



HAL
open science

Understanding and harnessing chaperone-mediated autophagy (CMA) in the rainbow trout (*Oncorhynchus mykiss*)

Simon Schnebert

► **To cite this version:**

Simon Schnebert. Understanding and harnessing chaperone-mediated autophagy (CMA) in the rainbow trout (*Oncorhynchus mykiss*). Cellular Biology. Université de Pau et des Pays de l'Adour, 2023. English. NNT : 2023PAUU3090 . tel-04726272

HAL Id: tel-04726272

<https://theses.hal.science/tel-04726272v1>

Submitted on 8 Oct 2024

HAL is a multi-disciplinary open access archive for the deposit and dissemination of scientific research documents, whether they are published or not. The documents may come from teaching and research institutions in France or abroad, or from public or private research centers.

L'archive ouverte pluridisciplinaire **HAL**, est destinée au dépôt et à la diffusion de documents scientifiques de niveau recherche, publiés ou non, émanant des établissements d'enseignement et de recherche français ou étrangers, des laboratoires publics ou privés.

THÈSE

UNIVERSITE DE PAU ET DES PAYS DE L'ADOUR

École doctorale 211 - SCIENCES EXACTES ET LEURS
APPLICATIONS

Présentée et soutenue le 11 Décembre 2023
par **Simon SCHNEBERT**

pour obtenir le grade de docteur

de

l'Université de Pau et des Pays de l'Adour

Spécialité : Doctorat Aspects moléculaires et cellulaires de la biologie

UNDERSTANDING AND HARNESSING CHAPERONE-
MEDIATED AUTOPHAGY (CMA) IN THE RAINBOW
TROUT (*Oncorhynchus mykiss*)

MEMBRES DU JURY

RAPPORTEURS

- Marta MARTINEZ VICENTE Senior Researcher/Vall d'Hebron Research Institute (UAB)
- José Luís SOENGAS Professor/University of Vigo

EXAMINATEURS

- Mathieu BOURDENX Senior research fellow/UK Dementia Research Institute (UCL)
- Beth CLEVELAND Research Physiologist/U.S. Department of Agriculture

DIRECTEUR

- Iban SEILIEZ Research Director/NuMéA INRAe



Acknowledgements

I want to thank Marta Martinez Vicente, Beth Cleveland, José Luis Soengas and Mathieu Bourdenx for accepting to evaluate my work and be part of my thesis committee.

A huge thank to the CMA team, Iban and Emilio. You both have taught me how to build myself as a confident scientist, in the lab but also in life. I will also remember great times during conferences as the 4 of us (with Max) tried to convince people CMA in fish would be the next big thing (dream on...).

Emilio, I've learned so much from you. I will always try to remember your attention to every, - I mean EVERY - detail and carry it with me, as I'm sure it will make me a better scientist in the future. I really hope I can become an aspiring, generous scientist and person as you are, so thank you.

Iban, je pense que tu as cru en mon potentiel depuis le début et je te remercie pour cela. On a eu des moments de stress mais aussi d'euphorie et je pense que c'est la science que tu voulais me montrer et celle que j'affectionne le plus. J'adore ta façon de chercher et tu m'y as donné goût, merci pour ces trois ans. Merci aussi d'avoir été cool en dehors du labo, à la pala ou au petit cochon. A quand la prochaine bière à gantxiki ?

Thank you Beth Cleveland, Lisa Radler and the USDA team for having generated and grown the 'alien' trouts, they really are special.

Un énorme merci à Karine pour sa gentillesse, sa patience, son rire (!!!) et Vincent (aka mon miroir) pour les meilleures jams, conversations rock et matchs de ping-pong ! Vous avez été d'une aide immense pour moi pendant 3 ans.

Quiero agradecer a Isabel por el trabajo tan dedicado y la amistad durante su estancia en Saint Pée, realmente disfruté tenerte cerca. También quiero agradecer a Sarita, eres la mejor profesora de castellano y nunca dejas de sonreír, te sienta muy bien.

Merci à Adèle, Béa, Cécile, Amaury et Julien de m'avoir accueilli et guidé à LPGP. Je remercie aussi les doctorants de Rennes (Antoine, Manon, Maxime et Aude). J'y ai passé un mois mais il m'a marqué et j'ai beaucoup apprécié ces moments.

Milesker Maité, Pantxika eta Ibai euskara ikasgaiengatik.

Merci aux pisciculteurs qui font un travail exceptionnel. Merci Fred, Antho et une pensée pour Franck qui prenait toujours le temps de me parler de la nature et des poissons.

Je remercie le labo Ecoflop (les grognasses, les Belges, les joueurs de pala etc...) pour avoir mis une superbe ambiance. Je me suis senti intégré dans une grande famille et c'est surtout grâce à vous.

Merci aussi à NuMÉA pour le soutien technique et administratif. Merci Anne, Emilie, Ludo.

J'ai aussi rencontré de super stagiaires qui ont rendu cette thèse encore plus agréable. Merci Axelle, Julu, Hector, Oihana et Antoine.

Merci à Teiva pour des leçons de surf et de crypto monnaie que je n'ai jamais payé. Merci à Nathan pour des blagues plus que douteuses, tes plats étoilés et Léa pour ta bonne humeur et tes suggestions cinéma.

Merci à mon groupe de copains avec qui on a pu faire les 400 coups. Il y a eu des soirées couvre-feu, des jams de musique, des foires au jambon, du surf, mais aussi des moments reposant. Comme dans cette chanson de Sticky Fingers, ensemble, on pourra toujours passer des moments cools et calmes. J'espère que l'on se retrouvera vite mais en attendant je pense à vous. Merci Laura pour tes blagues et d'avoir toujours été à l'écoute. Loïc, *yeux au ciel* sans commentaire. Je remercie ma besta Soak, la plus brillante des transporteuses, de m'avoir transmis ses skills en bois. Un énorme merci à Marius, mon coach, avec qui j'irais au bout du monde.

Merci à Borys et Olivier, mes frères belges qui m'ont envoyé le soleil bruxellois quand ils pouvaient.

Je remercie Ben, Robin et Arthur que je pouvais toujours appeler pour décompresser et pour ces super sessions Rocket League avant de démarrer la semaine. Merci à Sarah et à mes parents qui m'ont toujours soutenu. On a eu la chance de (re)vivre ensemble 1 an et c'était génial. Vous m'avez transmis la soif de connaissance, l'amour de la recherche et de l'éthique, c'est grâce à vous que je fais cette thèse, merci.

Je remercie ma plus grande supportrice et meilleure amie, Lucie, qui m'a apporté beaucoup de rires, de sérénité, de confiance et d'amour.

P ublications and communication

Publications

- [Schnebert, S.](#), Goguet, M., Vélez, E. J., Depincé, A., Beaumatin, F., Herpin, A., & Seiliez, I. (2022). Diving into the Evolutionary History of HSC70-Linked Selective Autophagy Pathways: Endosomal Microautophagy and Chaperone-Mediated Autophagy. **Cells**, 11(12), 1945. DOI: 10.3390/cells11121945
- [Schnebert, S.](#), Vélez, E.J., Goguet, M., Dias, K., Véron, V., García-Pérez, I., Beaumatin, F., Herpin, A., Cleveland, B. and Seiliez, I. Chaperone-Mediated Autophagy in fish: a key function amid a changing environment. (**submitted**)
- Vélez, E.J., [Schnebert, S.](#), Goguet, M., Balbuena-Pecino, S., Dias, K., Beauclair, L., Fontagné-Dicharry, S., Véron, V., Depincé, A., Beaumatin, F., Herpin, A. and Seiliez, I. (2023). Chaperone-Mediated Autophagy Protects Against Hyperglycemic Stress. **Autophagy**. DOI: 10.1080/15548627.2023.2267415
- Goguet, M., Vélez, E.J., [Schnebert, S.](#), Dias, K., Véron, V., Depincé, A., Beaumatin, F., Herpin, A., and Seiliez, I. Chaperone-Mediated Autophagy: the zebrafish joins the dance. (**In preparation**)

Communication

Talks

- [Schnebert, S.](#), Vélez, E.J., Goguet, M., Dias, K., Veron, V., Pinel, K., Beaumatin, F., Herpin, A., Cleveland, B. and Seiliez, I. Physiological relevance of stress-induced chaperone-mediated autophagy in major metabolic pathways in the rainbow trout. 14th International Congress on the Biology of Fish, Montpellier, France, July 2022.
- [Schnebert, S.](#), Vélez, E.J., Goguet, M., Dias, K., Veron, V., Beaumatin, F., Herpin, A., Cleveland, B. and Seiliez, I. Chaperone-mediated autophagy in fish: a key function in the midst of a stressful environment. Autophagy UK Network Meeting 2023 at University of Birmingham, England, June 2023.
- Goguet, M., Vélez, E.J., [Schnebert, S.](#), Veron, V., Depincé, A., Herpin, A. and Seiliez, I. Chaperone-Mediated Autophagy: the zebrafish joins the dance. 4th CAB. Bordeaux Autophagy Club. Bordeaux, France, April 2022.
- Goguet, M., Vélez, E.J., [Schnebert, S.](#), Veron, V., Depincé, A., Herpin, A. and Seiliez, I. Chaperone-Mediated Autophagy: the zebrafish enters the dance. CFATG 10 – 10th Scientific Days on Autophagy (The Francophone Autophagy Club), Besancon-Dijon, France, May-June 2022.

- Vélez, E.J., Schnebert, S., Goguet, M., Dias, K., Beauclair, L., Pinel, K., Veron, V., Beaumatin, F., Herpin, A. and Seiliez, I. First *in vitro* assessment of chaperone-mediated autophagy and its metabolic implications in rainbow trout hepatocytes. 14th International Congress on the Biology of Fish, Montpellier, France, July 2022.
- Vélez, E.J., Schnebert, S., Goguet, M., Balbuena-Pecino, S., Dias, K., Beauclair, L., Véron, V., Beaumatin, F., Herpin, A. and Seiliez, I. First *in vitro* assessment of Chaperone-Mediated Autophagy (CMA) and its metabolic implications in rainbow trout hepatocytes. Aquaexcel3.0 annual meeting, Heraklion, Greece, October 2022.
- Vélez, E.J., Schnebert, S., Goguet, M., Balbuena-Pecino, S., Dias, K., Beauclair, L., Véron, V., Depincé, A., Beaumatin, F., Herpin, A. and Seiliez, I. Dissecting the regulation of CMA in a natural model of impaired glucose homeostasis, the rainbow trout. SEFAGIA 2022 (Sociedad Española de Autofagia), Toledo, Spain, November 2022.
- Vélez, E.J., Schnebert, S., Goguet, M., Dias, K., Beauclair, L., Véron, V., Beaumatin, F., Herpin, A. and Seiliez, I. Lighting Chaperone-Mediated Autophagy in fish. Séminaire Poissons INRAE Rennes, France, January 2023.
- Vélez, E.J., Schnebert, S., Goguet, M., Balbuena-Pecino, S., Dias, K., Beauclair, L., Véron, V., Depincé, A., Beaumatin, F., Herpin, A. and Seiliez, I. Fishing for clues of the role of Chaperone-Mediated Autophagy in hyperglycemia-induced stress. MetaBoDay 2023, Talence, France, May 2023.
- Vélez, E.J., Schnebert, S., Goguet, M., Balbuena-Pecino, S., Dias, K., Beauclair, L., Fontagné-Dicharry, S., Véron, V., Depincé, A., Beaumatin, F., Herpin, A. and Seiliez, I. Dissecting the role of chaperone-mediated autophagy in the intolerance to carbohydrates of the rainbow trout (*Oncorhynchus mykiss*). Aquaculture Europe 2023, Vienna, Austria, September 2023.
- Vélez, E.J., Schnebert, S., Goguet, M., Balbuena-Pecino, S., Dias, K., Beauclair, L., Fontagné-Dicharry, S., Véron, V., Depincé, A., Beaumatin, F., Herpin, A. and Seiliez, I. Chaperone-Mediated Autophagy safeguards against hyperglycemic stress. CFATG 11 – 11th Scientific Days on Autophagy (The Francophone Autophagy Club), Lyon, France, November 2022.

Posters

- Schnebert, S., Vélez, E.J., Goguet, M., et al. 2021. Fishing for new tools to study Chaperone-mediated Autophagy (CMA) - Women in Autophagy (WIA) 2nd Annual Symposium, e-conference, United States. November 2021.
- Vélez, E.J.*, Schnebert, S.*, Goguet, M., Balbuena-Pecino, S., Dias, K., Beauclair, L., Veron, V., Pinel, K., Beaumatin, F., Herpin, A., Cleveland, B., and Seiliez, I. (*equal contribution). Menu of the day: Trout, sweets and CMA. CFATG 10 - 10th Scientific Days on Autophagy (The Francophone Autophagy Club), Besancon-Dijon, France, May-June 2022.
- Goguet, M., Vélez, E.J., Schnebert, S., Veron, V., Depincé, A., Herpin, A. and Seiliez, I. Chaperone-Mediated Autophagy: the zebrafish joins the dance. Autophagy UK Network Meeting 2023 at University of Birmingham, England, June 2023.

Table of contents

General introduction.....	8
State of the art and Aims of thesis.....	10
1. Fish homeostasis challenged as environment changes.....	12
a. New threats for fish in the wild at physiological level.....	12
i. Temperature rise	
ii. Eutrophication	
iii. Oxygen minimum zones	
iv. Ocean acidification	
v. Starvation	
vi. Pollution	
b. Salmonids aquaculture in a changing world.....	16
i. State of aquaculture	
ii. New concerns in salmonids aquaculture	
iii. New feeding strategies and welfare concerns	
iv. Animal welfare in aquaculture	
c. Fish welfare and resilience.....	19
i. The physiology of stress in fish.....	19
1. Stress response and sensory systems	
2. Oxidative stress and cellular homeostasis	
a. Reactive oxygen species (ROS) and antioxidants	
b. The effects of external factors on oxidative stress	
ii. Overview and limitations of tools to assess fish welfare and resilience.....	22
a. Welfare	
b. Resilience	
2. CMA, a key function to maintain protein homeostasis (proteostasis) under stress in mammals	
a. Discovery and presentation of autophagy.....	27
i. From the discovery of autophagy to Chaperone-Mediated Autophagy (CMA)	
ii. Different types of autophagy	
1. Macroautophagy	
2. Microautophagy	
3. Endosomal Microautophagy	
4. CMA	
b. History and mechanism.....	34
c. Main actors of CMA.....	36
i. KFERQ	
ii. HSC70 and cofactors	
iii. LAMP2A	
d. Regulation of CMA.....	38
i. LAMP2A-independent mechanisms	

1. Post-translational modifications	
2. Lysosomal pH	
ii. LAMP2A-dependent mechanisms	
a. Transcriptional regulation of CMA	
1. Nrf2/NFE2L2	
2. NFAT and calcium signaling	
3. ATRA	
b. LAMP2A lysosomal biogenesis and transport	
c. LAMP2A stability at lysosomal membrane	
e. The many physiological roles of CMA.....	42
i. Protein quality control	
ii. Starvation	
iii. Metabolic pathways	
iv. Transcriptional regulation	
v. Immune response	
vi. Cell cycle	
vii. Circadian clock	
viii. Neuronal proteostasis	
f. Measuring CMA activity.....	46
i. Lysosome isolation and GAPDH uptake assay	
ii. Photoconvertible CMA reporter	
iii. The KFERQ-Dendra transgenic mouse	
iv. A novel approach to infer CMA status: CMA score	
3. CMA in fish.....	52
a. CMA restricted to mammals and birds: myth or reality?	
b. Existence of CMA activity in medaka challenges the tetrapod paradigm	
Aims of thesis.....	56
Results.....	58
a. Publication 1: <i>Diving into the evolutionary history of HSC70-linked selective autophagy pathways: endosomal microautophagy and chaperone-mediated autophagy</i>	60
b. Publication 2: <i>Chaperone-mediated autophagy in fish: a key function amid a stressful environment</i>	77
c. Additional results: CMA score increases upon Mercury exposure.	125
d. Additional results: CMA as a regulator of food intake?.....	128
General discussion.....	134
a. L2AC31 inactivation and compensation of other proteolytic pathways	
b. The interplay between CMA and eMI	
c. Mysteries of lamp2a in RT	
d. First in vivo CMA activity assay in a fish species	
e. A previously uncovered role for CMA?	
f. Compromised homeostasis and new perspectives for CMA in fish	
Conclusion.....	144
References.....	145

General introduction

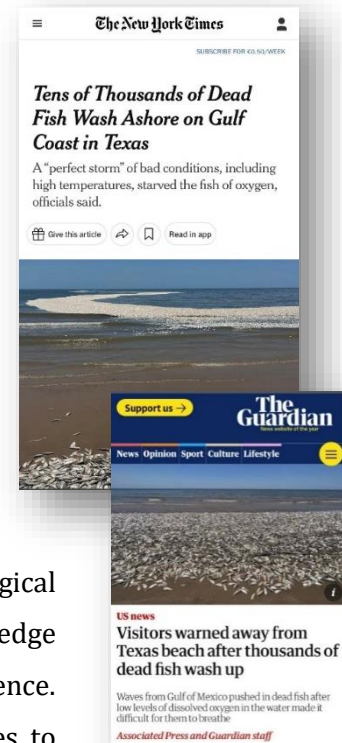
Chaperone-mediated Autophagy (CMA) is a lysosomal-dependent pathway responsible for protein degradation. By regulating the state of the proteome, it maintains cellular proteostasis (protein homeostasis) in the face of various stressors like starvation, oxidative stress, and hypoxia. Although extensively studied in mammals, the recent confirmation of CMA's existence in fish raises the possibility of significant roles previously unexplored in these species.

As fish in the environment are enduring increasing stressful situations, particular attention must be brought on their physiological responses to environmental pressures. Currently, there is limited knowledge regarding the physiological pathways involved in fish stress and resilience. This emphasizes the necessity for the development of new strategies to uncover the mechanisms underlying fish resilience and to establish tools for gauging their homeostasis.

In this context, the primary aim of this PhD thesis was to investigate the evolutionary characteristics of CMA throughout vertebrate evolution and explore the possibility of a functional CMA in salmonids, particularly in rainbow trout (RT - *Oncorhynchus mykiss*). Our initial investigations revealed the presence of key CMA components in RT. Subsequently, we embarked on characterizing CMA in RT, which confirmed the existence of CMA activity. To delve deeper into CMA's role, we developed a genetically modified RT line to modulate CMA, allowing us to investigate the pathways it regulates.

The data unveiled that CMA played a pivotal role in maintaining cellular homeostasis, particularly when RT faced environmental stressors. This suggests a potential correlation between CMA activation and cellular stress in RT. As a result, we adapted the 'CMA score' as a tool for assessing and quantifying cellular homeostasis in RT, with the potential for broader applications in fish research.

This PhD manuscript begins by introducing the current state of knowledge regarding fish homeostasis and its susceptibility to anthropogenic pressures. Subsequently, it delves into the topic of autophagy, with a particular focus on CMA, and highlights the existing gaps in CMA and fish research. Finally, the results presented in this study provide the first characterization of CMA's role in RT and explore its potential broader application in researching fish resilience within the context of environmental change.



S

tate of the art

PART 1: Fish homeostasis challenged as environment changes

1. New threats for fish in the wild at physiological level
 - c. Temperature rise
 - d. Eutrophication
 - e. Oxygen minimum zones
 - f. Ocean acidification
 - g. Starvation
 - h. Pollution

2. Salmonids aquaculture in a changing world
 - a. State of aquaculture
 - b. New concerns in salmonids aquaculture
 - c. New feeding strategies and welfare concerns
 - d. Animal welfare in aquaculture

3. Fish welfare and resilience
 - a. The physiology of stress in fish
 - i. Stress response and sensory systems
 - ii. Oxidative stress and cellular homeostasis
 1. Reactive oxygen species (ROS) and antioxidants
 2. The effects of external factors on oxidative stress
 - b. Overview and limitations of tools to assess fish welfare and resilience
 1. Welfare
 2. Resilience

PART 1: Fish homeostasis challenged as environment changes

1. New threats for fish in the wild at physiological level

While the importance of ocean health is widely recognized, this resource is still degrading. Anthropogenic pollution, climate change and overexploitation are affecting the health of this ecosystem. Robust governmental strategies and rigorous enforcement measures are necessary to protect and preserve the oceans¹. The physiology of fish and aquatic organisms depends on their surrounding environment. Parameters like salinity, temperature, pH or chemical composition can vary and induce a stress. The resilience and physiological adaptability of fish are then crucial to maintain homeostasis and overcome environmental stressors².

a. Temperature rise

With a predicted average increase of 3.1 °C in ocean surface temperature by 2100³ and the higher occurrence of climate events (El Niño–Southern Oscillation (ENSO), Pacific Decadal Oscillation (PDO), and Atlantic Multi-Decadal Oscillation (AMO) that vary in frequency and amplitude⁴, fish populations are enduring higher stress⁵. Following temperature rise, the stress response in fish consists in the release of catecholamines and cortisol⁶. The hormones trigger neural and metabolic pathways that distribute energy sources, which can subsequently be utilized by muscles and other tissues to generate a behavioral response⁷. These behavioral responses include food acquisition, predator avoidance and habitat selection⁸.

If the stress becomes chronic or recurrent, the stress response can be harmful, even for the progeny, as shown under high temperature⁹. In addition to affecting growth of large individuals of various fish species, high temperatures also potentially translate into less successful fertilization and reproduction¹⁰. Although early-life exposition to high temperature can shape fish neural response¹¹, the adaptation of fish populations to global warming is still unknown, especially considering that other stressors will have to be considered⁶.

As global warming impacts lakes on a global scale¹², Till et al. examined the potential link between extreme summer conditions and fish die-offs through a comprehensive synthesis of *in situ* and satellite-derived lake data. Their analysis encompassed a database of 502 freshwater fish die-offs, paired with simulated lake-specific temperature profiles for north temperate lake ecosystems. Their findings established a direct correlation between elevated local environmental temperatures and the incidence of severe ecological events, potentially contributing to a global reconfiguration or depletion of freshwater environments¹².

b. Eutrophication

Eutrophication arises from nutrient-rich human waste (mainly N and P), agriculture, and nitrogen deposition from fossil fuel combustion¹³. These factors promote algae growth, increasing biomass, which results in higher delivery of degradable organic matter to bottom waters. Oxygen depletion then occurs because of aerobic microbial decomposition. Restoring higher oxygen levels ultimately becomes challenging due to behavioral and biogeochemical feedbacks¹⁴ (Fig 1).

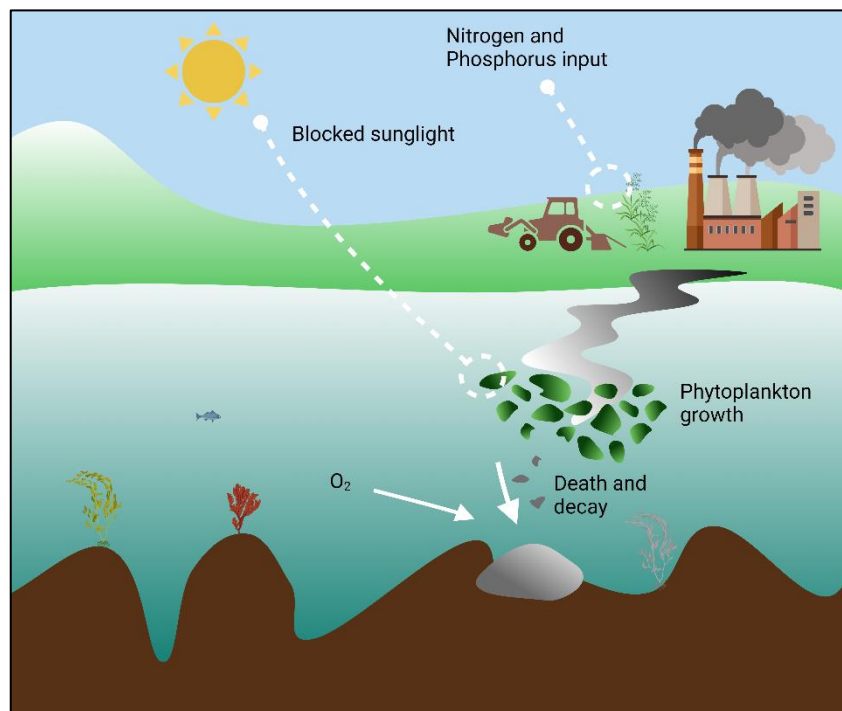


Figure 1: Illustration of the eutrophication process. Excess nutrient input causes algal growth. The overgrowth of algae consumes O_2 and blocks sunlight. Bacterial decay also reduce levels of O_2 .

Depending on the severity of the hypoxia, colonizing species can take years to recover¹⁵. In addition, species recovery often follows a distinct pattern of establishment compared to the pattern of species loss, wherein past events can influence current dynamics of a system. This results in a biodiversity response called hysteresis¹⁵. As an example, in the case of the Black Sea, an increase in nutrient input in 1975 increased phytoplankton blooms, causing oxygen depletion¹⁴. It led to a higher mortality of mussels and other benthic filter feeders, which resulted in an escalation of particulate organic carbon accessible for microbial respiration, causing further oxygen depletion¹⁶. To mitigate these effects, a management framework was developed in the 1990s, aiming at reducing nutrient inputs¹⁷. As the hypoxic area declined, there was a significant decrease in phytoplankton biomass, and the composition shifted towards diatoms, indicating an enhancement in ecosystem health¹⁸. Nevertheless, certain

species (*Mytilus galloprovincialis* and *Phyllophora truncate*) did not recover, underscoring that sensitive ecosystem components might not have had adequate time to recuperate after the return to normal oxygen levels. This strengthens the concept of hysteresis in the ecosystem's revival from hypoxia¹⁴.

c. Oxygen minimum zones

Oxygen levels in the open ocean and coastal waters have been declining since the mid-20th century, ranking as one of the most important changes in marine ecosystems. This reduction in oceanic oxygen content affects productivity, biodiversity, and biogeochemical cycles¹⁹. The concerning ongoing expansion of open-ocean oxygen minimum zones (OMZs) is a threat for marine life and biodiversity, as hypoxia could affect far more coastal ecosystems than previously thought²⁰. As oceans warm, oxygen solubility is expected to decrease and metabolic rates of marine organisms to escalate^{19,21}. All obligate aerobic organisms can compensate for oxygen depletion but only to a certain extent. Major physiological processes are affected by low oxygen levels, such as survival, growth, behavior or reproduction^{15,22}, and the epigenetic changes engendered can be expressed in future generations²³. A recent study shows that if greenhouse gases emissions continue, the Pacific oxygen minimum zone will certainly expand. Through modeling, they show that it will grow 6 to 8 million cubic kilometers - about 0.6% of the volume of the world's oceans by 2100²⁴. Marine species, ecosystems and ecosystems services could be severely impacted.

d. Ocean acidification

The increased human CO₂ emissions alter seawater carbonate chemistry and reduce the pH²⁵. While most marine organisms depend on the surrounding water's biochemistry, this phenomenon is expected to increase in time²⁶. The calcifying organisms are the most at risk, but fish are still vulnerable to pH variation²⁷. Their metabolic performance²⁸, behavior²⁹ and population dynamics³⁰ are currently being threatened.

In 2023, Dong et al. conducted an eight-month experiment simulating ocean acidification conditions to measure the effects on living benthic foraminifera³¹. They sampled organisms from four sites of the Yellow Sea and increased the carbon dioxide levels of the system. The experiments revealed that as salinity increased, there was a general decline in the abundance of benthic foraminifera. Additionally, shell diameter and thickness (and consequently weight) decreased due to the reduced availability of calcium carbonate in the surrounding environment, which serves as the building material for their shells. Nevertheless, an intriguing observation was the rise in diversity, driven by the demanding conditions that favor the emergence of less common species. In summary, their findings led them to

assert that they envision an ongoing "biocalcification crisis" stemming from ocean acidification³¹. Although the physiological well-being of fish might be influenced by declining pH through the formation of calcium carbonate structures in their inner ears³², the research by Dong et al. demonstrates that marine communities could experience repercussions, thus potentially exerting an impact on fish ecosystems as well.

e. Starvation

Survival of fish larvae is closely tied to the presence of prey. Given the high susceptibility of fish larvae to malnutrition, their survival depends on the average size of prey, their seasonal occurrence, and overall abundance³³. The concept known as the match-mismatch hypothesis³⁴ highlights the importance of synchronizing the production of first feeding larvae with the availability of planktonic food. As climate change influences primary and secondary production, it potentially could disrupt the distribution of fish larvae, hence fish populations and potential indirect effects on the structure of food webs³⁵.

In 2016, Hedström et al. conducted a study to examine the impact of water brownification on fish mortality in Northern climates³⁶. This phenomenon, anticipated to intensify with climate change, stems from the terrestrial export of colored organic matter^{37,38}. The researchers assessed the survival of young-of-the-year three-spined stickleback (*Gasterosteus aculeatus*) under experimental conditions involving increased humic water input³⁶. The outcomes revealed heightened mortality rates, reduced body condition, and decreased ingested prey biomass. The findings led the researchers to conclude that augmented water brownification hindered the predator's search efficiency, and led to starvation³⁶.

f. Pollution

A concern for the repercussions of increasing release of contaminants and pollutants in the aquatic environment has been growing for about 30 years³⁹. Pollutants from agricultural or industrial activities are the main contaminants³⁹ but the predicted growth in plastic pollution now also accounts for one of the major threats on the marine environment⁴⁰. It has been shown that effects of pollutants are widely spread among teleost species. In addition to stress⁴¹, major physiological functions are affected: reproduction³⁹; cardiac function⁴²; integrity of gills⁴³ and others.

Recently, a higher attention has been brought to the toxicity and danger of methylmercury (MeHg). It is naturally present in the environment but industrial and agricultural activities led to a higher contamination of surface waters and sediments⁴⁴. This pollutant biomagnifies through food chains and is known to be efficiently absorbed and distributed into organs⁴⁵. Levels of MeHg found in the

environment are enough to induce biological harm, affecting both individuals and entire populations within specific ecosystems⁴⁵.

One of the most thoroughly investigated current threats to fish is microplastics. These pollutants have seen a significant increase in oceanic surface waters over the past four decades, stemming from sources like synthetic clothing fibers, fragments from the deterioration of larger plastic items, and aquaculture practices including nets and floats^{46,47}. While fish are used to ingesting various indigestible particles such as sand, fish scales, shells, many studies have pointed out severe consequences of microplastics ingestion on gastrointestinal tract⁴⁸, gill function⁴³, reproduction⁴⁹, brain and nervous system^{50,51}.

2. Salmonids aquaculture in a changing world

a. State of aquaculture

The world aquaculture production has lately reached its highest growth, with a 56% increase over the 2008-2018 decade. Global aquaculture production now exceeds the capture fisheries aimed at human consumption, and is planned to expand⁵². In the year 2020, the primary contributors to fisheries and aquaculture production for aquatic animals were Asian nations, constituting 70% of the total output. They were followed by countries in the Americas (12%), Europe (10%), Africa (7%), and Oceania (1%)⁵². Although Europe's fisheries and aquaculture production has exhibited a gradual decrease since the late 1980s (with a slight recovery in recent years up to 2018, followed by another decline), and the Americas have witnessed fluctuations since their peak in the mid-1990s, Africa and Asia have nearly doubled their production over the past two decades (Fig 2)⁵².

France stands out as a prominent European nation in terms of aquaculture production volume, the quality of its education and research systems, and the robust support provided by producers' organizations. Although France experienced an initial period of growth in marine fish production during the 1990s, its progress has stabilized. In contrast, countries such as Greece, Spain, and Turkey have rapidly developed a significant sector, particularly focused on producing seabass and seabream (*Sparus aurata L.*)⁵³.

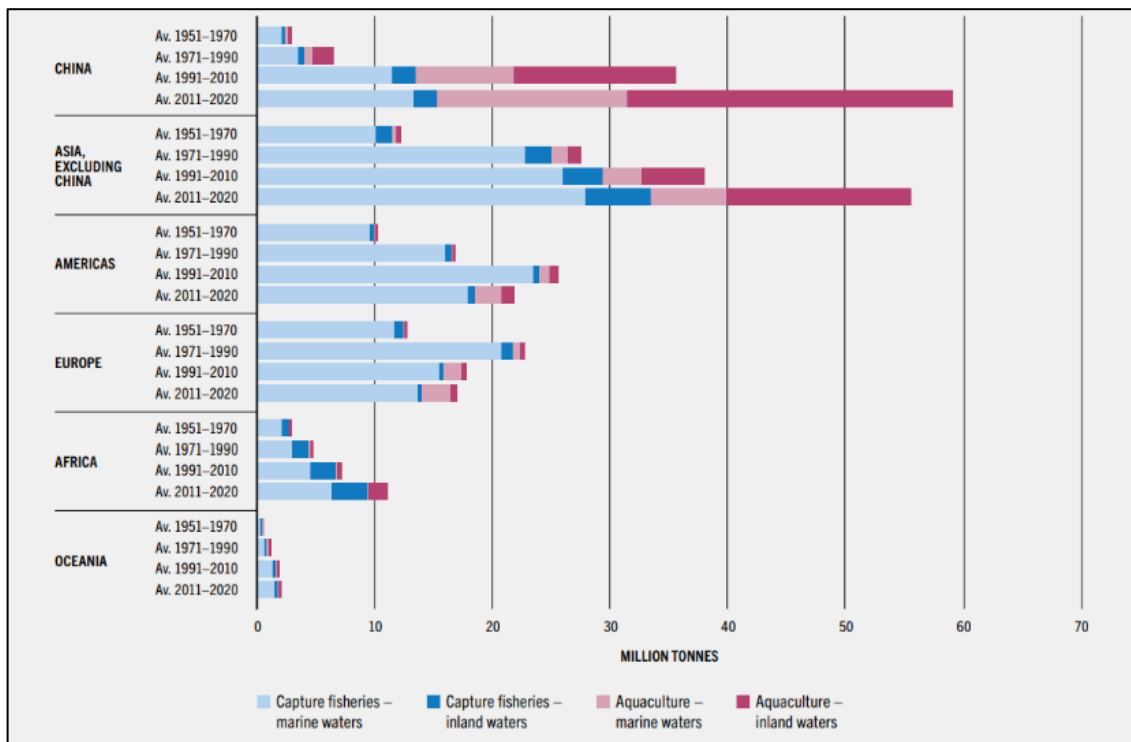


Figure 2: Regional contribution to world capture fisheries and aquaculture production since 1951 until 2020. Extracted from “The State of World Fisheries and Aquaculture 2022”⁵²

Aquaculture has a long-standing history in France, with a particular focus on mollusk production and trout farming. The shellfish industry in France stands out as the European leader in terms of volume and ranks second in value. In 2004, approximately 35,128 tons of rainbow trout (RT) were cultivated, amounting to a market value of approximately €135 million. France is the third largest producer of RT after Chile and Norway and in fact RT is the most important species farmed in France⁵³.

France is facing current challenges, such as competing for space and water use in the coastal zone or remaining competitive against Mediterranean, Southeast Asian and North Atlantic countries. This challenge is particularly pronounced due to the changing climate, which is set to pose difficulties for the cultivation of salmonid species⁵³.

b. New concerns in salmonids aquaculture

Salmonids aquaculture accounts for about 7% of the world’s fish production and represents 18% of total traded in value in 2020⁵² therefore is of great importance in this industry. The most farmed salmonids include Atlantic salmon (*Salmo salar*) and RT⁵². These species are currently exposed to major threats such as diseases^{54,55}, pathogens^{56,57} and environmental change⁵⁸. The risk of disease outbreaks is expected to increase due to climate change.

As an example, the amoebic gill disease (AGD) initially identified in 1985 in the United States, Tasmania, and Australia⁵⁹, has now evolved into a global challenge for Atlantic salmon aquaculture. Furthermore, this issue has extended its impact to encompass various other commercially cultivated marine fish species. It arises from the infection of fish gills by the facultative parasite *Neoparamoeba perurans*, and causes mortalities as high as 80% when left untreated⁶⁰. Observable clinical indications of AGD encompass respiratory difficulties, sluggish behavior, and reduced appetite, all of which are linked to visibly apparent gill lesions. Since its initial discovery, AGD has emerged as a significant global health concern within the marine salmonid industry⁵⁵. A recent meta-analysis that reviewed all AGD reports to date has suggested that disease outbreaks are more strongly linked to localized temperature anomalies rather than just absolute temperature levels⁶¹. With the anticipated increase in ocean temperatures and changes in rainfall patterns due to climate change, there is a growing concern that the costs associated with AGD will continue to rise for the salmonid industry in the future⁵⁵. While aquaculture continues to expand, more threats appear and call for new approaches to assess fish health⁶²

c. New feeding strategies and welfare concerns

As human population is increasing⁶³, new challenges emerge concerning the feasibility of achieving both adequate and sustainable fish production. New aquatic food systems need to be based on minimizing ecosystem impacts, promoting social equity, and addressing the repercussions of climate change. Life cycle assessment studies have consistently shown that aquafeeds frequently stand out as the primary source of detrimental environmental effects linked to commercial aquaculture operations. Valuable aquaculture species like salmonids, seabass, and shrimp demand protein-rich diets, historically reliant on fishmeal and fish oil sourced from wild pelagic fish stocks - a resource crucial not only for food security but also for ecological balance⁶⁴. To sustain such production, substantial feed volumes are essential, providing affordable protein, essential amino acids, additives, omega-3 fatty acids, minerals, vitamins, and energy sources. In addition, the fish used in the production of fishmeal and fish oil usually originate from well-managed resources; however, some countries are developing fishmeal production without considering the sustainability of their fisheries. In West Africa, fisheries products aimed at human consumption are neglected due to the increasing amount of catches reduced into fishmeal and exported⁶⁴.

Reducing the production of fishmeal and fish oil is now a real incentive for the aquafeed industry, thus many researchers are trying to find alternatives to these diets⁶⁴. It could represent a solution but also could improve resource sustainability, animal welfare, social equality or biodiversity. The main candidates to replace fishmeal and fish oil are plant by-products, algae (micro- and macro-), insects,

fish and land animal by-products, and single-cell proteins (including from bacteria and yeast)^{64,65}. Other innovative practices are also studied, such as precision technology, integrated multitrophic aquaculture (IMTA), integrated agriculture-aquaculture (IAA) or bivalve aquaculture⁶⁴. Overall, new formulated feeds and technological advances could enhance a 'cleaner' aquaculture but it would depend on the efficiency of technology transfer among countries and partners⁶⁴.

d. Animal welfare in aquaculture

The intensification of the aquaculture industry poses serious threats for the environment and the European Commission has clearly shown its desire to work toward a more sustainable production, through respect for animal welfare⁶⁶. Many initiatives constitute the establishment of an ethical responsibility, like the 2030 Agenda for Sustainable Development, the Sustainable Development Goals (SDGs) and the Paris Agreement of the Conference of the Parties (COP21) of the United Nations Framework Convention on Climate Change^{67,68}. Multiple fields involving animal research or consumption have incorporated welfare as part of their activities, but the welfare of aquatic animals in farmed systems is only recently discussed⁶⁹.

In 2018, the FAO reported 82.12 million metric tons of farmed aquatic animals from 6 phyla and at least 408 species. While analyzing this data, Franks et al. 2021⁷⁰ found welfare information for only 30% of individuals. For the remaining 70%, they either had no welfare data or were of unknown species. Their findings underline the importance of allocating immediate efforts to assess the welfare of these understudied species.

3. Fish welfare and resilience

a. The physiology of stress in fish

i. Stress response and sensory systems

Upon a given stress, the perception of a threatening situation in fish induces a response. Like in other vertebrates, the responses are primarily orchestrated through the activation of two hormonal axes: the sympatho-chromaffin (SC) axis and the hypothalamic-pituitary-interrenal (HPI) axis (Fig 3)⁴¹. The SC axis initiates a swift stress response, influencing the cardio-respiratory system by increasing breathing and heart rates, heart stroke volume, and blood perfusion in gills and muscles. This sequence ensures glucose supply to essential tissues, with adrenaline as a pivotal mediator. On the other hand, a triggered HPI axis contributes to resource restructuring through increased catabolic pathways, provision of carbohydrate sources, utilization of fatty acids for energy, and the restraint of energy-

demanding and extended functions like immune responses. The plasmatic cortisol plays a pivotal role as key mediator in the HPI pathway (Fig 3)⁷¹.

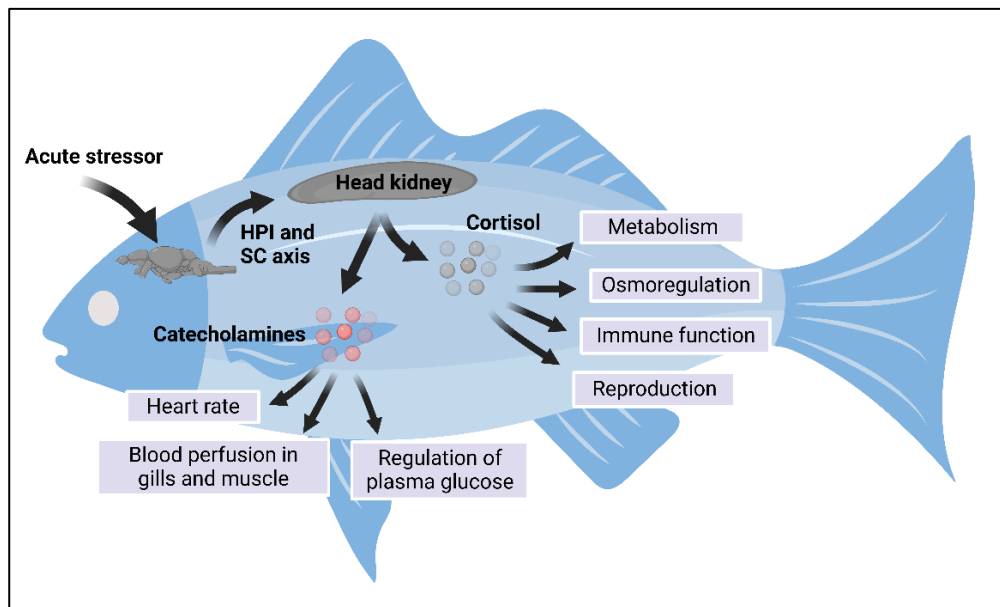


Figure 3: Schematic representation of the roles of the sympatho-chromaffin (SC) and hypothalamic-pituitary-interrenal (HPI) axis response to stress. Adapted from Vallejos-Vidal et al. 2022⁷²

After being produced in the head kidney and released in the blood⁷³, cortisol binds to glucocorticoid (GR) or mineralocorticoid (MR) receptors, which can affect cardiovascular function, immune and stress response, cell cycle, growth, reproduction, and allostatic balance^{74,75}.

Considering its physiological roles, cortisol has been used as a biomarker in stress-related surveys⁷⁴. However, the individual- and species-specific variations of the physiological effects of the stressors tend to distort the measure of stress⁷¹. Given the variability of cortisol levels due to circadian cycles⁷⁶ and environmental conditions such as captivity or the wild state⁷⁷, a comprehensive approach encompassing multiple parameters is essential for evaluating stress in fish⁷⁴.

Other plasma metabolites related to stress response, like glucose and lactate, can also serve as indicators to evaluate compromised welfare, as their levels increase upon stressful situations⁷⁸. Glucose, a vital carbohydrate in animal bioenergetics, plays a significant role driven by cortisol action, utilizing pathways like gluconeogenesis and glycogenolysis⁷⁹. These processes enable animals to meet energy demands spurred by stressors, supporting the 'fight or flight' response. Lactate is a byproduct of anaerobic glycolysis originating from glucose. Measuring plasma lactate and glucose to assess stress present inconsistencies, with reports suggesting that glucose content holds less precision as a stress indicator compared to cortisol⁸⁰. By affecting glycogen stores, extrinsic factors such as diet, life stage, and season of the year, etc., considerably influence glucose and lactate results. This implies that they

cannot stand as the solitary parameters for stress assessment⁸¹. In the assessment of welfare, it is vital to monitor diverse stress responses, incorporating behavior, neurophysiology, pathology, and molecular markers to establish robust conclusions regarding an individual's state. A comprehensive grasp of these elements, coupled with species-specific biological knowledge, well-founded behavioral observations, and supplementary stress indicators like plasma glucose and lactate, is indispensable for accurately interpreting individual well-being⁸¹, thus new welfare indicators are needed for fish.

ii. Oxidative stress and cellular homeostasis

1. Reactive oxygen species (ROS) and antioxidants

Around six decades ago, the identification of ROS within biological systems established a connection with diseases and aging⁸². Since then, investigating these ROS and oxidative stress – involving the generation of biomolecular oxidative damage due to an imbalance between ROS and protective antioxidant mechanisms – has surged in significance, emerging as a central theme in fields including medicine, molecular biology, physiology, and more recently, ecology⁸³.

When oxygen is partially reduced, it produces reactive compounds like the superoxide radical ($O_2^{\cdot-}$), singlet oxygen (1O_2), hydrogen peroxide (H_2O_2), and the hydroxyl radical (HO^{\cdot})⁸⁴. These compounds are collectively referred to as ROS. ROS are generated by all photosynthetic and aerobic organisms as part of their regular metabolism, or in the mitochondrial electron transport chain at two specific points: (i) complex I (NADH dehydrogenase) and (ii) between ubiquinone and complex III⁸⁵. Their level of production is directly linked to the oxygen concentration within an organism⁸⁶. If the increase in ROS production surpasses the organism's capacity to neutralize these reactive species, it results in oxidative stress, which harms cellular components⁸⁴.

To protect themselves against the toxicity of ROS, organisms have designed mechanisms to either prevent or repair the effects of oxidative stress. Antioxidants serve as a means of prevention, taking the shape of either enzymes (like superoxide dismutase (SOD), catalase (CAT), and glutathione peroxidase (GPX)) or non-enzymatic molecules (such as ascorbic acid (vitamin C), glutathione, α -tocopherol (vitamin E), carotenoids, and other small compounds). These components are naturally present in the environment^{87,88}, and are commonly used in fish biology to measure oxidative stress⁸³. Cellular homeostasis in aquatic animals, like in other organisms, relies on the equilibrium between ROS production and antioxidant defenses. Fish, due to factors like temperature fluctuations, oxygen levels, osmotic changes (e.g., anadromous species), and pollution, face heightened exposure to these challenges⁸³.

2. The effects of external factors on oxidative stress

The 2 °C rise in temperature predicted by the end of the century³ has the potential to severely affect fish physiology. It is known to increase oxygen consumption, thus an elevated flux at the level of the electron transport chain and a greater ROS production⁸⁴. Even though, some specific species have developed the ability to modulate their antioxidant capacity, they can only do it to a certain level. This was demonstrated on the bald notothen (*Pagothenia borchgrevinki*, Nototheniidae), a species endemic to Antarctica⁸⁹. Despite being able to cope with increased temperatures, the fish's enhanced antioxidant defenses reached a limit when exposed to chronic temperature elevation⁸⁹. Similar studies have been conducted on goldfish⁹⁰, North Sea eelpout⁹¹, leading to the consensus that the impact of heightened temperature on antioxidant capacity varies based on tissue and species. Examining three populations of three-spined sticklebacks (*Gasterosteus aculeatus*, Gasterosteidae), Nikinmaa et al. evaluated transcription and redox enzyme activities under stable conditions and in reaction to sudden temperature shifts. Their findings revealed divergence in markers connected to antioxidant response, suggesting that mechanisms regulating redox equilibrium might serve as key selection targets in driving adaptive divergence within this fish species⁹².

Certain fish species have demonstrated adaptation to low oxygen (hypoxic) or no oxygen (anoxic) conditions. They achieve this by strengthening their ability to control the generation of ROS and increasing their antioxidant capacity when they return to normal oxygen levels⁹³. Yet, in fish species not inherently acclimated to reduced oxygen levels, hypoxic conditions seem to trigger antioxidant activity, particularly in enzymes like SOD and catalase⁹⁴.

In an experiment by Martinez-Álvarez et al., sturgeons (*Acipenser naccarii*, Acipenseridae) were acclimated to seawater over a 20-day period. Subsequently, enzyme activities for CAT, GPX, and SOD were measured⁹⁵. While parameters like muscle water content, plasma osmolality, and cellular constants had reverted to their normal states, cortisol levels, antioxidant activity, and lipid peroxidation exhibited unusual measurements. It showed that osmoregulation had induced substantial physiological impacts, leading to increased oxidative stress. Unlike diadromous species, pelagic fish do not undergo periodic salinity changes throughout their life. Consequently, it might be expected that they display decreased resistance to oxidative stress⁸³.

b. Overview and limitations of tools to assess fish welfare and resilience

i. Welfare

The concept of fish welfare is developing, but the lack of reliable indicators and methods for welfare assessment entail new strategies to address this issue⁹⁶. Given the extensive diversity among teleost species, welfare indicators ought to consider species-specific physiology, anatomy, behavior and their corresponding environmental demands⁸¹.

To ensure the well-being and health of fish, it is widely believed that five conditions must be upheld and preserved⁹⁷ (Fig 4). These parameters can be gauged with different physiological and behavioral indicators⁸¹. In evaluating instances of compromised fish welfare, assessments typically rely on the measurement of stress-related metabolites in the bloodstream. These include cortisol, glucose, and lactate. Cortisol, a glucocorticoid hormone secreted in the bloodstream after activation of the hypothalamo–pituitary–adrenal/interrenal axis (HPI)⁹⁸, is an acute stress indicator. However, it does not necessarily imply chronic stress due to HPI desensitization from allostatic overload⁹⁸. As measuring plasma cortisol appears inconsequential during chronic stress⁸¹, it indicates the need to investigate further physiological pathways related to stress in fish.

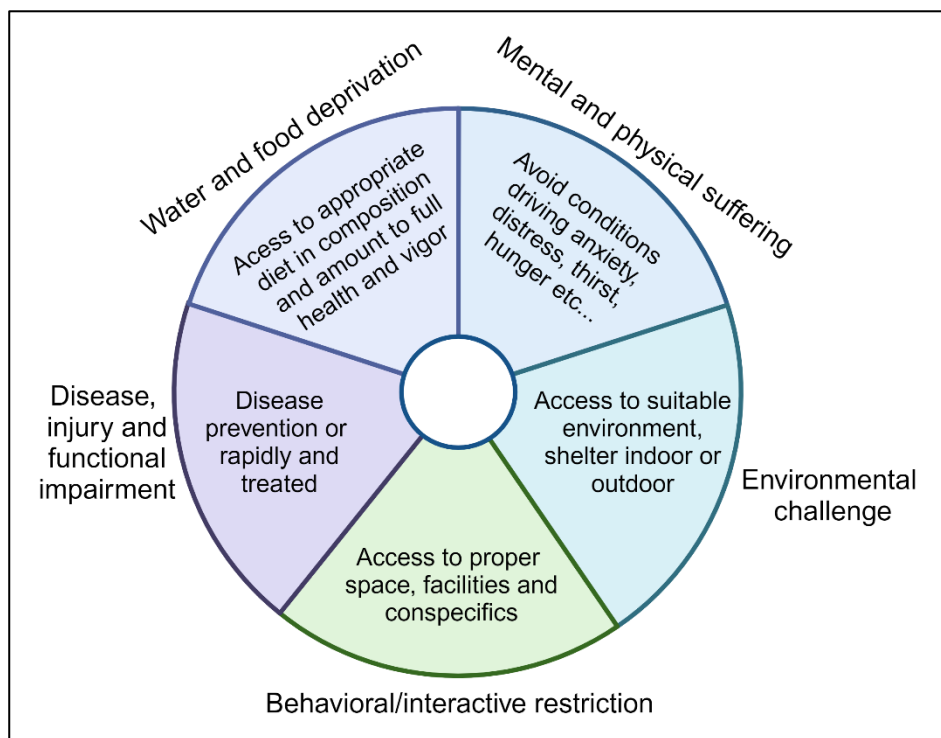


Figure 4: Five domains to assure and assess welfare of animal reared and kept under artificial conditions. Adapted from the Brambell (1965) by UK Farm Animal Welfare Council⁹⁷

ii. Resilience

Research conducted on fish provides empirical evidence that early exposure to various stressors triggers the adaptability of the HPI axis when subjected to subsequent stressors^{99,100}. A phenomenon called ‘thermal imprinting’ has been described as the long-lasting impacts on individual physiology and the subsequent capacity to manage similar or new environmental demands⁶. For instance, a study conducted on adult seabream showed that exposure to elevated temperatures during their

developmental stage resulted in a decreased cortisol reaction to stress caused by confinement¹¹. The response to cold stress was more pronounced in individuals that were raised under higher temperatures during the embryonic phase¹¹. Additionally, alterations in the transcription of genes involved in regulating the HPI axis (*gr* and *pomca2*) were observed following thermal imprinting. These changes could potentially be associated with coping mechanisms.

The limited availability of experimental setups that expose aquatic ectothermic animals to warming conditions over significant periods has posed a challenge to comprehending their ability to withstand the effects of climate warming. Nonetheless, the team of Jutfelt¹⁰¹ had access in 2016 to the Biotest enclosure, a distinct coastal ecosystem in the Baltic Sea subjected to natural thermal oscillations. The European perch (*Perca fluviatilis*, L.) from this area experienced a 5–10 °C temperature rise by a nuclear power plant for over three decades¹⁰¹. They have shown that fish under chronic warming exhibit rapid growth in their early life stages and morphological shifts as adults, including smaller relative organ sizes. Moreover, they show that this resilience arises from the thermal compensation of resting cardiovascular functions and basal energy needs, which are notably reduced when compared to fish experiencing acute warming¹⁰¹.

Although perch from the Biotest enclosure displayed physiological adaptability, their maximum cardiorespiratory traits and critical thermal maximum exhibited minimal or no thermal compensation. As a result, their warming tolerance was significantly diminished, likely rendering them more susceptible to abrupt heat waves. This underscores the limitations of fish resilience¹⁰¹.

Having shown that perch can modulate physiological traits to cope with chronic warming, Sandblom et al. underscore the concept of thermal plasticity in fish. However, it is plausible that additional mechanisms contribute to fish resilience when facing environmental challenges on varying scales. Exposure to environmental threats could potentially have long-term consequences for stress physiology, thus modifying the capacity to endure additional stressors⁶. This strongly indicates the need for investigating novel cellular or molecular pathways in fish.

Interestingly, recent studies from Moore and coauthors have focused on other cellular pathways related to stress to develop biomarkers and increase our understanding of the impact of a fluctuating environment on the cell¹⁰²⁻¹⁰⁴. In particular, Moore et al. investigated how blue mussels (*Mytilus edulis* and *Mytilus galloprovincialis*) react to different environmental stressors¹⁰³. That research focused on autophagy and the lysosome (which will be described in the second part of this thesis), and highlighted their protective role against ROS and oxidative stress induced by various stressors. Those authors introduced parameters to quantify autophagic activity¹⁰⁵ (lipofuscin, lysosomal membrane stability) in mollusks and hinted at the strong possibility of integrating them as new biomarkers to assess the impacts of environmental changes on animals. Exploring other cellular systems is of great

significance, as it is essential to gain a more extensive understanding of the antioxidant protection mechanisms that enable animals to respond and adjust to environmental changes.

PART 2: CMA, a key function to maintain protein homeostasis (proteostasis) under stress in mammals

- a. Discovery and presentation of autophagy
 - i. From the discovery of autophagy to Chaperone-Mediated Autophagy (CMA)
 - ii. Different types of autophagy
 1. Macroautophagy
 2. Microautophagy
 3. Endosomal Microautophagy
 4. CMA
- b. History and mechanism
- c. Main actors of CMA
 - i. KFERQ
 - ii. HSC70 and cofactors
 - iii. LAMP2A
- d. Regulation of CMA
 - i. LAMP2A-independent mechanisms
 1. Post-translational modifications (PTMs)
 2. Lysosomal pH
 - ii. LAMP2A-dependent mechanisms
 1. Transcriptional regulation of CMA
 - a. Nrf2/NFE2L2
 - b. NFAT and calcium signaling
 - c. Nuclear retinoic acid receptor- α (RAR α)
 2. LAMP2A lysosomal biogenesis and transport
 3. LAMP2A stability at lysosomal membrane
- e. The many physiological roles of CMA
 - i. Protein quality control
 - ii. Starvation
 - iii. Metabolic pathways
 - iv. Transcriptional regulation
 - v. Immune response
 - vi. Cell cycle
 - vii. Circadian clock
 - viii. Neuronal proteostasis
- f. Measuring CMA activity
 - i. Lysosome isolation and GAPDH uptake assay
 - ii. Photoconvertible CMA reporter
 - iii. The KFERQ-Dendra transgenic mouse
 - iv. A novel approach to infer CMA status: CMA score

PART 2: CMA, a key function to maintain protein homeostasis (proteostasis) under stress in mammals

CMA, a selective autophagy pathway, is recognized for its role in mammalian cellular stress responses and the maintenance of homeostasis.

a. Discovery and presentation of autophagy

Proteins are integral to nearly every biological process, and their functional efficacy relies on the fine tuning of their levels within cells and maintaining their proper conformational integrity. Adequate levels and integrity of proteins, in turn, enables organisms to thrive¹⁰⁶. However, in the face of cellular stress or adverse environmental circumstances, proteostasis may be compromised. Molecular chaperones and their regulators (responsible for *de novo* folding and refolding), the ubiquitin-proteasome system (UPS) and autophagy are responsible for protein quality control¹⁰⁶.

i. The discovery of autophagy

In 1955, Christian de Duve discovered and described the existence of a new type of organelle, resembling a "saclike structure surrounded by a membrane and containing acid phosphatase", that he called "lysosome"¹⁰⁷. Following the discovery of the lysosome, Werner Strauss and his group sought to understand how extracellular molecules entered the cell and discovered that previously labeled proteins were found in the lysosomes in a fragmented form¹⁰⁸. He therefore concluded that proteins were degraded in the lysosome. In 1963, Zanvil Cohn explored the nature of the molecules accumulating inside the lysosomes and observed that in addition to extracellular material, other types of intracellular content (lipids, carbohydrates, amino acids) could accumulate¹⁰⁹. Overall, it was established that the lysosome functions as the "cell's digestive system", degrading material from outside the cell but also intracellular components. Using electron microscopes, researchers then discovered different types of vesicles including autophagosomes¹¹⁰. In 1966, de Duve described this sequestering organelle as a vacuole that contains morphologically recognizable cytoplasmic components¹¹¹. While de Duve and others continued on characterizing the terminal stages of autophagy, Per Seglen's laboratory focused on the early and intermediate stages¹¹². It led to the discovery of the phagophore, an expanding membrane sac that subsequently matures into the autophagosome¹¹³ but also the amphisome¹¹⁴, which connects the endocytic and autophagic pathways. In 1992, Yoshinori Ohsumi revealed the existence of autophagy in yeast¹¹⁵. This discovery showed that autophagy was not restricted to mammals and established the foundations for further studies based on this organism.

Many researchers carried on characterizing the actors, functions and pathways encompassed within autophagy but then some focused on the link between autophagy and disease. Beth Levine and colleagues showed the importance of the *Beclin1/Atg6* (Autophagy-related gene 6) gene and tumor development¹¹⁶ (Fig 5). Eileen White and Shengkan Jin demonstrated that autophagy could protect against DNA damage and prevent tumorigenesis¹¹⁷.

For a long time, autophagy was considered as a non-selective process. Since the proteasome system was able to tag specific proteins, it was widely regarded as the exclusive pathway for selective proteolysis¹¹⁸. Many sub-types of autophagy, which can be selective, have been now well established. These include macroautophagy, microautophagy, and CMA, all of which involve the transport of substrates to the lysosome for degradation.

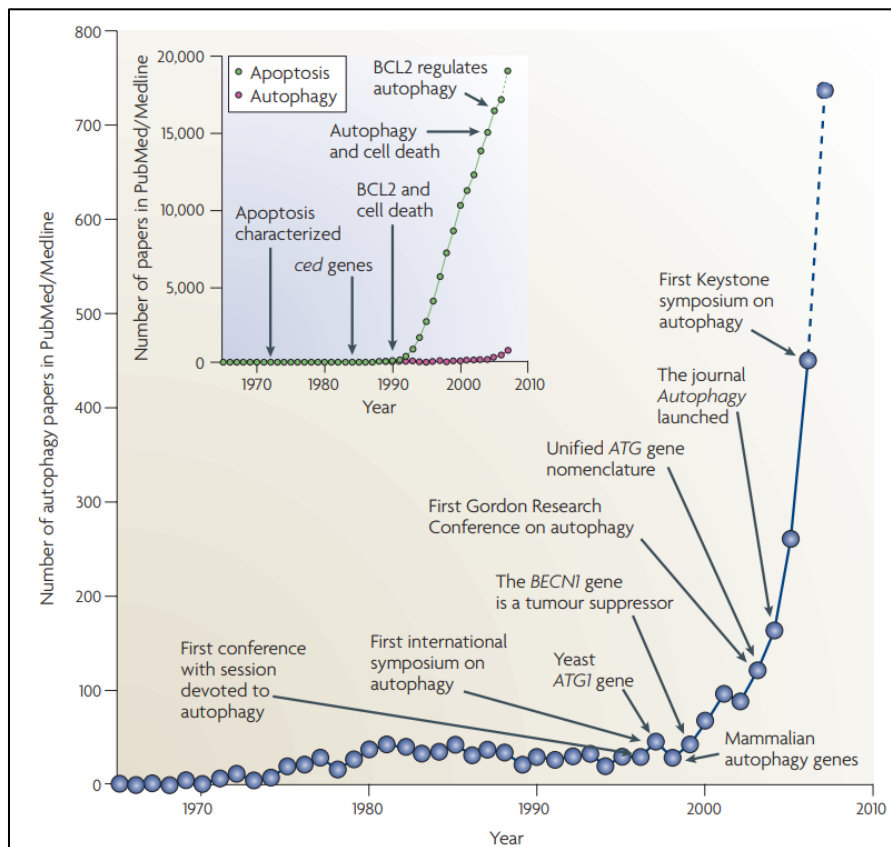


Figure 5: Evolution of autophagy research. Extracted from Klionsky (2007)¹¹².

ii. Different types of autophagy

1. Macroautophagy

Autophagy is a cellular mechanism that involves the breakdown of cytoplasmic components within the lysosome/vacuole, leading to the recycling of the resulting macromolecules¹¹⁹. Three main types of

autophagy are now described: macroautophagy, microautophagy and CMA. The best-characterized form of autophagy, macroautophagy, is a specific type of autophagic process where substrates are sequestered in double-membrane vesicles called autophagosomes. Macroautophagy can be selective or non-selective. Non-selective autophagy degrades bulk cytoplasm during periods of starvation. On the other hand, selective autophagy is designed to remove damaged or unnecessary organelles like mitochondria, peroxisomes, and invasive microbes. Each process has a common machinery but also involves specific components, and they are termed differently - mitophagy for targeted mitochondrial degradation, pexophagy for peroxisomes, and xenophagy for microbes, etc...¹²⁰⁻¹²². Once degraded, the resulting breakdown products are released back into the cytosol to recycle macromolecular components and generate energy, enabling cells to maintain viability under unfavorable conditions and protect themselves during various stressful situations^{123,124}.

In short, macroautophagy begins with the initiation stage (Fig 6), in which the unc51-like kinase (ULK - autophagy activating kinase) complex and ATG (autophagy-related proteins) proteins assemble to form a structure that will be used as a scaffold for autophagosome formation¹²⁵. Autophagy initiation relies on two primary receptors that sense intracellular or extracellular stress and trigger the ULK complex and downstream signaling pathways. The first of these receptors is the mammalian target of rapamycin (mTOR), a significant serine/threonine protein kinase highly responsive to fluctuations in nutrient levels, growth factors, and cellular stressors¹²⁶⁻¹²⁸. When nutrients are abundant, mTOR complex 1 (mTORC1) comes into play, phosphorylating ULK and ATG13. This leads to reduced ULK complex activity and subsequent inhibition of autophagy¹²⁹. However, in conditions of nutrient scarcity, inhibition of mTORC1 occurs rapidly. This results in ATG13 dephosphorylation and the translocation of the ULK complex to the membrane nucleation site, facilitating the initiation of autophagy^{130,131}.

The second receptor involved in regulating autophagy initiation is 5'-AMP-activated protein kinase (AMPK). When glucose is scarce, AMPK becomes activated and suppresses mTORC1 activity, removing the phosphorylation-mediated block on the ULK complex^{132,133}. This activated ULK complex subsequently triggers the activation of class III phosphatidylinositol 3-kinase (PI3KC3). PI3KC3 complex I consists of PI3KC3, VSP15, Beclin 1, and ATG14L, and it plays a crucial role in nucleating and forming the isolation membrane (phagophore)¹³⁴. Furthermore, AMPK can also phosphorylate PI3KC3 and Beclin 1, leading to the activation of PI3KC3 complex I¹³⁵.

The second phase, called elongation (Fig 6), consists in the expansion of the phagophore (i.e., precursor to the autophagosome). The molecular mechanism is now well described. It is believed that ATG2 connects the ER membrane to the phagophore membrane for phospholipids transfer. The ATG9 scramblase complex then redistributes the ER-derived phospholipids to the phagophore membrane for its elongation¹³⁶⁻¹³⁸. Many interactions among the ATG8 family proteins and ATG proteins are

recognized as essential for autophagosome formation¹³⁹. In a review, Nakatogawa summarized the mechanisms behind this pathway¹⁴⁰. The E1 enzyme Atg7 and the E2 enzyme Atg10 collaborate to attach Atg12 to a lysine residue within Atg5. The resulting Atg12–Atg5 conjugate then forms a complex with Atg16. In parallel, Atg8 undergoes initial processing at its C-terminus by Atg4, a related enzyme to ubiquitin-processing enzymes. Subsequently, Atg8 is activated by Atg7 (which is also involved with Atg12) and, with the assistance of the E2 enzyme Atg3, it is conjugated to the amino group of the lipid PE (phosphatidylethanolamine). The Atg12–Atg5–Atg16 complex serves as an E3 enzyme in the conjugation process of Atg8. It enhances the activity of Atg3 and specifies the location for Atg8–PE production on autophagy-related membranes. Atg8–PE plays a crucial role in multiple stages of autophagosome formation, including membrane expansion and closure. Furthermore, Atg4 cleaves Atg8–PE to release Atg8 from membranes for reuse, a process that also regulates autophagosome formation. These two ubiquitin-like systems are closely intertwined and play a pivotal role in driving the formation of autophagosomal membranes¹⁴⁰.

Following elongation, the phagophore membrane eventually closes to create a double-membraned autophagosome. This process is coordinated by the endosomal sorting complex required for transport (ESCRT), which facilitates membrane scission of the two membranes¹⁴¹. The newly-closed autophagosome then matures. The maturation stage (Fig 6) is characterized by the removal of most Atg proteins and the maintenance of a sufficient quantity of Atg8 (called LC3 in metazoans, Microtubule-associated protein 1A/1B-light chain 3) for the formation of new autophagosomes¹⁴². Supported by the microtubular system, mature autophagosomes move along microtubule pathways, guiding them toward the perinuclear region wherein they can merge either with endosomes or lysosomes. Ultimately, the outer membrane of the autophagosomes merges with the lysosomal membrane, giving rise to autolysosomes¹⁴³. The fusion depends on multiple protein complexes, such as RUBICON (RUN domain and cystein-rich domain containing, Beclin-1-interacting protein), UVRAG (UV irradiation resistance-associated gene), RAB proteins (RAB7 et RAB11), ESCRT-III (Endosomal Sorting Complexes Required for Transports), SNARES (Soluble N-ethylmaleimide sensitive factor Attachment protein REceptor) and lysosomal membrane proteins LAMP1 and LAMP2B (Lysosomal-Associated Membrane Proteins)^{142,144}. Those molecules regulating maturation define whether the autophagosomes fuse with endosomes or lysosomes, but also the acidification of autophagic compartments and the recycling of intralysosomal material¹⁴⁵.

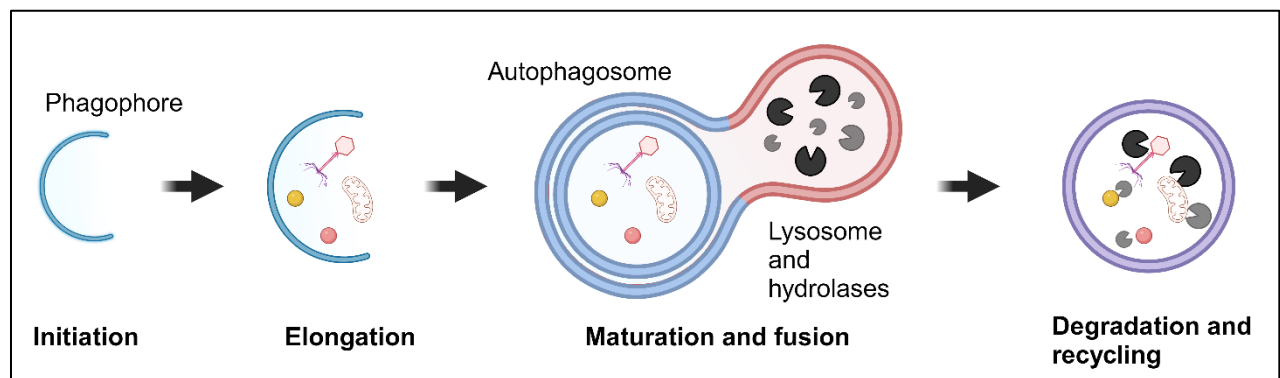


Figure 6: The five steps of macroautophagy.

2. Microautophagy

As most of autophagy-related research has focused on macroautophagy, much less is known about microautophagy. Like in macroautophagy, microautophagy can be selective or non-selective depending on the cellular context¹⁴⁶. In a non-selective manner, lysosomes are able to take up different cargoes (methaemoglobin, ovalbumin, lysozyme, ferritin and/or Percoll particles, to name a few) through membrane invagination, which forms intralysosomal vesicles¹⁴⁷.

Based on molecular machineries, three distinct types of microautophagy have been described, type 1, with lysosomal or vacuolar protrusion; type 2, with lysosomal or vacuolar invagination; and type 3, with endosomal invagination (Fig 7)¹⁴⁸.

Since there has been a clear interest for selective macroautophagy with the discoveries of mitophagy (mitochondria), reticulophagy (endoplasmic reticulum (ER)), lysophagy (lysosome), aggrephagy (protein aggregates), ribophagy (ribosome) and xenophagy (microorganisms)¹⁴⁹, selective forms of microautophagy also have been recently investigated. Numerous types have been discovered, each believed to fulfill distinct functions and to be subjected to distinct molecular regulatory processes¹⁴⁷. Those types of selective microautophagy include micromitophagy, micronucleophagy and endosomal microautophagy (eMI). Each of these is believed to serve unique functions and to be governed by specific molecular mechanisms¹⁴⁷. As eMI and CMA both involve a common biochemical component in their pathways, our primary emphasis will be on eMI.

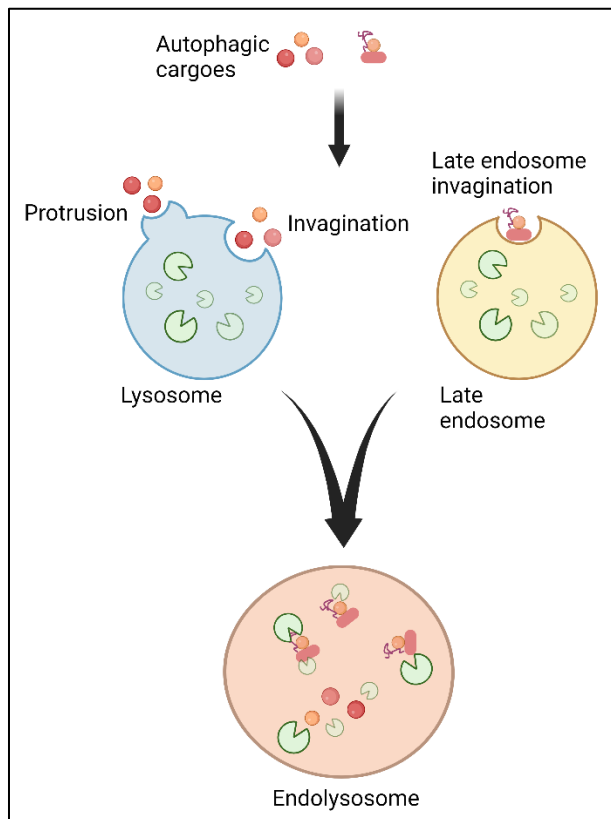


Figure 7: Microautophagy in mammals. Adapted from Wang et al. 2023¹⁴⁷. In microautophagy, autophagic contents are directly engulfed by lysosomes and late endosomes through membrane protrusion and invagination. Autophagic materials is then degraded in the endolysosomal lumen.

3. Endosomal Microautophagy

While searching for a mammalian mechanism homologous to yeast microautophagy, researchers discovered eMI, a microautophagy subtype in which cytosolic proteins are directed to late endosome (LE) for degradation¹⁵⁰ (Fig 8). It was originally thought that eMI constituted a process of bulk degradation¹⁴⁷, but recent studies show that it is operated by the heat shock protein HSPA8 (HSC70) that recognizes the KFERQ-like motif, a pentapeptide sequence sharing biochemical similarity to KFERQ (lysine-phenylalanine-glutamate-arginine-glutamine)¹⁵⁰.

Upon a stimulus, HSC70 recognizes and binds a substrate presenting a KFERQ-like motif. HSC70 then interacts with HSP40 (also known as DNAJB1), stress-induced phosphoprotein 1 (STIP1; also known as HOP) and negatively charged phosphatidylserine via its carboxy-terminal lid domain, all present on late endosome/ multivesicular bodies (LE/MVB) membrane. HSC70 then interacts with Bag6 to trigger the internalization of the substrate into endosomes through invaginations of the LE/MVB limiting membrane (Fig 8)¹⁵¹⁻¹⁵³. The ESCRT machinery, an ancient system for membrane remodeling and

scission, organizes these membrane invaginations^{150,154}. Beyond its involvement in protein internalization via eMI and other microautophagy-related pathways, the LE/MVB compartment also has the ability to take up extracellular cargo through heterophagy pathways such as pinocytosis, phagocytosis, and endocytosis¹⁵¹. Additionally, it plays a crucial role in degrading ubiquitinated plasma membrane receptors via the ESCRT pathway¹⁵⁵. This further highlights the compartment's significance in the process of protein degradation.

As its discovery is still considered recent, its physiological relevance is still unclear. The activation of eMI depends on stimuli, such as iron starvation in mammalian cells¹⁵⁶, or sucrose starvation, DNA damage and oxidative stress in *Drosophila melanogaster*¹⁵⁷.

CMA and eMI both target the KFERQ-like motif, through the activity of the same chaperone protein HSC70. Nevertheless, eMI does not require substrate unfolding prior to degradation¹⁵⁰. While eMI has been observed in mice and fruit flies^{158,159}, and an eMI-like pathway has been identified in yeast¹⁶⁰, CMA documentation has been limited to mammals, birds, and fish. This contrast raises questions about the evolutionary origins of each pathway.

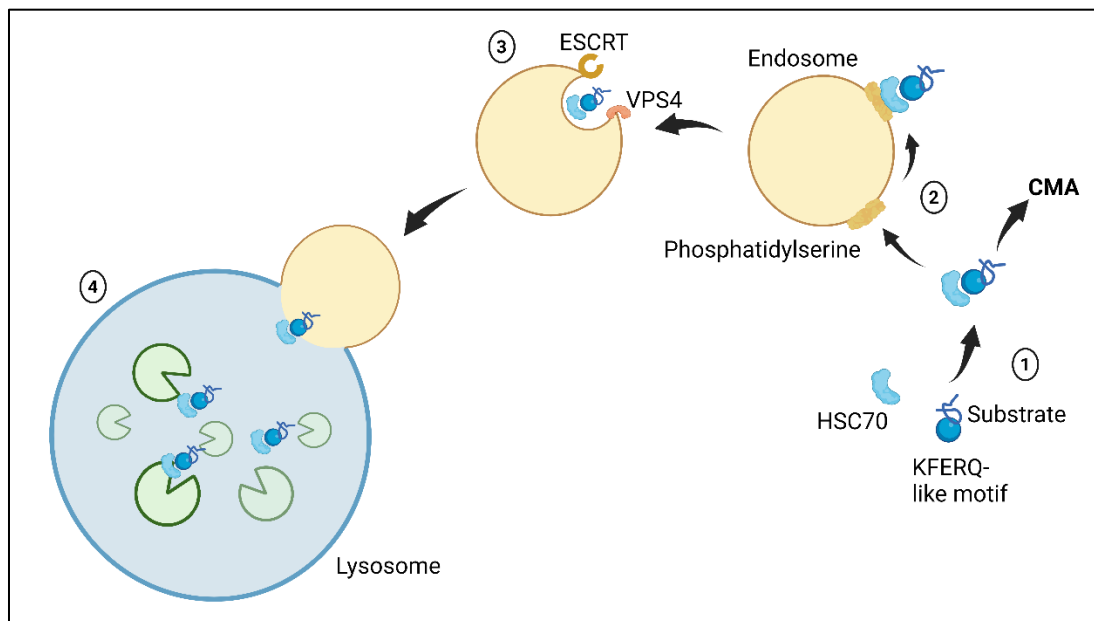


Figure 8: Endosomal microautophagy (eMI) in mammals. Adapted from Wang et al. 2023¹⁴⁷. There are three main steps eMI: binding, invagination and degradation. Binding is the recognition of a substrate nearing a KFERQ-like motif by HSC70. During invagination, the HSC70/substrate complex binds phosphatidylserine at the endosome membrane. ESCRTs and vacuolar protein sorting-associated protein 4 (VPS4) then regulate the complex's invagination into the endosome. Substrates undergo degradation within the late endosome itself or upon their fusion with a lysosome. Alternatively, eMI could mediate extracellular protein releases due to the ability of LE to fuse with the plasma membrane.

4. Chaperone-mediated Autophagy (CMA)

CMA constitutes the core of this thesis. It is therefore described thoroughly in the following chapters, in which we will successively present the history of its discovery, the underlying mechanisms as well as the main actors, its physiological role and the methods and skills developed for its investigation.

b. CMA: history and mechanism

In 1983, Jonathan Backer (Dice's laboratory) discovered that the rate of degradation of proteins could differ depending on the nature of amino acids in proteins. He microinjected two types of proteins in human fibroblasts: RNase A, and the S-protein¹⁶¹. Both proteins were similar except for a 20 amino acids sequence missing in the latter. He noticed that the two proteins behaved differently after the microinjection. RNase A underwent rapid degradation upon serum removal from the culture media, while S-protein remained notably stable under these conditions. Dice and collaborators then realized they were seeking a new lysosomal pathway¹⁶¹. After drawing more attention on the nature of the peptide, his research team unveiled significant findings (Fig 9).

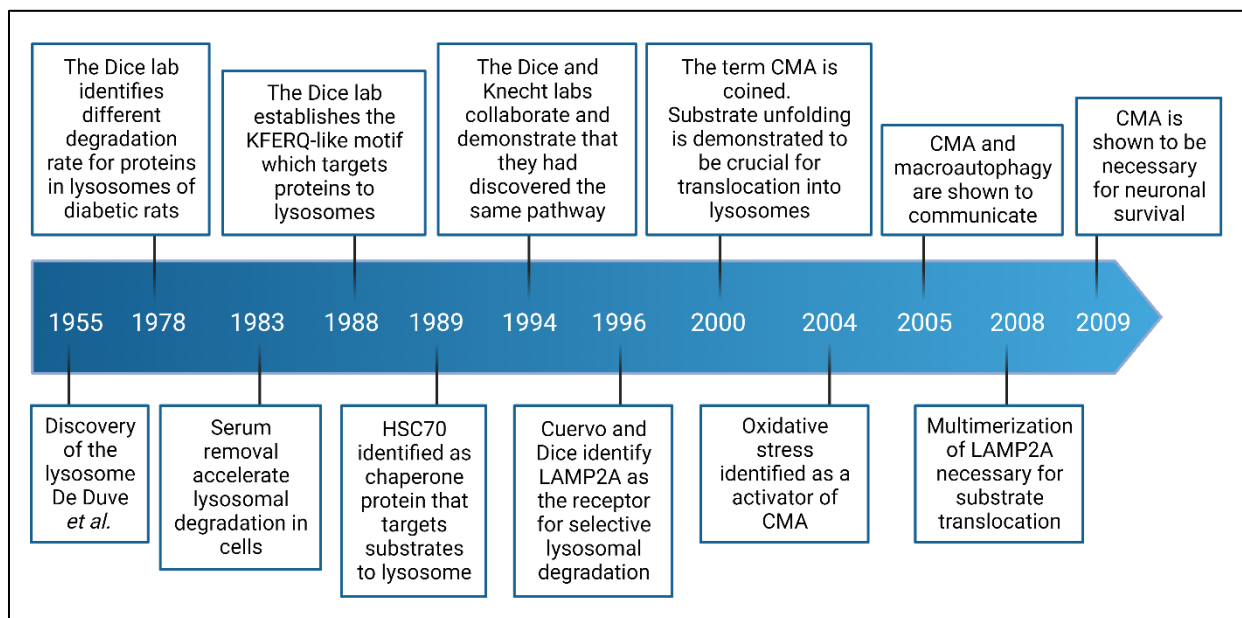


Figure 9: From the discovery of the lysosome to CMA. Adapted from Cuervo (2011)¹¹⁸.

They identified a pentapeptide motif (KFERQ motif) near the N terminus of RNase A, within the peptide, essential for its subsequent targeting and degradation in lysosomes¹⁶² (Fig 10). Furthermore, they described that this motif is used by the chaperone heat shock cognate 71-kDa protein (HSC70) to

bind the substrate protein and direct it to the lysosomal membrane¹⁶³. It was later described that this substrate/HSC70 complex was directed toward lysosomal membrane, to bind to the lysosome-associated membrane protein type 2A (LAMP2A), one of the three variants generated by alternative splicing of *LAMP2* gene¹⁶⁴ (Fig 10). While the substrate unfolds, multiple LAMP2A proteins then assemble and multimerize into a translocation complex^{165,166} with the help of a lysosomal HSC70. This HSC70, present at the surface of the lysosome, is responsible for substrate unfolding and disassembly of the translocation complex after substrate internalization¹⁶⁵. An HSP90 protein is also present on both sides of the lysosomal membrane: the cytosolic HSP90 attaches to substrate proteins while they unfold thus prevent unwanted interactions¹⁶⁷, the luminal HSP90 binds to LAMP2A to stabilize it while it multimerizes¹⁶⁵. LAMP2A then enables the import and degradation of KFERQ-like motif bearing proteins within lysosomes¹⁶⁴. Finally, Dice's lab demonstrated that the degradation of a protein bearing a KFERQ-like motif in isolated lysosomes was enhanced after adding HSC70, in an ATP-dependent manner^{163,168,169}. After years of discoveries regarding this selective pathway, the name "chaperone-mediated autophagy" (CMA) was finally established in 2000¹⁷⁰. Thereafter, more elements of CMA pathways and regulators were described, including factors that enhance CMA, such as stressful conditions like starvation or oxidative stress¹⁷¹.

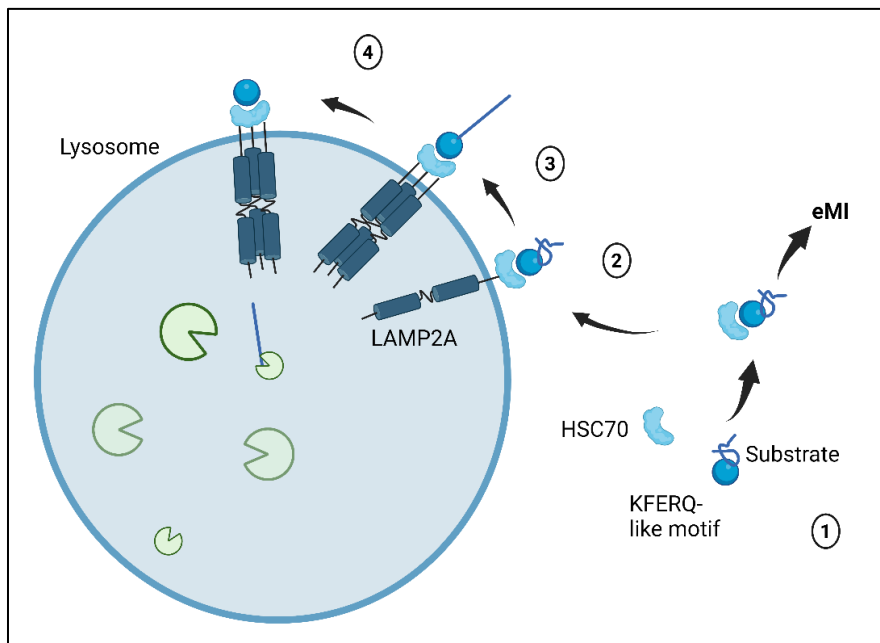


Figure 10: Main actors and mechanism of chaperone-mediated autophagy (CMA). Hsc70 recognizes and binds to sequences with the KFERQ motif. The HSC70/substrate complex specifically binds to the cytosolic tail of the lysosome-associated membrane protein type 2A (LAMP2A). Substrate binding triggers LAMP2A multimerization into a protein complex that mediates translocation of the substrate into lysosomes.

c. Main actors of CMA

i. KFERQ

The KFERQ motif establishes the nature of cargo selectivity in CMA (and eMI). The specific recognition mechanism between the substrate proteins and HSC70 is what defines selectivity of CMA (and eMI). This motif is necessary and sufficient for protein degradation by CMA. When the pentapeptide is altered via mutation, it prevents the lysosomal degradation of RNase A¹⁶². Conversely, when the initial 11 amino acids of RNase A are introduced into non-CMA substrate proteins, it directs them towards lysosomal degradation¹⁷². However, it has been demonstrated that the chemical properties of the motif will define the affinity of the binding, regardless of the exact nature of the amino acid¹⁶⁹. In short, a glutamine (Q) has to be present on one side of the motif (since the pentapeptide operates as a targeting sequence in both directions) (Fig 11). It consists of one or two positive lysine (K) or arginine (R) residues, along with one or two hydrophobic residues phenylalanine (F), leucine (L), isoleucine (I), or valine (V), and one negatively charged E or D residue. Furthermore, post-translational modifications (PTMs) can generate a motif with biochemical characteristics similar to that of a canonical KFERQ protein, thereby increasing the pool of potential CMA substrates¹⁷³⁻¹⁷⁵ (Fig 11). The PTMs are phosphorylation or acetylation of the amino acid residues along protein regions that do not originally show the mentioned properties. Besides, these PTMs outside the KFERQ motif can modulate CMA by altering or masking the motif¹⁷⁶. It is also interesting to mention that the reason why a protein is directed toward eMI or CMA is still unknown as of today. Nevertheless, it is believed that protein's inherent characteristics, such as mutations, PTMs, its state of oligomerization, could influence the substrate's switch between these autophagic routes. For instance, the endogenous Tau protein can be simultaneously degraded by both pathways, but when it undergoes pathogenic mutations, the proportion of the protein degraded by each pathway may shift¹⁷⁷.

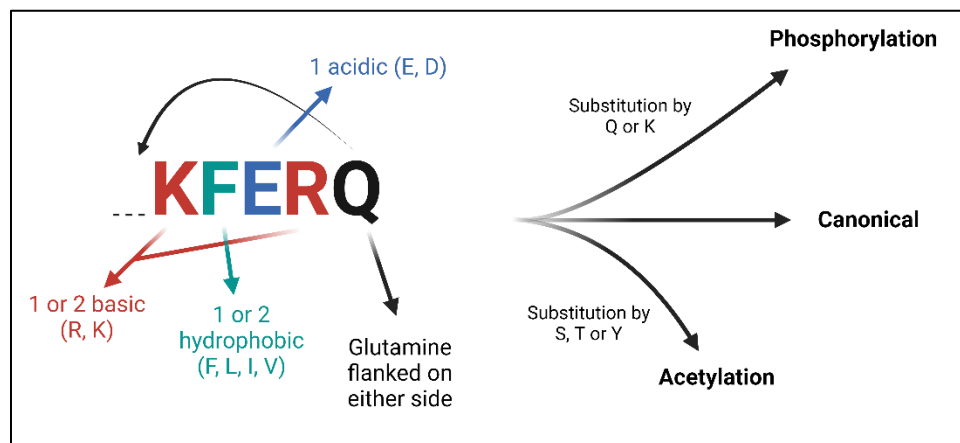


Figure 11: KFERQ-like motif in CMA and PTMs.

In order for a motif to become a degradation target, it must be amenable to interaction with HSC70. Around 40% of proteins in the mammalian proteome feature a canonical KFERQ-like motif¹⁷⁶. Certain proteins typically lack an exposed motif in regular circumstances, yet conditions that promote protein disassembly, such as oxidative stress, render this motif accessible for binding with HSC70¹⁷⁸. As the proteome contains both constitutive and PTM-generated KFERQ-like motifs, it is plausible to assume that proteins with buried motifs may exhibit a higher prevalence of canonical motifs, in contrast to proteins where the motif resides in a readily accessible region. The latter could use generation of motifs through PTMs as a strategy to prevent continuous degradation by CMA. Therefore, it was anticipated that proteins containing specific motifs would be more suitable for certain cellular processes than others¹⁷¹. In 2019, Kirchner et al. conducted an enrichment analysis on the biological processes enriched in each type of motif, which unveiled an association between the specific types and combinations of KFERQ-like motifs in proteins and their participation in particular biological processes. For example, they discovered that proteins with canonical motifs were linked to protein phosphorylation, those with phosphorylation-generated motifs were associated with nucleic acid metabolism and transcription, while proteins featuring acetylation-generated motifs were connected to RNA transport and localization¹⁷¹. This led to believe that CMA has a diversity of roles in biological functions through the multiple combination protein targeting motifs.

ii. HSC70 and cofactors

Although HSC70 is the only cytosolic chaperone that specifically recognizes the KFERQ-like motif, its binding is modulated by cochaperones: carboxyl terminus of HSC70-interacting protein (CHIP), heat shock protein 40 (HSP40; also known as DNABJ1) and HSP70–HSP90 organizing protein HOP^{179,180}. As seen in Fig 8 and 10, HSC70 occupies a central position at the intersection between eMI and CMA.

While the LAMP2A receptor is present in all lysosome types, not all lysosomes have the ability to perform CMA. CMA ability of a lysosome depends on the presence of HSC70 within it¹⁸¹. The chemical properties of this HSC70 differ from its cytosolic counterpart, as it has to thrive in an acidic environment with high concentrations of proteases¹⁸². Lysosomes without luminal HSC70 cannot perform CMA, showing its necessity for substrate translocation¹⁷⁶. The manner in which HSC70 gains access to the lysosomal lumen is, however, still unknown.

iii. LAMP2A

When the team of Fred Dice discovered that trypsinization of the lysosomal surface compromised the binding and internalization of KFERQ-like motif containing substrate proteins (RNase A, GAPDH), they presumed that a receptor protein could be responsible for their translocation into the lumen¹⁸³. LAMP2A originates from the alternative splicing of the *LAMP2* gene¹⁸⁴. All three splice variants, LAMP2A, LAMP2B, LAMP2C share identical luminal regions but present different transmembrane and cytosolic regions. LAMP2A is the only one involved in CMA^{164,185}. As of now, LAMP2A blockage is still the most specific and efficient way to inhibit CMA¹⁷⁶.

The HSC70/substrate complex docks at LAMP2A through a specific binding to its 12-amino-acid cytosolic tail. The substrate recognition and lysosomal docking can occur simultaneously, as they are coupled processes^{164,186}. Subsequently, LAMP2A assembles into a 700 kDa multimeric protein complex as critical step for substrate translocation¹⁶⁵. Firstly, LAMP2A forms a homotrimer (three identical units) to increase substrate affinity while it unfolds. The cytosolic HSC70 binds LAMP2A monomers and homotrimers, although it is released before the operational translocation complex comes together^{187,188}. During LAMP2A multimerization, the luminal HSP90 located at the lysosomal membrane, stabilizes LAMP2A and potentially protects the protease-sensitive regions¹⁸⁸.

d. Regulation of CMA

CMA is a gatekeeper of proteostasis and contributes to cellular quality control¹⁸⁹. Stressors that hinder proteostasis are more distressing upon CMA blockage, which eventually causes the accumulation of oxidized and aggregated proteins¹⁹⁰. Main stimuli that trigger CMA include starvation^{191,192}, oxidative stress¹⁷⁸, chemicals¹⁹³ and hypoxia¹⁹⁴.

i. LAMP2A-independent mechanisms

a. PTMs

Numerous proteins likely have KFERQ motifs that are buried inside their structure, making them unable to initiate CMA. Nevertheless, misfolding, partial unfolding, or even conformational changes caused by PTMs (phosphorylation, ubiquitination or acetylation) might reveal the CMA-targeting motif, potentially leading to CMA activation¹⁷⁸. For example, the ubiquitination of hypoxia-inducible factor 1 α (HIF1 α) exposes the CMA-targeted motif leading to its degradation¹⁹⁵.

PTMs can directly affect the KFERQ motif or its vicinity and influence substrate targeting through CMA. If a motif contains only four of the canonical residues, missing the negatively charged one, but has serine (S), tryptophan (T) or tyrosine (Y), they can be phosphorylated and the protein turned into a CMA substrate¹⁷⁶. If a motif has a K, it can be acetylated and obtain properties similar to Q, which allow targeting for CMA degradation¹⁹⁶.

b. Lysosomal pH

The proper function of CMA relies on the presence and action of lys-HSC70, with lysosomal pH playing a pivotal role in regulating its stability. Even minor increases in pH can lead to increased degradation of substrates¹⁹⁷. Lysosomal pH is also critical for the effective functioning of lysosomal proteases¹⁹⁸. It is maintained by proton-pumping v-ATPase, chloride channels, and ion transporters located in the lysosomal membrane¹⁹⁹.

ii. LAMP2A-dependent mechanisms

LAMP2A levels and dynamics govern the rate of CMA¹⁷⁶.

a. Transcriptional regulation of LAMP2A

In the presence of mild oxidative stress, CMA activation is achieved by directly increasing LAMP2A transcriptional regulation. This is mediated by factors like NRF2/NFE2L2²⁰⁰, nuclear factor of activated T-cells 1 (NFAT1)²⁰¹, and all-trans retinoic acid (ATRA)²⁰² allowing for the handling of oxidized CMA cargo¹⁷⁸.

1. NFE2L2/NRF2

One of the ways that *LAMP2A* gene transcription is triggered during oxidative stress involves a transcription factor called NFE2L2/NRF2. In 2018, Cuadrado and collaborators discovered that NRF2/NFE2L2 binds to two specific regulatory sites in the promoter region of *LAMP2*²⁰⁰. They also found that when NFE2L2 is partially inactivated (in fibroblasts) or completely removed (in mouse livers), the expression of *LAMP2A* significantly decreases. Importantly, this does not affect other forms of the *LAMP2* gene (variants 2B and 2C). Additionally, activating NFE2L2 with certain drugs increases

both *LAMP2A* expression and CMA activity. All these findings confirm that NFE2L2/NRF2 plays a vital role in regulating *LAMP2A* expression²⁰⁰.

2. NFAT and calcium signaling

The calcineurin-NFAT pathway was the initial signaling pathway discovered that regulates *LAMP2A* transcription, thus CMA. It is essential for CMA activation in T cells. Many potential NFAT1 binding sites were discovered in the promoter region proximal to the *LAMP2* gene. When exposed to ROS, the transcription factor NFAT binds to the *LAMP2A* promoter region and increases the transcriptional expression of *LAMP2A*^{201,203}.

3. Nuclear retinoic acid receptor- α (RAR α)

The nuclear retinoic acid receptor- α (RAR α), but not other members of this nuclear receptor family (RAR β , RAR γ or RXR), negatively regulates *LAMP2A* transcription²⁰³. The fact that their substrate, all-trans-retinoic acid (ATRA) has been well described allowed the design of pharmacological modulators to enhance CMA²⁰². Despite being originally designed as therapeutic targets, CMA modulators could also be used to alter CMA in adjusted environmental conditions (e.g., mesocosm systems). This could help understand the role of CMA under environmental stressors.

c. *LAMP2A* lysosomal biogenesis and transport

Lysosomal membrane proteins, such as *LAMP2A*, are synthesized within the endoplasmic reticulum (ER) and subsequently traverse the Golgi apparatus and the trans-Golgi network (TGN). Once within the TGN, these newly formed proteins undergo one of two paths: (i) direct transportation to endosomes or lysosomes, or (ii) routing to the cell's plasma membrane before being processed by endocytic mechanisms²⁰⁴. This transport is performed by clathrin-coated vesicles and facilitated by "clathrin-adaptor proteins"²⁰⁴ that recognize specific address patterns in the cytosolic domains of these proteins. Lysosomal membrane proteins, such as *LAMP2* (regardless of isoform), contain a GYXX ϕ motif recognized by clathrin adaptor AP-1 at the TGN and AP-2 at the plasma membrane²⁰⁵.

b. *LAMP2A* stability at lysosomal membrane

Under normal physiological conditions, the presence of *LAMP2A* on the lysosomal membrane is regulated through a process involving its cleavage and breakdown by lysosomal proteases¹⁸⁶. This degradation occurs in several steps. Initially, *LAMP2A* moves laterally to a specific lipid microdomain within the lysosomal membrane, which is rich in cholesterol or glycosphingolipids (Fig 12). This lateral

movement effectively hinders its ability to bind to substrate complexes/HSC70²⁰⁶. Following this, LAMP2A is cleaved through the actions of cathepsin A and a yet-to-be-characterized metalloproteinase^{207,208}.

When CMA is activated, LAMP2A is relocated from the lipid-rich microdomain to serve as a membrane receptor for substrate complexes/HSC70²⁰⁶. Once the internalization of substrates is complete, the LAMP2A multimeric complex undergoes a transformation back to its original monomeric state. This transformation is orchestrated by two proteins working in tandem: "Glial Fibrillary Acidic Protein (GFAP)" and "Elongation Factor 1 alpha (EF1 α)". GFAP exists in two forms on the lysosomal membrane - an unphosphorylated form (GFAP) that binds to and stabilizes LAMP2A within the multimeric complex, and a phosphorylated form (pGFAP) that remains associated with the lysosomal membrane but outside of the complex. (Fig 12). When GTP is present, EF1 α separates from pGFAP. This separation enables pGFAP to enlist the unphosphorylated form of GFAP, which is linked to the multimeric complex. Consequently, this recruitment initiates the breakdown of monomeric LAMP2A¹⁶⁶.

Interestingly, the lipid composition of the lysosomal membrane can affect the lipid microdomain thus LAMP2A stability. Upon a lipid challenge, mice have shown an accelerated degradation of LAMP2A due to a modified lipid membrane composition¹⁷⁶.

The modulation of AKT or mTOR can regulate the targeting and uptake of CMA substrates without affecting LAMP2A transcription²⁰⁷. Inhibiting AKT1 or mTOR *in vitro* increases the number of reporter puncta, therefore CMA activity²⁰⁷. Kinase AKT1, which is under the control of mTORC2 (mammalian Target Of Rapamycin Complex 2) control, phosphorylates GFAP and therefore regulates the stability of LAMP2A at lysosomal membrane. When CMA is activated, PHLPP1 prevents the inhibitory action of AKT1 on GFAP. GFAP can stabilize the multimeric state of LAMP2A on lysosomal membrane. When CMA is not necessary, GFAP disengages the multimeric complex and binds phosphorylated GFAP.

Recent findings from Endicott et al.²⁰⁹ showed that CMA is under fine regulation of the INS-PI3K-PDPK1 pathway (insulin-phosphatidylinositol 3-kinase-3-phosphoinositide-dependent protein kinase 1), as it modulates AKT. Inhibiting class I PI3K pathway *in vivo* can modulate lysosomal GFAP and activate CMA. In addition to proposing a novel pathway to investigate, the development of a pharmacological tool to modulate the INS-PI3K-PDPK1 pathway is promising to investigate situations wherein CMA could be altered²⁰⁹.

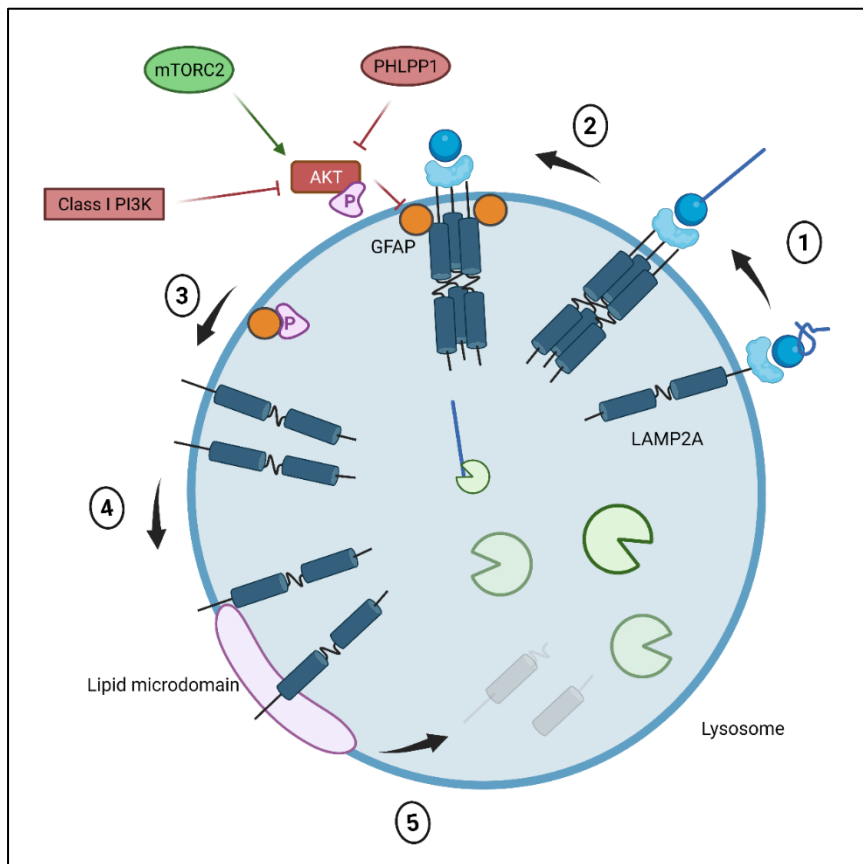


Figure 12: CMA depends on the stability of LAMP2A mimeric state at lysosomal membrane. Upon CMA activation, PHLPP1 prevents the inhibitory action of AKT on GFAP. GFAP can stabilize the mimeric state of LAMP2A on lysosomal membrane. In physiological conditions in which CMA is not necessary, GFAP disengages the mimeric complex and binds phosphorylated GFAP. mTORC2 phosphorylates AKT1, which phosphorylates GFAP, preventing stabilization of the mimeric complex. LAMP2A is then transferred to a lipid microdomain and degraded inside the lumen.

e. The many physiological roles of CMA

Confirmed canonical and putative CMA substrates are very diverse and numerous, which indicates the broad range of physiological processes CMA is involved in¹⁷⁶. CMA was originally thought to be mainly involved in protein quality control, by degrading abnormally synthesized proteins or post-translationally damaged KFERQ-containing proteins¹⁷⁸. After discovering that upon starvation, proteins could be targeted by CMA despite not being damaged revealed the many physiological pathways that could be impacted by CMA¹⁷⁶ (Fig 13).

i. Protein quality control

The identification of CMA substrates within aggregated proteins that accumulate upon stressors such as mild oxidative stress¹⁷⁸, hypoxia²¹⁰ or when CMA is not functional demonstrate the role of CMA in the maintenance of proteostasis. Although CMA is unable to deliver aggregated proteins to lysosomes, it plays a part in preventing aggregation, as it targets partially damaged or unfolded substrates^{211,212}.

ii. Starvation

The lack of nutrients induces CMA in numerous organs and cell types¹⁷⁶. In mammals, CMA is triggered after an 8 h starvation, after macroautophagy activity is already high²¹³. This activation contributes to replenishing the pool of intracellular amino acid¹⁸³, enhancing gluconeogenesis¹⁹², and maintaining adequate ATP supply²¹⁴. Overall, upon starvation, CMA can selectively remodel part of the proteome related to cellular energetics to fulfill physiological needs¹⁷⁶.

iii. Metabolic pathways

CMA targets specific enzymes involved in lipid and glucose metabolism (Fig 13) therefore participates in their regulation¹⁷⁶. For example, upon starvation CMA can halt hepatic glycolysis. If CMA does not function properly, it results in high rates of hepatic glycolysis and subsequent energy deficiency in peripheral organs¹⁹². For example, mice knocked out for *LAMP2A* displayed elevated activity levels of glycolytic enzymes such as glyceraldehyde 3-phosphate dehydrogenase (GAPDH) and pyruvate kinase (PK)¹⁹². Aside from glucose catabolism, CMA is also involved in lipid metabolism. CMA substrates include lipogenesis enzymes, lipid carriers and lipid droplet coat proteins^{192,215}. For example, selectively targeting the proteins PLIN2 and PLIN3 on the surface of lipid droplets through CMA removal facilitates easier access for lipolytic enzymes, promoting lipolysis and lipophagy²¹⁵. Furthermore, lipid nutritional levels can regulate CMA activity. High lipid intake will cause CMA activation to increase lipolysis and decrease lipogenesis, as a way of finely tune intracellular lipid levels¹⁹².

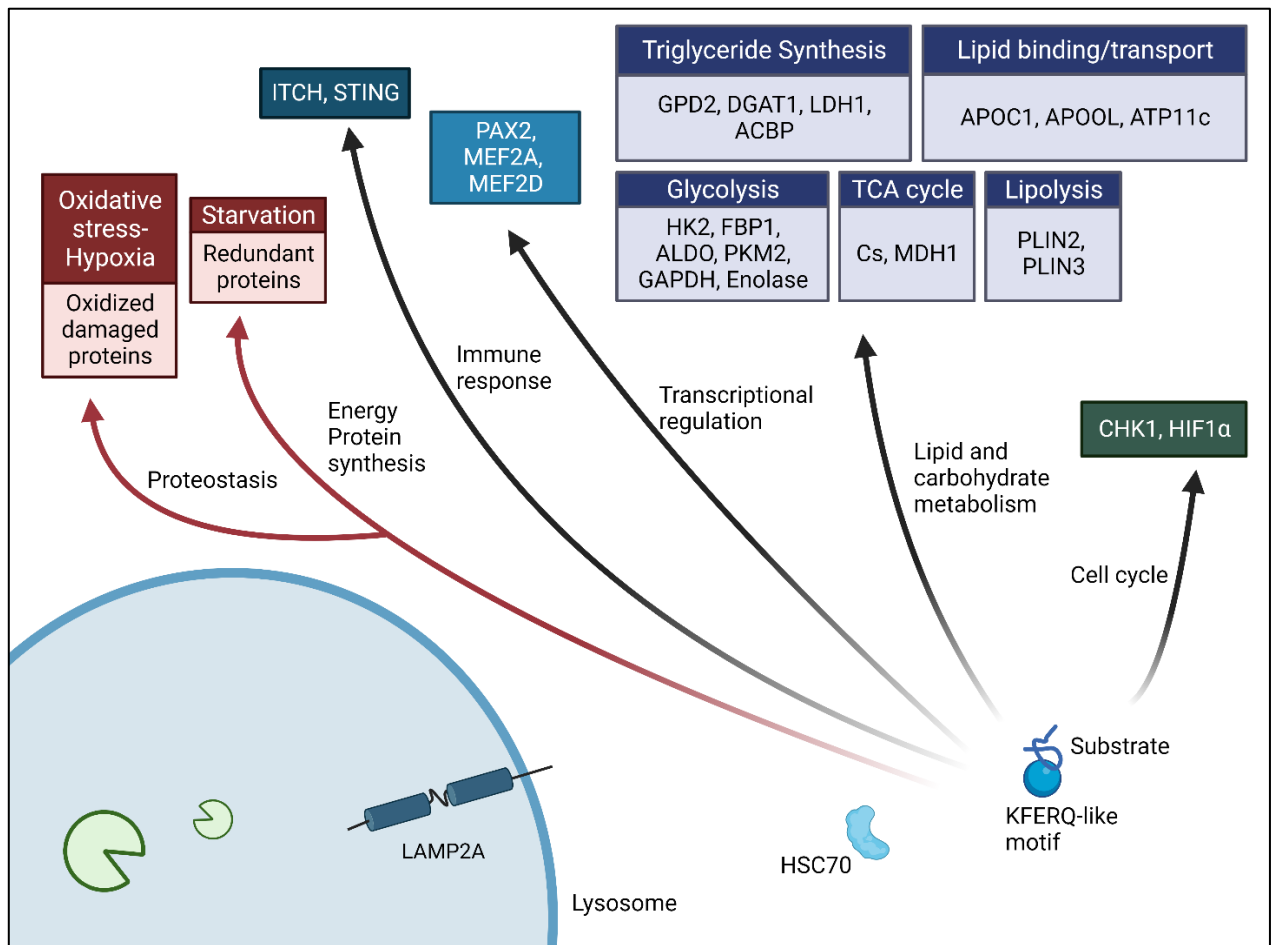


Figure 13: Main physiological roles of CMA and its substrates. Adapted from Kaushik & Cuervo 2018.¹⁷⁶

iv. Transcriptional regulation

After identifying the NF- κ -B inhibitor- α ($\text{I}\kappa\text{B}\alpha$) as a CMA substrate, a role in transcriptional regulation was evidenced for CMA (Fig 13)²¹⁶. $\text{I}\kappa\text{B}\alpha$ inhibits the NF- κ B transcription factor, which controls multiple transcriptional pathways²¹⁷. Other CMA substrates involved in transcriptional regulation were identified such as paired-box protein PAX2, implicated in cell proliferation and differentiation²¹⁸, or the myocyte-specific enhancer factors 2A (MEF2A) and 2D (MEF2D), which contribute to neuronal survival^{219,220}.

v. Immune response

CMA substrates also include negative regulators of T cell receptor (TCR) signaling, ubiquitin ligase ITCH and the calcineurin inhibitor RCAN1, which implies that CMA holds an important role in CD4⁺ T cell activation (Fig 13)²⁰¹. When blocking CMA after LAMP2A inactivation in T cells, responses to

infection with *Listeria monocytogenes* were impaired²⁰¹. Furthermore, CMA was shown to be involved in the regulation of innate immunity as it can target the stimulator of interferon genes protein (STING). At late phase of viral infection, desumoylation of STING will unveil its KFERQ-like motif to turn off innate immune response²²¹.

More recently, Cuervo's lab presented in a Women In Autophagy (WIA) conference in 2022 a novel work on the regulation of Regulatory T cells (Tregs) function by the selective remodeling of their proteome. The study focused on analyzing the role of CMA in Tregs function and first revealed that *LAMP2A* expression and CMA activity increased in activated Tregs. They also generated a CMA deficient Treg mouse line, which showed less survival, meaning that CMA in Tregs is crucial to maintain Treg function of self-tolerance under homeostatic conditions (unpublished data).

vi. Cell cycle

The findings of Park et al. 2015¹⁷⁴ demonstrated an upregulation of CMA in response to genotoxic stress, and impaired CMA function results in decreased cell viability and genomic instability. They found that selective degradation of activated checkpoint kinase 1 (Chk1) following genotoxic insults ensures genome integrity. When CMA is not functional, nuclear Chk1 accumulates leading to the disruption of cell cycle progression and persistence of DNA damage¹⁷⁴.

vii. Circadian clock

In 2022, the team of Ana Maria Cuervo evidenced that CMA regulates physiological circadian cycling²²². Circadian rhythmicity is sustained by the periodic fluctuations in the levels of clock proteins. They showed that CMA regulates the central and peripheral degradation of the core clock proteins, a process they refer to as 'selective chronophagy'²²². They investigated changes in CMA activity during the light/dark cycle and found that during the day, liver CMA activity reached maximal activity whereas it was the opposite for kidney and heart²²². While demonstrating that clock proteins are CMA substrates, meaning that CMA modulates circadian rhythm, they also show that the regulation is interdependent. Some circadian clock proteins (e.g., ARNTL/BMAL1) can inhibit *LAMP2A* expression by activating the negative regulator RAR α ²²². Hence, the circadian clock also has the capacity to temporally regulate tissue-specific CMA activity, thereby modulating a distinct subproteome at different circadian phases²²².

viii. Neuronal proteostasis

Loss of protein homeostasis (proteostasis) has been shown to occur with age and in neurodegenerative disorders such as Alzheimer disease (AD)²²³. In 2021, Bourdenx et al.

demonstrated that in neurons, CMA targeted part of the proteome at risk of aggregation²²⁴. In neurodegenerative pathologies, these proteins tend to aggregate if they are not properly degraded, which increases toxicity and loss of their function¹⁷⁶. By designing a CMA activator optimized for *in vivo* studies, they were also able to improve the behavior and pathology AD mouse models. These findings underscore the crucial role of proper CMA function in maintaining neuronal proteostasis¹⁷⁶.

f. Measuring CMA activity

As CMA plays such a major part in the protein quality control and cellular response to stress, many experimental approaches have been designed to measure CMA activity, some of which are described below.

i. Lysosome isolation and GAPDH uptake assay

The first studies on CMA relied mainly on *in vitro* measurements of the different steps of the process on isolated lysosomes^{225,226}. For that, a few criteria have to be satisfied: only CMA-active lysosomes have to be isolated when studying CMA²²⁵, as they contain the lysosomal HSC70 in the lumen¹⁹⁷. The second criteria refers to the integrity of the isolated lysosomes, to ensure intralysosomal degradation of substrates.

To isolate lysosomes, a piece of liver is grinded and subjected to ultra-high speed centrifugation in a discontinuous metrizamide gradient^{225,227}. Based on density, a gradient of four fractions is created with, from bottom to top: mitochondria, a mix of mitochondria and lysosomes, CMA-active and non-active lysosomes, CMA-active lysosomes (Fig 14).

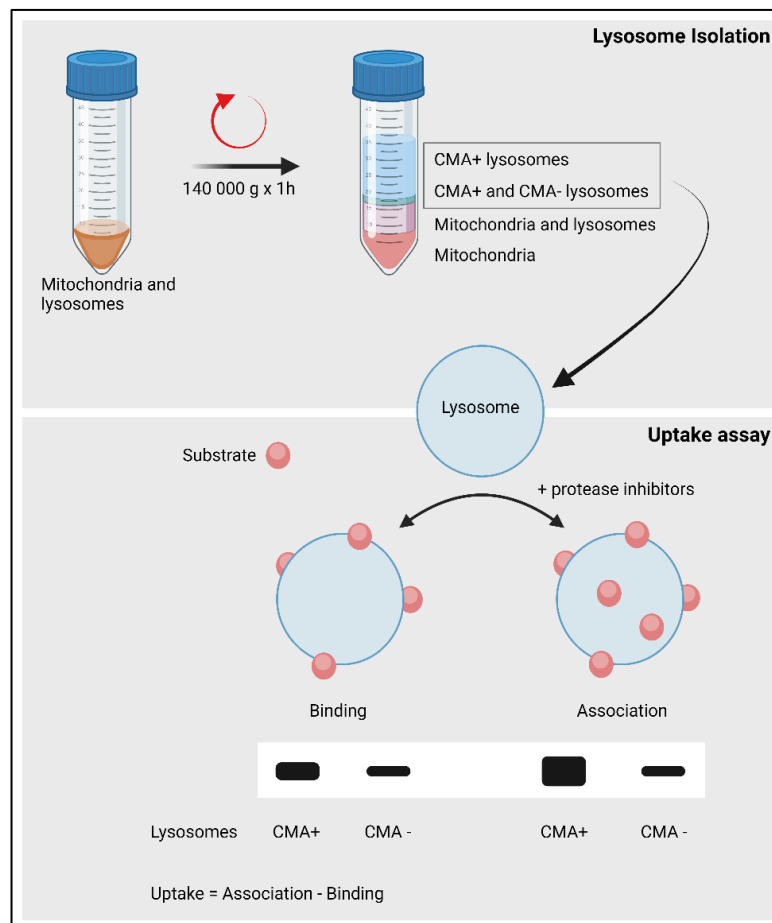


Figure 14: Main physiological roles of CMA and its substrates. Adapted from Juste & Cuervo et al. 2019²²⁶. Measurement of CMA *in vitro*. CMA-active lysosomes isolated by centrifugation in a discontinuous gradient of metrizamide. Bottom: lysosomes pre-treated or not with inhibitors of lysosomal proteases incubated with CMA substrates to quantify substrate binding and uptake inside the lysosomal lumen.

The isolation of CMA-active lysosomes allows an *in vitro* quantification of substrate binding, lysosomal uptake and lysosomal degradation²²⁵. Lysosomes can be incubated with a CMA substrate (e.g., GAPDH) so that they can bind, translocate and degrade these substrates. In addition, adding ammonium chloride/leupeptin will block lysosomal proteolysis to be able to quantify binding and uptake (known as association). The difference between association and binding is then calculated to obtain the uptake (Fig 14)¹⁹⁷.

Although these experiments provided major advances in our understanding of the detailed processes involved in CMA as well as their regulation at the whole tissue level²²⁵, they fail to provide insights at the cellular level and/or to discriminate cell type differences in CMA. A significant step forward in the

field was then reached with the development and validation of a fluorescent CMA reporter system described thereafter, which allow monitoring of CMA activity in living cells¹⁷².

ii. Photoconvertible CMA reporter

Monitoring the uptake and degradation of CMA substrate is possible via the use of artificial fluorescent CMA reporters. Koga, Martinez-Vicente and collaborators¹⁷² designed a photoactivable fluorescent reporter attached to a KFERQ motif (KFERQ-PA-mCherry1), which is initially non-fluorescent but fluoresces in red on irradiation using 405 nm light. Photoactivation is triggered at a certain time point, and then the association to the lysosome can be followed as they appear as red fluorescent puncta upon CMA activation²²⁸ (Fig 15).

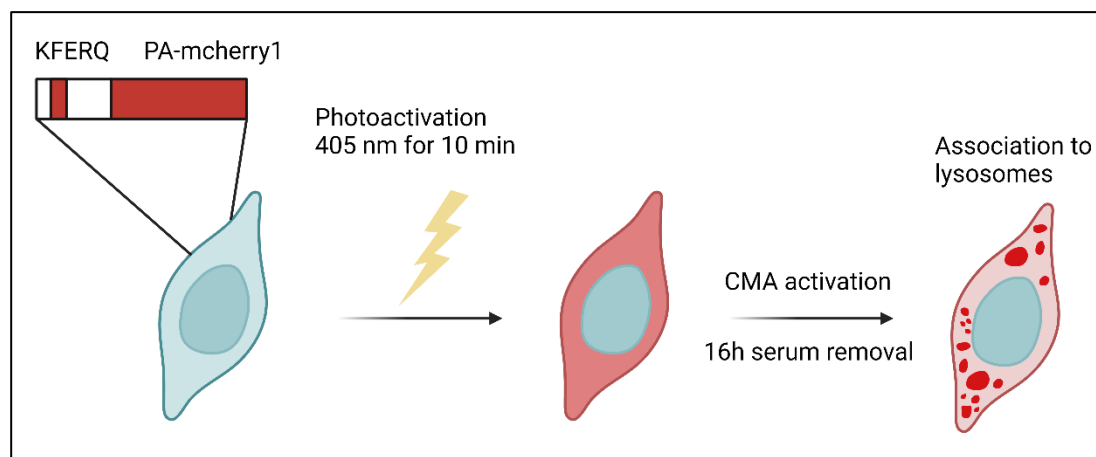


Figure 15: The photoactivable fluorescent reporter (KFERQ-PA-mCherry1). Adapted from Koga et al. 2011¹⁷²

The CMA reporter can be used in a broad variety of cells, and it became clear that levels of basal and inducible CMA activity are cell-type dependent²²⁸. However, the use of this reporter is limited to *in vitro* models and studies on animal tissues still rely on the measurement of CMA activity on isolated lysosomes. Regarding the latter, some questions remain unanswered with regard to cell type-dependent differences in CMA inside tissues. This marked a second critical step in CMA research, with the recent development and validation of a transgenic mouse model ubiquitously expressing a fluorescent CMA reporter (KFERQ-Dendra) that allows monitoring and quantifying this process *in vivo* at cellular resolution²²⁹.

iii. The KFERQ-Dendra transgenic mouse

In 2020, Dong et al. developed a transgenic mouse in which the photoconvertible fluorescent tag DENDRA coupled with a KFERQ motif²²⁹. This technique allows a live measurement of CMA activity *in vivo* but also can inform of organ-specific dynamics. The tissue-specificity of this model was used to reveal the role of CMA in adipocyte differentiation²³⁰ (Fig 16), haematopoietic stem cells function²³¹, Parkinson's disease²³², but also its link to the circadian clock²²².

iv. A novel approach to infer CMA status: the CMA score

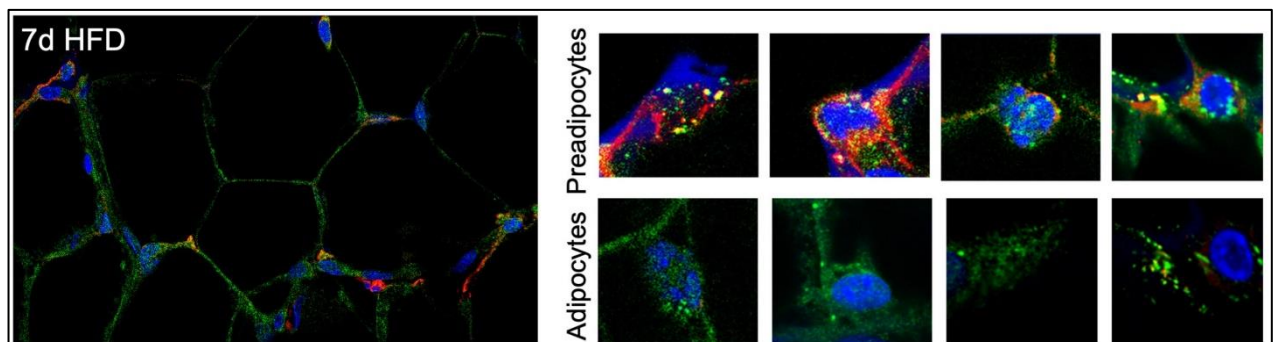


Figure 16: Immunostaining for epididymal white adipose tissue from KFERQ-Dendra-mice maintained on high-fat diet for 7 days (7d HFD) Extracted from Kaushik et al. 2022²³⁰. Nuclei are highlighted with DAPI. Adipogenesis was induced in a mouse model expressing the same CMA reporter (KFERQ-Dendra2 mice) by feeding for 1 week a high-fat diet (HFD). Dendra+ puncta (CMA activity) can be seen in the perinuclear region of adipocytes.

Since the methods to study CMA imply the establishment of transgenic lines or lysosome isolation from readily available fresh tissues or cells, limitations arise when focus is brought on novel species or hard-to-get samples (at least in the fresh state, which is a prerequisite for obtaining lysosomes^{233,234}. For that matter, Bourdenx et al. designed the CMA activation score²²⁴, with the goal of inferring CMA status in different cell types and tissues of patient at different pathological stages. This method was then used in organs or cell types in which lysosome isolation can be complex, such as carotid artery²³⁵, excitatory and inhibitory neurons²³⁶, and retinal organoids²³⁴. This method now represents a reliable indicator of potential CMA activity in tissues or species in which methods to monitor CMA activity are unsuitable. Based on gene expression data, the CMA activation score encompasses all genes modulating CMA (Fig 17). All elements of the CMA network are assigned a weight of 1, except for *LAMP2A*, which is given a weight of 2 due to its significant role as a rate-limiting factor in CMA. Whether the modulator activates or inhibits CMA, it is given a direction of 1 or -1.

The formula is as follows,

$$CMA\ score = (\sum \log_{10} \cdot RE \cdot weight\ of\ gene \cdot (modulating\ sign))$$

RE = relative expression of paralog/gene

Modulating sign= 1 or -1

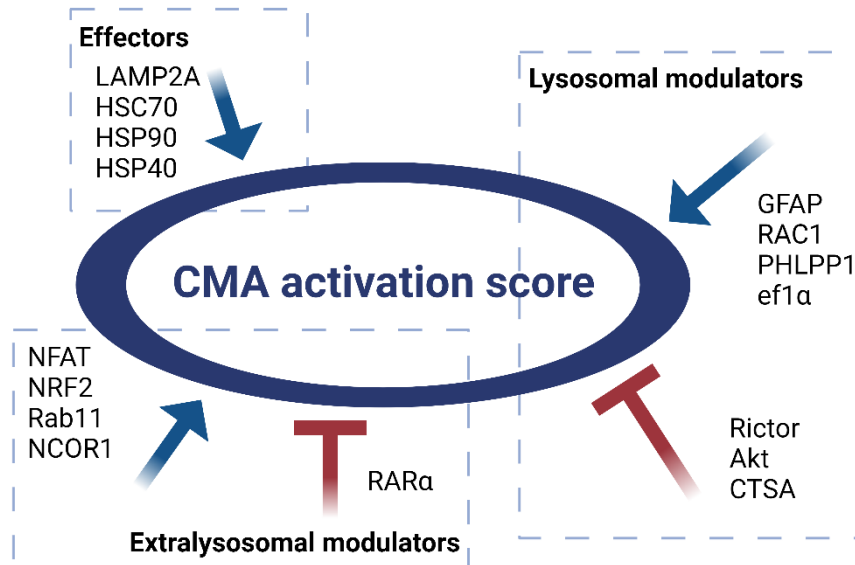


Figure 17: CMA score with target genes of CMA network. Adapted from Bourdenx et al. 2021.²²⁴

PART 3: CMA in fish

1. CMA restricted to mammals and birds: myth or reality?
2. Existence of CMA activity in medaka challenges the tetrapod paradigm

PART 3: CMA in fish

1. CMA restricted to mammals and birds: myth or reality?

It has been well-established that macro- and micro-autophagy processes emerged relatively early in evolution. This assertion is supported by the presence of homologous genes such as ATG5, ATG7, ATG10, ATG12, and ATG8, which play central roles in the autophagic pathway and have been identified in all eukaryotic model organisms studied to date²³⁷. Extensive evidence, including genetic, electron microscopy, and sequence-based findings, supports the existence of macroautophagy in various eukaryotic groups, including plants (such as *Arabidopsis thaliana*), amoebozoa (like *Dictyostelium discoideum*), yeasts (including *Saccharomyces cerevisiae*, *Pichia pastoris*, *Hansenula polymorpha*, and *Pichia methanolica*), and metazoa (such as *Caenorhabditis elegans*, *Drosophila melanogaster*, *Oncorhynchus mykiss*, and *Mus musculus*)²³⁷⁻²⁴⁰. Similarly, both ultrastructural and genetic studies have confirmed the presence of effective microautophagy in yeasts (*Saccharomyces cerevisiae*, *Pichia pastoris*, *Hansenula polymorpha*), plants (*Arabidopsis thaliana*), and mammalian cells¹⁴⁷. In contrast, the evolutionary history of CMA has long remained elusive.

Until recently, CMA was thought to be restricted to mammals and birds^{181,241}. The absence of an established evolutionary history for LAMP2A beyond tetrapods led to the formulation of certain assumptions. Nevertheless, the recent analysis of RNA-seq databases (PhyloFish) from 23 different ray-finned fish species revealed the existence of several sequences homologous to mammalian *LAMP2A*²⁴². Within these sequences, key motifs necessary for the proper function of the protein were shown to be conserved. These motifs included: the GY dipeptide, the hydrophobic phenylalanine residue, both required for targeting to lysosomes^{243,244} 3 of the 4 positively charged amino acids essential to bind substrate proteins¹⁸⁵ and 1 or 2 glycine residues involved in LAMP2A multimerization¹⁸⁸ (Fig 18).

These findings suggested the presence of LAMP2A outside of the tetrapod clade and opened up new perspectives in CMA research.

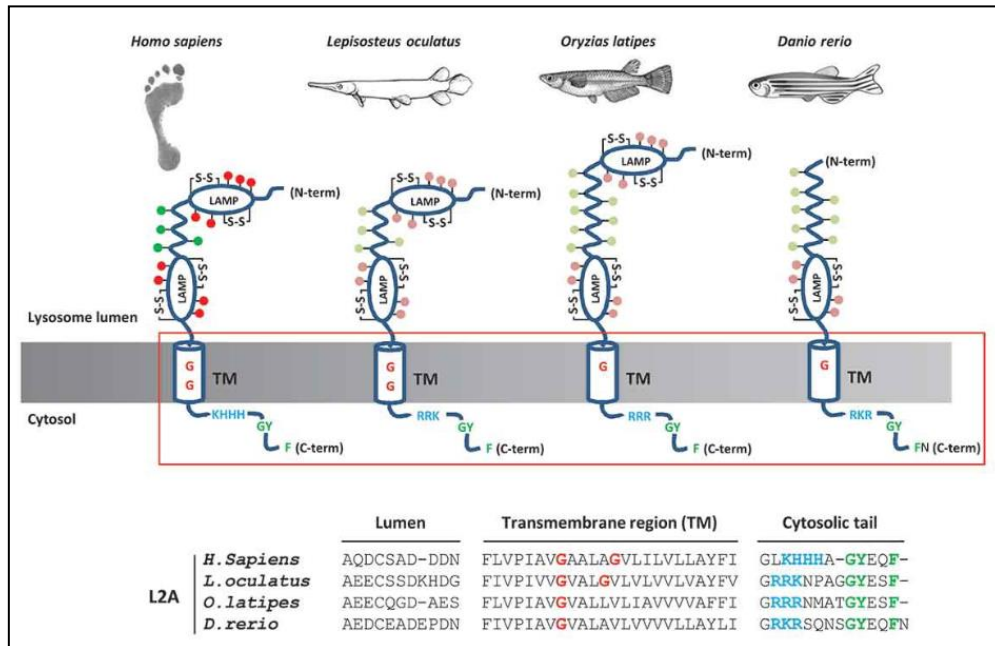


Figure 18: Protein Structure and gene organization of Lamp2A in fish. Extracted from Lescat et al. 2018.²⁴² Representation of vertebrate LAMP2A structure with human LAMP2A as reference. It shows a luminal region comprising 2 LAMP domains of approximately 160 residues separated by a 'hinge' region. The transmembrane (TM) domain, harboring 2 glycine residues (red G) is involved in LAMP2A multimerization. The schematic drawing of fish Lamp2A was done based on sequence complementarity with human LAMP2A. Sequence alignment of the boxed region of the 3 LAMP2/Lamp2 variants is shown below.

2. Existence of CMA activity in medaka challenges the tetrapod paradigm

By challenging the well-established concepts around the apparition of *lamp2* gene in evolutionary history, more information was needed regarding Lamp2A in fish. In 2020, Lescat et al.²⁴⁵ demonstrated that *lamp2* actually appeared at the root of vertebrate lineage. After the first and second rounds of vertebrate whole-genome duplications, the *lamp* genes arose. *Lamp1/2* and *lamp3/4* appeared after the first round and then resulted in *lamp1*, *lamp2* and *lamp3*, *lamp4* following the second round, around ~500 million years ago²⁴⁵. Among the studied vertebrates, including fish species, all exhibited the *lamp2* gene with the three alternative exons (B, A, and C), highlighting the high degree of conservation of the *lamp2* genomic structure across vertebrates²⁴⁵.

Interestingly, Lescat's findings demonstrate that the spotted gar, whose lineage diverged prior to the Teleost-specific Genome Duplication (TGD), has only one *lamp2*, while the eel and arowana, which diverged shortly after the TGD event, harbor two *lamp2* genes (Fig 19). Among the two *lamp2* genes found in these two species, only one still exhibits the exon A. The absence of this exon in the second *lamp2* in these two species, belonging to distinct superorders, could thus result either from

independent losses or from the loss of this exon in the common ancestor of teleosts shortly after the TGD event. In this context, it appears that the second *lamp2* (lacking exon A) in the eel and arowana is seemingly absent in all other teleost species examined (Fig 19). Indeed, genome analyses of zebrafish, cave tetra, codfish, and medaka only reveal the presence of a single copy of the *lamp2* gene containing exons B, A, and C. This could be due to a phenomenon called pseudogenization, wherein genes or gene portions can be lost after duplication^{246,247}.

In 2020, Lescat et al. aimed at determining if medaka displayed CMA activity. For that, they transfected a medaka fibroblast cell line with a photoactivable (PA) KFERQ-PA-mCherry1 fluorescent reporter originally developed by Koga et al¹⁷². It showed a high number of puncta after a 24 h starvation indicating the existence of a CMA activity. By transfecting medaka cells with a PA-mCherry1 construct lacking the KFERQ motif, they were able to demonstrate that the formation of puncta depends on the presence of the KFERQ-motif. In addition, they show that serum removal in morpholino (MO)-mediated knockdown of *lamp2a* cells did not display puncta²⁴⁵. In summary, these findings strongly confirm the presence of a CMA response in a fish cell line. This response, when induced by prolonged fasting, selectively targets KFERQ-proteins in a Lamp2a-dependent manner, as seen in mammalian CMA.

Then, in order to unravel the physiological pathways in which CMA played a role, they generated a Lamp2a knockout medaka line using the CRISPR-Cas9 tool. After a 16 h fasting period, Lamp2a-Ko female fish (but not males) displayed notably enlarged livers, increased lipid droplet levels (LD), and a significant reduction in glycogen content within their livers compared to the control group²⁴⁵. Furthermore, these fish exhibited impaired degradation of enzymes responsible for glycolysis and lipid storage, such as Gapdh, Enolase, and Aldolase (associated with glycolysis) or Mdh1 (linked to the TCA cycle), and Bhmt (associated with lipid storage)²⁴⁵. The compromised degradation of these enzymes could potentially be the cause of the observed disruptions in the metabolic balance in the mutant fish. Overall, these first insights into CMA in fish not only unveiled its presence in other vertebrates, previously overlooked, but also raised the exciting possibility of novel functions due to the distinct evolutionary trajectories they have taken.

Throughout her doctoral thesis, Lescat also described that salmonids (rainbow trout and Atlantic salmon) display two *lamp2* genes with the three exons, which probably stemmed from the Salmonids whole Genome Duplication (SaGD) that occurred around 80 million years ago^{247,248} (Fig 19). Investigating CMA in these species, equipped with two CMA rate-limiting factors Lamp2A raises curiosity toward the potential roles it could harbor.

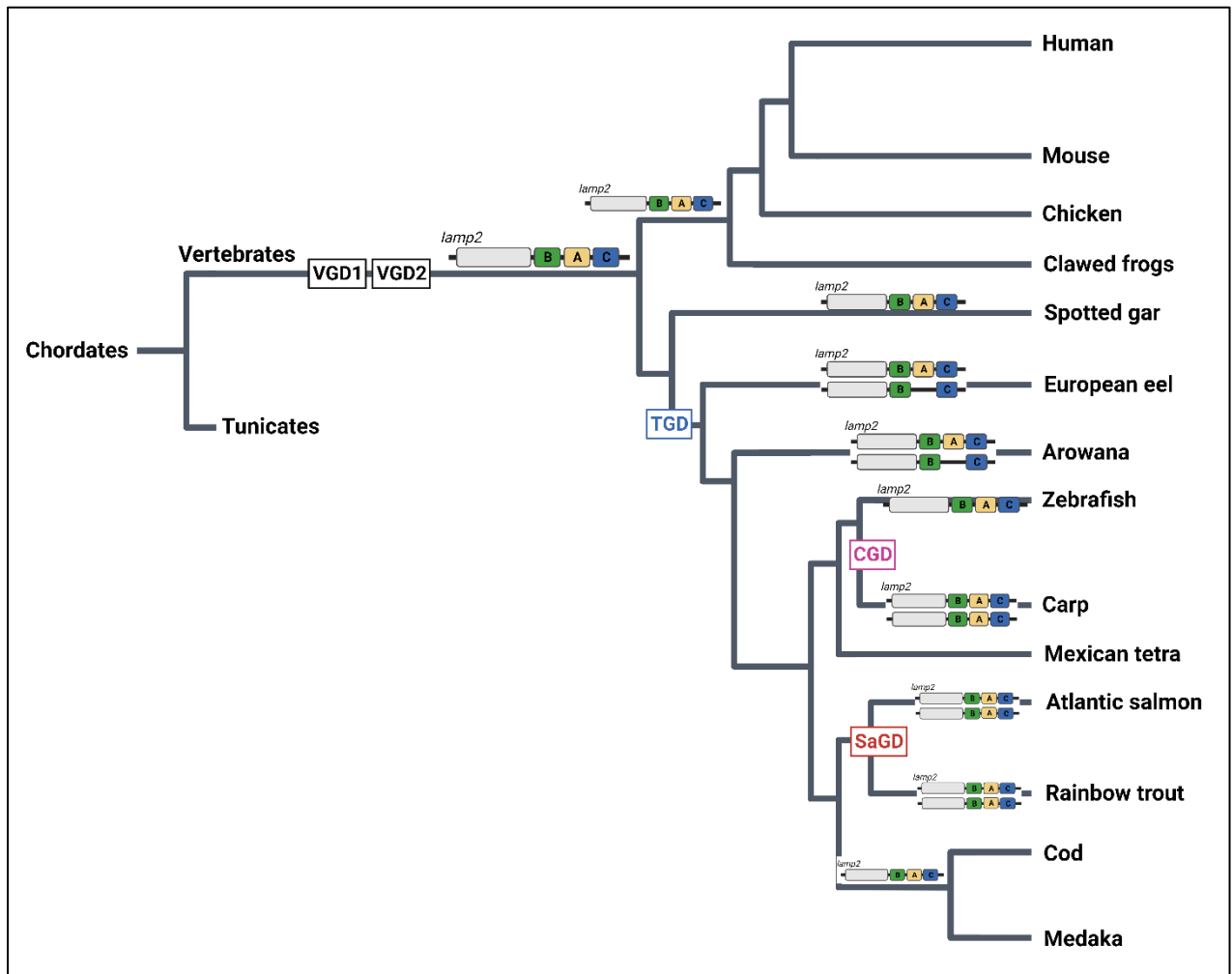


Figure 19: Hypothetical reconstruction of the evolutionary history of *lamp2*. Adapted from Lescat, 2019.²⁴⁷ If no information is provided on the branch, it indicates that the LAMP2 gene is present in a single copy, encompassing exons from all three variants: B, A, and C. VGD1: Vertebrates Genome Duplication 1, VGD2: Vertebrates Genome Duplication 2, TGD: Teleost Genome Duplication, SaGD: Salmonids Genome Duplication, and CGD: Cyprininae Genome Duplication.

Aims of thesis

In light of the current state-of-the-art, which describes the gradual evolution of ongoing environmental stress threatening fish populations, there is a pressing need to assess their stress and resilience. These assessments are vital for the development of effective conservation strategies, while maintaining animal welfare and improving breeding conditions. However, little is known about the maintenance of cellular homeostasis in these species. In this regard, I proposed to investigate the potential role of CMA in fish resilience, especially in the face of environmental threats. To do so, I planned to explore this mechanism in the RT, given its ecological and economic significance.

Part 1: Diving into the evolutionary history of HSC70-linked selective autophagy pathways: endosomal microautophagy and chaperone-mediated autophagy

The limited information available on CMA in fish prompted us to delve into the evolutionary trajectory of selective autophagy across eukaryotic development. The cytosolic chaperone HSC70 is central to both CMA and eMI, as they both target specific substrates to the lysosome. Nonetheless, this principle does not universally apply, and variations arise among species concerning the simultaneous existence of these two autophagic pathways. The aim of this part was to investigate the evolutionary lineage of key elements within CMA or eMI. Furthermore, we deliberated on how the identified variations among species could enhance our comprehension of these dual functions and their interplays.

Part 2: Chaperone-mediated autophagy in fish: a key function in the midst of a stressful environment

The preliminary overview of CMA main actors across vertebrate evolution in the first part unmistakably highlights the potential for a functional CMA in the RT. Subsequently, our objective was to characterize the mRNA expression of CMA-related genes throughout the developmental stages as well as within the adult tissues of RT. Contemplating the genetic basis for CMA in most of fish species including RT, we then planned to isolate RT lysosomes. This step involved an *in vitro* assay that allows the measurement of CMA activity by incubating them with a known CMA substrate. The initial two stages mark the foundational establishment of CMA in RT. However, the subsequent pivotal phase was

focused on unraveling the function of CMA in RT. To achieve this, our plan involved employing the CRISPR-Cas9 gene editing tool to create knockout (KO) RT lacking the Lamp2A splice form. Moreover, subjecting these RTs to a high carbohydrate diet would replicate an acute stress situation, given their status as a natural model for glucose intolerance.

As CMA in mammals is involved in the maintenance of cellular homeostasis, we anticipated that a similar role could be encountered in RT. As such, we planned to adapt the CMA score as a tool to assess cellular homeostasis in RT, and potentially other fish species. After designing the optimal methods for adequate CMA score calculations, RTs were subjected to moderate hypoxia. We then used the CMA score to evaluate whether CMA machinery could have been activated as a response to maintain homeostasis. This tool could potentially find application in fish species currently facing rising environmental challenges.

R

esults

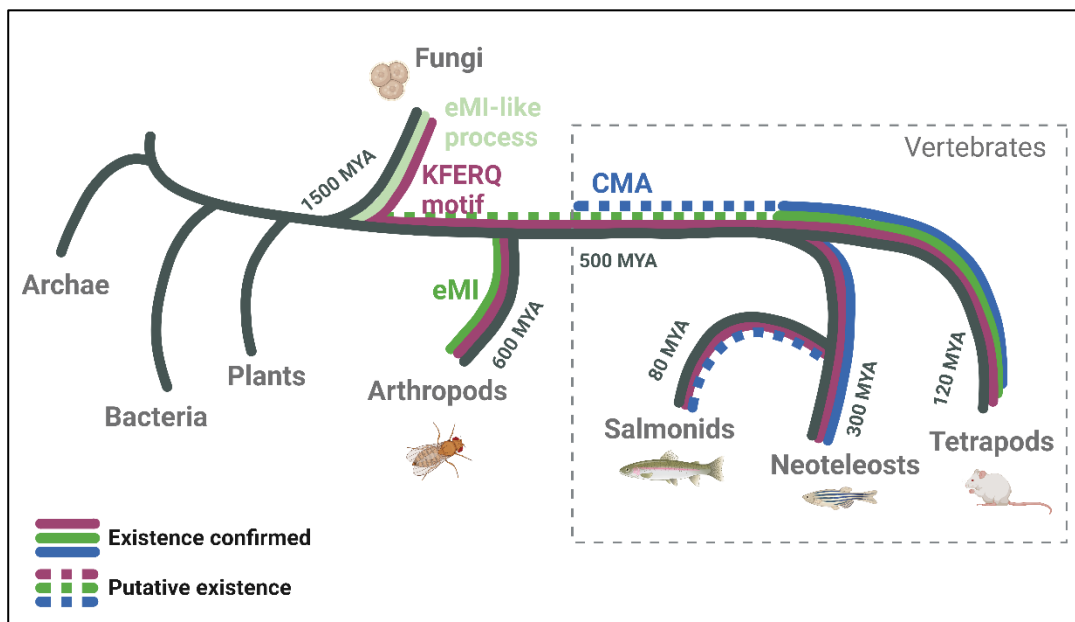
- Publication 1: Diving into the evolutionary history of HSC70-linked selective autophagy pathways: endosomal microautophagy and chaperone-mediated autophagy
- Publication 2: Chaperone-mediated autophagy in fish: a key function in the midst of a stressful environment
- CMA score increases upon Mercury exposure
- CMA as a regulator of food intake? New perspectives.

PUBLICATION 1: Diving into the evolutionary history of HSC70-linked selective autophagy pathways: endosomal microautophagy and chaperone-mediated autophagy

Objectives

As the main interests of the PhD project were to characterize and unravel the CMA intricacies in the RT, a first glance into the evolutionary specificities of this mechanism was necessary.

CMA and eMI use the same chaperone HSPA8 for targeting specific substances to lysosomes. By delving into the evolution of CMA and eMI components (HSC70, KFERQ-like motif, LAMP2A), this review investigates and exposes the species differences in these routes, which raises questions regarding the potential sequential apparition of both mechanisms throughout eukaryotes evolution.



Main results and conclusions

- Most of the core proteins/components of eMI are already present at the onset of eukaryotic evolution although the functional evidence of eMI was only found in mice and drosophila.
- The *LAMP2* gene appeared at the root of vertebrate radiation indicating that CMA, as defined, is specific to vertebrates. Nonetheless, the variability of *LAMP2A* functional domains suggest that CMA has evolved differently among species.

These findings raise new perspectives: the interrogation toward the coexistence of two closely related proteolytic pathways in vertebrates that target the same group of substrate proteins with the same chaperone HSC70. Also, *lamp2* evolution could indicate that CMA has evolved differently in some fish species.

Diving into the Evolutionary History of HSC70-Linked Selective Autophagy Pathways: Endosomal Microautophagy and Chaperone-Mediated Autophagy

Simon Schnebert ^{1,†}, Maxime Goguet ^{1,†}, Emilio J. Vélez ^{1,†}, Alexandra Depincé ², Florian Beaumatin ¹, Amaury Herpin ^{2,*} and Iban Seiliez ^{1,*}

¹ E2S UPPA, INRAE, NUMEA, Université de Pau et des Pays de l'Adour, 64310 Saint-Pée-sur-Nivelle, France; simon.schnebert@inrae.fr (S.S.); maxime.goguet@inrae.fr (M.G.); emilio-jose.velez-velazquez@inrae.fr (E.J.V.); florian.beaumatina@inrae.fr (F.B.)

² UR1037 Laboratory of Fish Physiology and Genomics, Campus de Beaulieu, INRAE, F-35042 Rennes, France; alexandra.depince@inrae.fr

* Correspondence: amaury.herpin@inrae.fr (A.H.); iban.seiliez@inrae.fr (I.S.)

† These authors contributed equally to this work.

Abstract: Autophagy is a pleiotropic and evolutionarily conserved process in eukaryotes that encompasses different types of mechanisms by which cells deliver cytoplasmic constituents to the lysosome for degradation. Interestingly, in mammals, two different and specialized autophagic pathways, (i) the chaperone-mediated autophagy (CMA) and (ii) the endosomal microautophagy (eMI), both rely on the use of the same cytosolic chaperone HSPA8 (also known as HSC70) for targeting specific substrates to the lysosome. However, this is not true for all organisms, and differences exist between species with respect to the coexistence of these two autophagic routes. In this paper, we present an in-depth analysis of the evolutionary history of the main components of CMA and eMI and discuss how the observed discrepancies between species may contribute to improving our knowledge of these two functions and their interplays.

Keywords: chaperone-mediated autophagy; CMA; LAMP2A; HSC70; KFERQ; endosomal microautophagy; eMI; evolution



Citation: Schnebert, S.; Goguet, M.; Vélez, E.J.; Depincé, A.; Beaumatin, F.; Herpin, A.; Seiliez, I. Diving into the Evolutionary History of HSC70-Linked Selective Autophagy Pathways: Endosomal Microautophagy and Chaperone-

Mediated Autophagy. *Cells* **2022**, *11*, 1945. <https://doi.org/10.3390/cells11121945>

Academic Editor: Takahiro Seki

Received: 29 May 2022

Accepted: 15 June 2022

Published: 16 June 2022

Publisher's Note: MDPI stays neutral with regard to jurisdictional claims in published maps and institutional affiliations.



Copyright: © 2022 by the authors. Licensee MDPI, Basel, Switzerland. This article is an open access article distributed under the terms and conditions of the Creative Commons Attribution (CC BY) license (<https://creativecommons.org/licenses/by/4.0/>).

1. Introduction

In the late 80s, Fred J Dice's work was pioneered when it first described a lysosomal pathway selectively degrading soluble proteins [1]. At that time, selectivity in lysosomal degradation had not yet been established or even considered. This notion has since gained ground, and the mechanism that Fred J Dice discovered is nowadays known as chaperone-mediated autophagy (CMA, Figure 1). In detail, during this process, cytosolic proteins containing a pentapeptide sequence sharing biochemical similarity to KFERQ (lysine-phenylalanine-glutamate-arginine-glutamine) are first recognized by the heat-shock protein family A [Hsp70] member 8 (HSPA8/HSC70) and co-chaperones (including Hsp90, Hsp40, the Hsp70-Hsp90 organizing protein (Hop), the Hsp70-interacting protein (Hip), and the Bcl2-associated athanogene 1 protein (BAG-1)) [2,3]. The substrate-chaperone(s) complex then docks at the lysosomal membrane through a specific binding to the cytosolic tail of the lysosomal-associated membrane protein 2A (LAMP2A), which is considered to be the rate-limiting and essential protein for CMA [4]. LAMP2A then organizes into a multimeric complex that allows substrates to translocate across the lysosomal membrane [5,6], where they are ultimately degraded by acid hydrolases. Beyond these primary modalities, in recent years, many research efforts have been carried out to decipher the ins and outs of how the pleiotropic physiological function(s) of CMA exert and are regulated to obtain specificity [7]. Hence, recent findings emphasized the fundamental role(s) of CMA

in regulating numerous cellular functions, including cellular energetics, transcriptional programs, cell death, cell survival mechanisms, and even DNA repair, whose main players harbor one or more KFERQ domains.

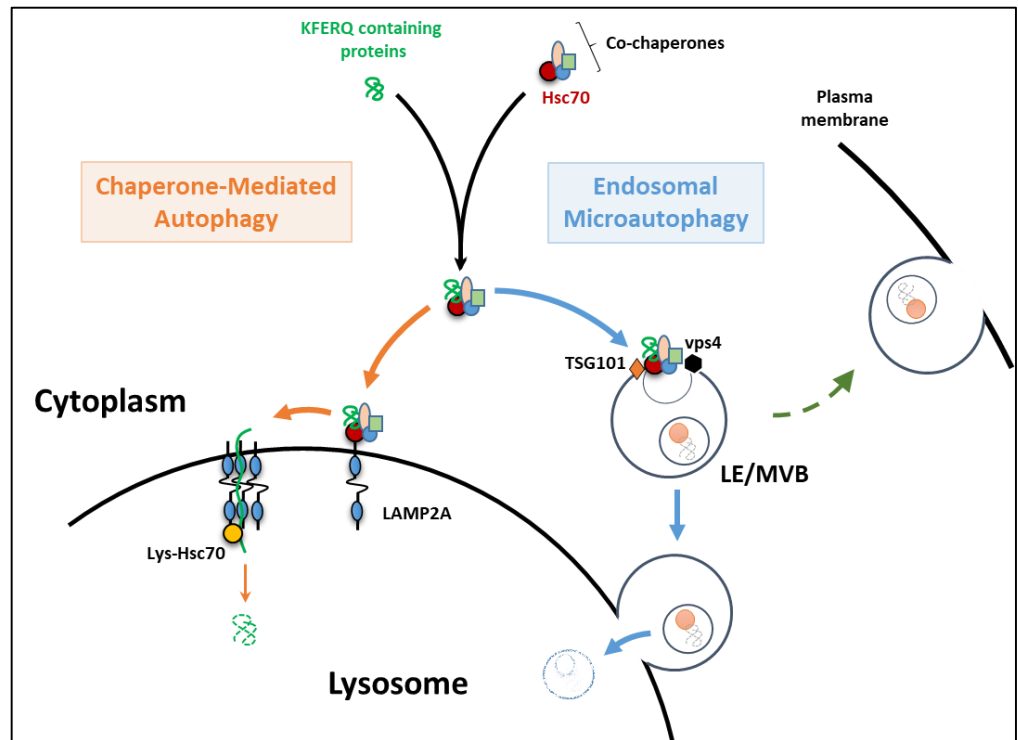


Figure 1. Chaperone-mediated autophagy (CMA) and endosomal microautophagy (eMI) as described in mammals. The first step (dark arrows) of recognition of the KFERQ motif-containing proteins by HSC70 and its co-chaperones is shared by both pathways. During CMA (orange arrows), the substrate-chaperone complex is then directed to the lysosomal membrane through specific binding to the cytosolic tail of the lysosomal-associated membrane protein 2A (LAMP2A). LAMP2A then organizes into a multimeric complex that allows substrates to translocate across the lysosomal membrane and reach the lumen for degradation by lysosomal hydrolases. During eMI (blue arrows), the substrate-chaperone complex is transported to late endosomes/multivesicular bodies (LE/MVB) by direct binding of HSC70 to phosphatidylserine residues on the LE/MVB membrane. Members of the ESCRT machinery (including VPS4 and TSG101) will then mediate the internalization of the substrate into intraluminal vesicles. eMI substrates may then be degraded within the LE/MVB itself or upon their fusion with a lysosome. Alternatively, eMI could mediate extracellular protein releases due to the ability of LE/MVB to fuse with the plasma membrane (green dashed arrow).

Very recently, along with the emergence of new concepts in the field of autophagy, Sahu et al. evidenced that KFERQ domain-containing proteins can additionally be subjected to parallel degradation in late endosomes/multivesicular bodies (LE/MVB) through a pathway referred to as endosomal microautophagy (eMI) [8]. This alternative process contributes to the in bulk degradation of cytosolic proteins trapped in vesicles forming at the LE membrane. Interestingly, some proteins bearing a KFERQ domain can also be selectively recognized and degraded by eMI through a LAMP2A-independent mechanism but are in need of the “Endosomal Sorting Complex Required for Transport” (ESCRT) machinery (Figure 1) [9].

Briefly, after being recognized by HSC70 (a common step between CMA and eMI), the substrates targeted by eMI are then transported to the LE/MVB after the direct binding of HSC70 to phosphatidylserine residues on the LE/MVB membrane [10]. Members of the ESCRT machinery, including VPS4 and TSG101, then gather around this area and form a membrane invagination internalizing the substrate into intraluminal vesicles [8]. eMI substrates might then be degraded either within the LE/MVB itself (i.e., Tau [11]) or upon subsequent fusion with a lysosome [8,11]. Alternatively, eMI could also act as a gateway for extracellular protein release due

to the ability of LE/MVB to fuse with the plasma membrane and release their luminal content (exosomes) [12]. However, in this latter case, the fate of the cargo is different. Thus, it has been proposed to use the term eMI only for cytosolic proteins loaded in the LE/MVB that undergo degradation in this compartment or during lysosomal fusion and not for those targeted for extracellular release by exocytosis [9]. The characterization of the eMI now raises several questions about the relationship and interplay between CMA and eMI. In particular, the mechanisms underlying the routing of KFERQ-containing substrates to one or the other of these degradation pathways remain to be determined. The respective roles and functional complementarities/overlapping/compensation of these pathways also need to be considered.

Notwithstanding, to date, the co-existence of these two autophagic pathways has only been demonstrated in mammals, and factually, this scenario does not seem to apply to all species. Indeed, the recent discovery that the *LAMP2* gene (encoding LAMP2A) emerged at the root of the vertebrate lineage [13] indicates that invertebrates are de facto unable to perform any mammalian-type of CMA activity [7], or at least a LAMP2A-dependent CMA process such as that recently described in fish [13]. As such, although flies (*Drosophila melanogaster*) appear to be a CMA-incompetent species, they nevertheless perfectly cope with eMI only [14], meaning that eMI could fulfill all the functions shared with CMA in mammals. Interestingly, in fission yeast (*S. pombe*), Liu et al. reported the existence of an ESCRT-dependent eMI-like process that relies on the NBR1 protein (which shares a partial homology with the mammalian macroautophagy receptor NBR1) to deliver two hydrolytic enzymes (LAP2 and APE2) from the cytosol to the vacuole [15]. However, unlike the eMI process described in mammals and *D. melanogaster*, the yeast alternative, termed NBR1-mediated vacuolar targeting (NVT), singularly relies on the ubiquitination of NBR1 and/or its associated proteins and not on HSC70, suggesting that NVT and eMI are indeed two distinct mechanisms. Considering this data, it is tempting to build a scenario in which eMI and CMA would have appeared sequentially during the course of evolution. The oldest eukaryotic lineages would be eMI- and CMA- incompetent, invertebrates (ectodyszoans and lophotrochozoans) would barely perform eMI, and only vertebrates would use both of the pathways, eMI and CMA. To go a step further, the apparent sequence variability of LAMP2A in vertebrates (particularly in its cytosolic Cterminal region that is involved in substrate-chaperone complex recognition) between phylogenetically distant species [16] additionally addresses the possibility of a still ongoing evolution of the mechanisms underlying CMA activity across vertebrates.

In the present review, we summarized the current understanding of the evolutionary history of the main components necessary for CMA and eMI functions and discussed how the observed disparities between species can improve our knowledge of these two functions and their interplays from an evolutionary perspective.

2. The Essentials of eMI and CMA

2.1. The KFERQ Motif

A common and essential step between eMI and CMA is the recognition by HSC70 of the KFERQ-like motif-containing proteins. The existence of either of these processes (eMI or CMA) in a given species, therefore, requires the presence of proteins bearing this motif or, at least, a sequence related to this motif, but how was this motif defined? Pioneering studies performed by Fred J Dice using bovine pancreatic ribonuclease A (RNase A) initially identified an 11-amino acid region within the protein, and later on, this motif was narrowed down to the pentapeptide KFERQ, which is necessary and sufficient to target proteins for lysosomal degradation [16]. However, the exact sequence, -KFERQ-, is only contained in

RNase A. Further studies conducted by the same team also demonstrated that the physical properties of the residues constituting the motif, rather than the specific amino acids per se, determine the ability of the chaperone HSC70 to bind this region [17]. Accordingly, these authors defined that a canonical KFERQ-like motif is always flanked by a glutamine (Q) on either side and must contain (i) one or two of the positive residues K and R, (ii) one or two of the hydrophobic residues F, L, I, or V, and (iii) one of the negatively-charged residues E or D (Figure 2). Recently, other studies have demonstrated that KFERQ-like motifs can be generated via post-translational modifications. Thus, phosphorylation or acetylation of the amino acid residues along protein regions that do not originally display the mentioned properties dramatically increases the repertoire of putative HSC70 substrates (Figure 2) [18–20].

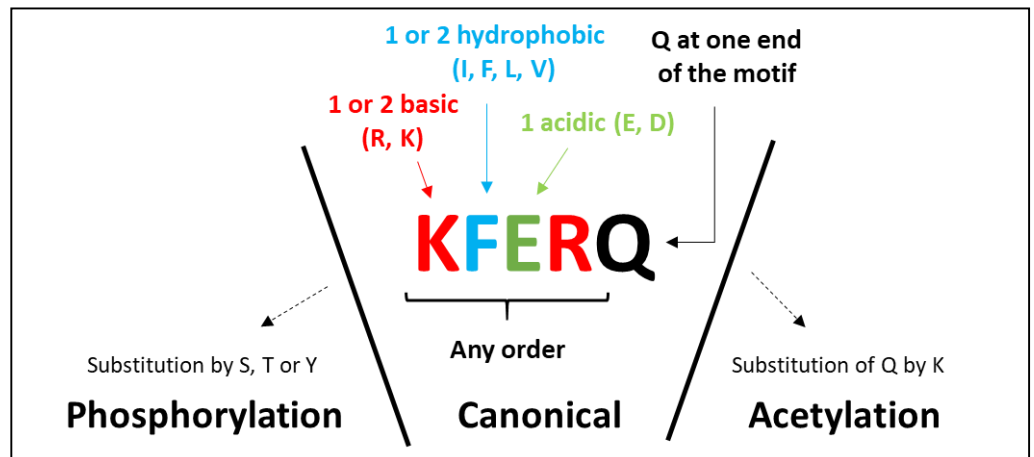


Figure 2. Building rules of canonical, phosphorylation-, and acetylation-generated KFERQ-like motifs (adapted from [21]). The KFERQ-like motif may contain up to two hydrophobic residues (isoleucine (I), phenylalanine (F), leucine (L), or valine (V)), up to two positive residues (arginine (R) or lysine (K)), and a single negatively-charged residue (glutamate (E) or aspartate (D)) flanked at either the N- or C-terminus of the pentapeptide by a single glutamine (Q) residue. KFERQ-like motifs can also be generated via post-translational modifications, such as phosphorylation or acetylation of the amino acid residues along protein regions that do not originally show the mentioned properties.

According to the above-described definition of the KFERQ-like motif, approximately 46% of proteins in human proteome contain at least one canonical motif, 20% contain no canonical motif but a phosphorylation-generated one, and 9% contain only acetylation-generated motifs [22]. Interestingly, the overall percentages of proteins bearing each of the KFERQ-like-types motifs are similar between the proteome of *Mus musculus* (which is both CMA- and eMI-competent), *Drosophila melanogaster* (which is eMI-competent but CMA-incompetent), and *Saccharomyces cerevisiae* (unable to perform CMA and whose ability to perform a “mammalian-type” eMI has not been demonstrated) [22]. These results suggest that the emergence of the KFERQ-like motif most likely preceded the establishment of the CMA function (and possibly that of eMI as well) and that the proportion of these proteins in the proteome of a given species is thus not predictive of its ability to perform any of these selective autophagy pathways. Nonetheless, a recent comparison of more than 500 orthologs of human proteins harboring a single canonical KFERQ motif in 50 different species predicted to be either CMA-competent or -incompetent, revealed that about 45% of the investigated proteins displayed a more preserved motif in “CMA-proficient” species than in “CMA-deficient” ones [22]. This suggests a substantial degree of evolution of this motif in different species. Whether the evolution of this region is dependent on their ability to perform either eMI, CMA, or both remains to be further investigated.

2.2. HSC70

The chaperone HSC70, a member of the heat shock protein 70 family (HSP70), is mostly constitutively expressed. It is involved in diverse cellular processes, including protein folding and protein degradation. We do not intend here to give a detailed description of all the various functions fulfilled by this protein. It has already been well described in excellent reviews that we encourage to consult [23–25]. Instead, we will rather discuss the evolutionary history of this chaperone and draw up a scenario that highlights how the two autophagic functions (eMI and CMA) might have specifically evolved, although using/sharing an initial common component.

Proteins of the HSP70 family appeared very early during evolution and are found in a wide range of living organisms, from archaea to mammals [26–28]. Interestingly, significant differences in the number of genes belonging to this family are clearly visible between species. Thus, a recent screen for the presence of HSP70 in 5551 representative prokaryotic genomes revealed that the number of HSP70 genes in individual prokaryotic genomes ranges from 0–23 (99.1% of the genomes contain at least one HSP70 gene) [29]. Similarly, it is well known that most eukaryotic cells also display several genes coding for HSP70/HSC70 proteins. For example, the yeast *Saccharomyces cerevisiae* has more than 10 genes coding for proteins of this family [30], which have all been shown to present both overlapping and divergent functions [31]. Furthermore, at least 12 genes encoding 14 proteins of the HSP70 family are found in the human genome [23]. Although all of them display an overall high sequence identity (more than half share 80% of their amino acid sequence), these proteins are nevertheless likely involved in distinct functions due to, notably, specific spatio-temporal distributions [23].

Most of the HSP70 family members are cytosolic proteins. They have further been classified into either inducible HSP70s or constitutively expressed HSC70s, but until recently, their evolutionary relationship remained elusive, mainly due to the lack of cross-phylum comparisons. However, a recent in-depth phylogenetic study reviewing 125 complete HSP70/HSC70s genes from a wide range of species across different phyla has clarified the complex evolution of this gene family [32]. According to this study, HSP70 family members associate with mitochondria and the endoplasmic reticulum form two monophyletic groups (Figure 3). Members of the cytosolic HSP70 family form a third monophyletic group, which also includes yeast cytosolic HSP70s (with both inducible and constitutive *ssa1–4* genes). Within metazoan cytosolic HSP70/HSC70s, two large lineages are distinct. These two lineages most certainly formed before the separation of vertebrates and invertebrates. One lineage includes a relatively limited number of genes from many invertebrate phyla, none of which have been shown to be constitutively expressed. The second lineage contains both inducible and constitutive genes from various phyla. This second lineage has further diversified within some phyla (including at least *Platyhelminthes*, *Rotifera*, *Nematoda*, and *Chordata*). In this regard, some genes from the second lineage have certainly either gained or lost their stress-inducible response capacity (through convergent evolution), which may explain the sporadic distribution of “HSP70” and “HSC70” in previous phylogenetic analyses. However, due to the presence of inducible and constitutive HSP70 gene members in many clades (including yeast), it is still difficult to predict the ancestral state.

Interestingly, an inter-clade comparison of the synonymous and nonsynonymous substitution rates revealed that all HSP70/HSC70 family members are under strong purifying selection [32]. The presence of such a purifying selection was already reported for mammalian [33], nematode [34], molluscan [35], and protist [36] HSP70/HSC70 genes. That positive selection would most likely operate to preserve

functions performed by HSP70s, including heat shock response, folding of newly synthesized proteins, protein transport, and autophagy.

Overall, this set of data supports an ancient origin of the chaperone HSC70, and its relatively high sequence conservation between phyla suggests preserved functions during the evolution. This being said, one might be tempted to speculate that the presence of both KFERQ-containing proteins and orthologs of HSC70 in yeast (i.e., *ssa1p*) signs a hallmark of an ancient origin of eMI and/or CMA. However, these two autophagic pathways also rely on other factors, such as members of the ESCRT machinery (in the case of eMI) and LAMP2A (in the case of CMA). Hence, a critical question is whether these factors also appeared very early during evolution or whether eMI/CMA functions formed later on from pre-existing and evolutionary conserved components.

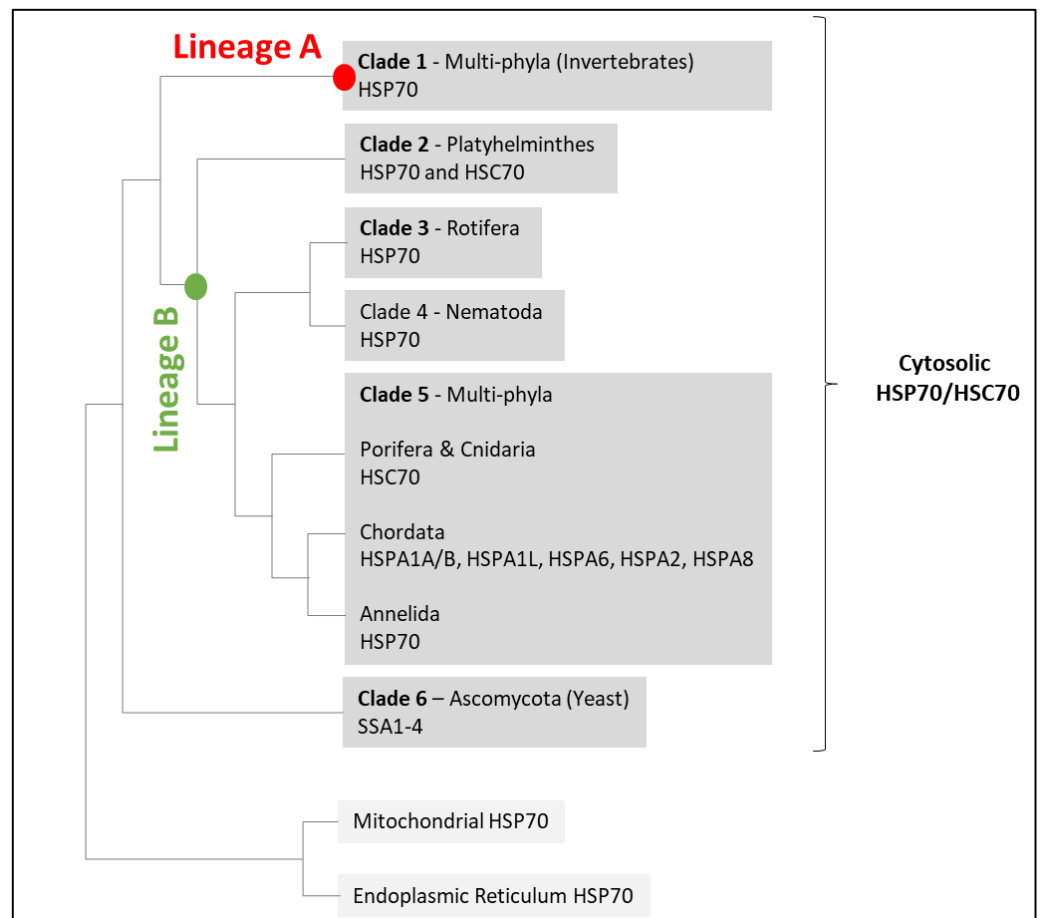


Figure 3. Proposed tree topology of HSP70/HSC70 family members in metazoans (adapted from Yu et al. [32]). Red and green circles show the nodes that give birth to Lineage A of invertebrate HSP70s (clade 1) and Lineage B of both vertebrate and invertebrate HSP70s and all HSC70 genes, respectively.

This second lineage has further diversified within diverse phyla: *Platyhelminthes* (clade 2), *Rotifera* (clade 3), *Nematoda* (clade 4), and *Chordata* (clade 5). Clades 1 to 6 include only cytosolic members of the HSP70 family.

3. Endosomal Microautophagy

After its initial description and characterization in mammals in the late 1980s [37,38], most progress in the microautophagy area has been achieved by research made in yeast, ranging from the microautophagy of peroxisomes [39,40], mitochondria [41], portions of nuclei [42], lipid droplets [43], endoplasmic reticulum [44], certain cytosolic enzymes [15], and vacuole membrane proteins [45]. Altogether, these findings provided evidence that the microautophagy function emerged very early during the evolution and that it can virtually target any cellular structure. However, the diversity of the mechanisms involved in handling/processing these different cellular constituents has led many authors to

wonder about the relevance of gathering these distinct types of autophagy under the same “microautophagy” process(es) (or at least terminology) [46].

The present review focused on a specific “subtype” of microautophagy that was first characterized in murine dendritic cells [8]. This process, termed eMI, contributes to in bulk degradation of proteins present in the cytosol and that are embedded in vesicles formed from the LE membrane. However, some cytosolic proteins can also be selectively degraded by eMI after HSC70 recognizes their KFERQ motifs and binds to endosomes via phosphatidylserine [8]. Members of the ESCRT machinery (including at least VPS4 and TSG101) then induce membrane invagination and subsequent internalization of the substrates into intraluminal vesicles [8]. Cargo degradation then occurs either in the LE/MVB compartment or after the fusion of LE/MVB with lysosomes.

More recently, the existence of a similar eMI process was described in the fat body of flies [14]. Akin to mammals, components of the ESCRT machinery have been proven to be necessary for eMI in *Drosophila*. However, in contrast to mammals, eMI in flies involves additional autophagy-related genes (such as *ATG1* and *ATG13*) and is induced after fasting [14]. Of note, genotoxic and oxidative stresses have also been shown to upregulate eMI in *Drosophila* [47]; although in these cases, the dependence on HSC70 is only partial, pointing out the importance of carefully discriminating between HSC70-dependent and HSC70-independent types of eMI.

Although an HSC70-dependent type of eMI has attracted much attention after it was just discovered, very few data are actually available regarding its regulation and functional implications compared to other forms of autophagy. To our knowledge, this particular mechanism has only been documented in mice [8] and *Drosophila* [14,48]. It is still unclear whether this singular autophagic pathway exists in other living organisms. Interestingly, extensive comparative genomic and phylogenetic studies have demonstrated that ESCRT genes are conserved throughout the eukaryotic lineage [49], as well as in Archaea with respect to some genes [50,51]. That broad distribution in eukaryotes (and some Archaea) supports the early evolutionary origin of the ESCRT machinery and by inference, possibly, of an eMI-like pathway similar to the one described in mice and *Drosophila*. In this context, Liu et al. reported the existence of an ESCRT-dependent eMI-like process relying on the NBR1 protein in fission yeast (*S. pombe*) [15]. However, while this pathway has been proven to be dependent on the ubiquitination of NBR1 and/or its associated proteins, it does not involve HSC70.

4. Chaperone-Mediated Autophagy

CMA activity is tightly correlated with (i) the amount of LAMP2A at the lysosomal membrane [52] and (ii) the assembly/disassembly efficiency of LAMP2A complexes in this compartment [5]. As such, analyzing either the presence/absence of the gene coding for that protein, or the variability observed within the different functional protein domains between phylogenetically distant species, would certainly help decipher the evolutionary history of this function.

4.1. Origin and Evolution of LAMP2

LAMP2A originates from the alternative splicing of the *LAMP2* gene, which also generates two other different splice variants, LAMP2B and LAMP2C. While these three splice variants all share a common luminal domain, they also display different and specific cytosolic and transmembrane™ regions (Figure 4A) [53,54]. In contrast to LAMP2A, neither LAMP2B nor LAMP2C has been shown to be involved in CMA. Instead, LAMP2B is involved in macroautophagy [55,56] and the LAMP2C in the uptake and degradation of DNA and RNA molecules by lysosomes [57,58].

Recently, Lescat et al. provided a comprehensive picture of the evolutionary history of the *LAMP2* gene in vertebrates. They demonstrated that *LAMP2* appeared after the second round of whole-genome duplication (WGD) at the root of the vertebrate lineage, ~500 Ma [13]. More precisely, phylogenetic analyses and synteny conservation data strongly suggest that a single copy of *LAMP* was already present in the common vertebrate ancestor, and that the two successive WGDs that occurred at the root of the vertebrate lineages [59] engendered *LAMP1/2* and *LAMP3/4* (from WGD1), and then *LAMP1*, *LAMP2*, *LAMP3*, and *LAMP4* (from WGD2) that are common to all vertebrates (Figure 4B). Hence, data support the idea that invertebrates would not factually be able to perform CMA, or at least a *LAMP2A*-dependent CMA process similar to the one described in mammals [7] and fish [13].

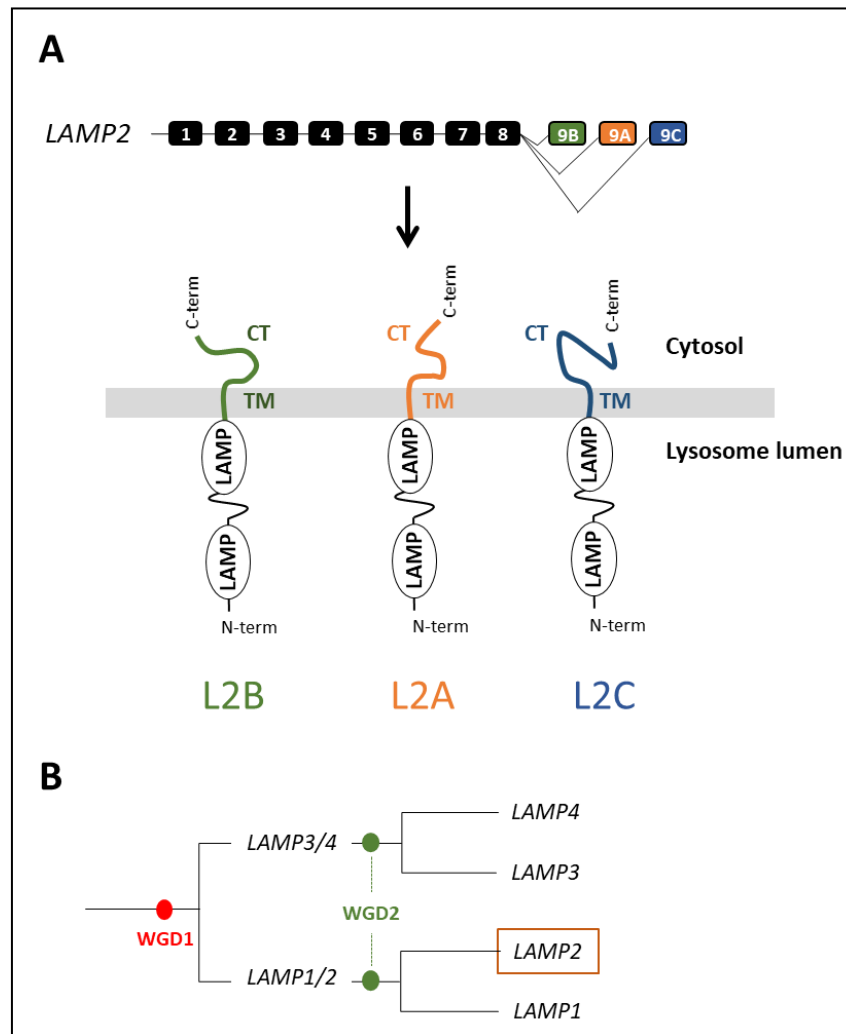


Figure 4. (A) Gene organization of the gene *LAMP2* and protein structure of three splice variants displaying a common luminal domain (with two LAMP domains) but different transmembrane (TM) domain and cytosolic tail (CT). The boxed numbers denote exons. (B) Schematic scenario of the evolutionary history of lamp family genes.

It is also worth noting that, despite the significant genomic rearrangements that some vertebrate lineages have experienced [60], the number of *LAMP2* genes is constant across vertebrate genomes. Indeed, the third WGD, which occurred 320–350 million years ago in the teleost fish ancestor (namely, the teleost-specific round of WGD or TGD), theoretically implies that two orthologs (co-orthologs) of each human *LAMP* gene would be expected in teleost species, unless lost. Accordingly, both the European eel (*Anguilla anguilla*) and the Asian bonytongue (*Scleropages formosus*), whose lineages diverged shortly after the TGD, display two *LAMP2* genes, with one paralog bearing the three alternative exons and the other only the exons B and C [13] (Figure 5).

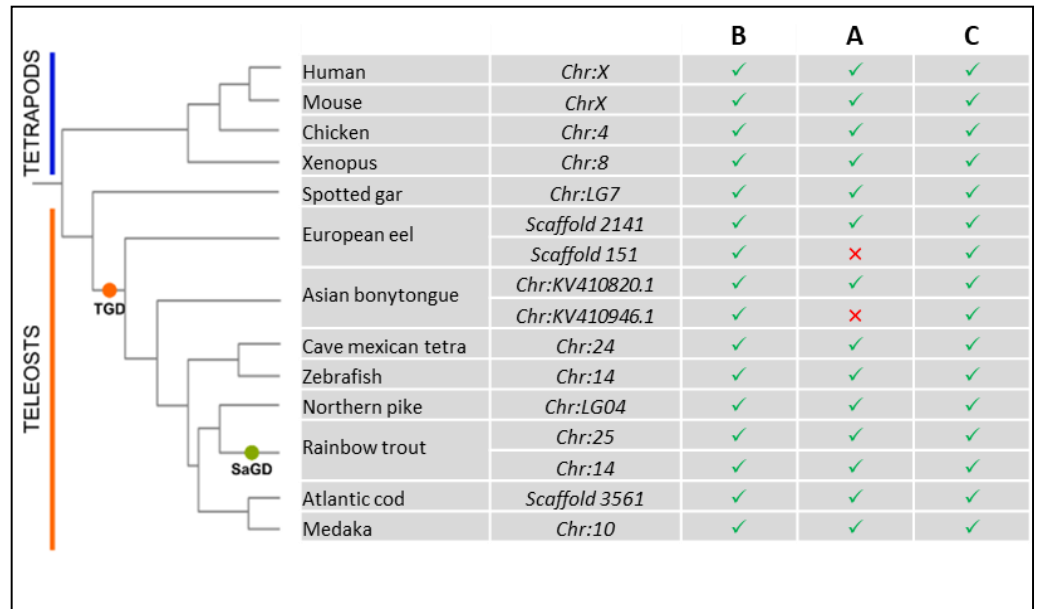


Figure 5. Presence of the three alternative exons (**B**, **A**, and **C**) in the *LAMP2* gene in four tetrapod species—human (*H. sapiens*), mouse (*M. musculus*), chicken (*G. gallus*), and frog (*X. tropicalis*)—and nine fish species—spotted gar (*L. oculatus*), European eel (*A. anguilla*), Asian bonytongue (*S. formosus*), cave Mexican tetra (*A. mexicanus*), zebrafish (*D. rerio*), Northern pike (*E. lucius*), rainbow trout (*O. mykiss*), Atlantic cod (*G. morhua*), and medaka (*O. latipes*). The phylogenetic tree is a representative tree of life. The presence or absence of each alternative exon (**B**, **A**, and **C**) is represented by a green check mark or a red cross mark, respectively. For each species, the location of the gene is specified in the table. TGD, teleost-specific whole-genome duplication; SaGD, salmonid-specific whole-genome duplication.

The absence of exon A in the second *LAMP2* paralog of these two species, belonging to different super-orders, could be due to either independent losses or the specific loss of this exon in the common ancestor of teleost shortly after the TGD. However, this second *LAMP2* gene, which likely results from the TGD, appears to have been lost in all other teleost species investigated [13]. Accordingly, in cave Mexican tetra (*Astyanax mexicanus*), zebrafish (*Danio rerio*), Northern pike (*Esox lucius*), Atlantic cod (*Gadus morhua*), and medaka (*Oryzias latipes*), a unique *LAMP2* is found with all three alternative exons (Figure 5). Interestingly, genome analyses of various salmonid species have revealed the presence of two *LAMP2* genes bearing the three alternative exons A, B, and C, which likely originated from the fourth round of WGD that occurred in the common ancestor of salmonids (SaGD) about 100 million years ago. However, a re-analysis of the PhyloFish RNA-seq database—providing gene expression data from 23 different ray-finned fish species [61]—confirmed the expression of a single *LAMP2A* transcript in all considered salmonids [16]. This suggests that the loss of expression of the second *LAMP2A* transcript is of a common origin, probably in the ancestor of salmoniforms, shortly after the SaGD. Together, these data suggest that evolution tends to promote the presence of a single *LAMP2A* protein. Indeed, duplication of the *LAMP2* genes following WGD appears to be systematically followed by the loss of one duplicate, the loss of the A exon, or the lack of expression of one of the two copies (in the case of the recent SaGD). This last point certainly deserves to be clarified in the future.

4.2. Structure Evolution of *LAMP2A* across Vertebrates

In mammals, the structure of the lysosomal membrane proteins belonging to the LAMP family is now well documented [62–66]. These proteins consist of a large luminal region at the N-terminus, a TM domain of about 20 amino acids, and a short Cytosolic (C-terminal) Tail (CT) stretching from 10–12 amino acids (Figure 4A). In addition, these proteins possess a number of conserved motifs required for protein lysosomal targeting and function (see [5,52,67,68] for details). Although the

general architecture of this protein is relatively well conserved among vertebrates, some differences are noticed within the different functional domains of LAMP2A between phylogenetically distant species. Taking advantage of that “evolution in motion” will certainly be of great value for identifying evolutionarily conserved, or species-dependent, key residues necessary for further deciphering the structure–function relationship of this protein.

4.2.1. The GYXX ϕ Motif

According to the literature, the C-terminal ends of LAMP proteins carry a recognition signal for lysosomal targeting, which is characterized by the canonical GYXX ϕ motif (where ϕ is a hydrophobic amino acid) [52]. In mammalian LAMP2A, ϕ is the hydrophobic phenylalanine (F) residue, whose deletion has been shown to impair the proper addressing of LAMP2A to the lysosomal membrane [52]. Further analysis of LAMP2A sequences additionally revealed that this hydrophobic F residue is actually highly conserved in vertebrates (Figure 6). Excepting the absence of that “F” in *Xenopus tropicalis* and *Perca fluviatilis*, the only variations identified are the presence of one or two extra amino acids at the C-terminus in some fish species belonging to ostariophysans (a superorder comprising about 8000 species of bony fish, including catfishes, characins, electric knifefishes, and the zebrafish). In addition, recent findings showing that extra amino acids (i.e., a triple FLAG tag) at the C-terminus of LAMP2A do not impair neither its lysosomal addressing nor its ability to properly target well-known CMA substrates (such as GAPDH) fused to the HaloTag protein (GAPDH-HT) [62] indicate that these extra C-terminus residues are undeniably not crucial for a proper CMA function.

It should also be noted that, while in the majority of the vertebrate species analyzed the GY dipeptide is conserved when focusing on the cytosolic tail sequence of LAMP2A, it is nevertheless not “retained” in some (e.g., in the common wombat (*Vombatus ursinus*), the blind cave tetra (*Astyanax mexicanus*), the coelacanth (*Latimeria chalumnae*), the channel catfish (*Ictalurus punctatus*), the European perch (*Perca fluviatilis*), and one of the two LAMP2A found in the rainbow trout) (Figure 6). These data might suggest that LAMP2A in these species is (possibly) not correctly targeted to the lysosomal membrane. However, previous studies carried out on the LAMP1 protein (human and mouse), which also presents the GY dipeptide, clearly demonstrated that only tyrosine (Y) is required for the localization of the protein at the lysosomal membrane [67,68]. In contrast, while mutating the glycine does not impair the correct addressing of LAMP1 to the lysosomal membrane [67], on the other hand, it does affect its routing to the lysosomes [69,70].

Together, these data suggest that the LAMP2A proteins, as far as the large majority of the vertebrates is concerned, do require the presence of the minimal YXXF motif in their cytosolic tails to be correctly addressed to the lysosomal membrane.

4.2.2. Positively-Charged Amino Acids

Although the presence of the YXXF motif identified within the cytosolic tail of the LAMP2A from most vertebrate species suggests that these proteins can, in theory, be properly delivered to the lysosomal membrane, the activity of this protein also relies on several other motifs nested within the C-terminal region. In mammals, it is commonly accepted that the presence of 3–4 positively charged residues within the cytosolic tail of LAMP2A is necessary for the proper recognition and binding of the substrate/chaperone complex [52]. In that direction, isolated lysosomes containing a mutated version of LAMP2A for the four positive residues displayed a lower binding ability against GAPDH when compared to native LAMP2A residues [52].

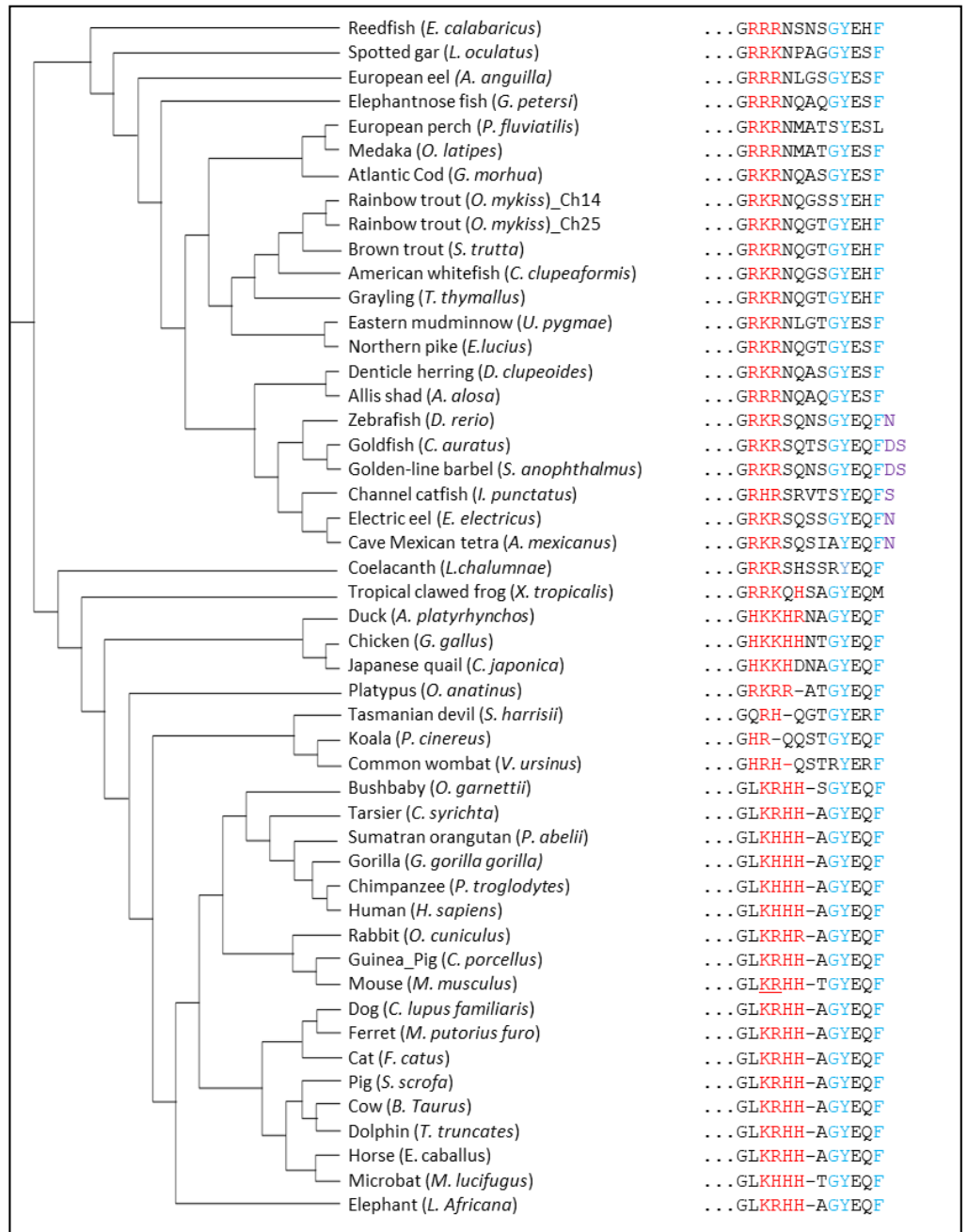


Figure 6. Protein sequence alignment of the short CT tail of LAMP2A from different vertebrates. Positively-charged amino acids required for the binding of substrate proteins are colored in red. The GY dipeptide as well as the hydrophobic F required for the targeting of LAMP2A to lysosomes are in blue. The additional residues at the C-terminus of LAMP2A from fish belonging to ostariophysans are in purple. The K406 and R407 of mouse LAMP2A are underlined.

Very recently, using a site-specific photo-reactive crosslinking experiment, Ikami et al. evidenced the direct interaction of the cytoplasmic tail of mouse LAMP2A together with HSC70 [66]. More precisely, a UV-dependent crosslinking was observed at two positively charged amino acids (K406 and R407 of mouse LAMP2A), which are located immediately after the TM region (underlined residues for the mouse sequence in Figure 6). This finding supports the conclusions drawn after monitoring by nuclear magnetic resonance (NMR)-based chemical shift perturbation (CSP) assay of the interactions between human TMLAMP2A (369–410, consisting of the transmembrane domain and cytoplasmic tail) and the substrate-binding domain of HSC70 [64]. In the presence of the substrate-binding domain of HSC70, residues K401 and H402 (corresponding to K406 and R407 in mouse LAMP2A, respectively) showed significant CSPs, while those of the TM residues were essentially unchanged [64]. Together, these findings support an

intrinsic affinity of HSC70 for the cytoplasmic tail of LAMP2A and an important role of the two positively charged residues in this affinity. Of note, a similar pattern of CSPs was also observed when a CMA substrate, RNase A, was added to TM-LAMP2A [64], further emphasizing the role of these residues in substrate affinity and specificity.

Interestingly, sequence analysis of vertebrates LAMP2A shows the presence (in the majority of the species considered) of at least three positively charged amino acids (including the two amino acids corresponding to K406 and R407 in mouse LAMP2A) (Figure 6). These results suggest that, in addition to bearing the lysosome membrane addressing motifs discussed above (see Section 4.2.1), the analyzed LAMP2A from most of the vertebrates also carry the motifs necessary for substrate recognition and binding.

4.2.3. Glycine Residues in the Transmembrane Region

The GAALAG motif, located at the TM region of LAMP2A (382–387 in *H. sapiens*), is known to be involved in dimerization. More precisely, it is important for the oligomerization of LAMP2A and, consequently, for the translocation of target proteins inside lysosomes [71]. Site-directed mutagenesis of the two glycine (G) residues to alanine (A) has been shown to impair the oligomerization of LAMP2A and, by implication, substrates translocation [5,64,71]. Recently, an in-depth analysis of the coding sequences of LAMP2A from 45 mammalian species belonging to the nine major placental orders (*Chiroptera*, *Carnivora*, *Perissodactyla*, *Artiodactyla*, *Soricomorpha*, *Erinaceomorpha*, *Primates*, *Lagomorpha*, and *Rodentia*) and three marsupials reported that these two glycines are indeed conserved across mammals [72]. While few exceptions should be noticed in the star-nosed mole (*C. cristata*), for which the second glycine is substituted by an isoleucine, in two megabats, *P. alecto* and *P. vampyrus*, as well as in the *Muridae* family of rodents, *M. musculus*, *M. pahari*, *R. norvegicus*, and *M. caroli*, species for which the motif is converted to GTALAG and GAALGG, respectively, it is not clear whether these variations do significantly affect the dimerization and function of LAMP2A. Nevertheless, the overall high preservation of the GAALAG motif within the vertebrate clade would support purifying selection during evolution.

Two glycines are also found in the TM region of LAMP2A in three fish species analyzed (spotted garfish, European eel, and arowana). However, one of these two glycines are absent in all other fish considered in our analyses, supporting the existence of functional variation of LAMP2As between species. Nevertheless, effects related to a single glycine mutation have so far not been reported.

4.2.4. The LAMP Domains

In mammals, all LAMP2 proteins (B, A, and C) display two conserved domains—the LAMP domains—being both located in the intra luminal compartment of the lysosomes (Figure 4A). Data reporting on the possible role(s) of these two domains (N- and C- domains) are sparse, but a recent study suggests that the N-domain may act as a negative regulator of the (self)multimerization step between LAMP2 proteins [65]. Interestingly, sequence analysis of the different LAMP2As retrieved from the above-mentioned [72] placental mammals clearly indicates that the N-domain is less conserved compared to the second luminal C-domain. The same holds when compared to the TM and CT regions. These results suggest that a relaxation of the purifying selection may have occurred for this distal luminal domain, allowing it to harbor functional diversity during mammalian evolution. In this regard, it is noteworthy that, in fish species belonging to the Ostariophyses (including zebrafish), this luminal N-domain displays major structural variations (Figure 7), further supporting the possibility that it may play an important role

accounting for the functional variation of LAMP2A between vertebrates. However, further functional analyses will be required to support this hypothesis.

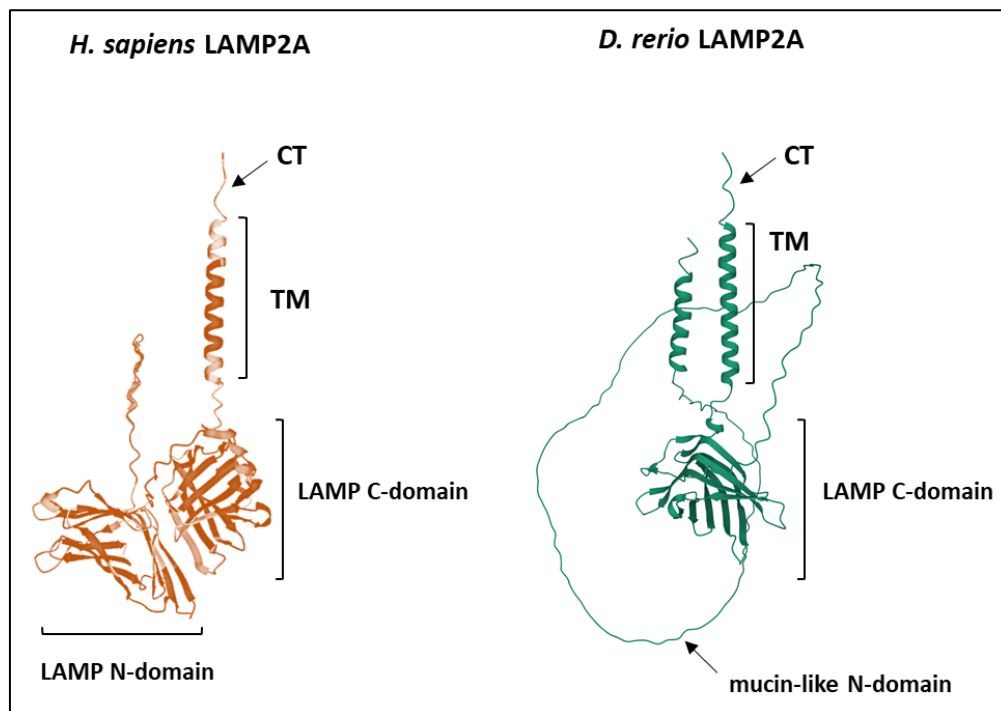


Figure 7. Structure prediction of *Homo sapiens* and *Danio rerio* LAMP2As showing the strong structural divergence of the two proteins at the membrane-distal LAMP domain (Source: AlphaFold Protein Structure Database [73,74]). Instead of a beta-sheet structure classically observed in most vertebrates, the zebrafish N-domain exhibits a mucin-like structure. CT, cytoplasmic tail; TM, transmembrane domain; LAMP C-domain, membrane-proximal LAMP domain; LAMP N-domain, membrane-distal LAMP domain.

Overall, these data show that the sequences of LAMP2As from different vertebrates contain the motifs necessary for (i) addressing the lysosomal membrane, (ii) recognizing the substrates to be degraded, and (iii) acquiring the conformation necessary for translocation across the lysosomal membrane. It thus suggests that most vertebrates may have a CMA (or CMA-like) activity similar to that described in humans and mice (and recently in fish). However, depending on the species considered, these motifs nevertheless harbor numerous variations compared to the “canonical” human or mice LAMP2As. Which residues are dispensable, required, or absolutely crucial for the proper functioning of LAMP2A remain to be functionally tested.

5. Concluding Remarks and Pending Questions

In mammals, the coexistence of CMA and eMI, both of which rely on the recognition of a KFERQ-like motif by the chaperone HSC70, raises many questions dealing with the respective roles of these two pathways and their interplay [9]. However, this dichotomic picture does not seem to apply to all species, and the presence of only one of both functions, or even none of them, has already been reported in some organisms [22]. Such a diversity of situations offers the opportunity to better appreciate the respective role(s) of each of these functions independently and from a comparative/evolutionary point of view. However, it also raises fundamental questions about the evolutionary history of these two functions: when did they appear? How did they evolve? How did they conjointly evolve? Can they functionally substitute each other?

Overall, the data we aggregated in the present review provide unequivocal evidence that the *LAMP2* gene appeared at the onset of vertebrate radiation [13], de facto indicating that CMA (as currently described) is specific to this lineage.

However, the existing sequence variability within the different functional domains of LAMP2A between phylogenetically distant vertebrates may suggest that CMA function has evolved differently between species, ultimately resulting in a variety of different cellular/physiological functions. In the future, the study of the structure/function relationship of LAMP2A in diverse vertebrates will certainly help decipher the functional importance of the several different domains of this protein and, more generally, will provide new insights into the species-specificities of this function in non-mammalian species.

The origin and the evolutionary trajectory of eMI are not that straightforward. Indeed, although most of the core proteins/components of eMI (including the chaperone HSC70, KFERQ-motif containing proteins, as well as major components of the ESCRT machinery) are already present at the onset of eukaryotic evolution, functional validations of this function (as currently defined) have only been provided for mice and *Drosophila* [8,14]. On the other hand, the existence of an ESCRT-dependent eMI-like process has been reported in fission yeast (*S. pombe*), arguing for a much more ancient origin of this process [15]. However, and unlike the eMI process described in mammals and *Drosophila*, the yeast pathway does not rely on HSC70, suggesting that these should be considered as two distinct mechanisms. Hence, the question of the origin and evolution of the eMI still remains open and will certainly provide new exciting avenues for autophagy research in the next coming years.

Author Contributions: Conceptualization, I.S. and A.H.; writing—original draft preparation, S.S. M.G., and E.J.V.; writing—review and editing, F.B., A.D., I.S. and A.H.; visualization, S.S., M.G. and E.J.V.; supervision, I.S. and A.H.; project administration, I.S.; funding acquisition, I.S. All authors have read and agreed to the published version of the manuscript.

Funding: This work was supported by (i) I-site E2S: Energy and Environmental Solutions from the University of Pau and Pays de l'Adour (S.S., PhD fellowship: UPPA contract 2020-11); (ii) La Communauté d'Agglomération Pays Basque (M.G., PhD fellowship: INRAE contract 00004643); (iii) FONDS EUROPEEN POUR LES AFFAIRES MARITIMES ET LA PECHE (VITASWEET project n° PFEA470019FA1000005). This work was additionally supported by the TUNESAL (Research Project- HAVBRUK2, PN: 294971) and AquaExcel3.0 (Grant Agreement No. 871108) projects to AH, AD and IS.

Institutional Review Board Statement: Not applicable.

Informed Consent Statement: Not applicable.

Data Availability Statement: Not applicable.

Conflicts of Interest: The authors declare no conflict of interest.

References

1. Chiang, H.L.; Dice, J.F. Peptide Sequences That Target Proteins for Enhanced Degradation during Serum Withdrawal. *J. Biol. Chem.* **1988**, *263*, 6797–6805. [[CrossRef](#)]
2. Chiang, H.L.; Terlecky, S.R.; Plant, C.P.; Dice, J.F. A Role for a 70-Kilodalton Heat Shock Protein in Lysosomal Degradation of Intracellular Proteins. *Science* **1989**, *246*, 382–385. [[CrossRef](#)] [[PubMed](#)]
3. Agarraberes, F.A.; Dice, J.F. A Molecular Chaperone Complex at the Lysosomal Membrane Is Required for Protein Translocation. *J. Cell Sci.* **2001**, *114*, 2491–2499. [[CrossRef](#)] [[PubMed](#)]
4. Cuervo, A.M.; Dice, J.F. A Receptor for the Selective Uptake and Degradation of Proteins by Lysosomes. *Science* **1996**, *273*, 501–503. [[CrossRef](#)]
5. Bandyopadhyay, U.; Kaushik, S.; Varticovski, L.; Cuervo, A.M. The Chaperone-Mediated Autophagy Receptor Organizes in Dynamic Protein Complexes at the Lysosomal Membrane. *Mol. Cell. Biol.* **2008**, *28*, 5747–5763. [[CrossRef](#)]
6. Bandyopadhyay, U.; Sridhar, S.; Kaushik, S.; Kiffin, R.; Cuervo, A.M. Identification of Regulators of Chaperone-Mediated Autophagy. *Mol. Cell* **2010**, *39*, 535–547. [[CrossRef](#)]
7. Kaushik, S.; Cuervo, A.M. The Coming of Age of Chaperone-Mediated Autophagy. *Nat. Rev. Mol. Cell Biol.* **2018**, *19*, 365–381. [[CrossRef](#)]

8. Sahu, R.; Kaushik, S.; Clement, C.C.; Cannizzo, E.S.; Scharf, B.; Follenzi, A.; Potolicchio, I.; Nieves, E.; Cuervo, A.M.; Santambrogio, L. Microautophagy of Cytosolic Proteins by Late Endosomes. *Dev. Cell* **2011**, *20*, 131–139. [[CrossRef](#)]
9. Tekirdag, K.; Cuervo, A.M. Chaperone-Mediated Autophagy and Endosomal Microautophagy: Joint by a Chaperone. *J. Biol. Chem.* **2018**, *293*, 5414–5424. [[CrossRef](#)]
10. Morozova, K.; Clement, C.C.; Kaushik, S.; Stiller, B.; Arias, E.; Ahmad, A.; Rauch, J.N.; Chatterjee, V.; Melis, C.; Scharf, B.; et al. Structural and Biological Interaction of Hsc-70 Protein with Phosphatidylserine in Endosomal Microautophagy. *J. Biol. Chem.* **2016**, *291*, 18096–18106. [[CrossRef](#)]
11. Caballero, B.; Wang, Y.; Diaz, A.; Tasset, I.; Juste, Y.R.; Stiller, B.; Mandelkow, E.-M.; Mandelkow, E.; Cuervo, A.M. Interplay of Pathogenic Forms of Human Tau with Different Autophagic Pathways. *Aging Cell* **2018**, *17*, e12692. [[CrossRef](#)]
12. Caballero, B.; Bourdenx, M.; Luengo, E.; Diaz, A.; Sohn, P.D.; Chen, X.; Wang, C.; Juste, Y.R.; Wegmann, S.; Patel, B.; et al. Acetylated Tau Inhibits Chaperone-Mediated Autophagy and Promotes Tau Pathology Propagation in Mice. *Nat. Commun.* **2021**, *12*, 2238. [[CrossRef](#)] [[PubMed](#)]
13. Lescat, L.; Véron, V.; Mourot, B.; Péron, S.; Chenais, N.; Dias, K.; Riera-Heredia, N.; Beaumatin, F.; Pinel, K.; Priault, M.; et al. Chaperone-Mediated Autophagy in the Light of Evolution: Insight from Fish. *Mol. Biol. Evol.* **2020**, *37*, 2887–2899. [[CrossRef](#)] [[PubMed](#)]
14. Mukherjee, A.; Patel, B.; Koga, H.; Cuervo, A.M.; Jenny, A. Selective Endosomal Microautophagy Is Starvation-Inducible in *Drosophila*. *Autophagy* **2016**, *12*, 1984–1999. [[CrossRef](#)] [[PubMed](#)]
15. Liu, X.-M.; Sun, L.-L.; Hu, W.; Ding, Y.-H.; Dong, M.-Q.; Du, L.-L. ESCRTs Cooperate with a Selective Autophagy Receptor to Mediate Vacuolar Targeting of Soluble Cargos. *Mol. Cell* **2015**, *59*, 1035–1042. [[CrossRef](#)]
16. Lescat, L.; Herpin, A.; Mourot, B.; Véron, V.; Guiguen, Y.; Bobe, J.; Seiliez, I. CMA Restricted to Mammals and Birds: Myth or Reality? *Autophagy* **2018**, *14*, 1267–1270. [[CrossRef](#)] [[PubMed](#)]
17. Dice, J.F. Peptide Sequences That Target Cytosolic Proteins for Lysosomal Proteolysis. *Trends Biochem. Sci.* **1990**, *15*, 305–309. [[CrossRef](#)]
18. Lv, L.; Li, D.; Zhao, D.; Lin, R.; Chu, Y.; Zhang, H.; Zha, Z.; Liu, Y.; Li, Z.; Xu, Y.; et al. Acetylation Targets the M2 Isoform of Pyruvate Kinase for Degradation through Chaperone-Mediated Autophagy and Promotes Tumor Growth. *Mol. Cell* **2011**, *42*, 719–730. [[CrossRef](#)]
19. Kaushik, S.; Cuervo, A.M. Degradation of Lipid Droplet-Associated Proteins by Chaperone-Mediated Autophagy Facilitates Lipolysis. *Nat. Cell Biol.* **2015**, *17*, 759–770. [[CrossRef](#)]
20. Bonhoure, A.; Vallentin, A.; Martin, M.; Senff-Ribeiro, A.; Amson, R.; Telerman, A.; Vidal, M. Acetylation of Translationally Controlled Tumor Protein Promotes Its Degradation through Chaperone-Mediated Autophagy. *Eur. J. Cell Biol.* **2017**, *96*, 83–98. [[CrossRef](#)]
21. Jackson, M.P.; Hewitt, E.W. Cellular Proteostasis: Degradation of Misfolded Proteins by Lysosomes. *Essays Biochem.* **2016**, *60*, 173–180. [[CrossRef](#)] [[PubMed](#)]
22. Kirchner, P.; Bourdenx, M.; Madrigal-Matute, J.; Tian, S.; Diaz, A.; Bartholdy, B.A.; Will, B.; Cuervo, A.M. Proteome-Wide Analysis of Chaperone-Mediated Autophagy Targeting Motifs. *PLoS Biol.* **2019**, *17*, e3000301. [[CrossRef](#)] [[PubMed](#)]
23. Stricher, F.; Macri, C.; Ruff, M.; Muller, S. HSPA8/HSC70 Chaperone Protein: Structure, Function, and Chemical Targeting. *Autophagy* **2013**, *9*, 1937–1954. [[CrossRef](#)] [[PubMed](#)]
24. Liao, Y.; Tang, L. The Critical Roles of HSC70 in Physiological and Pathological Processes. *Curr. Pharm. Des.* **2014**, *20*, 101–107. [[CrossRef](#)] [[PubMed](#)]
25. Bonam, S.R.; Ruff, M.; Muller, S. HSPA8/HSC70 in Immune Disorders: A Molecular Rheostat That Adjusts Chaperone-Mediated Autophagy Substrates. *Cells* **2019**, *8*, E849. [[CrossRef](#)]
26. Gupta, R.S.; Singh, B. Phylogenetic Analysis of 70 KD Heat Shock Protein Sequences Suggests a Chimeric Origin for the Eukaryotic Cell Nucleus. *Curr. Biol.* **1994**, *4*, 1104–1114. [[CrossRef](#)]
27. Hunt, C.; Morimoto, R.I. Conserved Features of Eukaryotic Hsp70 Genes Revealed by Comparison with the Nucleotide Sequence of Human Hsp70. *Proc. Natl. Acad. Sci. USA* **1985**, *82*, 6455–6459. [[CrossRef](#)]
28. Lindquist, S.; Craig, E.A. The Heat-Shock Proteins. *Annu. Rev. Genet.* **1988**, *22*, 631–677. [[CrossRef](#)]
29. Pan, Z.; Zhang, Z.; Zhuo, L.; Wan, T.; Li, Y. Bioinformatic and Functional Characterization of Hsp70s in *Myxococcus Xanthus*. *mSphere* **2021**, *6*, e00305-21. [[CrossRef](#)]
30. Werner-Washburne, M.; Craig, E.A. Expression of Members of the *Saccharomyces Cerevisiae* Hsp70 Multigene Family. *Genome* **1989**, *31*, 684–689. [[CrossRef](#)]
31. Boorstein, W.R.; Ziegelhoffer, T.; Craig, E.A. Molecular Evolution of the HSP70 Multigene Family. *J. Mol. Evol.* **1994**, *38*, 1–17. [[CrossRef](#)] [[PubMed](#)]
32. Yu, E.; Yoshinaga, T.; Jalufka, F.L.; Ehsan, H.; Welch, D.B.M.; Kaneko, G. The Complex Evolution of the Metazoan HSP70 Gene Family. *Sci. Rep.* **2021**, *11*, 17794. [[CrossRef](#)] [[PubMed](#)]

33. Hess, K.; Oliverio, R.; Nguyen, P.; Le, D.; Ellis, J.; Kdeiss, B.; Ord, S.; Chalkia, D.; Nikolaidis, N. Concurrent Action of Purifying Selection and Gene Conversion Results in Extreme Conservation of the Major Stress-Inducible Hsp70 Genes in Mammals. *Sci. Rep.* **2018**, *8*, 5082. [[CrossRef](#)] [[PubMed](#)]
34. Nikolaidis, N.; Nei, M. Concerted and Nonconcerted Evolution of the Hsp70 Gene Superfamily in Two Sibling Species of Nematodes. *Mol. Biol. Evol.* **2004**, *21*, 498–505. [[CrossRef](#)] [[PubMed](#)]
35. Kourtidis, A.; Drosopoulou, E.; Nikolaidis, N.; Hatzi, V.I.; Chintiroglou, C.C.; Scouras, Z.G. Identification of Several Cytoplasmic HSP70 Genes from the Mediterranean Mussel (*Mytilus Galloprovincialis*) and Their Long-Term Evolution in Mollusca and Metazoa. *J. Mol. Evol.* **2006**, *62*, 446–459. [[CrossRef](#)]
36. Krenek, S.; Schlegel, M.; Berendonk, T.U. Convergent Evolution of Heat-Inducibility during Subfunctionalization of the Hsp70 Gene Family. *BMC Evol. Biol.* **2013**, *13*, 49. [[CrossRef](#)]
37. Marzella, L.; Ahlberg, J.; Glaumann, H. Autophagy, Heterophagy, Microautophagy and Crinophagy as the Means for Intracellular Degradation. *Virchows Arch. B Cell Pathol. Incl. Mol. Pathol.* **1981**, *36*, 219–234. [[CrossRef](#)]
38. Mortimore, G.E.; Lardeux, B.R.; Adams, C.E. Regulation of Microautophagy and Basal Protein Turnover in Rat Liver. Effects of Short-Term Starvation. *J. Biol. Chem.* **1988**, *263*, 2506–2512. [[CrossRef](#)]
39. Tuttle, D.L.; Lewin, A.S.; Dunn, W.A. Selective Autophagy of Peroxisomes in Methylotrophic Yeasts. *Eur. J. Cell Biol.* **1993**, *60*, 283–290.
40. Sakai, Y.; Koller, A.; Rangell, L.K.; Keller, G.A.; Subramani, S. Peroxisome Degradation by Microautophagy in *Pichia Pastoris*: Identification of Specific Steps and Morphological Intermediates. *J. Cell Biol.* **1998**, *141*, 625–636. [[CrossRef](#)]
41. Campbell, C.L.; Thorsness, P.E. Escape of Mitochondrial DNA to the Nucleus in Yme1 Yeast Is Mediated by Vacuolar-Dependent Turnover of Abnormal Mitochondrial Compartments. *J. Cell Sci.* **1998**, *111*, 2455–2464. [[CrossRef](#)]
42. Roberts, P.; Moshitch-Moshkovitz, S.; Kvam, E.; O'Toole, E.; Winey, M.; Goldfarb, D.S. Piecemeal Microautophagy of Nucleus in *Saccharomyces Cerevisiae*. *Mol. Biol. Cell* **2003**, *14*, 129–141. [[CrossRef](#)] [[PubMed](#)]
43. Van Zutphen, T.; Todde, V.; de Boer, R.; Kreim, M.; Hofbauer, H.F.; Wolinski, H.; Veenhuis, M.; van der Klei, I.J.; Kohlwein, S.D. Lipid Droplet Autophagy in the Yeast *Saccharomyces Cerevisiae*. *Mol. Biol. Cell* **2014**, *25*, 290–301. [[CrossRef](#)] [[PubMed](#)]
44. Schuck, S.; Gallagher, C.M.; Walter, P. ER-Phagy Mediates Selective Degradation of Endoplasmic Reticulum Independently of the Core Autophagy Machinery. *J. Cell Sci.* **2014**, *127*, 4078–4088. [[CrossRef](#)] [[PubMed](#)]
45. Yang, X.; Zhang, W.; Wen, X.; Bulinski, P.J.; Chomchai, D.A.; Arines, F.M.; Liu, Y.-Y.; Sprenger, S.; Teis, D.; Klionsky, D.J.; et al. TORC1 Regulates Vacuole Membrane Composition through Ubiquitin- and ESCRT-Dependent Microautophagy. *J. Cell Biol.* **2020**, *219*, e201902127. [[CrossRef](#)]
46. Schuck, S. Microautophagy—Distinct Molecular Mechanisms Handle Cargoes of Many Sizes. *J. Cell Sci.* **2020**, *133*, jcs246322. [[CrossRef](#)]
47. Mesquita, A.; Glenn, J.; Jenny, A. Differential Activation of EMI by Distinct Forms of Cellular Stress. *Autophagy* **2021**, *17*, 1828–1840. [[CrossRef](#)]
48. Uytterhoeven, V.; Lauwers, E.; Maes, I.; Miskiewicz, K.; Melo, M.N.; Swerts, J.; Kuenen, S.; Wittcox, R.; Corthout, N.; Marrink, S.-J.; et al. Hsc70-4 Deforms Membranes to Promote Synaptic Protein Turnover by Endosomal Microautophagy. *Neuron* **2015**, *88*, 735–748. [[CrossRef](#)]
49. Leung, K.F.; Dacks, J.B.; Field, M.C. Evolution of the Multivesicular Body ESCRT Machinery; Retention Across the Eukaryotic Lineage. *Traffic* **2008**, *9*, 1698–1716. [[CrossRef](#)]
50. Spang, A.; Saw, J.H.; Jørgensen, S.L.; Zaremba-Niedzwiedzka, K.; Martijn, J.; Lind, A.E.; van Eijk, R.; Schleper, C.; Guy, L.; Ettema, T.J.G. Complex Archaea That Bridge the Gap between Prokaryotes and Eukaryotes. *Nature* **2015**, *521*, 173–179. [[CrossRef](#)]
51. Hatano, T.; Palani, S.; Papatziadou, D.; Salzer, R.; Souza, D.P.; Tamarit, D.; Makwana, M.; Potter, A.; Haig, A.; Xu, W.; et al. Asgard Archaea Shed Light on the Evolutionary Origins of the Eukaryotic Ubiquitin-ESCRT Machinery. *Nat. Commun.* **2022**, *13*, 3398. [[CrossRef](#)] [[PubMed](#)]
52. Cuervo, A.M.; Dice, J.F. Unique Properties of Lamp2a Compared to Other Lamp2 Isoforms. *J. Cell Sci.* **2000**, *113*, 4441–4450. [[CrossRef](#)] [[PubMed](#)]
53. Gough, N.R.; Hatem, C.L.; Fambrough, D.M. The Family of LAMP-2 Proteins Arises by Alternative Splicing from a Single Gene: Characterization of the Avian LAMP-2 Gene and Identification of Mammalian Homologs of LAMP-2b and LAMP-2c. *DNA Cell Biol.* **1995**, *14*, 863–867. [[CrossRef](#)] [[PubMed](#)]
54. Hatem, C.L.; Gough, N.R.; Fambrough, D.M. Multiple MRNAs Encode the Avian Lysosomal Membrane Protein LAMP-2, Resulting in Alternative Transmembrane and Cytoplasmic Domains. *J. Cell Sci.* **1995**, *108*, 2093–2100. [[CrossRef](#)] [[PubMed](#)]
55. Nishino, I.; Fu, J.; Tanji, K.; Yamada, T.; Shimojo, S.; Koori, T.; Mora, M.; Riggs, J.E.; Oh, S.J.; Koga, Y.; et al. Primary LAMP-2 Deficiency Causes X-Linked Vacuolar Cardiomyopathy and Myopathy (Danon Disease). *Nature* **2000**, *406*, 906–910. [[CrossRef](#)]

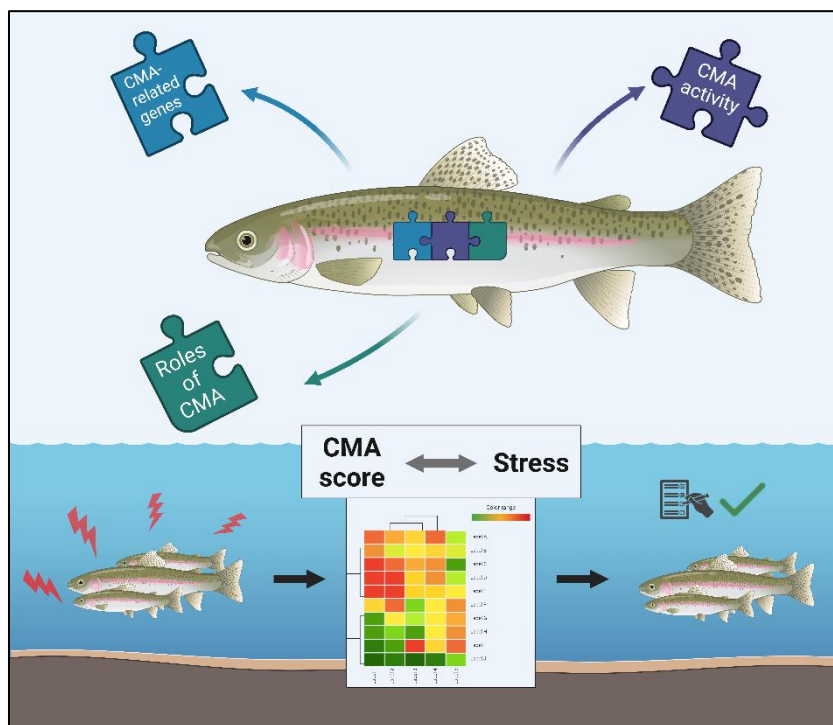
56. Chi, C.; Leonard, A.; Knight, W.E.; Beussman, K.M.; Zhao, Y.; Cao, Y.; Londono, P.; Aune, E.; Trembley, M.A.; Small, E.M.; et al. LAMP-2B Regulates Human Cardiomyocyte Function by Mediating Autophagosome–Lysosome Fusion. *Proc. Natl. Acad. Sci. USA* **2019**, *116*, 556–565. [[CrossRef](#)]
57. Fujiwara, Y.; Furuta, A.; Kikuchi, H.; Aizawa, S.; Hatanaka, Y.; Konya, C.; Uchida, K.; Yoshimura, A.; Tamai, Y.; Wada, K.; et al. Discovery of a Novel Type of Autophagy Targeting RNA. *Autophagy* **2013**, *9*, 403–409. [[CrossRef](#)]
58. Fujiwara, Y.; Kikuchi, H.; Aizawa, S.; Furuta, A.; Hatanaka, Y.; Konya, C.; Uchida, K.; Wada, K.; Kabuta, T. Direct Uptake and Degradation of DNA by Lysosomes. *Autophagy* **2013**, *9*, 1167–1171. [[CrossRef](#)]
59. Dehal, P.; Boore, J.L. Two Rounds of Whole Genome Duplication in the Ancestral Vertebrate. *PLoS Biol.* **2005**, *3*, e314. [[CrossRef](#)]
60. Ravi, V.; Venkatesh, B. The Divergent Genomes of Teleosts. *Annu. Rev. Anim. Biosci.* **2018**, *6*, 47–68. [[CrossRef](#)]
61. Pasquier, J.; Cabau, C.; Nguyen, T.; Jouanno, E.; Severac, D.; Braasch, I.; Journot, L.; Pontarotti, P.; Klopp, C.; Postlethwait, J.H.; et al. Gene Evolution and Gene Expression after Whole Genome Duplication in Fish: The PhyloFish Database. *BMC Genom.* **2016**, *17*, 368. [[CrossRef](#)] [[PubMed](#)]
62. Terasawa, K.; Kato, Y.; Ikami, Y.; Sakamoto, K.; Ohtake, K.; Kusano, S.; Tomabechei, Y.; Kukimoto-Niino, M.; Shirouzu, M.; Guan, J.-L.; et al. Direct Homophilic Interaction of LAMP2A with the Two-Domain Architecture Revealed by Site-Directed Photo-Crosslinks and Steric Hindrances in Mammalian Cells. *Autophagy* **2021**, *17*, 4286–4304. [[CrossRef](#)] [[PubMed](#)]
63. Wilke, S.; Krausze, J.; Büsow, K. Crystal Structure of the Conserved Domain of the DC Lysosomal Associated Membrane Protein: Implications for the Lysosomal Glycocalyx. *BMC Biol.* **2012**, *10*, 62. [[CrossRef](#)]
64. Rout, A.K.; Strub, M.-P.; Piszczek, G.; Tjandra, N. Structure of Transmembrane Domain of Lysosome-Associated Membrane Protein Type 2a (LAMP-2A) Reveals Key Features for Substrate Specificity in Chaperone-Mediated Autophagy. *J. Biol. Chem.* **2014**, *289*, 35111–35123. [[CrossRef](#)] [[PubMed](#)]
65. Terasawa, K.; Tomabechei, Y.; Ikeda, M.; Ehara, H.; Kukimoto-Niino, M.; Wakiyama, M.; Podyma-Inoue, K.A.; Rajapakshe, A.R.; Watabe, T.; Shirouzu, M.; et al. Lysosome-Associated Membrane Proteins-1 and -2 (LAMP-1 and LAMP-2) Assemble via Distinct Modes. *Biochem. Biophys. Res. Commun.* **2016**, *479*, 489–495. [[CrossRef](#)] [[PubMed](#)]
66. Ikami, Y.; Terasawa, K.; Sakamoto, K.; Ohtake, K.; Harada, H.; Watabe, T.; Yokoyama, S.; Hara-Yokoyama, M. The Two-Domain Architecture of LAMP2A Regulates Its Interaction with Hsc70. *Exp. Cell Res.* **2022**, *411*, 112986. [[CrossRef](#)]
67. Williams, M.A.; Fukuda, M. Accumulation of Membrane Glycoproteins in Lysosomes Requires a Tyrosine Residue at a Particular Position in the Cytoplasmic Tail. *J. Cell Biol.* **1990**, *111*, 955–966. [[CrossRef](#)]
68. Guarnieri, F.G.; Arterburn, L.M.; Penno, M.B.; Cha, Y.; August, J.T. The Motif Tyr-X-X-Hydrophobic Residue Mediates Lysosomal Membrane Targeting of Lysosome-Associated Membrane Protein 1. *J. Biol. Chem.* **1993**, *268*, 1941–1946. [[CrossRef](#)]
69. Hunziker, W.; Harter, C.; Matter, K.; Mellman, I. Basolateral Sorting in MDCK Cells Requires a Distinct Cytoplasmic Domain Determinant. *Cell* **1991**, *66*, 907–920. [[CrossRef](#)]
70. Harter, C.; Mellman, I. Transport of the Lysosomal Membrane Glycoprotein Lgp120 (Lgp-A) to Lysosomes Does Not Require Appearance on the Plasma Membrane. *J. Cell Biol.* **1992**, *117*, 311–325. [[CrossRef](#)]
71. Russ, W.P.; Engelman, D.M. The GxxxG Motif: A Framework for Transmembrane Helix-Helix Association. *J. Mol. Biol.* **2000**, *296*, 911–919. [[CrossRef](#)] [[PubMed](#)]
72. Jalali, Z.; Parvaz, N. Molecular Evolution of Autophagy Rate-Limiting Factor LAMP2 in Placental Mammals. *Gene* **2020**, *727*, 144231. [[CrossRef](#)] [[PubMed](#)]
73. Jumper, J.; Evans, R.; Pritzel, A.; Green, T.; Figurnov, M.; Ronneberger, O.; Tunyasuvunakool, K.; Bates, R.; Židek, A.; Potapenko, A.; et al. Highly Accurate Protein Structure Prediction with AlphaFold. *Nature* **2021**, *596*, 583–589. [[CrossRef](#)] [[PubMed](#)]
74. Varadi, M.; Anyango, S.; Deshpande, M.; Nair, S.; Natassia, C.; Yordanova, G.; Yuan, D.; Stroe, O.; Wood, G.; Laydon, A.; et al. AlphaFold Protein Structure Database: Massively Expanding the Structural Coverage of Protein-Sequence Space with High-Accuracy Models. *Nucleic Acids Res.* **2022**, *50*, D439–D444. [[CrossRef](#)] [[PubMed](#)]

PUBLICATION 2: Chaperone-Mediated Autophagy in Fish: A Key Function Amid a Changing Environment

Objectives

After having shown that core components of CMA are present in the RT's genome, the first objectives were to characterize the expression of CMA-related factors and demonstrate the existence of CMA activity. Subsequently, by using the gene-editing tool CRISPR-Cas9 and deleting the most expressed of the 2 *lamp2a* present in the RT, the roles of CMA in this species could be addressed. Given the potential activation of CMA in stressful situations, we aimed at adapting a tool based on CMA-related factors gene expression as a proxy for stress and resilience.

Main results and conclusions



- CMA-related factors are ubiquitously expressed during early development as well as in several adult tissues of RT. Furthermore, RT exhibits CMA activity, which increases 21-fold during nutrient deprivation, a known CMA inducer.
- Knockout (KO) RTs lacking Lamp2A show significant physiological alterations under stress, including enhanced body size and altered organ indices, as well as substantial remodeling of the liver proteome.
- As CMA is necessary against oxidative stress, we propose the use of the CMA activation score as a potential biomarker for assessing fish homeostasis.

Chaperone-Mediated Autophagy in Fish: A Key Function Amid a Changing Environment

Simon Schnebert¹, Emilio J Vélez¹, Maxime Goguet¹, Karine Dias¹, Vincent Véron¹, Isabel García-Pérez¹, Lisa M Radler², Emilie Cardona¹, Stéphanie Fontagné-Dicharry¹, Pierre Van Delft³, Franziska Dittrich-Domergue³, Amélie Bernard³, Florian Beaumatin¹, Amaury Herpin⁴, Beth Cleveland², #, Iban Seiliez¹, #, *

¹Université de Pau et des Pays de l'Adour, E2S UPPA, INRAE, UMR1419 Nutrition Métabolisme et Aquaculture, F-64310 Saint-Pée-sur-Nivelle, France.

²National Center for Cool and Cold Water Aquaculture, ARS/USDA, 11861 Leetown Rd, 25430 Kearneysville, WV, USA.

³Laboratoire de Biogenèse Membranaire, UMR 5200, CNRS, Univ. Bordeaux, F-33140, Villenave d'Ornon, France.

⁴INRAE, UR1037 Laboratory of Fish Physiology and Genomics, Campus de Beaulieu, Rennes, F-35042, France.

These authors contributed equally to this work.

*Corresponding author:

Iban SEILIEZ

INRAE, UMR1419 NuMeA,

F64310 Saint Pée sur Nivelle, France.

Tel: (33) 5 59 51 59 99; Fax: (33) 5 59 54 51 52

Email: iban.seiliez@inrae.fr

Author Contributions: I.S. and B.C. got the funding; S.S., B.C. and I.S. conceived and planned the study; S.S., K.D., V.V., I-G.P., L.M.R., E.C., B.C., F.D., P.V.D. and A.B. performed the experiments; S.S. and I.S. analyzed the data; S.S., E.J.V., K.D., V.V., I-G.P., M.G., F.B., A.H., S.F-D., B.C. and I.S. discussed the data and future experiments; S.S. and I.S. wrote the original draft of the manuscript; S.S., E.J.V., F.B., A.H., M.G., B.C. and I.S. reviewed and edited the final version of the manuscript; I.S. and B.C. supervised the project and had primary responsibility for final content.

Competing Interest Statement: The authors declare no competing financial interests.

Classification: Biological sciences, cell biology.

Keywords: Chaperone-mediated autophagy; fish; Rainbow Trout; metabolism; stress; environment; CMA score

This file includes: Main Text; Figures 1 to 6

Abstract

Chaperone-mediated Autophagy (CMA) is a prominent lysosomal-dependent pathway responsible for protein degradation, maintaining cellular proteostasis in the face of various stressors like starvation, oxidative stress, and hypoxia. While extensively studied in mammals, CMA's existence in fish has only been confirmed recently, offering exciting insights into its role in species facing environmental stress. In this study, we first show that CMA-related factors are ubiquitously expressed during early development as well as in several adult tissues of rainbow trout (RT, *Oncorhynchus mykiss*), a species of both economic and ecological importance. In order to firmly establish the existence of functional CMA activity in this species, we then performed an in vitro CMA activity assay using isolated lysosomes. Our results show that RT undoubtedly exhibits CMA activity, which increases 21-fold during nutrient deprivation, a known CMA inducer. Finally, we used the CRISPR-Cas9 genome editing tool to generate a knock-out (KO) line lacking a key CMA rate-limiting protein, the lysosome-associated membrane protein 2A (Lamp2A). Lamp2A KO fish showed significant physiological alterations, including enhanced body size and altered organ indices, as well as substantial remodeling of the liver proteome. Furthermore, we propose the use of the CMA activation score as a potential biomarker for assessing fish cellular homeostasis, given its demonstrated involvement in stress response. Altogether, our data shows that in addition to being present in RT, CMA shapes a distinct part of the proteome related to major metabolic pathways, emphasizing its crucial role in evaluating the impact of environmental threats on fish.

Significance Statement

While CMA is extensively studied in the medical realm, its potential implications in environmental contexts remain unexplored. Our study fills this knowledge gap by demonstrating the existence and significance of CMA as a metabolic gatekeeper in rainbow trout (*Oncorhynchus mykiss*) exposed to an acute stress. Additionally, we uncovered the potential utility of CMA as a biomarker for assessing cellular homeostasis in fish. The data gathered in our current study provides a completely novel evolutionary perspective on CMA research. It bridges the domains of cell biology and ecological science, and has the potential to advance our understanding of cellular homeostasis for species facing increasing environmental challenges.

Introduction

The higher frequency of extreme climate events is likely to have an impact on fish populations, production and fisheries by causing a shift in their physiology thus survival^{1,2}. Parameters such as

growth³, osmotic balance⁴, reproduction⁵, and cellular processes⁶ are directly affected. Cellular homeostasis is hence key for resisting environmental stressors coming fish's way, and finding new ways of gauging it have become urgent.

In mammals, a lysosomal degradative process called autophagy involved in the recycling of proteins, damaged organelles and defense against pathogens is crucial to cellular homeostasis⁷. One of the selective forms of autophagy, chaperone-mediated autophagy (CMA), begins when cytosolic proteins bearing a KFERQ-like motif are recognized by the heat-shock protein family A HSP70 member 8 (HSPA8/HSC70) and brought to lysosomal membrane via specific binding to lysosome-associated membrane protein 2A (LAMP2A), the rate-limiting factor in CMA⁸. LAMP2A, one of the three splice variants (LAMP2A, B and C) of the *lamp2* gene, is the only one involved in CMA^{9,10,11}. Following the binding of the substrate/chaperone complex, LAMP2A multimerizes to form a translocation complex through which the substrate translocates for intralysosomal degradation¹². KFERQ-like motifs can be found in a large subset of the eukaryotic proteome in 2 different forms: canonical and putative. Putative motifs can be turned into KFERQ-like motifs after post-translational modifications such as phosphorylation or acetylation¹³. Proteins bearing canonical or putative KFERQ-like motifs have been associated with various biological processes like metabolism, cell cycle, immune response and transcriptional regulation¹². Upon oxidative stress, nutrient deprivation, hypoxia or pathologies, enhanced CMA activity has been shown to regulate energetics and metabolic processes to maintain cellular homeostasis^{14,15}. Fine tuning of the proteome and preservation of cellular homeostasis define CMA as a major cellular function in vertebrates.

Although previously thought to be restricted to mammals and birds, CMA was recently established in fish^{16,17}. This discovery brought new perspectives for a better understanding of the mechanisms involved in the adaptation of organisms amid environmental stress. The rainbow trout (RT, *Oncorhynchus mykiss*), a widely spread salmonid commonly found in aquaculture production¹⁸, is an extensively studied model organism in physiology, genetics, behavior and ecology¹⁹. In addition to stressful environmental events it has to endure²⁰, the RT also exhibits distinctive metabolic features like a high dietary protein requirement and glucose intolerance²¹. Therefore, it is an interesting candidate organism to study CMA and its potential role in regulating the proteome, particularly proteins responsible for maintaining metabolic and cellular homeostasis.

Recently, a homology-based search unveiled the presence of two *lamp2* paralogous genes within the genome of RT, located on chromosomes 14 (C14) and 31 (C31) respectively, with both genes harboring all three alternative exons (A, B, and C)^{16,17}. Furthermore, a first glimpse of *lamp2a* splice variants expression in different fish species provided a clue to the potential existence of CMA in the RT²².

In this study, we have shown that RT has all the genetic material to express CMA machinery, particularly in tissues involved in major metabolic processes. We conducted a lysosome isolation

combined with the Glyceraldehyde-3-phosphate Dehydrogenase (GAPDH) binding/uptake assay to measure CMA activity. It revealed that RT lysosomes can translocate GAPDH, a bona fide CMA substrate, depending on the presence of HSC70 and ATP. In addition, we showed that as in mammals, nutritional status regulates CMA activity. To fully unravel the physiological functions of CMA in RT, we used the genome-editing tool CRISPR-Cas9 and generated a knock-out (KO) line lacking LAMP2A from C31, the most expressed of both isoforms. Following LAMP2A C31 deletion, RTs were significantly larger than their wild type (WT) correlates and presented heavier livers and viscera weights. To further characterize the physiological roles of CMA in RT, we then used quantitative proteomics and found that upon nutritional stress, CMA is crucial to the preservation of cellular homeostasis by regulating oxidative stress response, energetics and metabolic processes. Finally, the adaptation and validation in RT of the "CMA score", a reliable indicator of the activation status of CMA based on the expression levels of key CMA effectors and regulators as developed by Bourdenx et al. 2021¹⁵, not only introduces a novel biomarker for fish cellular homeostasis but also enables the assessment of CMA potential in emerging models. Overall, this study emphasizes the importance of considering CMA as a major function in maintaining fish cellular homeostasis, particularly amid the rising occurrence of new environmental threats.

Results

The main CMA effectors are expressed in RT

A homology-based investigation of sequences of main CMA effectors in RT's genome allowed us to investigate their expression throughout development and in different tissues of adult individuals. As presented in Fig 1A, most of core CMA genes are gradually induced from oocyte stage to maximum expression at stage 22/23, during which the primitive liver and the primitive hepatic portal vein develop in RT²⁴⁹. Both *lamp2a* paralogs from C14 and C31 were then compared and in most tissues, *lamp2a* C31 shows a higher expression (Fig 1B). Nearly all tissues displayed *lamp2a* expression, particularly liver, intestine and kidney.

Following the high mRNA expression of both *lamp2a* paralogs in liver and intestine, we conducted a BaseScope assay to address spatial expression of the transcripts. *Lamp2a* transcripts quantity and distribution were analyzed in fed and starved RT, as starvation induces maximal CMA activation¹⁸³. BaseScope signal showed that mRNA was distributed evenly across sampled liver tissue (Fig 2A). Countings confirmed previous data validating a higher expression of *lamp2a* C31 compared to *lamp2a* C14, regardless of nutritional status (Fig 2C).

In the distal part of the intestine, *lamp2a* mRNA was mostly found in enterocytes (epithelium) in contrast to lamina propria, serous and submucous layer (Fig 2B). Regarding the expression of *lamp2a* paralogs and effect of nutritional status, similar results were found in the intestine, with a higher expression of both *lamp2a* paralogs in starved conditions and *lamp2a* C31 being the most expressed transcript (Fig 2D).

The expression of CMA-related genes showed undisputable signs that RT carries all the genetic material required to express the CMA machinery, although a demonstration of its activity was required.

RT exhibits CMA-active lysosomes able to bind and uptake GAPDH

To truly grasp whether CMA is functional in RT, we referred to the gold standard for *in vivo* CMA activity quantification, which consists of measuring the binding and uptake of a given CMA substrate in isolated CMA-competent (CMA+) lysosomes²⁵⁰. In this aim, we relied on the technique described by Juste & Cuervo's²⁵¹ to isolate trout liver lysosomes. Four interphases were separated after the ultracentrifugation step theoretically containing, from top to bottom: CMA+ lysosomes, a mix population of CMA-competent and CMA-non-competent lysosomes (CMA+/- lysosomes), a mixture of lysosomes and mitochondria (Lyso/Mito) and mitochondria (Mito) (Fig 3A).

To ensure that each interphase contained its expected content, we conducted western blotting to quantify key proteins from each fraction. We first quantified Tim23, a component of the mitochondrial inner membrane²⁵². The mitochondrial fraction displayed a higher level of Tim23 compared to other phases (Figs 3B and C). We then quantified levels of lysosome-associated membrane protein 1 (Lamp1), commonly used as a lysosomal marker¹⁹⁷ as well as the CMA-key Hsc70 chaperone. We found a higher abundance of Lamp1 in fractions that contained lysosomes (Figs 3B and 3D). Interestingly, Hsc70 was present at higher levels in the CMA+ fraction than in its CMA- counterpart (Figs 3B and 3E), in accordance with the higher content of lysosomal Hsc70 in CMA+ lysosomes^{197,236}. Overall, these results clearly show that RT contains lysosomes displaying characteristics of CMA+ lysosomes.

After confidently having isolated CMA+ lysosomes, we needed to find evidence for their capacity to perform CMA. To assess CMA activity, we referred to the Juste & Cuervo's protocol, which involves testing the ability of a given CMA substrate (e.g., GAPDH) to bind to and be taken up by CMA+ lysosomes²⁵¹. Briefly, 5 different conditions were used to test CMA activity in RT (Fig 3F; quantification in Fig 3G). In condition 1, CMA+ lysosomes were left untreated. The thin GAPDH band observed by western blotting likely stems from endogenous RT GAPDH. In condition 2, we incubated CMA+ lysosomes with GAPDH. This resulted in a more pronounced band, indicating the binding of the CMA substrate to the lysosomal membrane (Figs 3F and 3G). To confirm the binding of GAPDH to the

lysosomal membrane, we then introduced proteinase K (PK) in condition 3, which degraded all proteins associated with the cytosolic side of the lysosomal membrane. Consequently, the band disappeared, validating that GAPDH binds specifically to the lysosomal membrane (Figs 3F and 3G). In condition 4, we pre-treated CMA+ lysosomes with inhibitors of lysosomal proteases to prevent the degradation of translocated substrates. This led to a stronger band compared to condition 2 (Figs 3F and 3G), providing evidence that GAPDH binds to the lysosomal membrane and is subsequently translocated inside CMA+ lysosomes. Lastly, in condition 5, CMA+ lysosomes were pre-treated with inhibitors of lysosomal proteases and then incubated with PK (Figs 3F and 3G). A thinner band appeared, which likely represents the fraction of GAPDH taken up by CMA+ lysosomes. Additionally, we were able to measure the uptake by calculating the difference in GAPDH quantity between conditions 4 (association) and 2 (binding) or through the use of PK (condition 5). No difference was found between both uptake values (Fig 3H), strengthening our results and supporting that RT exhibits CMA+ lysosomes able to bind and uptake GAPDH.

To characterize the mechanisms at play more comprehensively, we then verified whether GAPDH binding and uptake by CMA+ lysosomes depend on the presence of ATP and HSC70, as demonstrated in mammals²⁵⁰. We incubated freshly isolated RT liver CMA+ lysosomes with all factors required for binding/uptake of GAPDH and added PK to reveal uptake (Fig 3I, condition 1). In conditions 2 and 3, we repeated the treatments, but without ATP or HSC70, respectively. Our findings clearly demonstrate that GAPDH uptake was significantly diminished (if not completely suppressed) in the absence of ATP or HSC70 (Figs 3I and 3J), witnessing the essential part they play in the ability of RT CMA+ lysosomes to bind and translocate the added GAPDH.

Finally, since nutrient deprivation commonly induces CMA in mammals¹⁸³ and higher *lamp2a* gene expression was found in starved RT (Figs 2A – 2D), we investigated the effects of starvation on GAPDH uptake by RT CMA+ lysosomes. Our findings revealed that CMA+ lysosomes isolated from starved RT exhibited a significantly higher ability to uptake GAPDH compared to lysosomes from fed RT (Figs 3K and 3L), hinting at a higher CMA activity following nutrient deprivation akin to that occurring in mammals..

Taken together, these results indicate that RT contains lysosomes able to perform CMA or CMA-like activity.

Lamp2a C31 deletion leads to enhanced body size, altered organ indices, and metabolic dysregulation in RT

Having demonstrated the existence of CMA activity in RT, we then focused on unraveling its physiological role. Using the genetic tool CRISPR-Cas9, we generated RT models knocked-out for

lamp2a C31 (hereafter referred to as L2AC31-KO), as it is the most expressed of both paralogs (Figs 1B and 2A - 2D), and *lamp2a* C14's contribution to CMA appears marginal, as seen in our recent *in vitro* study²⁵³. More specifically, the generated fish line displayed a deletion of a 322 bp region in exon 9 of the *lamp2* gene (from C31) that encodes for the specific cytosolic and transmembrane domains of the Lamp2a protein (Fig 4A and S1A). As expected, levels of *lamp2a* C31 mRNA were undetectable in the tissues of L2AC31-KO RTs (Fig 4B). Surprisingly, higher expression of *lamp2a* C14 mRNA was found in L2AC31-KO RTs when compared to their WT counterparts (Fig 4C), suggesting the existence of compensatory mechanisms. Differential regulations of other *lamp2* splice variants transcripts (*lamp2b* and *lamp2c*) from both C31 and C14 were also observed (Figs S1B - S1E), in agreement with the reported specific regulation of expression of these 2 isoforms²⁰⁰, which do not participate in CMA.

To further appreciate the impact of the *lamp2a* C31 deletion on the overall CMA network, we then used the CMA score, as recently defined by Bourdenx et al²⁵⁴. The score is a weighted average of the expression level of every known effector and both positive and negative modulators of CMA (Fig S2A and Table S1), with recent studies showing that it represents a reliable proxy for CMA activation status^{236,235,234}. We first validated this score experimentally using RT cells expressing the KFERQ-PA-mCherry1 CMA reporter, a widely utilized method for monitoring CMA in mammalian cells²²⁸ and more recently validated in fish cells^{245,253}. These cells were cultured under conditions known to induce CMA activation: starvation (serum-free) and mild-oxidative stress (H₂O₂, 25 μ M) (Fig S2B). CMA activity (number of puncta/cell) was quantified after 4, 8, 16, 24 and 48h of treatment. The highest CMA activation was observed upon mild-oxidative stress and starvation at 16 hours (Figs S2C and S2D). The CMA score was then calculated at that time point using mRNA levels of all CMA network elements (Fig S2E). The significant higher CMA score encountered upon these 2 CMA activators respect to the control condition (Fig S2F) ensured its adequacy and the opportunity to use it as a potential proxy for CMA's functional output in RT as well. After we validated the CMA activation score *in vitro*, we then calculated it for liver, intestine and brain samples of WT versus L2AC31-KO RTs. We found significant decrease of the CMA score in L2AC31-KO RTs in the different tissues analyzed (Fig 4D), suggesting a decline in CMA activity following *lamp2a* C31 KO. Interestingly, we found no significant alteration in the steady state levels of LC3-II, a well-established marker for autophagosome formation²⁵⁵, in the livers of L2AC31-KO RTs compared to WT fish (Figs 4E and 4F), highlighting the suitability of these animals to study the consequences of compromised CMA activity independent of any effects induced by macroautophagy compensation.

Considering the critical role(s) of CMA in the control of hepatic metabolism^{192,245}, we then investigated the physiological consequences of *lamp2a* C31 deletion. In a first phase, we tracked the biometrical parameters/growth of both L2AC31-KO and WT fish for approximately 23 weeks, and observed that L2AC31-KO animals presented both significantly higher body weight and length than

their WT counterparts both at 97 and 159 days of rearing (Figs 4G and 4H), suggesting that the lack of Lamp2a C31 induces metabolic alterations in these species. To go further, and as the RT is considered a natural model for glucose intolerance²⁵⁶, we then subjected both L2AC31-KO and WT fish to a diet rich in carbohydrates (HCHO diet, 30% of the diet). This dietary challenge aimed to investigate the nutritional stress response of RTs unable to perform CMA. Interestingly, after 7 weeks of feeding the high carbohydrate diet, L2AC31-KO fish still presented significantly higher body weights and lengths than WT (Figs 4G and 4H). Furthermore, at the last time point, L2AC31-KO fish exhibited significantly higher levels of hepatosomatic (HSI) and gastro-somatic (GSI) indexes (Fig 4I), as well as a trend towards reduced postprandial plasma glucose levels (Fig 4J), suggesting defects in their metabolism. Given the important phenotypical consequences observed in L2AC31-KO RTs, we inspected the specific metabolic pathways affected by *lamp2a* C31 inactivation. We found that glycogen levels were unaltered upon *lamp2a* C31 inactivation (Fig 4K), indicating that the liver enlargement in L2AC31-KO RTs was not caused by accumulated glycogen. Accordingly, we measured the hepatic lipid content and found similar levels of saturated fatty acids (Sat) in WT and L2AC31-KO RTs (Fig 4L). However, L2AC31-KO RTs displayed an accumulation of monounsaturated fatty acids (MUFA) and a depletion in polyunsaturated fatty acids (PUFA) (Fig 4L), a fatty acid composition found in nonalcoholic fatty liver²⁵⁷.

Lamp2a C31 deletion in RT leads to substantial remodeling of the hepatic proteome.

To unveil how Lamp2a C31 deficiency leads to the phenotypic changes observed, we first measured the expression of select genes involved in glucose and lipid metabolism. We found that mRNA expression levels of glucose metabolism-related enzymes in the livers of WT and L2AC31-KO RTs did not differ significantly (Fig 5A). In contrast, L2AC31-KO fish exhibited a significant upregulation of the genes involved in lipid metabolism (Fig 5A), hinting at an enhanced potential to synthesize fatty acids.

To investigate whether L2AC31-KO RTs also underwent liver proteome perturbations, we conducted a quantitative proteomic analysis of the liver samples obtained from both WT and L2AC31-KO fish fed the HCHO diet. Overall, we identified 5489 proteins, among which 2.5% (137 proteins) were significantly up-regulated and 2.6% (144 proteins) were significantly down-regulated in L2AC31-KO RTs compared to WT (Fig 5B, Tables S2 and S3). Remarkably, the analysis of CMA-targeting motifs in these up- and down-regulated proteins revealed a higher percentage of proteins containing either the canonical or a phosphorylation-generated KFERQ motif in the former group compared to the latter group (Fig 5C), potentially suggesting an accumulation of putative CMA substrates in L2AC31-KO RTs.

To obtain a global picture of pathways affected by Lamp2a inactivation in RT, we first conducted an enrichment map analysis. We found that proteins up-regulated in L2AC31-KO RTs, were mainly related to cellular and metabolic processes (Fig 5D and Table S2). The gene ontology analysis then provided us with a closer look at specific pathways affected by Lamp2A C31 disruption (Fig 5E). Notably, among the proteins that were up-regulated, the biological processes most prominently observed were the TCA cycle and pathways associated with glucose and isocitrate metabolism. In detail, we found several proteins involved in the metabolic use of glucose as well as fatty acid biosynthesis and transport (Table S2). These include notably (i) hexokinase (HK) and fructose biphosphate A (ALDOA) involved in glycolysis, (ii) isocitrate dehydrogenase (IDH) and malate dehydrogenase (MDH) involved in the TCA cycle, and (iii) ATP citrate synthase (ACLY), very long-chain acyl-CoA synthetase (ACSVL) and fatty-acid-binding proteins (FABP) involved in fatty acid biosynthesis and transport. Although this analysis cannot reveal whether these proteins (whose levels are induced in L2AC31-KO versus WT fish) are directly targeted by CMA, it is worth noting that a number of them have already been described as *bona fide* CMA substrates in mammals²⁵⁸ and possess one or more KFERQ motifs in RT (Table S4). Whether this upregulation of proteins involved in hepatic metabolism is direct or indirect, it supports an enhanced capacity of L2AC31-KO RT liver for glucose utilization and fatty acid biosynthesis, in agreement with the already mentioned reduced glucose circulating levels and altered hepatic lipid profile (Figs 4J and 4L). However, a significant number of proteins associated with metabolic processes were also found to be downregulated in KO fish compared to their WT counterparts (Fig 5F and Table S3). Among them, we noticed the presence of Apo lipoprotein B100 (ApoB-100), which is involved in the assembly and secretion of very low density lipoprotein (VLDL) associated with the distribution of excess triglycerides from the liver to peripheral tissues²⁵⁹. Thus, this finding supports defects in the hepatic lipid metabolism/trafficking.

Another cluster identified through enrichment mapping and gene ontology analysis is associated with mitochondria biogenesis and function (Figs 5D - 5G). Despite an increase in proteins related to mitochondrial biogenesis (Fig 5D and Table S2), we observed a decrease in the levels of electron transport chain complexes (Figs 5F and 5G, and Table S3). Specifically, various subunits of mitochondrial complex I (FOXRED1, NDUFV1, NDUFA7, NDUFA12) and complex IV (COX-7c) were found to be downregulated upon Lamp2a C31 inactivation (Table S3), suggesting potential alterations in mitochondrial respiration within the liver of L2AC31-KO RTs. Notably, our analysis also revealed elevated levels of several proteins associated with glutathione (GSH) metabolism and antioxidant functions in mutant fish, including glutamate cysteine ligase (GCL), Glutathione S-transferase omega (GSTO1), thioredoxin, thioredoxin reductase (TR), glutaredoxin, and glucose-6-phosphate dehydrogenase (G6PD) (Fig 5D and Table S2), possibly reflecting the establishment of an adaptive response to mitigate oxidative stress caused by a compromised mitochondrial function. In that

direction, further investigation unveiled an upregulation of Glutathione-Disulfide Reductase (*gsr*) mRNA expression along with a decrease in the ratio of reduced glutathione (GSH) to oxidized glutathione (GSSG) in the liver of L2AC31-KO RTs (Figs 5H and 5I), supporting a situation of compromised redox status in CMA-defect animals.

Finally, we turned our attention to the cluster associated with proteolytic pathways evidenced by the enrichment map of the up-regulated proteins (Fig 5D). We witnessed an increase of key components of the endosomal sorting complexes required for transport (ESCRT) machinery such as vacuolar protein sorting 4 homolog B (VPS4B) (Table S2), considered to be an ESCRT accessory protein whose expression level controls the activation of endosomal microautophagy (eMI). Other proteins related to the ubiquitin-proteasome system (UPS), including Proteasome 26S subunit, ATPase 1 (PSMC1), UV excision repair protein RAD23 homolog A (RAD23) and Ubiquitin Conjugating Enzyme E2 K UBE2K, were also up-regulated in L2AC31-KO RTs (Table S2), overall suggesting that compensation of the CMA defect could occur via these two pathways.

Taken together, these results demonstrate that upon an acute nutritional stress such as the HCHO diet, loss of CMA leads to strong perturbations of the hepatic proteome, thus highlighting its critical role as a gatekeeper of hepatic proteostasis in RT.

Use of CMA score as a prognostic tool to assess cellular homeostasis in fish exposed to hypoxic conditions

After emphasizing the critical role of CMA in the regulation of hepatic proteostasis in RT exposed to an acute stress, we investigated the applicability of the CMA score as a tool to assess cellular homeostasis in fish facing environmental stress. In this aim, we subjected RTs to moderate hypoxic conditions (dissolved oxygen DO 5.6 ± 0.5 ppm), widely known to induce oxidative stress and organ failure in fish, as established by previous studies^{260,261}. After 4 weeks of moderate hypoxia, we collected the liver, gills and multiple brain parts of RT and calculated the CMA score (Fig 6A). We found a significant overall increase in the CMA score in RT tissues when exposed to hypoxia, suggesting the overall induction of the CMA network in response to this stressful condition (Fig 6B). Collectively, these findings highlight the activation of the CMA machinery following an environmental stress and emphasize the purpose of using the CMA score as an indicative marker for cellular homeostasis in organisms currently exposed to a changing environment.

Discussion

While extensively documented in the current literature, CMA is primarily investigated as a potential therapeutic target²⁶². However, recent studies opened up new avenues regarding the presence of this pathway in species beyond those traditionally investigated in biomedical research^{245,253}. The role of CMA in maintaining cellular homeostasis supports the idea that it could also be decisive for species exposed to numerous threats and a changing environment. Throughout this study, we have presented compelling evidence that supports the existence and crucial role of CMA in RT.

Firstly, we found that most genes of the CMA network are gradually activated throughout the development of the RT embryo. Then, quantification of the transcript levels of both CMA rate-limiting factors *lamp2a* paralogs revealed their presence in various tissues, especially those involved in metabolism, and a high heterogeneity of their expression levels, with *lamp2a* from C14 being very weakly expressed compared to its counterpart on C31. Interestingly, the low expression level of the former paralog associated with its apparent non or limited involvement in CMA activity²⁵³, suggests that it is under ongoing pseudogenization, as more than half of the genes duplicated during the 4th round of WGD (100 million years ago) that occurred in the salmonids ancestor²⁴⁸. Another noteworthy observation is the induction of the expression of both *lamp2a* paralogs by fasting. In mammals, although nutrient deprivation is a potent activator of CMA, it relies on reduced degradation of LAMP2A and relocation of this receptor at the lysosomal membrane¹⁸⁶ and not on the control of *LAMP2A* transcription. Overall, these data highlight general conservation of the CMA machinery in RT, but also show differences with mammals in the mechanisms involved in its regulation, which remain to be further investigated.

To demonstrate CMA activity in RT, we then isolated CMA-active lysosomes from liver samples and established their ability to bind and translocate a CMA substrate. To our knowledge, this is the first *in vivo* evidence for the existence of CMA activity (or CMA-like activity) in a non-mammalian organism. This finding is in line with the recent demonstration of CMA activity in medaka cell lines using the CMA reporter KFERQ-mCherry1²⁴⁵ and provides clear evidence of that the CMA mechanism is also functional in fish. Not only does the binding and uptake of GAPDH show the capability of RT lysosomes to carry out CMA, it also demonstrates their capacity to recognize a KFERQ-like motif. This finding raises new questions regarding the KFERQ-like motif conservation throughout vertebrate evolution and whether new CMA substrates are introduced in other species therefore diversifying the scope of influence of CMA.

To advance further into unraveling the physiological role of CMA in RT, we generated a unique RT line KO for *lamp2a* C31, as our latest in cell-based knockdown experiments show that Lamp2A C14 has minimal, if any, contribution to total CMA activity²⁵³. As expected, the mutant fish showed a total loss of C31 *lamp2a* mRNA expression. However, they also exhibited tissue-specific modulations of the

expression of the other two *lamp2* splice variant transcripts (namely, C31 *lamp2b* and C31 *lamp2c*) compared to WT. Although encoded by the same gene, previous studies reported distinct regulatory patterns for the 3 isoforms in response to various situations^{200, 185, 263, 264, 265}, providing evidence for the presence of post-transcriptional mechanisms that govern the expression of *lamp2* gene(s). These mechanisms may underlie the observed variations in the expression of *lamp2b* and *lamp2c* in L2AC31-KO fish and warrant further investigation. More surprising was the induction of C14 *lamp2a* mRNA expression (carried by a different gene) in mutant RTs, which support the existence of compensatory mechanisms whose molecular determinants remain to be determined.

At a phenotypic level, mutant fish presented increased growth, enlarged livers, greater visceral weights, and a trend of lower postprandial blood glucose levels, hinting at metabolic disturbances. By investigating the state of the proteome upon *lamp2a* inactivation, we obtained a closer glimpse at CMA's involvement in the regulation of the RT's metabolism. Overall, Gene Ontology and network analysis highlighted clusters related to metabolic processes, mitochondrial activity, antioxidant functions and proteolytic pathways, providing compelling evidence that CMA plays a critical role as a gatekeeper of hepatic proteostasis in RT. Interestingly, several metabolic enzymes identified as *bona fide* CMA substrates (e.g., ALDOA and MDH) in mice¹⁹² were up regulated upon *lamp2a* inactivation in RT, suggesting a conservation of at least some CMA targets across vertebrates. In this sense, it is worth noting that these enzymes present KFERQ-like motifs in RT as well. Looking ahead, it will be of major interest to determine precisely which proteins are specifically targeted by CMA in this species. Another important issue will be to compare the physiological consequences of the deletion of *lamp2a* C31 with that of *lamp2a* C14 or that of the two *lamp2as*.

As we witnessed the essential role of CMA to maintain cellular homeostasis upon an external stress, new questions arose as to the involvement of CMA in fish resilience and whether it could be harnessed as a stress gauge. To this end, we adapted and validated in RT the CMA score, as recently defined by Bourdenx et al²⁵⁴ to generate an index accounting for the CMA status. As CMA is activated in harmful situations such as oxidative stress, genotoxic damage or hypoxia²⁶², we subjected RTs to moderate hypoxic conditions. In response to reduced DO levels, our investigation of multiple tissues consistently revealed a significant increase in the CMA score. This level of precision shows that CMA machinery activation is finely tuned and depends on tissue- or even cell-type, as demonstrated in mammalian cells²⁵⁴. Furthermore, it opens new perspectives regarding the potential of quickly measuring CMA status in non-invasive tissues of fish (e.g. blood or mucus) but also in uncommon species, also subjected to increasing severity of climate events, especially when unable to measure CMA activity conventionally (e.g., lysosome isolation). Nonetheless, further investigation is required (e.g., identification of specific CMA substrates, exposure of L2AC31-KO fish to different environmental stressors) in order to truly identify the mechanisms through which CMA maintains proteostasis.

Materials and Methods

EXPERIMENTAL MODEL AND STUDY PARTICIPANT DETAILS

Ethical statements

All *in vivo* experiments were conducted according to EU legal frameworks related to the protection of animals used for scientific purposes (directive 2010/63/EU), the guidelines of the French legislation governing the ethical treatment of animals (decree no. 2001-464, 29 May 2001) and/or the Institutional Animal Care and Use Committee at the United States Department of Agriculture National Center for Cool and Cold Water Aquaculture.

Production, husbandry and treatments of L2AC31-KO fish

A commercial diet was provided for general rearing (Finfish G, Zeigler Bros, Inc., Gardners, PA), unless otherwise noted. Water flow was adjusted to maintain appropriate dissolved oxygen (> 8 ppm); water temperatures ranged from 12.5 – 13.5 °C.

Gene editing reagents were purchased from Integrated DNA Technologies (IDT) from the Alt-R CRISPR-Cas9 System product line. Online programs (crispr.wustl.edu/crispr/index.html, crispr.med.harvard.edu/sgRNAScorer/) were used to generate chromosome-specific crRNA sequences (5'-CCGTGCCCACTTTCTTTACT-3' and 5'-AGAAGCGGCTGTGTTAACGA-3') that cut on either side of the 9a exon of the lamp2a gene on C31, with the goal of excising the 9a exon to disrupt Lamp2a C31 protein function. Chromosome/gene specific forward primers internal to exon 9a and reverse primers within a downstream intron were used to assess whether an intact exon was present (5'-TCGGGGTTGCCTTGACTT-3' and 5'-GGTCATCTGGATAATTGTTGATTT-3'). Two crRNAs that cut on either side of the C31 9a exons were diluted to 100 µM, as was tracrRNA, in the supplied IDTE buffer. The gRNA solution was generated by combining 1.5 µL of each crRNA, 6 µL tracrRNA, and 8.0 µL Duplex buffer. The solution was heated at 95 °C for 5 min and cooled to room temperature. Cas9 protein was diluted to 2.0 µg/µL in Cas9 working buffer (20 mM HEPES, 150 mM KCl, pH 7.5) and combined with an equal volume of gRNA solution. Ribonucleoprotein (RNP) complexes were assembled by incubating the gRNA + Cas9 mixture at 37 °C for 10 min. Phenol red was used to visualize RNP delivery.

Eggs and milt were collected from two and three-year broodstock held at the facility. Prior to fertilization, eggs were rinsed with milt activation solution (102.8 mM NaCl, 10 mM Tris, 20 mM glycine, pH 9.0, 1 mM reduced glutathione). Each fertilization lot was produced using a single female crossed with a single male. The microinjection procedure was modified from previously published procedures for RT and Atlantic salmon^{266,267}. Fertilized eggs (embryos) were held in milt activation

solution in an incubator at 10 °C and injected 3 – 7 h post-fertilization. Immediately prior to injection, embryos were stabilized on a tray within a Petri dish and submerged in 10 °C isotonic saline solution (155 mM NaCl, 3.22 mM KCl, 2 mM CaCl₂). A handheld positive displacement microinjector was used to deliver between 100-200 nL of the RNP complex directly into the blastodisc, visualized using a stereomicroscope (Nikon SMZ1000). Once injected, embryos were transferred to spring water (10 – 14°C) for hatching. Injected embryos (potential mutants) and untreated embryos (controls) from the same fertilization lot were combined upon hatching for collective rearing. At approximately 20 g (~7 month old), fish were anesthetized with tricaine methanesulfonate (MS222, 100 mg/L), adipose fin clipped for genotyping, and tagged with passive integrated transponders (PIT tags) inserted in the intraperitoneal cavity. Genotyping was completed during the grow-out period to distinguish between 1) WT controls, 2) mutants with indels at target sites but retained the 9a exon (intact gene), and 3) mutants with excised exons at the lamp2a gene on C31. Twelve fish were identified that exhibited mosaicism for excision of the 9a exon; these fish, including WT controls from the same fertilization lots were used to produce an F1 generation. A subsample of 10 sacfry from each offspring lot were harvested after hatch to screen for gene mutagenesis. Approximately 50% of the F1 offspring from a single cross exhibited complete excision of the 9a exon on the C31 gene. This cross, along with the associated F1 control cross, were hatched and reared separately until PIT tagging and fin clipping at approximately 20 g body weight. After PIT tagging, fish were comingled for grow-out under standard rearing protocols.

At approximately one year of age, a subset of 68 fish from the F1 mutant (51 fish) and F1 control (17 fish) groups were stocked into two 800 L tanks and acclimated to these conditions for two weeks while consuming a commercially available diet. Feed was withheld for 18 hours before recording weights and fork lengths on individual fish; for the next seven weeks fish were fed to satiation with a high carbohydrate diet (Table S5A). Feed was provided using automatic feeders set to dispense feed at a fixed percent of tank biomass between 08:00 h and 14:00 h, with hand feeding at 14:30 h each day. Ration was adjusted so hand feeding to satiation was approximately 5 – 10% of the total daily ration. Weights and lengths were recorded after week 4 and at the end of the study (week 7). Feed was withheld the day of sampling. At the final sampling, a subset of mutants and controls (n = 9 per group, n = 4-5 per tank) were euthanized with a lethal dose of MS222 (300 mg/L). Blood was collected from caudal vasculature into heparinized tubes and placed on ice for subsequent processing for separation of plasma and storage at -80 °C. The viscera was removed and liver and gastrointestinal tract weights were recorded. Samples of liver and distal intestine were placed in histology cassettes and submerged in 10% neutral-buffered formalin with 4% formaldehyde prior to paraffin embedding. Subsamples of liver, distal intestine, and whole brain were frozen in liquid nitrogen and stored at -80 °C.

Other in vivo experiments

Samples used to investigate the expression of CMA-related genes during RT development were generated in a previously published study²⁶⁸. Briefly, spawns were fertilized synchronously with neomale sperm and reared in separate tanks at 8°C at the INRAE experimental facilities, Lees-Athas, France. Fish were sampled according to Vernier et al.1969²⁴⁹ at stages 2, 5, 6, 7, 8, 10, 12, 15, 22 and 23. Embryos were directly snap-frozen while juveniles anaesthetized and killed in benzocaine (60 mg/L). Fish were consistently sampled at 12:00 h for each ontogenetic stage, to avoid potential circadian effects.

Samples used to investigate the tissue-specific expression of both lamp2a genes were generated in a previously published study²⁶⁹. In details, all-female RT from a spring-spawning strain were used and kept under a natural photoperiod at 17°C at the INRAE experimental facilities in Donzacq, France. Twice a day, fish were manually fed ad libitum and considered to be satiated when only a few pellets remained on the bottom of the tank. At the end of experiment, fish were anesthetized and euthanized 6 h after the last meal. Then tissues were sampled and immediately stored at -80 °C.

For the hypoxia experiment, monosex female RTs from a spring-spawning strain were used and kept under a natural photoperiod²⁶⁹. The 12 fish studied were part of a pool of 240 fish (i.e., initial mean weight of 288 ± 9 g) randomly distributed in 12 tanks of 150 L each, for an initial mean biomass of 18 ± 1 kg/m³. A factorial experimental design was used to obtain two DO levels (normoxia vs. moderate hypoxia). The treatment was applied for four weeks.

Hypoxic conditions were created by reducing the water flow. DO concentrations were measured at the tank's outlet twice daily using an oximeter (HatchLange HQ 40D). The mean DO concentrations in the hypoxia and normoxia tanks were 5.6 ± 0.5 and 7.7 ± 0.3 ppm, respectively. Mean DO concentrations were higher than those needed to support positive growth, feeding and swimming activities. Total ammonia nitrogen (NH₄⁺-N), nitrite-nitrogen (NO₂⁻-N) and nitrate-nitrogen (NO₃⁻-N) were analyzed twice a week using a commercial kit based on colorimetric method (© Tetra). No trace of these elements was recorded. The temperature remained constant (17.0 ± 0.5 °C). We can therefore consider that the decrease in water level only caused a decrease in oxygen.

Twice a day, fish were manually fed ad libitum and considered to be satiated when only a few pellets remained on the bottom of the tank.

RTgutGC cell line

For in vitro experiments, the RTgutGC cell line²⁷⁰ derived from RT was routinely grown in Leibovitz's L-15 medium supplemented with 10% fetal bovine serum (FBS, #10270-106), 2 mM sodium pyruvate (NaPyr, #11360-070), 100 units/mL penicillin and 100 g/mL streptomycin (#14065-056), all provided by Gibco (Thermo Fisher scientific) and 25 mM HEPES (#BP299-1, Fisher Bioreagents, Fisher

Scientific SAS, Illkirch Graffenstaden, France). Cells were maintained at 18 °C, the medium was replaced twice a week and cells were passaged at 80% of confluence. Cell counting was achieved using a Cellometer K2 (Nexcelom Bioscience LLC, Lawrence, MA, USA) to plate cells prior to the experiments. Cells were seeded at a density of 50-60% for RNA isolation. Prior to the treatments, cells were washed twice with PBS before the exposure to the appropriate treatment. The treatments consisted in applying a mild-oxidative stress using CT medium supplemented with hydrogen peroxide (H₂O₂ 25 µM) or using a Hank's balanced salt solution (HBSS) (#14025-092, Gibco) supplemented with 25 mM HEPES as a starvation medium.

Nucleofector 2b Device (Lonza, Colmar, France) and the Cell line Nucleofector Kit T (Lonza, VCA-1002) were used for the plasmids cells transfections (1-5 µg). RTgutGC cells stably-transfected with the KFERQ-PA-mCherry1 construction were selected for the resistance to the selective geneticin antibiotic (G418; Gibco, 11811) before cell sorting using a FACS Aria 2-Blue 6-Violet 3-Red 5-YelGr, 2 UV laser configuration (BD Biosciences, Le Pont de Claix Cedex, France) in biosafety cabinet.

METHOD DETAILS

RNA extraction and quantitative RT-PCR analysis

To extract total RNA from individual samples, tissues were ground in TRIzol reagent (Invitrogen, Carlsbad, California, USA). 50-100 mg of tissue per mL of reagent were sampled and homogenized in a Precellys tissue homogenizer (Bertin Technologies, Montigny le Bretonneux, France). The Super-Script III RNase H-Reverse transcriptase kit (Invitrogen) was used with random primers (Promega, Charbonnières, France) to synthesize cDNA from 1µg of total RNA. The primer sequences used are listed in Tables S1 and S6. Primers were validated by testing their efficiency on pooled cDNA and subsequently sequencing the amplified products. A Roche Lightcycler 480 system (Roche Diagnostics, Neuilly-sur-Seine, France) was used for real-time RT-PCR following the protocol from Plagnes et al. 2008²⁷¹. Quadruplicates were analyzed and standardized with luciferase (Promega) or stably expressed housekeeping genes (18S, or β -actin). The E-method²⁷² was used for the developmental and tissue-specific expression analysis, and the Δ CT method²⁷³ for the expression of target genes in KO-RTs and CMA score calculation.

***In situ* hybridization**

The liver and distal portion of the intestine of starved fish (48h) and fish fed with a commercial diet were sampled and immediately fixed with 4% paraformaldehyde (PFA 4%). Samples were then rinsed in PBS, dehydrated through gradual ethanol and butanol baths, embedded in paraffin and cut in 7µM transversal sections. The sections were placed on superfrost adhesion slides (VWR®). The following steps were performed according to the BaseScope™ Detection Reagent Kit v2 – RED User Manual.

Samples were deparaffinized and dried after a series of xylene and alcohol baths. To facilitate target access and detection sensitivity, we applied a target retrieval, then a hydrophobic barrier was set and a tissue-specific protease applied. Both Basescope lamp2a probes, designed by ACD bio® were applied before the amplification phase during which multiple probes are hybridized to amplify the signal. A fast red substrate was then added to visualize the target RNA. A nanozoomer - slides scanner (Hamamatsu NANOZOOMER 2.0HT) was used to visualize whole tissue sections. To quantify the mRNA signal in the liver, equal size images of hepatocyte-covered area were used to count the particles (mRNA). However, as the signal was not evenly distributed in the distal intestine, each image was calibrated using ImageJ²⁷⁴ so as to only quantify the signal in epithelium area.

Lysosome isolation and GAPDH binding/uptake assay

The lysosome isolation protocol²⁵¹ was adapted to RT, as it is originally targeted to rat liver. A piece of starved fish liver was sampled (~1-1.5 g), washed with cold PBS, minced with a clean scalpel and homogenized in a conical tube. Some of the homogenate was put aside as a marker for total sample proteins (TLH) and the rest was filtered through a cotton gauze. After a series of centrifugation, a mix of mitochondria and the lysosomal fraction was collected. A discontinuous Nycodenz® (Proteogenix) gradient was then generated and ultracentrifuged (141000 g for one hour at 4°C) to create different interphases with specific content. From bottom to top were isolated mitochondria, a mixture of mitochondria and lysosomes, a mix population of lysosomes and lysosomes with high CMA activity. Those phases were collected with a Pasteur pipet and washed by centrifugation. The third interphase was resuspended and centrifuged to only be able to collect high CMA activity lysosomes.

For the GAPDH binding/uptake assay, protein concentrations were measured by Qubit assay (Thermo Fisher Scientific). Isolated lysosomes were incubated in the uptake assay buffer: 300 mM sucrose, 10 mM MOPS, pH 7.2, 10 mM ATP (Sigma A2383), 0.01 µg/µL biologically active HSC70 (AbCam, ab78431). For the conditions needing a CMA substrate, samples were incubated with 0.025 µg/µL GAPDH (LP00008). In conditions involving PK, samples were incubated with 1 µL of PK (Sigma P6556). To prevent lysosomal degradation, chymostatin (Sigma C7268) was used. All samples were centrifuged and the pellet was then washed and prepared for SDS-PAGE and western blotting.

To measure lysosomal integrity, isolated lysosomes were diluted in a buffer of 300mM sucrose, 10 mM MOPS, pH 7.2, and 10 mM ATP. Then the sample was centrifuged to separate the pellet (intact lysosomes) from the supernatant (broken lysosomes). Lysosomal integrity was measured by the β-hexosaminidase assay with the fluorogenic substrate 4-methylumbelliferyl-2-acetamido-2-deoxy-β-D-glucopyranoside (MUG) and only experiments with >90% intact lysosomes were considered.

Western blotting analysis

To verify if RT lysosomes display known characteristics of CMA+ lysosomes, the isolated fractions (CMA+ lysosomes, CMA+/- lysosomes, lysosomes/mitochondria and mitochondria) were subjected to SDS-PAGE and immunoblotted using the following antibodies: LAMP1 (ab24170), HSC70 (AS05 062) and TIM23 (BD611222). The total tissue homogenate was also quantified as it contains the biological components of all fractions (TLH). To quantify GAPDH, GAPDH (ab8245) was used. We used LC3B (CST3868S) to measure steady-state levels of autophagosome component LC3. After being washed, membranes were incubated with corresponding secondary antibodies such as: HRP anti-rabbit (926-80011) HRP anti-mouse (926-80010). Bands could be visualized by using the Invitrogen™ iBright™ FL1500 Imaging System and analyzed with the iBright analysis software (version 5.0). To ensure protein normalization, a No-Stain Protein Labeling Reagent (A44717) and β Actin (sc-47778) were used.

Plasma glucose levels

Blood glucose measurements were analyzed immediately upon collection using a Prodigy AutoCode glucometer (Prodigy Diabetes Care, LLC, Charlotte, NC, USA).

Glycogen content

Glycogen content of WT and L2AC31-KO RT was analyzed on lyophilized liver through a hydrolysis technique described by Good et al. (1933). Each sample was homogenized in 1 mol.L⁻¹ HCl (VWR, United States) and free glucose content was measured. Another measurement of free glucose occurred after a 10min centrifugation at 10.000 g using the Amplite Fluorimetric Glucose Quantification Kit (AAT Bioquest, Inc., United States) according to the manufacturer's instructions. The remainder ground tissue was boiled for 2.5 h at 100 °C before being neutralized with 5 mol.L⁻¹ KOH (VWR, United States). Total glucose (free glucose + glucose produced by glycogen hydrolysis) was measured then free glucose levels were subtracted to determine the glycogen content.

Lipid content

Lipids were extracted and purified according to Folch et al.1957²⁷⁵ and Alannan et al.2022²⁷⁶. Briefly, the lipids from about 100 mg of fresh weight were homogenized in an Eppendorf tube with 2 x 1 mL of ice-cold isopropanol with a TissueLyser. The homogenates were transferred in a glass tube and 1 mL of ice-cold isopropanol was used to rinse the Eppendorf tube. The samples were then placed at 85 °C for 30 min to inactive lipases. After letting the samples cool down, lipids were extracted with 3 mL of chloroform/methanol 2:1 for 2 h at room temperature, with 3 mL of chloroform overnight at 4 °C and then with 2 mL for an additional 4 h at room temperature. Between each extraction, the samples were centrifuged for 5 min at 3,500 g and the organic phase was collected and transferred to a fresh

tube where all organic phases were ultimately pooled (final volume = 11 mL). Polar contaminants such as proteins or nucleic acids were removed by adding 4 mL of NaCl 0.9 % 100 mM Tris and shaking vigorously. After phase separation by centrifugation (15 min at 3.500 g) the organic phase was collected and the solvent was evaporated. The lipids were then resuspended in chloroform:methanol (1:1, v/v) for a final concentration of 0,1 mg equivalent fresh weight/ μ L. For quantification of neutral lipids, 50 μ L (= 5 mg fresh weight) of total lipids were applied onto a silica-coated chromatography plate (Silicagel 60 F254, 10x 20 cm; Merck, Rahway, NJ) and developed with hexane/ethyl ether/acetic acid (21. 25:3.75:0.25, v/v) The plates were then immersed in a copper acetate solution (3% copper acid + 8 % phosphoric acid in distilled water) and heated at 115 °C for 30 min. Lipids were identified by co-migration with known standards and quantified by densitometry analysis using a TLC scanner 3 (CAMAG, Muttenz, Switzerland). Fatty acid methyl esters were obtained by transmethylation at 85 °C for 1 h with 0.5 M sulfuric acid in methanol containing 2 % (v/v) dimethoxypropane and 5 μ g/mL of heptadecanoic acid (C17:0) as internal standards. After cooling, 1 mL of NaCl (2.5 %, w/v) was added, and fatty acyl chains were extracted with 1 mL hexane. GC-FID was performed using an Agilent 7890 gas chromatograph equipped with a DB-WAX column (15 m x 0.53 mm, 1 μ m; Agilent) and flame ionization detection. The temperature gradient was 160 °C for 1 min, increased to 190 °C at 20 °C/min, increased to 210 °C at 5 °C/min and then remained at 210 °C for 5 min. FAMES were identified by comparing their retention times with commercial fatty acid standards (Sigma-Aldrich) and quantified using ChemStation (Agilent) to calculate the peak surfaces, and then comparing them with the C17:0 response

Quantification of GSH, GSSG in liver

AccQ-Fluor™ borate buffer was purchased from Waters® (Massachusetts, USA). Glutathione reduced (GSH), Glutathione oxidized (GSSG), EthyleneDiamineTetraacetic Acid (EDTA), Phosphoric acid (H3PO4), Potassium dihydrogen phosphate (KH2PO4) and MetaPhosphoric Acid (MPA) were purchased from Sigma-Aldrich® (Germany). Other reagents that used were of HPLC grade. All organic solvents used were gradient HPLC grade (ADL & Prochilab, Lormont, France). Ultrapure water was daily made with a MilliQ Direct8 system (Millipore, Bedford, MA, USA). Each sample (almost exactly 50 mg) was homogenized with Precellys® tissue homogenizer in 300 μ L of 20 mM phosphate buffer, 1 mM EDTA (pH = 6.5 \pm 0.05). After centrifugation (14.000 g, 20 min, 4 °C), deproteinization of the supernatant was performed with a volume-to-volume 10 % metaphosphoric acid solution. After centrifugation (14.000 g, 5 min, 4 °C), the supernatant was filtered with a 0.22 μ m PVDF unit. Metabolite mixtures were stored at -20°C (no more than 1 week) until LC-UV analysis. Chromatographic separation was achieved on Waters® Symmetry Shield RP18 column (4.6 mm x 150 mm i.d. 3.5 μ m). The column was operated at 30 °C. The injection volume was 50 μ L and the

flow rate was set at 0.7 mL/min. A ternary solvent system was used, consisting of (A) pH 2.7 20 mM phosphate buffer, (B) acetonitrile, (C) methanol. The mobile phase was filtered through in-line 0.2 µm membrane filters. The following gradient elution was employed: 0–10 min : 99.5 % A, 0 % B; 10.5 min : 40 % A, 60 % B; 10–13 min : 40 % A, 60 % B; 13.5 min : 99.5 % A, 0.5 % B ; 13.5 – 20 min (column equilibration) : 99.5 % A, 0.5 % B. The eluate was monitored with absorbance detection at 210 nm during the whole run. Waters® Empower™ Pro software was used for data acquisition. Metabolites were identified comparing their Retention Time (RT) to standard ones. Quantification was based on integration of peak areas and compared to the standard calibration curves (R² correlation > 0.999) of each metabolite of interest (6 biological levels, 3 repetitions). Calibration curves were linear from 0.2 to ~1 000 pmol/injection for GSSG and from 2 to ~10 000 pmol/injection for GSH.

Sample preparation for label-free proteomics analysis

Proteins from WT and KO25-trouts were extracted using the Thermo Scientific™ T-PER™ Tissue Protein Extraction Reagent (ref 78510). Protein concentrations were then measured by bicinchoninic acid (BCA) assay (Interchim; ref UP95424A). For each sample 50 µg of dried protein extracts were solubilized with 25 µL of 5% SDS. Proteins were submitted to reduction and alkylation of cysteine residues by addition of TCEP and chloroacetamide to a final concentration respectively of 10 mM and 40 mM. Protein samples were then processed for trypsin digestion on S-trap Micro devices (Protifi) according to manufacturer's protocol, with the following modifications: precipitation was performed using 216 µL S-Trap buffer, 4 µg trypsin was added per sample for digestion in 25 µL ammonium bicarbonate 50 mM.

NanoLC-MS/MS analysis of proteins

Tryptic peptides were resuspended in 35 µL of 2 % acetonitrile and 0.05 % trifluoroacetic acid and analyzed by nano-liquid chromatography (LC) coupled to tandem MS, using an UltiMate 3000 system (NCS-3500RS Nano/Cap System; Thermo Fisher Scientific) coupled to an Orbitrap Exploris 480 mass spectrometer equipped with a FAIMS Pro device (Thermo Fisher Scientific). 1 µg of each sample was injected into the analytical C18 column (75 µm inner diameter × 50 cm, Acclaim PepMap 2 µm C18 Thermo Fisher Scientific) equilibrated in 97.5 % solvent A (5 % acetonitrile, 0.2 % formic acid) and 2.5 % solvent B (80 % acetonitrile, 0.2 % formic acid). Peptides were eluted using a 2.5 % - 40 % gradient of solvent B over 62 min at a flow rate of 300 nL/min. The mass spectrometer was operated in data-dependent acquisition mode with the Xcalibur software. MS survey scans were acquired with a resolution of 60,000 and a normalized AGC target of 300 %. Two compensation voltages were applied (-45 v / -60 v). For 0.8 s most intense ions were selected for fragmentation by high-energy collision-induced dissociation, and the resulting fragments were analyzed at a resolution of 30,000, using a

normalized AGC target of 100 %. Dynamic exclusion was used within 45s to prevent repetitive selection of the same peptide.

Bioinformatics analysis of mass spectrometry raw files

Raw MS files were processed with the Mascot software (version 2.7.0) for database search and Proline55 for label-free quantitative analysis (version 2.1.2). Data were searched against Rainbow trout entries of Uniprot protein database (46.650 sequences; 17.861.404 residues). Carbamidomethylation of cysteines was set as a fixed modification, whereas oxidation of methionine was set as variable modifications. Specificity of trypsin/P digestion was set for cleavage after K or R, and two missed trypsin cleavage sites were allowed. The mass tolerance was set to 10 ppm for the precursor and to 20 mmu in tandem MS mode. Minimum peptide length was set to 7 amino acids, and identification results were further validated in Proline by the target decoy approach using a reverse database at both a PSM and protein false-discovery rate of 1%. For label-free relative quantification of the proteins across biological replicates and conditions, cross-assignment of peptide ions peaks was enabled inside group with a match time window of 1 min, after alignment of the runs with a tolerance of +/- 600 s. Median Ratio Fitting computes a matrix of abundance ratios calculated between any two runs from ion abundances for each protein. For each pair-wise ratio, the median of the ion ratios is then calculated and used to represent the protein ratio between these two runs. A least-squares regression is then performed to approximate the relative abundance of the protein in each run in the dataset. This abundance is finally rescaled to the sum of the ion abundances across runs. A Student t-test (two-tailed t-test, equal variances) was then performed on log₂ transformed values to analyze differences in protein abundance in all biologic group comparisons. Significance level was set at p = 0.05, and ratios were considered relevant if higher than +/- 2. The results were ranked based on fold change (>1.41) and p-value (<0.05) of t-test comparing WT and L2AC31-KO groups. Gene Ontology enrichment maps were generated in CytoScape (3.9.1) using EnrichmentMAP (3.3.5) plugin, and then annotated with AutoAnnotate (1.4.0) app. The presence of KFERQ motifs within the protein sequences was assessed using the KFERQ finder app V0.8¹⁷¹. Furthermore, an ontology analysis was conducted using Enrichr²⁷⁷. Clusters are grouped by major functional association.

CMA score

Each gene of the CMA network is attributed a weight. As some genes are present in multiple copies (paralogs) in RT, each paralog was attributed a weight of 1/n, with n copies. As LAMP2A is the rate-limiting factor in CMA, it was given a weight of 2 (1/paralog). Weight values for LAMP2A copies were measured with the relative contribution of each paralog to CMA activity in a RT cell line stably expressing the KFERQ-PA-mCherry1 reporter²⁵³. Furthermore, a modulating score (+1 or -1) was

applied to the values, whether the gene has a positive or negative impact on CMA. Finally, a sum of all values was calculated to obtain a final score.

QUANTIFICATION AND STATISTICAL ANALYSIS

Data is reported as means + SEM, percentages + SEM. Normality assumptions were tested before conducting statistical tests and parametric tests conducted only when they were met. Differences between more than two groups were evaluated by one-way ANOVA followed by Tukey's multiple comparison (same sample size) post-hoc test. In the case of non-parametric tests, Kruskal-Wallis or Friedman test followed by Dunn's multiple comparisons were conducted. When comparing two groups we used a parametric two-tailed unpaired Student's T-test, or a non-parametric Mann Whitney test. All statistical analyses were performed using GraphPad Prism version 8.0.1 for Windows (GraphPad Software, Inc., www.graphpad.com) and a p -value < 0.05 was set as a level of significance. All data generated in this study and presented in the figures are provided along with their statistic report in the Dataset S1-S3.

Acknowledgments

We thank Cécile Heraud (INRAe) for the GSSG:GSH measurements, Christel Poujol for technical assistance at the Bordeaux Imaging Center (BIC), CNRS-INSERM and Bordeaux University, member of the national infrastructure France BioImaging and supported by the French National Research Agency (ANR-10-INBS-04). Lipidomic analyses were performed on the Bordeaux Metabolome Facility-MetaboHUB (ANR-11-INBS-0010). We thank Alexandre Stella from the ProteoToul Services - Proteomics Facility of Toulouse for the proteomics analysis. We also acknowledge technical and animal caretaking contributions from NCCCWA personal Josh Kretzer, Vanessa Panaway, and Joe Beach. Mention of trade names is solely to provide accurate information and does not reflect endorsement by the USDA. The USDA is an equal opportunity employer and provider. We would also like to thank Lucie Marandel for kindly providing us with RT samples from her experiment⁴⁸ and L. Peron for manufacturing the light emitting device. S.S. received a doctoral fellowship from the E2S-UPPA.

References

1. Sydemann, W. J., Poloczanska, E., Reed, T. E. & Thompson, S. A. Climate change and marine vertebrates. *Science* 350, 772–777 (2015).
2. Brander, K. M. Global fish production and climate change. *Proc. Natl. Acad. Sci. U.S.A.* 104, 19709–19714 (2007).
3. Huang, M., Ding, L., Wang, J., Ding, C. & Tao, J. The impacts of climate change on fish growth: A summary of conducted studies and current knowledge. *Ecological Indicators* 121, 106976 (2021).
4. Islam, M. J., Slater, M. J. & Kunzmann, A. What metabolic, osmotic and molecular stress responses tell us about extreme ambient heatwave impacts in fish at low salinities: The case of European seabass, *Dicentrarchus labrax*. *Science of The Total Environment* 749, 141458 (2020).
5. Pankhurst, N. W. & Munday, P. L. Effects of climate change on fish reproduction and early life history stages. *Mar. Freshwater Res.* 62, 1015 (2011).
6. Clarke, A. Costs and consequences of evolutionary temperature adaptation. *Trends in Ecology & Evolution* 18, 573–581 (2003).
7. Rabinowitz, J. D. & White, E. Autophagy and Metabolism. *Science* 330, 1344–1348 (2010).
8. Cuervo, A. M. & Dice, J. F. A Receptor for the Selective Uptake and Degradation of Proteins by Lysosomes. *Science* 273, 501–503 (1996).
9. Nishino, I. et al. Primary LAMP-2 deficiency causes X-linked vacuolar cardiomyopathy and myopathy (Danon disease). *Nature* 406, 906–910 (2000).
10. Saftig, P., Von Figura, K., Tanaka, Y. & Lüllmann-Rauch, R. Disease model: LAMP-2 enlightens Danon disease. *Trends in molecular medicine* 7, 37–39 (2001).
11. Fujiwara, Y. et al. Discovery of a novel type of autophagy targeting RNA. *Autophagy* 9, 403–409 (2013).
12. Kaushik, S. & Cuervo, A. M. The coming of age of chaperone-mediated autophagy. *Nat Rev Mol Cell Biol* 19, 365–381 (2018).
13. Kirchner, P. et al. Proteome-wide analysis of chaperone-mediated autophagy targeting motifs. *PLoS Biol* 17, e3000301 (2019).
14. Tesseraud, S. et al. Autophagy in farm animals: current knowledge and future challenges. *Autophagy* 17, 1809–1827 (2021).
15. Bourdenx, M. et al. Chaperone-mediated autophagy prevents collapse of the neuronal metastable proteome. *Cell* 184, 2696–2714.e25 (2021).
16. Lescat, L. et al. Chaperone-Mediated Autophagy in the Light of Evolution: Insight from Fish. *Molecular Biology and Evolution* 37, 2887–2899 (2020).
17. Vélez, E. J. et al. Chaperone-mediated autophagy protects against hyperglycemic stress. *Autophagy* 15548627.2023.2267415 (2023) doi:10.1080/15548627.2023.2267415.
18. European Commission. Joint Research Centre. & Scientific, Technical and Economic Committee for Fisheries. The EU aquaculture sector: economic report 2020 (STECF 20 12). (Publications Office, 2021).
19. Thorgaard, G. H. et al. Status and opportunities for genomics research with rainbow trout. *Comparative Biochemistry and Physiology Part B: Biochemistry and Molecular Biology* 133, 609–646 (2002).
20. Muhlfeld, C. C. et al. Trout in hot water: A call for global action. *Science* 360, 866–867 (2018).
21. Wilson, R. P. Utilization of dietary carbohydrate by fish. *Aquaculture* 124, 67–80 (1994).
22. Lescat, L. et al. CMA restricted to mammals and birds: myth or reality? *Autophagy* 14, 1267–1270 (2018).
23. Vernier, J. M. Table chronologique du développement embryonnaire de la truite arc-en-ciel, *Salmo gairdneri* Rich. *Ann. Embryol. Morphogenet.* 2, 495–520 (1969).

24. Cuervo, A. M., Knecht, E., Terlecky, S. R. & Dice, J. F. Activation of a selective pathway of lysosomal proteolysis in rat liver by prolonged starvation. *American Journal of Physiology-Cell Physiology* 269, C1200–C1208 (1995).
25. Cuervo, A. M., Terlecky, S. R., Dice, J. F. & Knecht, E. Selective binding and uptake of ribonuclease A and glyceraldehyde-3-phosphate dehydrogenase by isolated rat liver lysosomes. *Journal of Biological Chemistry* 269, 26374–26380 (1994).
26. Juste, Y. R. & Cuervo, A. M. Analysis of chaperone-mediated autophagy. *Autophagy: Methods and Protocols* 703–727 (2019).
27. Donzeau, M. et al. Tim23 Links the Inner and Outer Mitochondrial Membranes. *Cell* 101, 401–412 (2000).
28. Cuervo, A. M., Dice, J. F. & Knecht, E. A Population of Rat Liver Lysosomes Responsible for the Selective Uptake and Degradation of Cytosolic Proteins. *Journal of Biological Chemistry* 272, 5606–5615 (1997).
29. Kuo, S.-H. et al. Mutant glucocerebrosidase impairs α -synuclein degradation by blockade of chaperone-mediated autophagy. *Sci. Adv.* 8, eabm6393 (2022).
30. Pajares, M. et al. Transcription factor NFE2L2/NRF2 modulates chaperone-mediated autophagy through the regulation of LAMP2A. *Autophagy* 14, 1310–1322 (2018).
31. Madrigal-Matute, J. et al. Protective role of chaperone-mediated autophagy against atherosclerosis. *Proc. Natl. Acad. Sci. U.S.A.* 119, e2121133119 (2022).
32. Gomez-Sintes, R. et al. Targeting retinoic acid receptor alpha-corepressor interaction activates chaperone-mediated autophagy and protects against retinal degeneration. *Nat Commun* 13, 4220 (2022).
33. Koga, H., Martinez-Vicente, M., Macian, F., Verkhusha, V. V. & Cuervo, A. M. A photoconvertible fluorescent reporter to track chaperone-mediated autophagy. *Nat Commun* 2, 386 (2011).
34. Klionsky, D. J. et al. Guidelines for the use and interpretation of assays for monitoring autophagy. *autophagy* 17, 1–382 (2021).
35. Schneider, J. L., Suh, Y. & Cuervo, A. M. Deficient Chaperone-Mediated Autophagy in Liver Leads to Metabolic Dysregulation. *Cell Metabolism* 20, 417–432 (2014).
36. Krishnan, J. & Rohner, N. Sweet fish: Fish models for the study of hyperglycemia and diabetes. *Journal of Diabetes* 11, 193–203 (2019).
37. Puri, P. et al. A lipidomic analysis of nonalcoholic fatty liver disease. *Hepatology* 46, 1081–1090 (2007).
38. Tasset, I. & Cuervo, A. M. Role of chaperone-mediated autophagy in metabolism. *The FEBS journal* 283, 2403–2413 (2016).
39. Schlegel, A. Zebrafish models for dyslipidemia and atherosclerosis research. *Front Endocrinol* 7: 159. (2016).
40. Wood, C. M. & Eom, J. The osmorepiratory compromise in the fish gill. *Comparative Biochemistry and Physiology Part A: Molecular & Integrative Physiology* 254, 110895 (2021).
41. Abdel-Tawwab, M., Monier, M. N., Hoseinifar, S. H. & Faggio, C. Fish response to hypoxia stress: growth, physiological, and immunological biomarkers. *Fish Physiol Biochem* 45, 997–1013 (2019).
42. Berthelot, C. et al. The rainbow trout genome provides novel insights into evolution after whole-genome duplication in vertebrates. *Nature communications* 5, 3657 (2014).
43. Cuervo, A. M. & Dice, J. F. Regulation of lamp2a levels in the lysosomal membrane. *Traffic* 1, 570–583 (2000).
44. Cuervo, A. M. & Dice, J. F. Unique properties of lamp2a compared to other lamp2 isoforms. *Journal of Cell Science* 113, 4441–4450 (2000).
45. Pérez, L. et al. LAMP-2C Inhibits MHC Class II Presentation of Cytoplasmic Antigens by Disrupting Chaperone-Mediated Autophagy. *The Journal of Immunology* 196, 2457–2465 (2016).

46. Kiffin, R. et al. Altered dynamics of the lysosomal receptor for chaperone-mediated autophagy with age. *Journal of Cell Science* 120, 782–791 (2007).
47. Murphy, K. E. et al. Lysosomal-associated membrane protein 2 isoforms are differentially affected in early Parkinson's disease: Early loss of LAMP2A protein in PD. *Mov Disord.* 30, 1639–1647 (2015).
48. Marandel, L., Véron, V., Surget, A., Plagnes-Juan, É. & Panserat, S. Glucose metabolism ontogenesis in rainbow trout (*Oncorhynchus mykiss*) in the light of the recently sequenced genome: new tools for intermediary metabolism programming. *Journal of Experimental Biology* jeb.134304 (2016) doi:10.1242/jeb.134304.
49. Kirchner, P. et al. Proteome-wide analysis of chaperone-mediated autophagy targeting motifs. *PLoS Biol* 17, e3000301 (2019).
50. Cleveland, B. M., Yamaguchi, G., Radler, L. M. & Shimizu, M. Editing the duplicated insulin-like growth factor binding protein-2b gene in rainbow trout (*Oncorhynchus mykiss*). *Sci Rep* 8, 16054 (2018).
51. Wargelius, A. et al. Dnd knockout ablates germ cells and demonstrates germ cell independent sex differentiation in Atlantic salmon. *Sci Rep* 6, 21284 (2016).
52. Cardona, E. et al. Tissue origin of circulating microRNAs and their response to nutritional and environmental stress in rainbow trout (*Oncorhynchus mykiss*). *Science of The Total Environment* 853, 158584 (2022).
53. Kawano, A. et al. Development of a rainbow trout intestinal epithelial cell line and its response to lipopolysaccharide. *Aquaculture Nutrition* 17, e241–e252 (2011).
54. Plagnes-Juan, E. et al. Insulin regulates the expression of several metabolism-related genes in the liver and primary hepatocytes of rainbow trout (*Oncorhynchus mykiss*). *Journal of Experimental Biology* 211, 2510–2518 (2008).
55. Gudrun, T. The E-Method: a highly accurate technique for gene-expression analysis. *Nat. Methods* 3, i–ii (2006).
56. Pfaffl, M. W. A new mathematical model for relative quantification in real-time RT-PCR *Nucleic Acids Res* 29: e45. Find this article online (2001).
57. Schindelin, J. et al. Fiji: an open-source platform for biological-image analysis. *Nat Methods* 9, 676–682 (2012).
58. Folch, J., Lees, M. & Sloane Stanley, G. H. A simple method for the isolation and purification of total lipids from animal tissues. *J Biol Chem* 226, 497–509 (1957).
59. Alannan, M. et al. Targeting PCSK9 in Liver Cancer Cells Triggers Metabolic Exhaustion and Cell Death by Ferroptosis. *Cells* 12, 62 (2022).
60. Kuleshov, M. V. et al. Enrichr: a comprehensive gene set enrichment analysis web server 2016 update. *Nucleic Acids Res* 44, W90–W97 (2016).

Figures and Tables

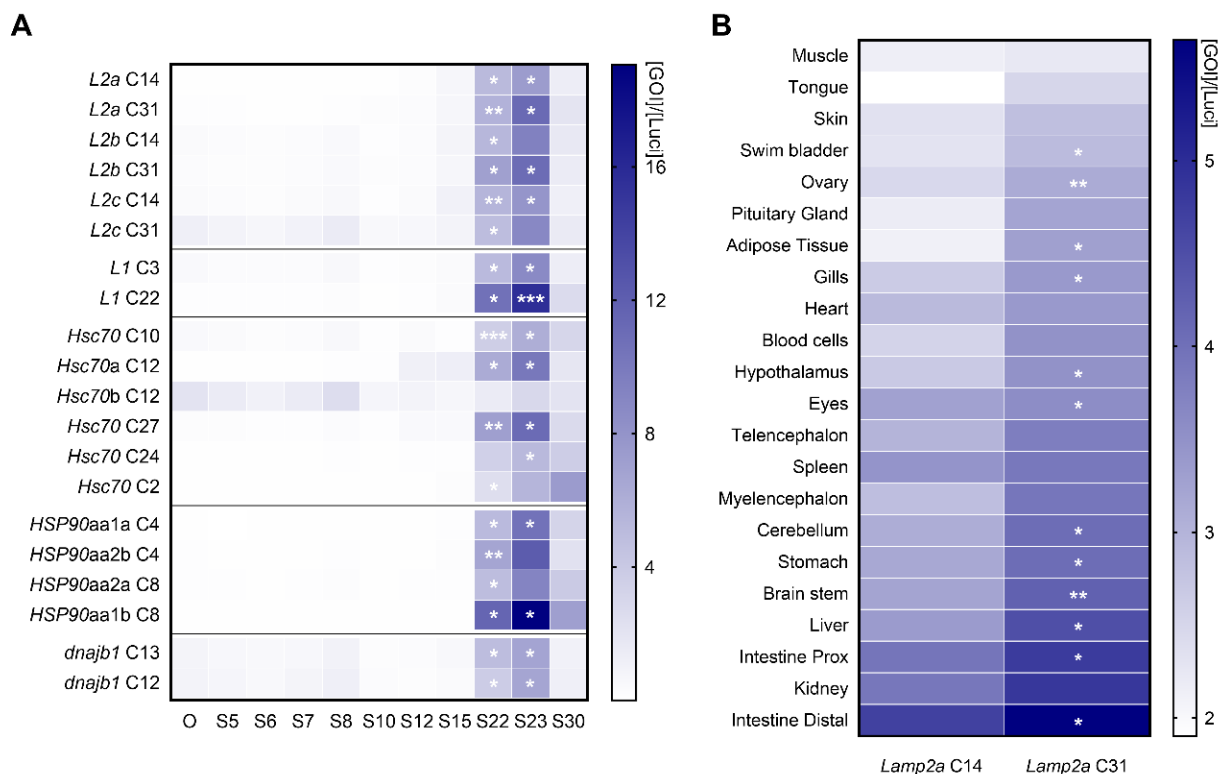


Figure 1. The expression of CMA-related genes in RT is induced during development and shows a tissue-specific pattern. (A) Expression of CMA-related genes throughout development from oocyte (O) stage (S) to hatching (S30). mRNA levels were normalized with luciferase. Parametric statistical t-tests were performed comparing all stages to oocyte stage (n=3 pools of embryos, one pool of 30 embryos per spawn) (*, p<0.05; **, p<0.01; ***, p<0.001). (B) Expression of lamp2a paralogs (from C14 and C31) in different tissues. mRNA levels were normalized with luciferase. A parametric statistical t-test was performed comparing both lamp2a paralogs (n=6) (*, p<0.05; **, p<0.01).

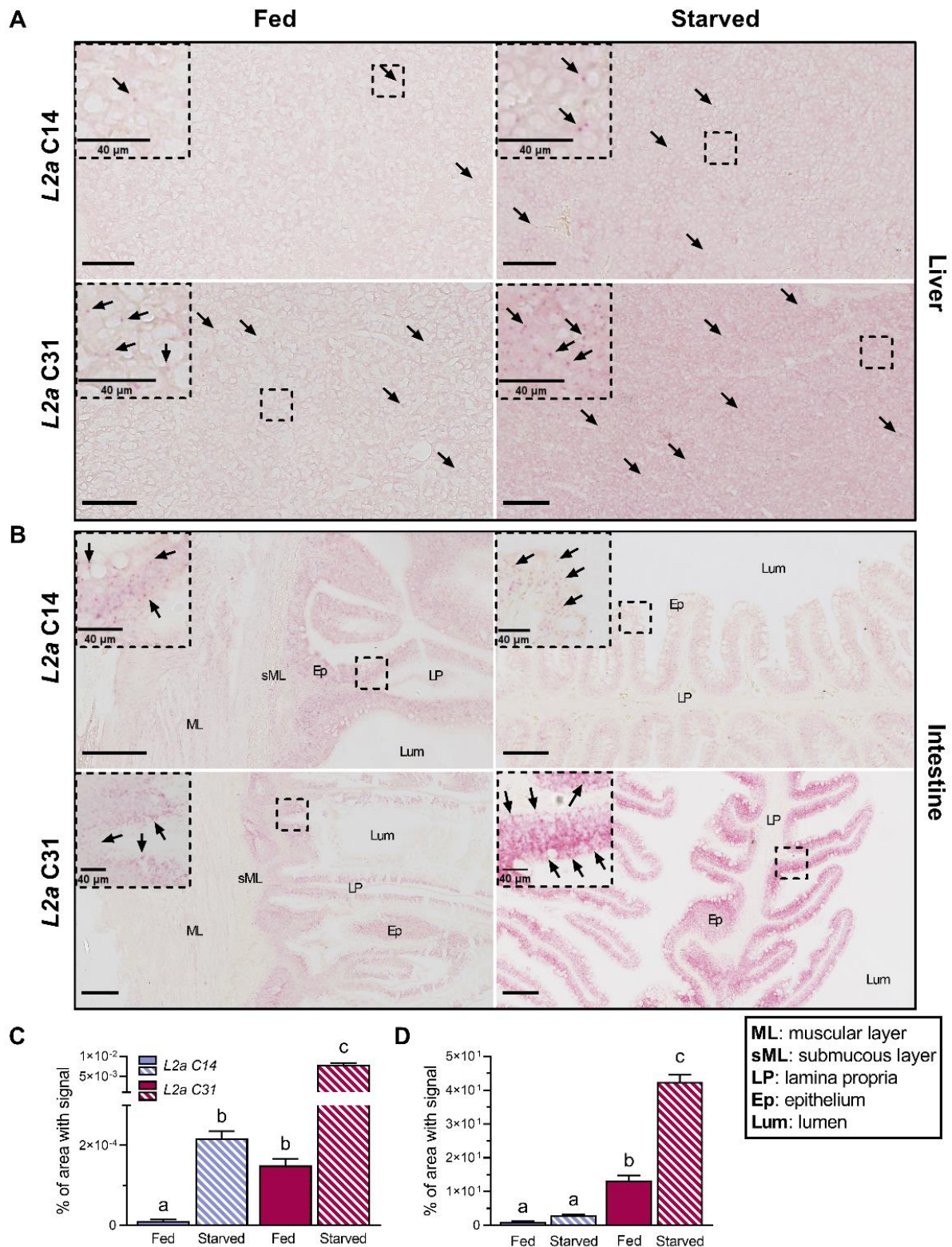


Figure 2. The expression of both RT lamp2a is induced by fasting and shows a similar spatial distribution although at different levels. (A) Signal of lamp2a C14 and lamp2a C31 probes (arrows) in liver sections from fed and starved RTs (Scale bars, 200 μ m). (B) Signal of lamp2a C14

and lamp2a C31 probes (arrows) in distal intestine sections from fed and starved RTs (Scale bars, 200 μm). Enlargements of the boxed region are shown to the top left of each image (Scale bar, 40 μm). (C) Quantification of liver mRNA signal between both paralogs in contrasted nutritional states (n=4). (D) Quantification of distal intestine mRNA signal between both paralogs in contrasted nutritional states (n=4). A Kruskal-Wallis test (C) and a one-way ANOVA (D) were conducted comparing all conditions. Letters indicate a significant difference between treatments ($p < 0.001$). All data is presented as mean \pm SEM.

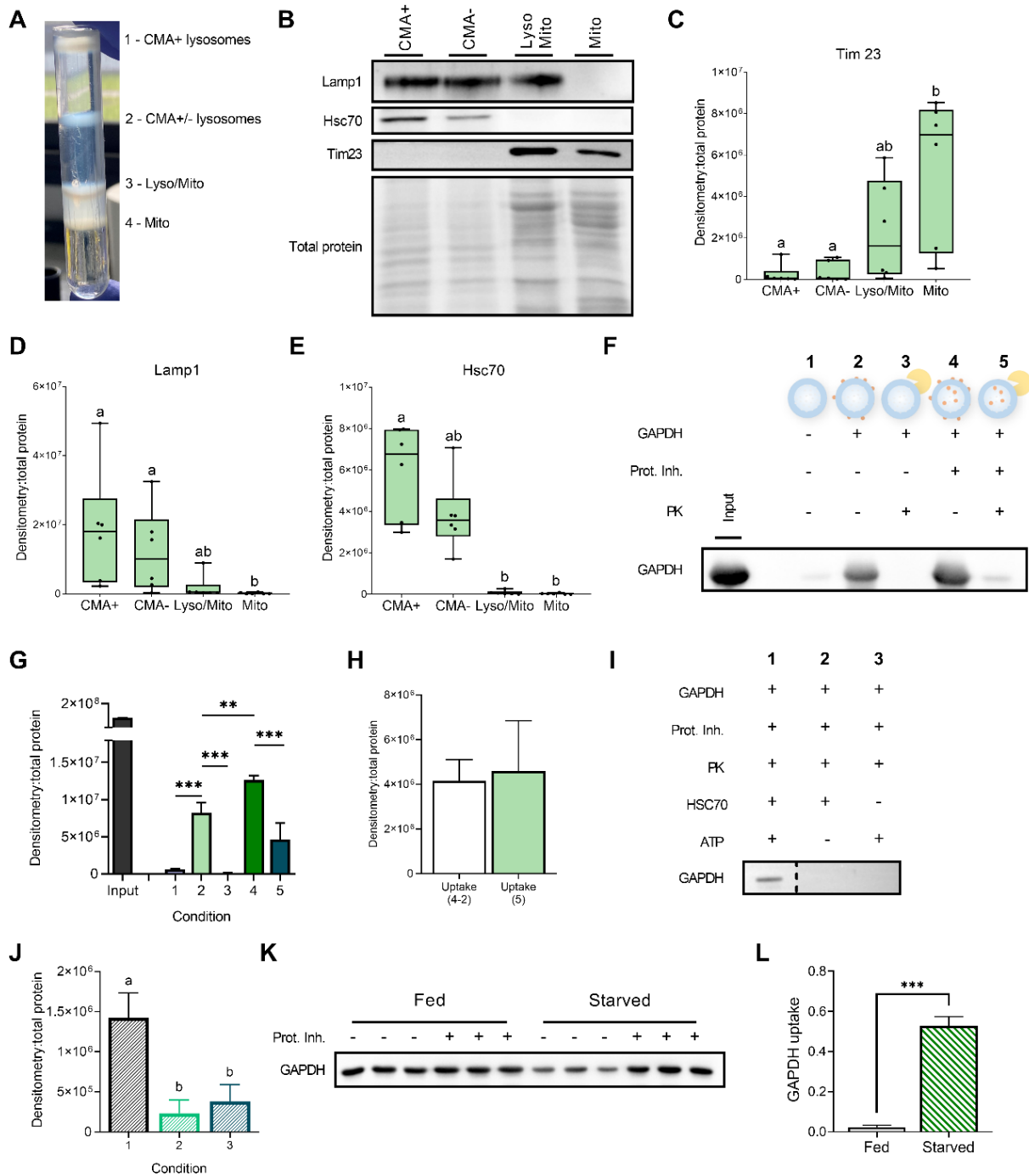


Figure 3. RT displays CMA-active lysosomes able to bind and uptake the CMA substrate GAPDH. (A) Different interphases obtained after centrifugation of RT liver homogenate on a discontinuous Nycodenz gradient. The mitochondria (Mito) are localized in the lowest interphase of the gradient, while the subsequent interphase consists of a mixture of lysosomes and mitochondria (Lyso/Mito). The third interphase from the bottom contains a heterogeneous population of CMA-competent and CMA-non-competent lysosomes (CMA+/- lysosomes), and the lysosomes with high CMA activity (CMA+) migrate to the upper interphase. (B) Immunoblots in those four different liver

fractions and densitometric quantification of TIM23 (C), LAMP1 (D), and HSC70 (E) proteins. All values are shown as min. to max. (n=6). A Friedman test with multiple comparisons was performed comparing all fractions. Letters indicate a significant difference between treatments ($p < 0.0001$). (F) Immunoblot showing RT CMA+ lysosome's ability to bind and uptake GAPDH. Conditions correspond to (1) untreated CMA+ lysosomes, (2) CMA+ lysosomes incubated with the CMA substrate GAPDH, (3) CMA+ lysosomes incubated with GAPDH and PK, (4) CMA+ lysosomes incubated with GAPDH and inhibitors of lysosome proteases, and (5) CMA+ lysosomes incubated with GAPDH, Prot. Inh. and PK. (G) Densitometric quantification of the Western blot shown in F. Values are expressed relative to total proteins (n=6). A t-test (**, $p < 0.01$; ***, $p < 0.001$) was conducted to stress the differences between association, binding and uptake. (H) Densitometric quantification of GAPDH uptake, comparing uptake from condition 5 and the uptake obtained from the arithmetic difference between condition 2 and 4. (I) Western blot showing RT's CMA activity depends on presence of Hsc-70 and ATP. (J) Densitometric quantification of GAPDH uptake in absence of Hsc70 and ATP, statistically compared with a one-way ANOVA ($p < 0.01^{**}$), (n=4). (K and L) GAPDH binding and uptake upon nutrient deprivation versus control condition. Representative Immunoblot (K) and quantification of GAPDH uptake (L) calculated as the difference between GAPDH association (+ Prot. inh.) and GAPDH binding (- Prot. inh.). A t-test was conducted comparing both nutritional conditions ($p < 0.001^{***}$), (n=3). All data is presented as mean + SEM.

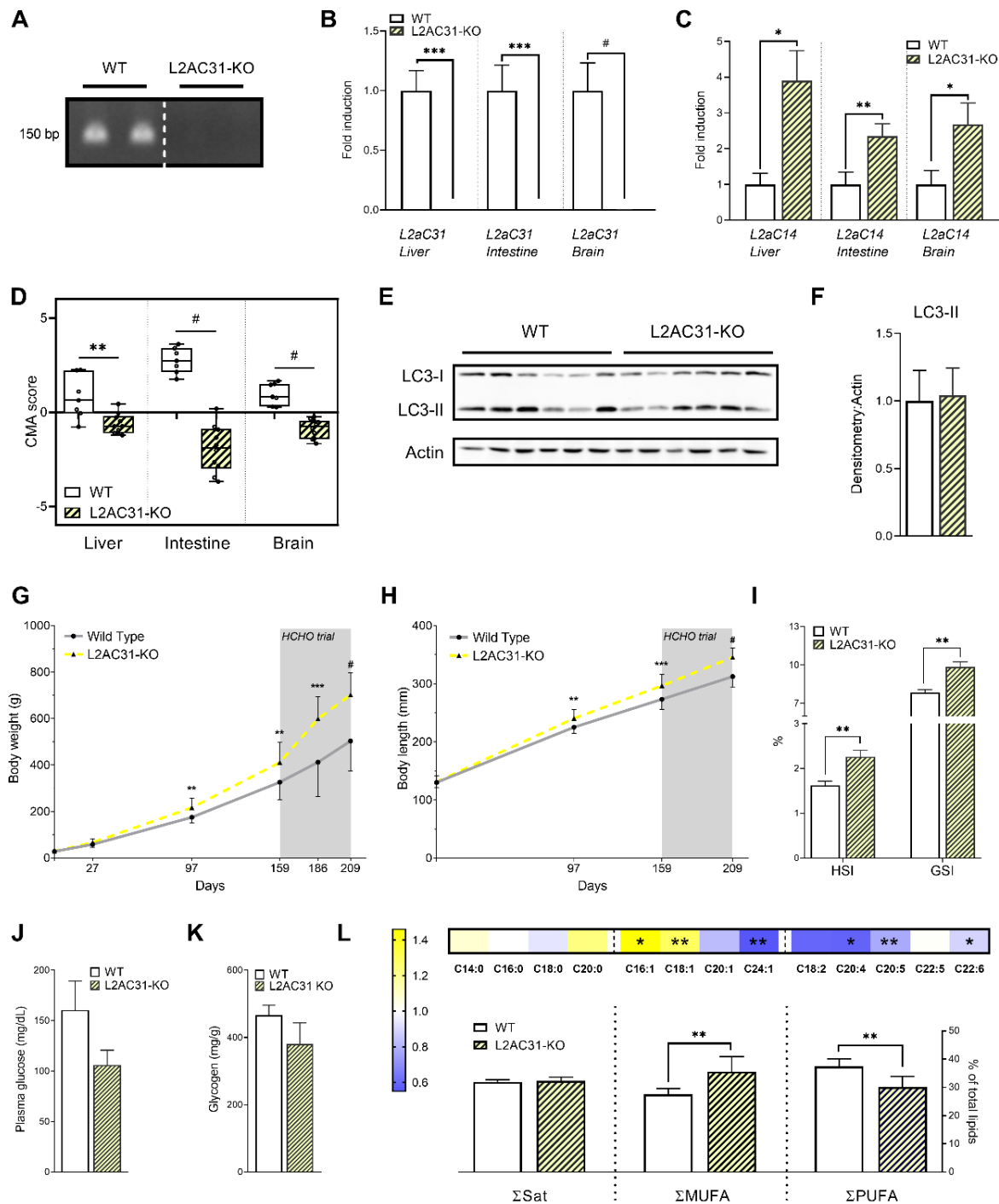


Figure 4. Lamp2a C31 deletion leads to enhanced body size, altered organ indices, and metabolic dysregulation in RT. (A) Genotyping of lamp2a allele was performed by PCR of fish fin generated by Crispr-Cas9 method. The primers used were specifically designed to bind exon A. (B) Liver, intestine and brain mRNA expression of lamp2a C31 in WT and L2AC31-KO RTs analyzed by RT-qPCR (n=7, values are mean + SEM shown by fold induction respect to WT fish). (C) Liver, intestine and brain mRNA expression of lamp2a C14 genes in WT vs L2AC31-KO RTs (n=7, values are mean + SEM shown by fold induction respect to WT fish). A Mann-Whitney test was performed comparing mRNA of WT and L2AC31-KO (*, p<0.05; **, p<0.01; ***, p<0.001; #, p<0.0001). (D) CMA

score based on expression of liver, intestine and brain CMA network genes in WT vs L2AC31-KO RTs. (n=7, all values shown min. to max.) (t-test; **, p<0.01; #, p<0.0001). (E) Representative immunoblot for LC3 I and LC3 II in homogenate liver from WT and L2AC31-KO RTs, quantified in (F), values are mean + SEM. (G) Body weights of WT vs L2AC31-KO RTs during 209 days of experiment. Mean +/- SD (*, p<0.05; **, p<0.01; ***, p<0.001; #, p<0.0001). (H) Body lengths of L2AC31-KO vs WT RTs during 209 days of experiment. Mean +/- SD (*, p<0.05; **, p<0.01; ***, p<0.001; #, p<0.0001). (I) Hepatosomatic ([liver weight/body weight]x100) and Gastrosomatic index ([weight of gastrointestinal tract /body weight]x100) of WT vs L2AC31-KO RTs sampled at day 209. Values are mean + SEM (**, p<0.01). (J) Postprandial plasma glucose in WT vs L2AC31-KO RTs at day 209. Values are mean + SEM. (K) Hepatic glycogen content (mg of glycogen per g of fresh tissue) of WT vs L2AC31-KO RTs at day 209. Values are mean + SEM. (L) Hepatic lipid profile of WT and L2AC31-KO RTs at day 209. The heatmap represents the % of each fatty acid type to total lipids in L2AC31-KO divided by the corresponding value from the WT group. In both groups, a sum of percentages was calculated per fatty acid category: saturated (Sat), monounsaturated (MUFA) and polyunsaturated (PUFA). Values are mean + SEM. A t- test was performed comparing each fatty acid content between groups (**, p<0.01).

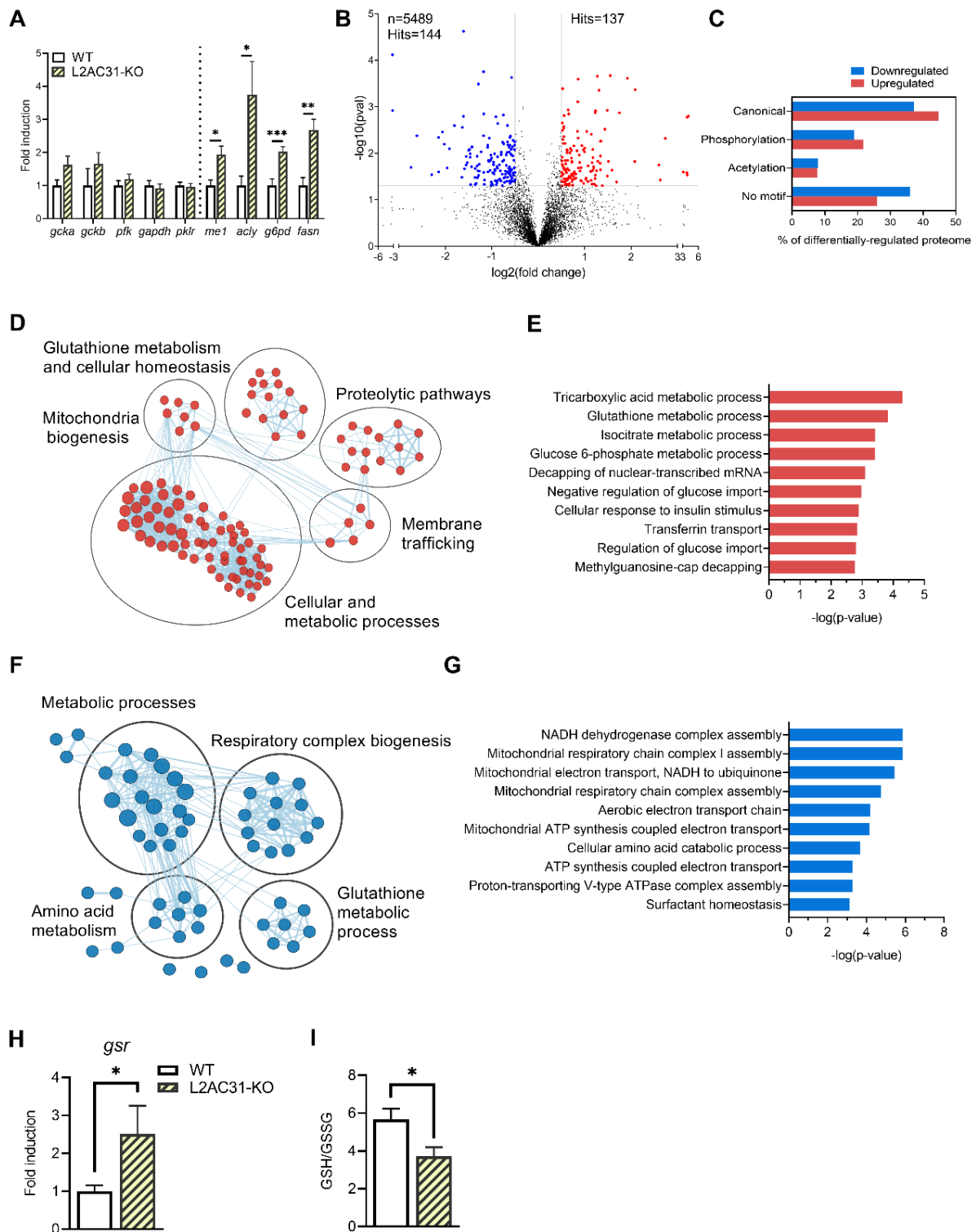


Figure 5. Deletion of Lamp2a C31 in RT leads to substantial remodeling of the hepatic proteome. (A) mRNA levels of several enzymes related to glucose and lipid metabolisms in liver homogenates from WT vs L2AC31-KO RTs (n=7, values are mean + SEM fold induction respect to WT group). *gcka*, *gckb*, glucokinase a and b; *pfk*, phosphofructokinase 1; *gapdh*, glyceraldehyde 3-phosphate dehydrogenase; *pklr*, pyruvate kinase; *me1*, malic enzyme 1; *acly*, ATP citrate lyase; *g6pd*, glucose-6-Phosphate dehydrogenase; *fasn*, fatty acid synthase. A Mann-Whitney test was performed

comparing mRNA of WT and L2AC31-KO (*, $p < 0.05$; **, $p < 0.01$; ***, $p < 0.001$). (B) Volcano plot of the quantitative proteomics analysis of liver L2AC31-KO VS WT RTS. Top left: number of identified proteins (n) and significantly down-regulated hits. Top right: number of significantly up-regulated hits. Blue and red dots indicate significantly down- and up-regulated proteins, respectively ($p < 0.05$ and fold change > 1.41). (C) Proportion of differentially-regulated proteins harboring distinct classes of KFERQ-like motifs. (D) Enrichment map showing biologically-related protein networks up-regulated upon Lamp2a blockage. (E) Gene ontology analysis of proteins up-regulated upon Lamp2a blockage. (F) Enrichment map showing biologically-related protein networks down-regulated upon Lamp2a blockage. (G) Gene ontology analysis of proteins down-regulated upon Lamp2a blockage. (H) Glutathione-Disulfide Reductase mRNA expression in liver L2AC31-KO VS WT RTS. Values are mean \pm SEM (n=7) shown by fold induction respect to WT group (Mann-Whitney test; *, $p < 0.05$). (I) Hepatic GSSG:GSH level in L2AC31-KO VS WT RTS. Values are mean \pm SEM (n=7; Mann-Whitney test; *, $p < 0.05$).

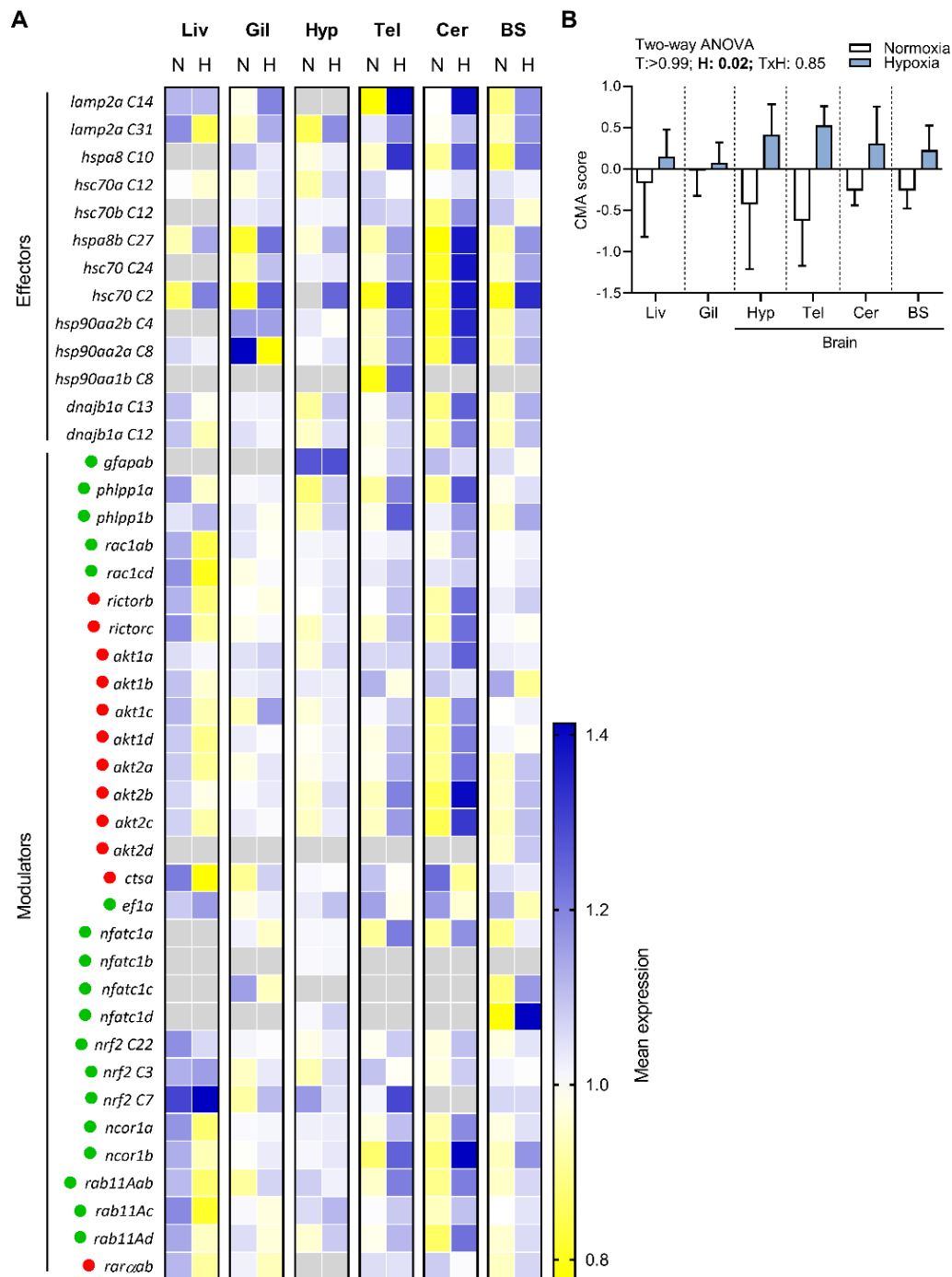


Figure 6. Use of CMA score as a prognostic tool to assess cellular homeostasis in fish exposed to stressful conditions. (A) Expression of CMA network genes in different tissues of RT under hypoxia relative to normoxia (n=6). N= normoxia; H= hypoxia; Liv= liver; Gil= gills; Hyp= hypothalamus; Tel= telencephalon; Cer= cerebellum; BS= brain stem. The CMA network components are organized into functional groups. Green and red dots indicate whether the element has a positive or negative impact on CMA activity, respectively. Gray squares of the heatmap indicate absence of expression. (B) CMA activation score based on expression of CMA network genes in different tissues of RT under hypoxia (n=6). Data represent mean \pm SEM (Two-way ANOVA). T= tissue and H= hypoxia.

Supporting Information for

Chaperone-Mediated Autophagy in Fish: A Key Function Amid a Changing Environment

Simon Schnebert¹, Emilio J Vélez¹, Maxime Goguet¹, Karine Dias¹, Vincent Véron¹, Isabel García-Pérez¹, Lisa M Radler², Emilie Cardona¹, Stéphanie Fontagné-Dicharry¹, Pierre Van Delft³, Franziska Dittrich-Domergue³, Amélie Bernard³, Florian Beaumatin¹, Amaury Herpin⁴, Beth Cleveland², #, Iban Seiliez¹, #, *

¹Université de Pau et des Pays de l'Adour, E2S UPPA, INRAE, UMR1419 Nutrition Métabolisme et Aquaculture, F-64310 Saint-Pée-sur-Nivelle, France.

²National Center for Cool and Cold Water Aquaculture, ARS/USDA, 11861 Leetown Rd, 25430 Kearneysville, WV, USA.

³Laboratoire de Biogenèse Membranaire, UMR 5200, CNRS, Univ. Bordeaux, F-33140, Villenave d'Ornon, France.

⁴INRAE, UR1037 Laboratory of Fish Physiology and Genomics, Campus de Beaulieu, Rennes, F-35042, France.

These authors contributed equally to this work.

*Corresponding author:

Iban SEILIEZ

INRAE, UMR1419 NuMeA,

F64310 Saint Pée sur Nivelle, France.

Tel: (33) 5 59 51 59 99; Fax: (33) 5 59 54 51 52

Email: iban.seiliez@inrae.fr

This file includes:

Figures S1 and S2

Table S1 to S6

Other supporting materials for this manuscript include the following:

Datasets S1 to S3

A

```

WT      ...TTAGCTGCAATAAATGGGAATGGAAATTGTGCATAAACTGGCGTGGACCATTGTAAATATTTTACAATATATATGGTCCCCGGACATTTTAGTAAA
L2AC31-KO ...TTAGCTGCAATAAATGGGAATGGAAATTGTGCATAAACTGGCGTGGACCATTGTAAATATTTTACAATATATATGGTCCCCGGACATTTTAGTAAA
*****

WT      TCCTCCTTTGTTTCCAACATATCTTGACTGAGAAGTGTCTATGATTGACCATGCATTCACCATTTTGATGTTTTACCTTTCTCCACCCTGCAACCCC
L2AC31-KO TCCTCCTTTGTTTCCAACATATCTTGACTGAGAAGTGTCTATGATTGACCATGCATTCACCATTTTGATGTTTTACCTTTCTCCACCCTGCAACCCC
*****

WT      CCGTGCCCACTTTCTTTACTGTGCATCCAGCGGAGGATTGCCAAGACGATACGACAGAGAGCTGGCTTGTTCCTATAGCGGTGGGGTTGCCTTGACTTT
L2AC31-KO CCGTG-----
*****

WT      ACTGGTCCCTCATTTGTTGGTTGCCTATTTTCATTGGAAGAAAGCGAAACCAGGGCCTGGCTATGAGCACTTCTAAATTATCTTCACTATGCTGAGGCTA
L2AC31-KO -----

WT      TAACTTCGGTCATCTGGATAATTGTTGATTTAATTTGACTAATATACTGTGCAGAGTTTACTTAATGGTGAATTCACCGGATGGAAAGCTCTTTCTCAT
L2AC31-KO -----

WT      GAAACAATGACTTGGAGAAGCGGCTGTGTTAACGATGGCATGTAACAGCTGTGTGTGTAATTAGAATTTATGATTTTATTGATGACACATCTTATATTCCT
L2AC31-KO -----TTAACGATGGCATGTAACAGCTGTGTGTGTAATTAGAATTTATGATTTTATTGATGACACATCTTATATTCCT
*****

WT      CATCACATGGTTGACTATAGATGGCTGATGACCAAAATGTTTTCCCTAATGCAATTAATGCCATGCTCTGACGGACCCTGATGAATATGCTTGGTT...
L2AC31-KO CATCACATGGTTGACTATAGATGGCTGATGACCAAAATGTTTTCCCTAATGCAATTAATGCCATGCTCTGACGGACCCTGATGAATATGCTTGGTT...
*****
    
```

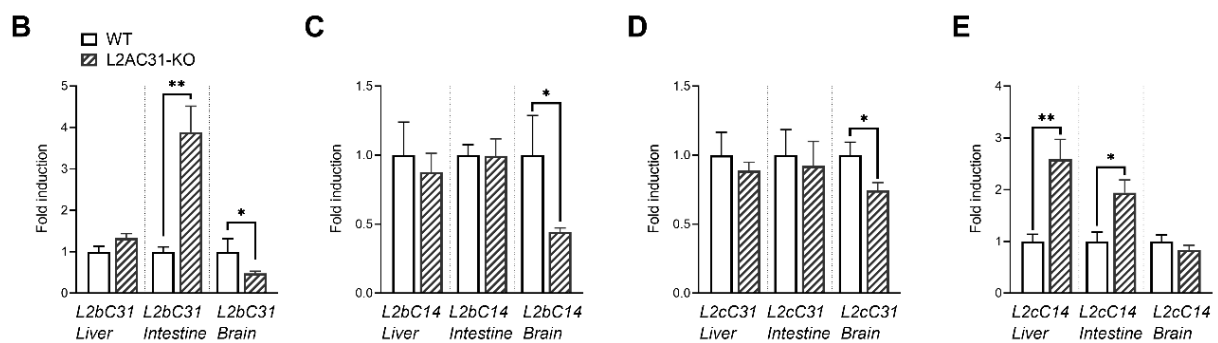


Figure S1. mRNA expression of lamp2b and lamp2c splice variants in WT vs L2AC31-KO RTs. (A) Sequence alignment of lamp2a in WT vs L2AC31-KO RT showing the loss of exon A (highlighted in yellow) and the CRISPR targets (red font). (B) and (C) show the mRNA expression of lamp2b from C31 and C14, respectively. (D) and (E) show the mRNA expression of lamp2c from C31 and C14, respectively. Values are mean + SEM (n=7) shown by fold induction respect to WT group. T-test was used to compare between groups (*, p<0.05; **, p<0.01).

Understanding and harnessing chaperone-mediated autophagy (CMA) in the rainbow trout (*Oncorhynchus mykiss*)

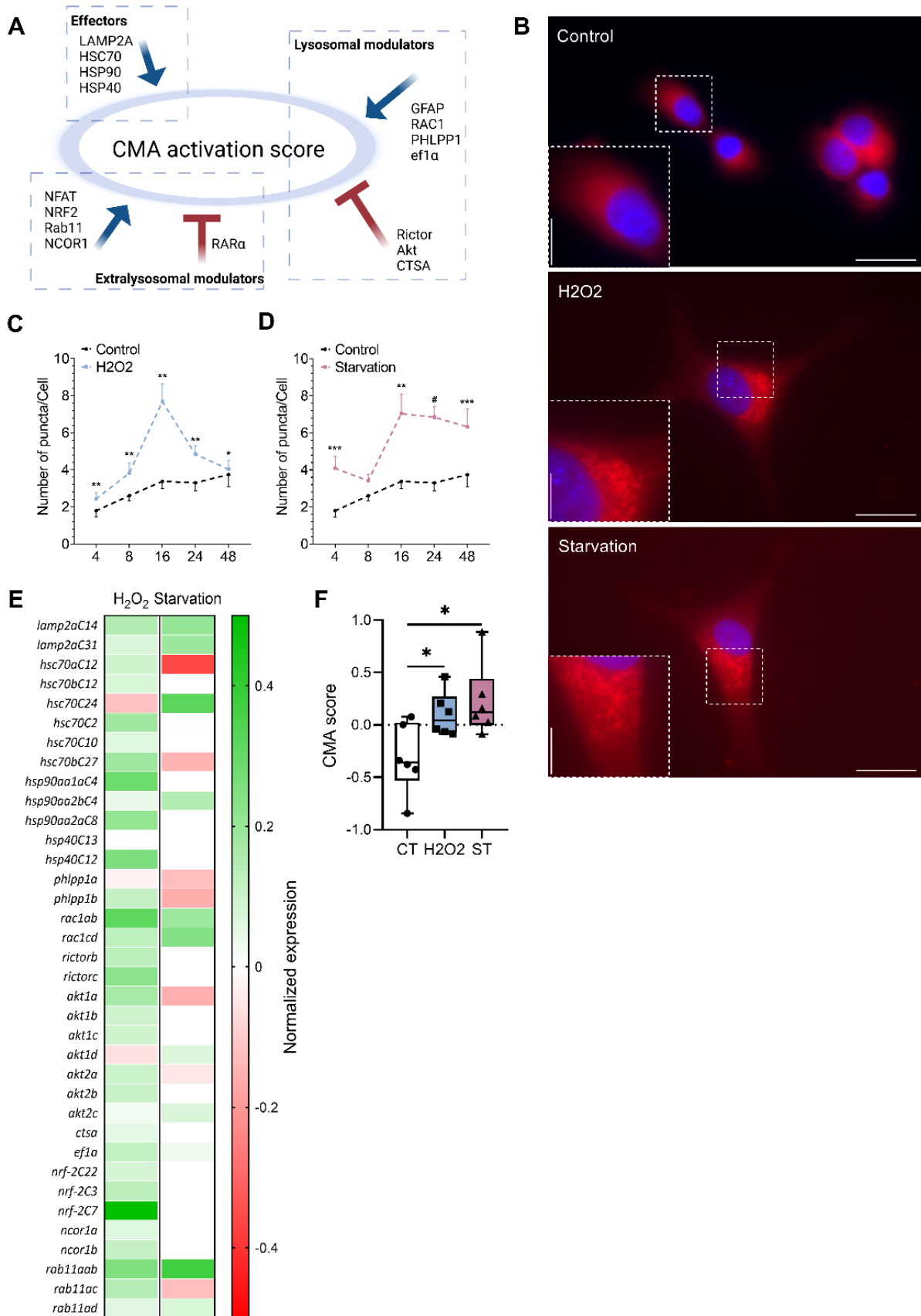


Figure S2. In vitro validation of the CMA score using KFERQ-PA-mCherry1 reporter in RTgutGC cells. (A) Graphical representation of the CMA network. Each group of proteins is based on function (effectors and modulators) and localization (lysosomal and extra-lysosomal) (modified from15). (B) Representative images of RT enterocytes cells visualized by fluorescence microscopy (scale bars, 20 μm) and zoomed image with scale bars of 5 μm . Cells were transfected with a photoactivable (PA) KFERQ-PA-mCherry1 fluorescent reporter (red) and then photoactivated for 10 min. Cells were untreated (Control), exposed to a mild-oxidative stress (H_2O_2 , 25 μM) or maintained in the absence of serum (starvation) for 16 h. CMA activity was measured as the total number of KFERQ-PA-mCherry1 fluorescent puncta normalized for the number of cells after 4, 8, 16, 24 or 48 h exposure of RT enterocytes to mild-oxidative stress (C) or starvation (D) and compared with control cells using Mann-Whitney tests (*, $p < 0.05$; **, $p < 0.01$; ***, $p < 0.001$; #, $p < 0.0001$) ($n = 3$ experiments, values are means \pm SEM). (E) Heatmap representing expression of CMA network genes in mild-oxidative stress and starvation conditions. mRNA levels were standardized with housekeeping gene 18S. ($n = 3$, values are mean). (F) CMA score based on expression of CMA network genes under both conditions. ($n = 3$, all values shown min. to max.). A t-test was performed comparing the control condition with each treatment condition (*, $p < 0.05$).

Table S1. CMA network genes and corresponding primers

Role	Name of gene	Forward sequence	Reverse sequence
Effectors	<i>lamp2a C14</i>	CAACAGGGAGCAGACATTAAC	CAATGAGGATCAGCACAGCC
	<i>lamp2a C31</i>	CAACAAGGAGCAGACCTTAAC	CCCTGGTTTCGCTTCTTCC
	<i>hspa8 C10</i>	TGCGTCCATTATATCCAGCA	CAAACGCTTAGCATCGAACA
	<i>hsc70a C12</i>	ACCTCCCCAACAAGCAAA	AGGCATTGTGACAAAGGAG
	<i>hsc70b C12</i>	GCCCAATCTGTAGTAAAGCCAAG	CTCCAGGACTCAAATGTAGACAAA
	<i>hspa8b C27</i>	ATGGCTTGGAAATGGACTGAA	CATTTATTGGCTAAACTGAAAACG
	<i>hsc70 C24</i>	TGCTGAAAGCAACCAATCAA	TGCAGTACAAAGGCAAAAACA
	<i>hsc70 C2</i>	GGCTCTTCTGTGGTCCAAC	GCTGTAGGAGTGTGCGGTAG
	<i>hsp90aa1a C4</i>	GAGGATTAGGACCAGTGAATACA	TGGCGTTTTCTGATCACTGT
	<i>hsp90aa2b C4</i>	GAGAAGAAAGATGGGGAGGAGAG	CTTGTCACATGCGCCGTCA
	<i>hsp90aa2a C8</i>	GAGGGAGACGAGGACACATC	GAACAAACATCAAAGTCATCCTG
	<i>hsp90aa1b C8</i>	TTTTCATGACTGCTGAGTCG	TTGAATAGGGTTGAAAACAGCA
	<i>dnajb1a C13</i>	TCAAGCGTACTTGACAGATACTTG	TCAGCTCCAGTGGACTTGT
<i>dnajb1a C12</i>	TCAAGCGTACTTGCGAGAC	TCAGCTCCAGTGGACTTGT	
Modulators	<i>gfapab</i>	GCTCCGTGGAACAAACGAGT	GATGACCCACCGTATCCTGG
	<i>phlpp1a</i>	AACAGGTTTCGGCAGAGGC	TGGGGCTTCCCTGCGTAA
	<i>phlpp1b</i>	TTGAAAACAGGGTGGGGG	TGTGGGGCTTCTGCGTAA
	<i>rac1ab</i>	GTACATCCCCACAGTGTGTTGA	ATCCCAAAGGCCCAAGTTGA
	<i>rac1cd</i>	ATGGCAAAAGAGATTGGAGCAG	CTTCTTCTTGTGACGGGCG
	<i>riCTORA</i>	GTCCATCTCTATGCCTTGGTTT	CTGTTGGAAGTAGGGCGTGT
	<i>riCTORB</i>	ATCATCTGTGAACCTGCTGTGA	TAGTGAAAGTCTGTGTACGGGG
	<i>riCTORC</i>	CCAGTAAGTCTCAGCCAGTATG	CGTCCGACAGGTACAGTTTC
	<i>akt1a</i>	ACCAAGCCCAAACCTCAAAGTG	GTGTGCTACTCATCTTTGCC
	<i>akt1b</i>	CGACGGTACATTATTGGCT	AGCTGACATTCTGGTGCTACT
	<i>akt1c</i>	CCACAAGATGTTGACGCGTTCCG	CTTTCGTCATTCTTCCCTCTCC
	<i>akt1d</i>	CATTGAGGCCGTAGCAGACAG	TTCAAAGTCGTGCATAGTCACTT
	<i>akt2a</i>	AAAGGACCCCAAGCAGAGGTTA	AAGTAGCGGGTGTGCGTC
	<i>akt2b</i>	GATCCCAAGCAAAGTTAGGG	TGCCACAGTCCAGGTTGGTAT
	<i>akt2c</i>	TGCCAAAGACGTGATGACACAG	TGAGTCTAAGCTGTACACTTGTCC
	<i>akt2d</i>	GATGCCCCACGAGGAGAGTA	GTAGGCAGCGATGACAAAC
	<i>ctsa</i>	GTTTCTCCCTGGGCTTCAA	GACATGCCATCGTTCTGAATCAAG
	<i>ef1a</i>	TCCTCTTGGTGGTTTCGCTG	ACCCGAGGGACATCCTGTG
	<i>nfatc1a</i>	TACCTTCCCAAACGTTCC	GATAAACCCCGACCAGGCAG
	<i>nfatc1b</i>	AGGACTCCTTCAAGTCTACCGC	AATGAACAGACAGCCCTGAG
	<i>nfatc1c</i>	AAGGACTCTGCAAGTCTACAT	CGTGGGGACACACCTGA
	<i>nfatc1d</i>	CAAGGACTCCTCAAATCTACATC	CCAGAACAATGCTTGGGACA
	<i>nrf2 C22</i>	CTAGCACCCAACAGCAGTCA	TCAGACATTGTGCTGAGCTCA
	<i>nrf2 C3</i>	CCTGTGGACGACTTCAACGA	AGCCACCTTATTCTTGCCCC
	<i>nrf2 C7</i>	ACACAAACCACTGGAACCGT	TCTCTCCAGGTCTGAGTCG
	<i>ncor1a</i>	GTCATCACCCCTCTCATGCCATC	CGTCGTCTCGATCGTGCTTG
	<i>ncor1b</i>	AGCACAAGCAGGACACACG	ACTGGTCTCTGACCCTCCA
	<i>rab11Aab</i>	CGGGCCTTCGAGAGAAAAAC	AGAATGGTCTGAAAGCCGTT
	<i>rab11Ac</i>	CTCCAGACCAATTCTGACTGAAATC	GGTGACATGTTGTGTCTTGCC
	<i>rab11Ad</i>	CTCCAGACCAATTCTGACTGAAATC	ACATGTGTTGTCTGCTCG
<i>raraab</i>	AGCTCGGAAGAGATAGTCCCC	CTCCGGAAGAAACCTTGACG	

Table S2. List of up-regulated proteins in L2AC31-KO vs WT RTs

Name of protein	Accession Number	log ₂ (KO/WT)	log ₁₀ (pval)
Isocitrate dehydrogenase (IDH)	AOA060W4K6	1.55	3.67
motile sperm domain-containing protein 2 MOSPD2	AOA060WQ66	1.27	3.65
Isocitrate dehydrogenase (IDH)	AOA8C7QHT2	1.92	3.61
Ubiquitin-conjugating enzyme E2 K (UBE2K)	AOA8C7V187	2.09	3.37
Transferrin receptor 1b (Tr1b)	AOA060YMI7	1.31	3.35
dhrs7b (Dehydrogenase/reductase 7)	AOA060WQL1	1.49	2.92
SGT1	AOA060YDC6	1.23	2.91
very long-chain acyl-CoA synthetase ACSVL	AOA060YZL8	1.23	2.87
Talin 1	AOA060Y5X6	1.75	2.87
RAD23A	AOA060YG13	4.05	2.80
MFN2 (mitofusin 2)	AOA060YG13	3.81	2.77
Glutamate-cysteine ligase (GCL)	AOA060WN13	1.44	2.51
ZO-1 tight junction protein	AOA060YR10	1.04	2.47
Prostaglandin E synthase 3 - chaperone p23	AOA060XMQ8	1.14	2.41
Galectin-8 LGALS8	AOA060YPK1	1.34	2.26
28S ribosomal protein S35, mitochondrial (MRPS35)	AOA060XNY9	2.74	2.32
TCB1 transposase	AOA060W525	1.35	2.26
DP-N-acetylglucosamine pyrophosphorylase (UAP1)	AOA060WK17	1.00	2.11
Aldose Reductase	AOA060W451	1.17	2.08
Mitochondrial protein LACTB	AOA060WDJ0	1.34	1.94
ALDOA - Aldolase - fructose-bisphosphate A	AOA060WUI1	1.18	1.90
Saccharopine dehydrogenase (SDH)	AOA060YW21	1.28	1.83
Phosphoserine transaminase - Phosphoserine Aminotransferase	AOA060YU89	1.51	1.82
Mustn1 musculoskeletal embryonic nuclear protein 1a	AOA060XD24	2.08	1.82
ALDOA - Aldolase - fructose-bisphosphate A	AOA060XHN5	1.16	1.80
Condensin complex subunit 1	AOA060XX58	1.33	1.78
Vacuolar protein sorting-associated protein 33B - VPS33B	AOA060WA63	1.07	1.73
Phosphoserine Aminotransferase	AOA060ZSW8	2.60	1.75
tmem97 - Transmembrane Protein 97	AOA060Y953	1.19	1.71
MROH2B maestro heat like repeat family member 2B	AOA060XSP9	1.19	1.68
Vacuolar protein sorting-associated protein 4B - VPS4B	AOA060X3F6	1.34	1.64
ADP-ribosylation factor-like 3 (Arl3)	AOA060WFD0	1.59	1.64
Nucleoporin 133 (Nup133)	AOA060XOR2	1.17	1.63
mRNA-decapping enzyme 1A (DCP1A)	AOA060YNK5	1.26	1.62
V-ATPase	AOA060XXM1	1.15	1.61
Histone deacetylase (HDAC)	AOA060Z7V8	1.13	1.61
Thioredoxin	C1BH85	3.08	1.59
TRAPPC8 (Trafficking Protein Particle Complex Subunit 8)	AOA060WA90	3.77	1.58
Elongation factor G 1, mitochondrial (GFM1)	AOA060VWB3	3.86	1.53
PTPN23 (Protein Tyrosine Phosphatase Non-Receptor Type 23)	AOA060WXG6	1.23	1.53
PRKAB1 - 5'-AMP-activated protein kinase subunit beta-1	AOA060XTP5	1.49	1.51
Influenza virus NS1A-binding protein (NS1BP)	AOA060W6C5	1.03	1.47
Replication protein A (RPA)	AOA060XWW5	1.22	1.46
ADP-ribosylhydrolase	AOA060XZF2	1.02	1.44

Understanding and harnessing chaperone-mediated autophagy (CMA) in the rainbow trout (*Oncorhynchus mykiss*)

Name of protein	Accession Number	log2(KO/WT)	log10(pval)
Complement component 8 c8g	A0A060XV51	1.14	1.41
5-oxoprolinase	A0A060WE17	1.07	1.39
Ubiquitin-protein ligase UBR5	A0A060WTW8	2.63	1.42
ATP citrate synthase (ACLY)	A0A060WTD0	1.69	1.38
Glucose-6-phosphate 1-dehydrogenase (G6PD)	A0A060WHZ0	1.16	1.34
Heat shock protein 75 kDa (TRAP1)	A0A060YT17	1.20	1.34
FAM185A	A0A060WBH4	1.21	1.34
5-oxoprolinase	A0A060WDM6	1.38	1.30
Hexokinase HK	A0A060WFB8	0.52	2.65
G6PD (glucose-6-phosphate dehydrogenase	A0A060XEX6	0.77	1.57
motile sperm domain-containing protein 2	A0A674F7Q4	1.27	3.65
Dual specificity phosphatase 23b (DUS23)	C1BIA0	0.86	3.59
argininosuccinate synthase (ASS)	A0A060WCU7	0.52	3.39
Integrator complex subunit 11 INTS11	A0A060X0J0	0.55	1.66
transferrin receptor 1b (Tr1b)	A0A060YPC2	1.31	3.35
Trans-L-3-hydroxyproline dehydratase	A0A060WY07	0.85	3.10
PTGES2 Gene - Prostaglandin E Synthase 2	A0A060Z7I8	0.65	2.93
Peroxisomal targeting signal 1 receptor (PTS1)	A0A060XU62	0.66	2.84
ACTR1B Beta-centractin	D5LNF9	0.56	2.81
Talin 1	A0A060Y5X6	1.75	2.87
RAD23	A0A060Y182	3.81	2.77
Malate dehydrogenase (MDH)	A0A8C7TVA0	0.55	2.57
Malate dehydrogenase (MDH)	A0A060XXI1	0.55	2.54
akr1a1a aldehyde reductase	A0A060W451	0.52	2.49
Phosphoprotein enriched in astrocytes-15 (PEA-15)	A0A060Z5M9	0.85	2.47
ZO-1 tight junction protein	A0A060YR10	1.04	2.47
PTGES3 Gene - Prostaglandin E Synthase 3	A0A060XMQ8	1.14	2.41
Septin 9 (SEPT9)	A0A060X5R9	0.55	2.36
Histone-lysine N-methyltransferase SETD5	A0A8C7RCG9	0.86	2.33
AFG3-like protein	A0A060X3F1	0.53	2.29
Glutamate-cysteine ligase (GCL)	A0A8C7VYS9	1.35	2.26
Igals8a galectin 8a	A0A8C7QLP1	1.34	2.26
ATP6V1C1 V-type proton ATPase subunit C 1	A0A060ZG28	0.54	2.21
glrx glutaredoxin (thioltransferase)	A0A673ZI75	0.58	2.21
3alpha(or 20beta)-hydroxysteroid dehydrogenase	A0A674DT84	0.77	2.16
ABCB6 ATP-binding cassette super-family B member 6, mitochondrial	A0A060X8Q2	0.98	1.35
Influenza virus NS1A-binding protein (NS1BP)	A0A060WEI1	0.67	1.31
Synaptobrevin homolog YKT6	A0A060XS36	0.58	1.32
unknown	A0A060WAB1	0.60	1.32
Mitochondrial amidoxime-reducing component 1 MOSC1	A0A060Z7S4	0.63	1.33
Mitochondrial outer-membrane protein FUNDC1	A0A060WG90	0.67	1.34
GSTO1 (Glutathione S-transferase omega) GSTTL	C1BFM5	0.73	1.39
Transaldolase	A0A060YV08	0.58	1.34
Protein ETHE1, mitochondrial	A0A8C7SHX1	0.92	1.41
Exocyst complex component 1 EXOC1	A0A060X3B4	0.93	1.40
mao Amine oxidase	P49253	0.73	1.43
Exocyst complex component 1 EXOC1	A0A060X3Y7	0.78	1.45

Understanding and harnessing chaperone-mediated autophagy (CMA) in the rainbow trout (*Oncorhynchus mykiss*)

Name of protein	Accession Number	log2(KO/WT)	log10(pval)
ARHGAP1 (Rho GTPase Activating Protein 1)	AOA8U0QMV8	0.81	1.46
NMRK1 nicotinamide riboside kinase 1	AOA060WPZ9	0.58	1.39
Protein transport protein Sec24B	AOA060W285	0.54	1.38
Protein kinase C PKC	AOA060X6F9	0.51	1.39
Kinesin-1 KIF5B	AOA060WML3	0.60	1.41
Thioredoxin reductases (TR)	AOA060XUV9	0.62	1.42
Methylmalonyl CoA epimerase MCEE	AOA060XNR5	0.56	1.45
Palmitoyl-protein hydrolase (lyplal1)	AOA060YP76	0.61	1.44
Probable ubiquitin carboxyl-terminal hydrolase FAF-X	AOA060XT85	0.64	1.45
2',3'-cyclic-nucleotide 3'-phosphodiesterase CNPase	AOA060W1Z9	0.65	1.47
Phosphatidylinositol transfer protein beta isoform PITPNB	AOA060XQV7	0.70	1.47
nudC domain-containing protein 3	AOA060Y4N3	0.76	1.50
atp6v1f ATPase H+ transporting V1 subunit F	AOA8C7QNX0	0.66	1.50
PTGES2 Gene - Prostaglandin E Synthase 2	AOA060YE60	0.50	1.51
Fibronectin FN	AOA060YRG9	0.54	1.55
Fibulin-1 FBLN1	AOA060XB63	0.72	1.53
GLRX5 Glutaredoxin 5 homolog	C1BI21	0.72	1.55
coenzyme Q : cytochrome c – oxidoreductase COMPLEX III	AOA060Z810	0.81	1.55
cAMP-regulated phosphoprotein 21 ARPP-21	AOA060Y8E9	0.61	1.58
PATL1	AOA060WEQ7	0.51	1.59
Calponin 2	AOA060YZQ0	0.78	1.60
bri3bp	AOA060XE57	0.59	1.62
cysS cysteine–tRNA ligase	AOA060W354	0.66	1.63
SLC27A4	AOA060XKK5	0.90	1.62
Histone deacetylase HDAC	AOA060Z7V8	1.13	1.61
V-ATPase	AOA060XXM1	1.15	1.61
5'-(N(7)-methylguanosine 5'-triphospho)-[mRNA] hydrolase / D10 decapping enzyme	AOA060YNK5	1.26	1.62
Heat Shock Protein Family A (Hsp70) Member 14 HSPA14	AOA060Y0Z6	0.57	1.67
Threo-3-hydroxyaspartate ammonia-lyase D-THA DH	AOA060YKPO	0.63	1.67
rcor1 REST corepressor 1	AOA674AG29	0.86	1.68
Isocitrate dehydrogenase IDH	AOA060Z6S7	0.92	1.69
Vacuolar protein sorting-associated protein 33B - VPS33B	AOA060WA63	1.07	1.73
Proteoglycan 4 or Lubricin	AOA060Z3V5	0.89	1.80
aifm2 Apoptosis inducing factor mitochondria associated 2	AOA060W214	0.53	1.72
Presequence protease (PreP)	AOA060WBN1	0.52	1.76
Dihydrolipoyl transacetylase dlat-1	AOA061A6R7	0.59	1.77
E3 ubiquitin-protein ligase NEDD4	AOA060Y4F6	0.73	1.81
Secretory carrier-associated membrane protein 2 (SCAMP2)	AOA060W547	0.72	1.82
Dynein cytoplasmic 1 heavy chain 1 DYNC1H1	AOA060XFE1	0.58	1.84
26S protease regulatory subunit 4 PSMC1	AOA060XW34	0.51	1.84
LIMA1 LIM domain and actin-binding protein 1	AOA060YJ77	0.72	1.89
RNA helicase MOV-10	AOA8C7LVX8	0.52	1.91
Caspase 3, apoptosis-related cysteine peptidase b	AOA060W2H2	0.88	1.96
TIP41-like protein	AOA060X165	0.68	2.01
Cdc42 effector protein 4 CDC42EP4	AOA060Z1R2	0.62	2.01
fatty-acid-binding protein (FABP)	AOA060YTS7	1.00	2.03
usp11 Ubiquitinyl hydrolase 1	AOA060XEN3	0.71	2.06
ACOT9 Acyl-CoA thioesterase 9	AOA060Y438	0.62	2.07
TIP41-like protein	AOA060WZQ8	0.83	2.05
UDP-N-acetylhexosamine pyrophosphorylase UAP1	AOA8C7UHI6	0.97	2.07
C-factor	AOA060WU91	0.69	2.10
UDP-N-acetylhexosamine pyrophosphorylase UAP1	AOA060WK17	1.00	2.11
Aldo-keto reductase family 1, member B1 (AKR1B1) - Aldose reductase	AOA060W451	1.17	2.08

Table S3. List of down-regulated proteins in L2AC31-KO vs WT RTs

Name of protein	Accession	log2(KO/WT)	log10(pval)
apolipoproteinB-100	A0A060W3H4	-1.61	4.62
apolipoproteinB-100	A0A060Y552	-3.23	4.12
homogentisate 1,2-dioxygenase (HGD)	A0A060YA42	-1.18	3.75
Carbonic anhydrase 1 (CA)	Q68YC2	-1.29	3.49
apolipoproteinB-100	A0A060Z709	-3.21	2.92
Sodium-coupled neutral amino acid transporter 4 (SNAT4)	A0A060X0J3	-1.17	2.85
Surfeit locus protein 2 SURF2	A0A060W7Q0	-1.61	2.79
D-aspartate oxidase	A0A060WJY0	-1.80	2.59
Gastrula zinc finger protein	A0A140F304	-1.64	2.56
venom factor isoform X1	A0A060XW02	-2.06	2.46
tRNA methyltransferase	A0A060WFW7	-2.61	2.38
Retinol dehydrogenase 12	A0A060X190	-2.15	2.34
SELENBP1 / methanethiol oxidase	A0A060XQH4	-1.18	2.38
ZNT7 Zinc transporter protein 7	A5PMX1	-1.05	2.32
Vitellogenin 1	Q92093	-2.02	2.19
Retinol-binding protein 2 (RBP2)	Q71B03	-1.09	2.17
MHC class I	A0A060WZV0	-1.43	2.13
Terminal uridylyl transferase 7 (TUT7)	A0A060YJN8	-1.09	2.13
Tropomodulin 3	A0A060ZI14	-1.91	2.10
Immunoglobulin kappa light chain	A0A060XIK2	-1.48	2.08
Sulfide:quinone oxidoreductase (SQOR)	A0A060YB67	-1.50	2.06
GSTM3 glutathione S-transferase mu 3	A0A060Y2H6	-1.23	2.03
C1-inhibitor (C1-inh)	A0A060WERO	-1.47	1.99
Ribosome-binding protein 1 (p180)	A0A060VRW0	-1.02	1.96
GTPase IMAP family member 8 (GIMA8)	A0A060YJA9	-1.32	1.94
Monocarboxylate transporter 7 (MCT7)	A0A060XZE8	-1.55	1.93
inactive rhomboid protein 2 (iRhom2)	A0A060WAR8	-1.46	1.91
Cu transport protein Antioxidant-1 (Atox1)	A0A060YR00	-1.01	1.90
NPC2 NPC intracellular cholesterol transporter 2	C1BGA1	-1.03	1.85
wdr92 - WD repeat-containing protein 92	A0A060XN54	-1.07	1.84
Phosphorylase kinase (PhK)	A0A060VME0	-1.05	1.83
Cathepsin F	A0A060WE48	-1.07	1.83
Aromatic L-amino acid decarboxylase (AADC or AAAD)	A0A060WI79	-1.53	1.80
Carboxypeptidase D	A0A060XHB4	-1.27	1.76
N-acetyltransferase 10 - NAT-10	A0A060WTM3	-1.55	1.75
PLRG1 - Pleiotropic regulator 1	A0A060XMA6	-1.31	1.73
Acyl-CoA thioesterase - ACOT	A0A060XF12	-1.44	1.71
Guanylate-binding protein 1 (GBP1)	A0A060X412	-2.74	1.69
dnttp2 deoxynucleotidyltransferase	A0A060WM03	-1.96	1.68
Butyrophilin subfamily 1 member A1 (BTN1A1)	A0A060X431	-1.36	1.67
Properdin	A0A060XDG4	-1.59	1.66
ZCHC4 - rRNA N6-methyltransferase	A0A060Y1B0	-1.03	1.63
FAD-dependent oxidoreductase 1 (FOXRED1)	A0A060VXJ0	-1.29	1.62
HIUHase, and 5-hydroxyisourate hydrolase	A0A8C7TKN0	-1.27	1.61
Golgi membrane protein 1 (GOLM1)	A0A060WNZ1	-1.01	1.38
Nucleobindin-2 - NUCB2	A0A060WJ28	-1.08	1.60

Understanding and harnessing chaperone-mediated autophagy (CMA) in the rainbow trout (*Oncorhynchus mykiss*)

Name of protein	Accession	log2(KO/WT)	log10(pval)
SLC27A6 - Long-chain fatty acid transport protein 6	AOA060YFS1	-2.15	1.60
Cytochrome c oxidase polypeptide VIIc	P80334	-1.17	1.59
PHYIP Phytanoyl-CoA hydroxylase-interacting protein	AOA060XE45	-2.29	1.54
Prolyl isomerase (also known as peptidylprolyl)	AOA060VQQ6	-1.28	1.52
Synaptosomal-Associated Protein, 25kDa (SNAP-25)	AOA060WCC0	-1.64	1.48
Cell adhesion molecule 1 (CADM1)	AOA060VYC8	-1.36	1.48
ubiquitin-like protein FUBI	C1BFG2	-1.31	1.48
CDGSH iron sulfur domain	C1BI29	-1.16	1.42
COMM domain-containing protein 9	AOA060XCH2	-1.34	1.35
GSTM3 - Glutathione S-transferase Mu 3	AOA060ZAG6	-1.00	1.34
NADH dehydrogenase (ubiquinone) 1 alpha NDUFA7	AOA060W5N8	-1.35	1.34
ACIN1 (Apoptotic Chromatin Condensation Inducer 1)	AOA060XGP3	-1.16	1.33
GPRC5C G-protein coupled receptor family C group 5	AOA060XR44	-1.45	1.32
ACIN1 (Apoptotic Chromatin Condensation Inducer 1)	AOA060Y2W1	-1.36	1.33
EARP-interacting protein homolog	AOA060XAA8	-1.01	1.31
Y-box binding protein YB-1	AOA060Y0T3	-0.77	1.31
UDP-glucuronosyltransferase 2A3 UGT2A3	AOA060YBS5	-0.90	1.32
EARP-interacting protein homolog	AOA060XAA8	-1.01	1.31
Cell division cycle and apoptosis regulator protein 1 CCAR1	AOA060XZF0	-0.98	1.32
Calcium/calmodulin-dependent protein kinase type 1 CAMK1	AOA060YCX0	-0.61	1.35
Thiopurine methyltransferase TPMT	AOA060WUW1	-0.73	1.37
Activating signal cointegrator 1 (ASC-1)	AOA060Z7U5	-0.68	1.40
ctsh cathepsin H	AOA8C7S3U7	-0.62	1.40
scavenger receptor class B type I (SR-BI)	AOA060WH67	-0.57	1.39
Sarcosine dehydrogenase	AOA060YZQ1	-0.58	1.41
OS9 endoplasmic reticulum lectin ERLEC1	AOA8C7TGM4	-0.53	1.40
Protein kinase C and casein kinase substrate PACSIN3	AOA060VSI0	-0.51	1.40
GTP-binding nuclear protein Ran	AOA060VZL7	-0.89	1.37
Carboxypeptidase Q	AOA060YCQ8	-0.89	1.41
UDP-glucuronosyltransferase	AOA060YHW2	-0.93	1.41
Estradiol 17-beta-dehydrogenase 8 HSD17B8	AOA060VRD9	-0.83	1.43
NADH dehydrogenase [ubiquinone] 1 beta NDUFB6	AOA060XUW9	-0.83	1.44
BTD Biotinidase	AOA060XNN4	-0.74	1.47
Lactoylglutathione lyase	AOA060WQQ3	-0.71	1.48
NDUFB11 NADH dehydrogenase 1 beta subcomplex subunit 11	AOA060XEM0	-0.56	1.47
Glycoprotein endo-alpha-1,2-mannosidase MANEA	AOA060XJZ5	-0.58	1.48
CD276 antigen-like	AOA060WBI1	-0.66	1.48
vtg1 Vitellogenin	Q92093	-2.02	2.19
Sulfide:quinone oxidoreductase (SQOR)	AOA060ZDL1	-0.91	2.78
Organic solute transporter subunit alpha (SLC51A) or OST-alpha	AOA060XRH2	-0.75	2.82
pm20d1 N-fatty-acyl-amino acid synthase/hydrolase	AOA060XQK1	-0.87	2.64
Ras-like GTP-binding protein Rho1	AOA060X4I6	-0.57	3.63
Lysosomal-associated membrane protein 1 (LAMP-1)	AOA8C7VQL2	-1.64	2.56
TM9SF2 transmembrane 9 superfamily member 2	AOA674CL93	-0.60	2.37
ndufv1 NADH:ubiquinone oxidoreductase	AOA674CHH5	-0.61	2.34
cytosolic non-specific dipeptidase CNDP2	B5X4T7	-0.54	2.28
Prefoldin subunit 5 PFDN5	AOA060WP50	-0.50	2.25
GDP-L-fucose synthase	AOA060YFS3	-0.66	2.24
POLR1C DNA-directed RNA polymerases I and III subunit RPAC1	AOA060WQ06	-0.77	2.24
Monocarboxylate transporter 10 SLC16A10	AOA060WBK6	-0.74	2.20
Integrin beta-1 (ITGB1), also known as CD29	AOA060X309	-0.65	2.18

Understanding and harnessing chaperone-mediated autophagy (CMA) in the rainbow trout (*Oncorhynchus mykiss*)

Name of protein	Accession	log2(KO/WT)	log10(pval)
Membrane-associated progesterone receptor component 2 PGRMC2	A0A8U0Q940	-0.61	2.17
Sarcosine dehydrogenase	A0A060YK79	-0.51	2.17
PRMT1 protein arginine methyltransferase 1	A0A060X602	-0.55	2.14
DHRS4 - Dehydrogenase/reductase SDR family member 4	A0A8U0QWT	-0.63	2.13
Adenylate cyclase	A0A060WN4	-0.58	2.08
TPK2 - Thiamine pyrophosphokinase 2	A0A060Z2Y2	-0.51	2.08
PTER - Phosphotriesterase-related protein	A0A060Y8N1	-0.62	2.02
60S acidic ribosomal protein P2	A0A060WJW	-0.67	2.02
DPYD dihydropyrimidine dehydrogenase	A0A060YFT0	-0.79	2.02
ACY3 Aspartoacylase	A0A060WF45	-0.94	1.99
CRYL1 Crystallin, lambda 1 or L-gulonate 3-dehydrogenase	A0A060XAB5	-0.80	1.97
GTP cyclohydrolase I feedback regulatory protein GFRP	C1BHD1	-0.69	1.96
GSTK1 glutathione S-transferase kappa 1	A0A060XKR8	-0.59	1.98
phr2aB Serine/threonine-protein phosphatase 2A regulatory	A0A060XGH8	-0.58	1.97
PXMP2 - Peroxisomal membrane protein 2	A0A060WGG	-0.87	1.92
TM9SF2 transmembrane 9 superfamily member 2	A0A8K9V045	-0.55	1.94
FAHD2A (Fumarylacetoacetate Hydrolase Domain Containing 2A)	A0A060W664	-0.74	1.85
Malate synthase	A0A060XNA5	-0.52	1.85
Hepatocyte nuclear factor 4 alpha (HNF4A)	A0A060X563	-0.77	1.83
Indoleamine 2,3-dioxygenase 2 (IDO2)	A0A060VVQ3	-0.96	1.81
KH domain-containing, RNA-binding, signal transduction-associated	A0A060YV02	-0.69	1.74
cysteine-rich with EGF-like domains 2 (CRELD2)	A0A8C7VXU9	-0.84	1.75
MYEF2 myelin expression factor 2	A0A061A2A1	-0.96	1.75
Acyl-CoA thioesterase 16 ACOT	A0A060YTU9	-0.89	1.72
Peroxidase	A0A060XUD1	-0.62	1.70
Atp11c - Phospholipid-transporting ATPase 11C	A0A060XC13	-0.52	1.69
Alpha-1-microglobulin/bikunin precursor AMBP	A0A060YFZ1	-0.63	1.68
Aldolase B ALDOB	A7L6A8	-0.62	1.67
Transportin-1	A0A060Y475	-0.57	1.65
Integrin beta-1 (ITGB1)	A0A060WSX3	-0.88	1.68
UDP-glucuronosyltransferase 2A1 UGT2A1	A0A060Y8W2	-0.94	1.65
Cytochrome c oxidase polypeptide VIIIc cox-7c	P80334	-1.17	1.59
Nucleobindin-2 - NUCB2	A0A060WJ28	-1.08	1.60
Dihydropyrimidinase	A0A060ZNP9	-0.93	1.62
Desmoplakin a	A0A060VWG	-0.82	1.62
Glycerol-3-phosphate dehydrogenase (GPDH)	A0A8C7P1A0	-0.61	1.63
UDP-glucose 6-dehydrogenase	A0A060WVE5	-0.95	1.56
uncharacterized protein LOC110526684	A0A060WA66	-0.78	1.55
Low-density lipoprotein receptor-related protein-1 (LRP1)	A0A060XD42	-0.71	1.54
Pyridoxine 5'-phosphate synthase DXP	A0A060W490	-0.60	1.53
cysteine-rich with EGF-like domains 2 (CRELD2)	A0A8C7VXU9	-0.71	1.61
UFM1 ubiquitin fold modifier 1	A0A060YYP8	-0.60	1.61
NOL5A Nucleolar protein 56	A0A060W4J3	-0.67	1.60
U6 snRNA-associated Sm-like protein LSM7	C1BH51	-0.64	1.57
Aldo-keto reductase family 1, member B1 (AKR1B1) - Aldose reductase	A0A060ZCT9	-0.61	1.56

Table S4. List of differentially-regulated proteins in L2AC31-KO vs WT RTs mentioned and potential KFERQ-like motifs

Upregulated proteins				
Name of protein	Accession number	log2(K)	log10(P)	KFERQ-like motif
Isocitrate dehydrogenase (IDH)	A0A060W4K6	1.55	3.67	1 canon. 1 acet.
Isocitrate dehydrogenase (IDH)	A0A8C7QHT2	1.92	3.61	1 acet. 1 phos.
Isocitrate dehydrogenase (IDH)	A0A060Z6S7	0.92	1.69	1 acet.
Ubiquitin-conjugating enzyme E2 K (UBE2K)	A0A8C7V187	2.09	3.37	3 canon. 4 acet.
very long-chain acyl-CoA synthetase ACSVL	A0A060YZL8	1.23	2.87	1 canon.
RAD23 homolog A	A0A060Y182	3.81	2.77	4 phos. 1 acet.
RAD23 homolog A	A0A060YG13	4.05	2.80	4 phos. 1 acet.
Aldolase - fructose-bisphosphate (ALDOA)	A0A060WUI1	1.18	1.90	1 canon. 2 phos. 1 acet.
Aldolase - fructose-bisphosphate A (ALDOA)	A0A060XHN5	1.16	1.80	1 canon. 1 phos. 1 acet.
Vacuolar protein sorting-associated protein 33B (VPS33B)	A0A060WA63	1.07	1.73	1 canon.
Vacuolar protein sorting-associated protein 4B (VPS4B)	A0A060X3F6	1.34	1.64	1 phos. 4 acet.
Thioredoxin	C1BH85	3.08	1.59	none
Protein Tyrosine Phosphatase Non-Receptor Type 23 (PTN23)	A0A060WXG6	1.23	1.53	2 canon. 6 phos. 2 acet.
Thioredoxin reductases (TR)	A0A060XUV9	0.62	1.42	1 phos. 2 acet.
ATP citrate synthase (ACLY)	A0A060WTD0	1.69	1.38	none
Glucose-6-phosphate 1-dehydrogenase (G6PD)	A0A060WHZ0	1.16	1.34	none
Glucose-6-phosphate 1-dehydrogenase (G6PD)	A0A060XEX6	0.77	1.57	1 canon. 1 phos. 1 acet.
Hexokinase (HK)	A0A060WFB8	0.52	2.65	5 canon. 6 phos. 1 acet.
Malate dehydrogenase (MDH)	A0A8C7TVA0	0.55	2.57	none
Malate dehydrogenase (MDH)	A0A060XXI1	0.55	2.54	none
Glutamate-cysteine ligase (GCL)	A0A8C7VYS9	1.35	2.26	1 canon.
phosphofructokinase-2 (PFK-2)	A0A060Y9T0	0.51	1.30	1 canon.
Vacuolar protein sorting-associated protein 33B (VPS33B)	A0A060WA63	1.07	1.73	1 canon.
26S protease regulatory subunit 4 (PSMC1)	A0A060XW34	0.51	1.84	1 canon. 1 acet.
fatty-acid-binding protein (FABP)	A0A060YTS7	1.00	2.03	none
Downregulated proteins				
Name of protein	Accession number	log2(K)	log10(P)	KFERQ-like motif
apolipoproteinB-100	A0A060W3H4	-1.61	4.62	9 canon. 3 phos. 8 acet.
apolipoproteinB-100	A0A060Y552	-3.23	4.12	none
apolipoproteinB-100	A0A060Z709	-3.21	2.92	3 phos. 1 acet.
FAD-dependent oxidoreductase 1 (FOXRED1)	A0A060VXJ0	-1.29	1.62	1 canon. 1 acet.
Adenylate cyclase	A0A060WN48	-0.58	2.08	4 canon. 3 phos. 1 acet.

ADDITIONAL RESULTS 3: CMA score increases upon Mercury exposure

ADDITIONAL RESULTS 3: CMA score increases upon Mercury exposure

After having used the CMA score to assess cellular homeostasis in fish facing a hypoxic stress, we decided to extend its application to assess the effects of environmental toxicity. To do so, we exposed first-feeding RT fry to a diet enriched in Methylmercury (Hg), a well-established inducer of oxidative stress and organ failure in fish, as demonstrated by previous studies^{278,279}. After 3 weeks of Hg-rich feed, we collected RT fry and calculated the CMA score in whole body (Fig 20A). The results suggested a slight increase in the CMA score in fish exposed to Hg contamination, suggesting an overall induction of the CMA network in response to this stressful condition (Fig 20A). In the light of these findings and to explore potential tissue-specific variations in the CMA score response to Hg exposure, we then conducted an additional experiment using 30 g juvenile RT, allowing us to isolate different tissues. While no variation in the CMA score was observed in the brain (Fig 20B), a significant increase was detected in the liver following 3 weeks of Hg exposure (Fig 20C). This level of precision shows that CMA machinery activation is finely tuned and depends on tissue- or even cell-type, as demonstrated in mammalian cells¹⁵. Furthermore, it opens new perspectives regarding the potential of quickly measuring CMA status in non-invasive tissues of fish (e.g. blood or mucus) but also in uncommon species, also subjected to increasing severity of climate events, especially when unable to measure CMA activity conventionally (e.g., lysosome isolation).

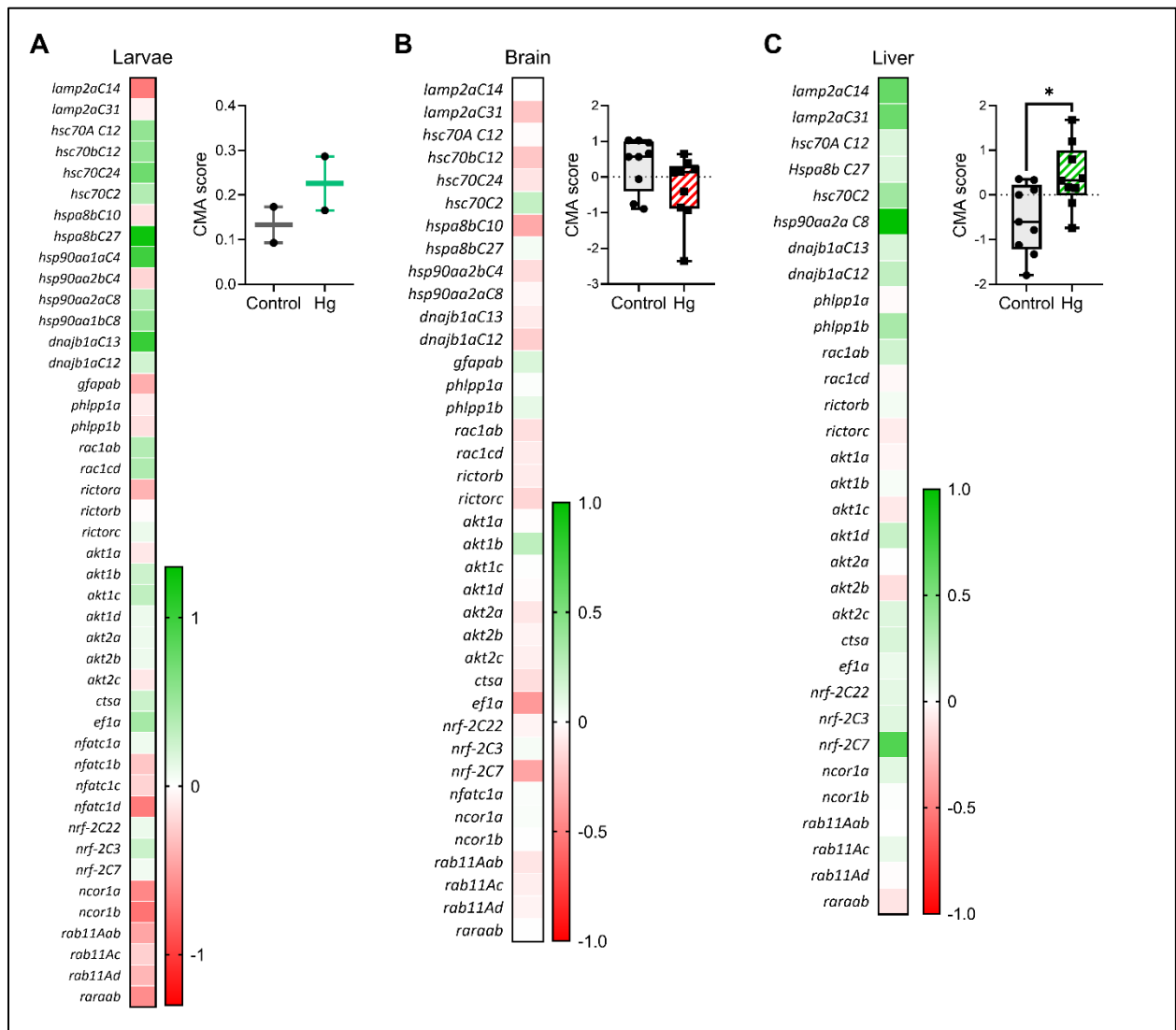


Figure 20: Use of CMA score as a prognostic tool to assess cellular homeostasis in fish exposed to stressful conditions (A) Left, Expression of CMA network genes in RT fry fed the Hg diet for 3 weeks relative to control fry. Right, CMA activation score based on expression of CMA network genes in RT fry fed with normal diet (control) vs high Hg diet (Hg) for 3 weeks (n=2 pools of 10 fry). (B and C) Left, Expression of CMA network genes in the brain (B) and the liver (C) of RT juveniles fed the Hg diet for 3 weeks relative to control fish. Right, CMA scores in the brain (B) and liver (C) based on the expression of CMA network genes (n=9). All values are shown as min. to max. \pm SEM (t-test; *, $p < 0.05$).

ADDITIONAL RESULTS 4: CMA as a regulator of food intake?

ADDITIONAL RESULTS 4: CMA as a regulator of food intake?

As the newly generated L2AC31-KO RTs grew, the observation of their feeding behavior suggested potential differences in food intake. Accordingly, we conducted a study focusing on feed intake parameters and mRNA expression of genes related to the regulation of feed intake in brain were measured. The experiment lasted 30 days and comprised of two tanks, each containing 17 individuals of either WT or L2AC31-KO RTs. Food intake was measured (Fig 21) and it suggested that the L2AC31-KO RTs displayed a different feeding behavior.

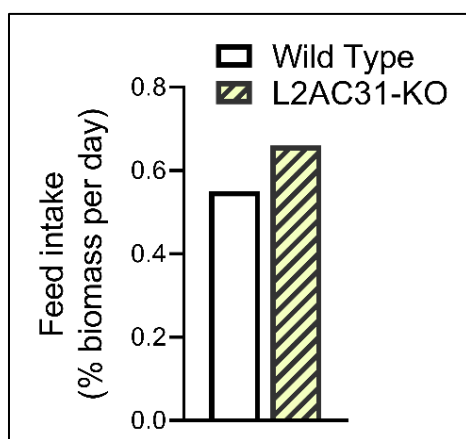


Figure 21: (A) Food intake in WT vs L2AC31-KO RTs. (n=1 pool of 17 RTs/line), values are mean.

The hypothalamus is the main center of control for the regulation of food intake²⁸⁰. Depending on the energy demand of the organism, the hypothalamus will transmit neuroendocrine factors that inhibit or stimulate feed intake (Fig 22). Within the mammalian hypothalamic arcuate nucleus, two distinct sets of neurons respond to increased levels of circulating metabolites like fatty acids, glucose, and amino acids. They exhibit a dual response: either downregulating agouti-related peptide (AgRP) and neuropeptide Y (NPY), or upregulating cocaine and amphetamine-related transcript (CART) and pro-opiomelanocortin (POMC) (Fig 22). These two neuronal populations mutually influence each other's actions and communicate with higher-level neurons in distinct regions. In these regions, different neuropeptides are released, eventually regulating food intake²⁸¹. Within the hypothalamus, POMC and AgRP both bind the melanocortin-4 receptor (MC4R), which mediate either anorexigenic or orexigenic signals to manage energy homeostasis²⁸². The critical role played by MC4R in mammals has also been described in teleost species^{283,284}.

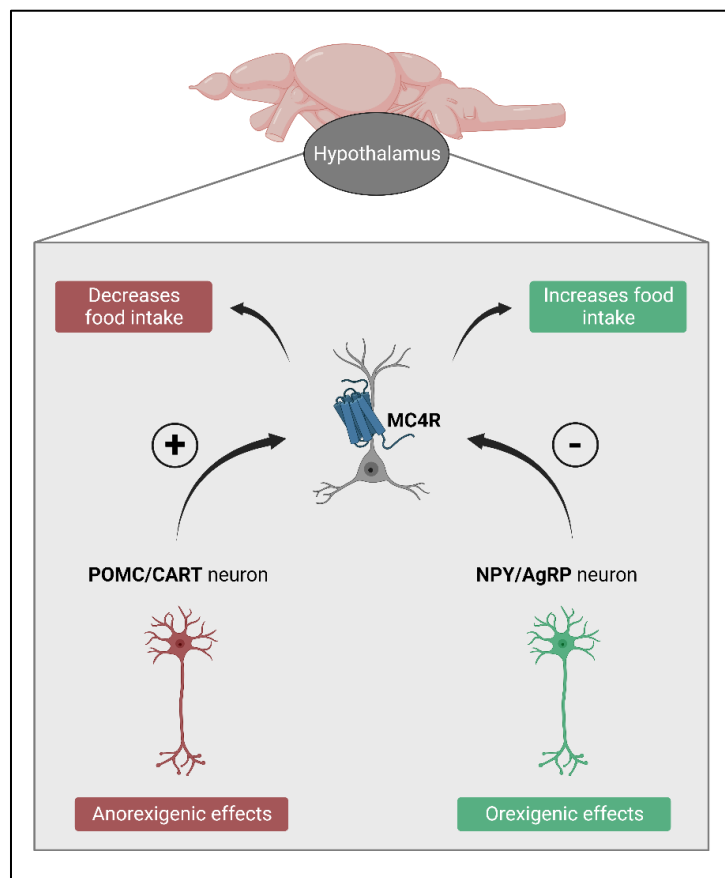


Figure 22: Mechanisms involved in the regulation of food intake. In response to negative energy balance, Agouti-related protein AgRP, coexpressed with the neuropeptide Y (NPY) on hypothalamic neurons, inhibits melanocortin 4 receptor (MC4R) to induce food intake. In the opposite situation, pro-opiomelanocortin (POMC) and cocaine- and amphetamine-regulated transcript (CART) in the hypothalamus suppress feeding.

An analogous form of arcuate nucleus, called nucleus lateralis tuberis (NL_{Tv}) is present in fish²⁸⁵, and contains the AgRP/NPY and POMC/CART neurons. As in mammals, studies have shown that food intake and energy expenditure can be regulated following sensing mechanisms of nutrient levels^{286,287}. The mRNA expression of the main actors of food intake regulation was investigated in brain of L2AC31-KO RTs (Fig 23). At first glance, we can notice the absence of expression of *lamp2a-C31* and a potential compensation of this absence in *lamp2a-C14* expression in L2AC31-KO RTs (Fig 23A). Levels of expression of both *mc4r* paralogs, which play a critical role in the control of appetite, decrease in the absence of L2AC31, hinting at orexigenic effects (Fig 22 and 23B). Potential orexigenic effects can also be hypothesized from the increase in *Agrp2* mRNA expression and decrease in *Cart* mRNA expression upon L2AC31 inactivation (Fig 22, 23C and 23D). Only the decrease in *Npyb* expression in L2AC31-KO RTs could indicate possible anorexigenic effects (Fig 22C). However, it is believed that *Npyb* likely does not contribute to feeding regulation, as shown in Nile tilapia²⁸⁸ and Atlantic salmon²⁸⁹.

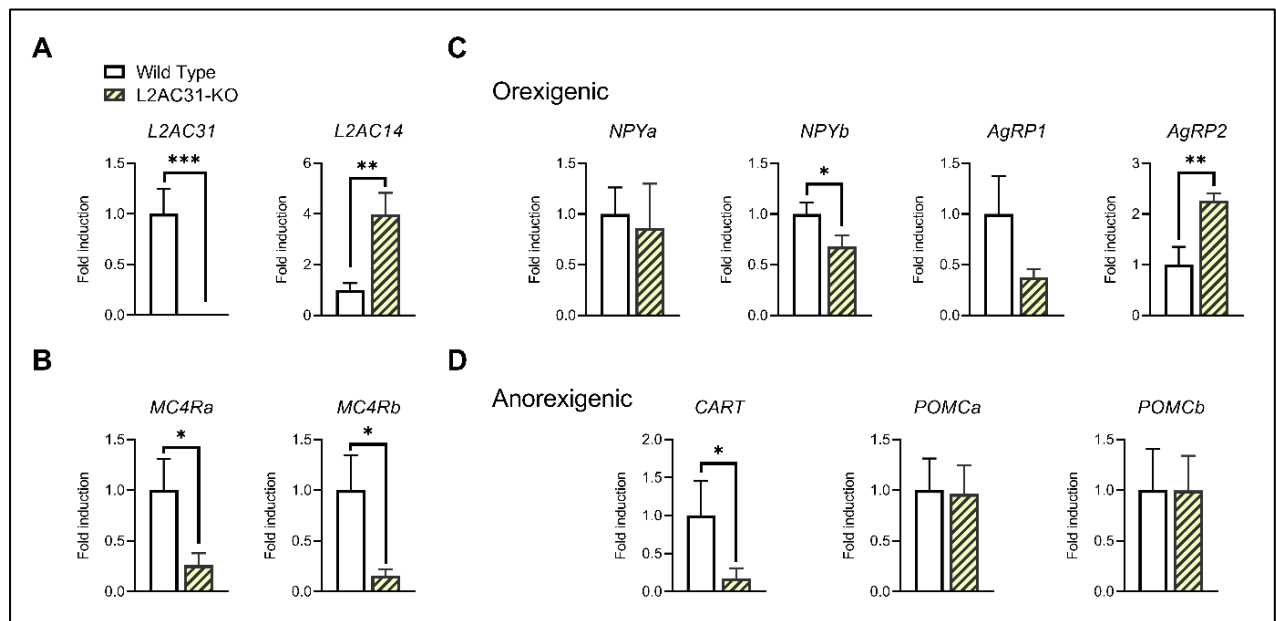


Figure 23: (A) Brain mRNA expression of *lamp2a* genes. (B), (C) and (D): Brain mRNA expression of food intake-related genes in WT vs L2AC31-KO RTs. (n=7, values are mean + SEM shown by fold induction respect to WT fish). A Mann-Whitney test was performed comparing mRNA of WT and L2AC31-KO (*, p<0.05; **, p<0.01; *, p<0.001).**

Taken together with the significant changes in mRNA levels of some appetite regulators, this data strongly suggest CMA is involved in the control of feed intake in RT. Nevertheless, more results are needed to identify the exact mechanism behind CMA regulation of appetite control.

In parallel, we also conducted a pilot quantitative proteomics analysis on the brain of L2AC31-KO RTs compared to the WT. We identified 5852 proteins, among which 1.09% (64 proteins) were significantly upregulated and 1.35% (79 proteins) were significantly downregulated in L2AC31-KO RTs compared to WT.

Among the downregulated proteins, we found the protein orthologs of mammalian *bona fide* CMA substrates hexokinase (HK) (Fig 24), which is one of the rate-limiting enzymes of glycolysis^{290,291} and ATP citrate lyase (ACLY), which initiates de novo lipid synthesis²⁹² (Fig 24). If they were indeed CMA substrates in RT, it would imply their upregulation in absence of CMA. Nonetheless, it is interesting to note that in the present study only the soluble protein fraction was extracted and analyzed. In 2021, Bourdenx et al. mention that CMA blockage in mice brains impacts the neuronal proteome, and CMA substrate proteins, like pyruvate dehydrogenase (PK), aldolase, and lactate, appeared to form aggregates and become insoluble²⁵⁴. It is then possible to suppose that the downregulation of Hk and Acly observed here in the soluble fraction following L2AC31 inactivation might have been caused by

an excessive accumulation of these aggregated proteins in the insoluble fraction. In addition, they also describe an enrichment of clathrin adaptor protein AP2 α and endocytosis-related proteins in the insoluble fraction of LAMP2A-KO mice brains²⁵⁴. Interestingly, we observed a downregulation of AP-2 complex subunit mu and clathrin coat assembly protein AP180 in the soluble fraction (Fig 24). This suggests a possible accumulation of insoluble forms of these proteins, indicating a shift towards insolubility in the CMA-deficient brain proteome. The list of downregulated enzymes encompasses several components of mitochondrial metabolism, such as mitochondrial carrier homolog 2 (MTCH2), translocase of outer mitochondrial membrane 40 homolog (TOMM40), NADH dehydrogenase 1 beta subcomplex subunit 1 (NDUFB1), and sorting and assembly machinery component SAMM50. These enzymes play critical roles in mitochondrial dynamics, morphology, and metabolism²⁹³⁻²⁹⁵. It is conceivable that enzymes involved in mitochondrial metabolism may also be targeted by CMA, potentially leading to the formation of aggregates that become insoluble when CMA is impaired. Situations of cellular stress, such as hypoxia in *C. elegans*, have been shown to result in the accumulation of mitochondrial components like the Complex III electron transport chain protein UCR-11²⁹⁶. Another hypothesis regarding the mitochondrial enzyme downregulation is that aggregates tend to inhibit mitochondrial function²⁹⁷. For example, in pathologies such as Alzheimer's and Parkinson disease, protein aggregates (e.g. A β , tau, α -synuclein) with a high probability of aggregating can inhibit mitochondrial trafficking²⁹⁸. Further research is required to precisely identify the mechanisms linking CMA and protein quality control with mitochondrial metabolism.

Multiple enzymes involved in nutrient sensing and lipid metabolism were found amongst downregulated and upregulated proteins (Fig 24). Phosphoinositide phospholipase C (Plc) was downregulated while inorganic diphosphatase (Ppase) and succinate-CoA ligase (Suglg2) were upregulated (Fig 24), indicating potential lipid catabolism²⁹⁹⁻³⁰¹. In addition, the upregulation of arachidonate--CoA ligase (Acsl4), ADP-dependent glucokinase (Adpgk), and of adenylate cyclase type 9-like (Adyc9) (Fig 24), point at a potential increased AMP production, which imply differential regulation of energy homeostasis and signal transduction. Additionally, the involvement of AMPk pathway in feed intake could be related to the L2AC31-KO RTs differential feed intake³⁰².

Overall, these findings highlight the importance of considering the solubility of proteins when identifying putative CMA substrates and points out significant alterations in the sensing and control of energy stores due to L2AC31 inactivation. Further research is needed to identify CMA substrates, their potential contribution to feed intake regulation and investigate the specific pathways in which CMA is involved.

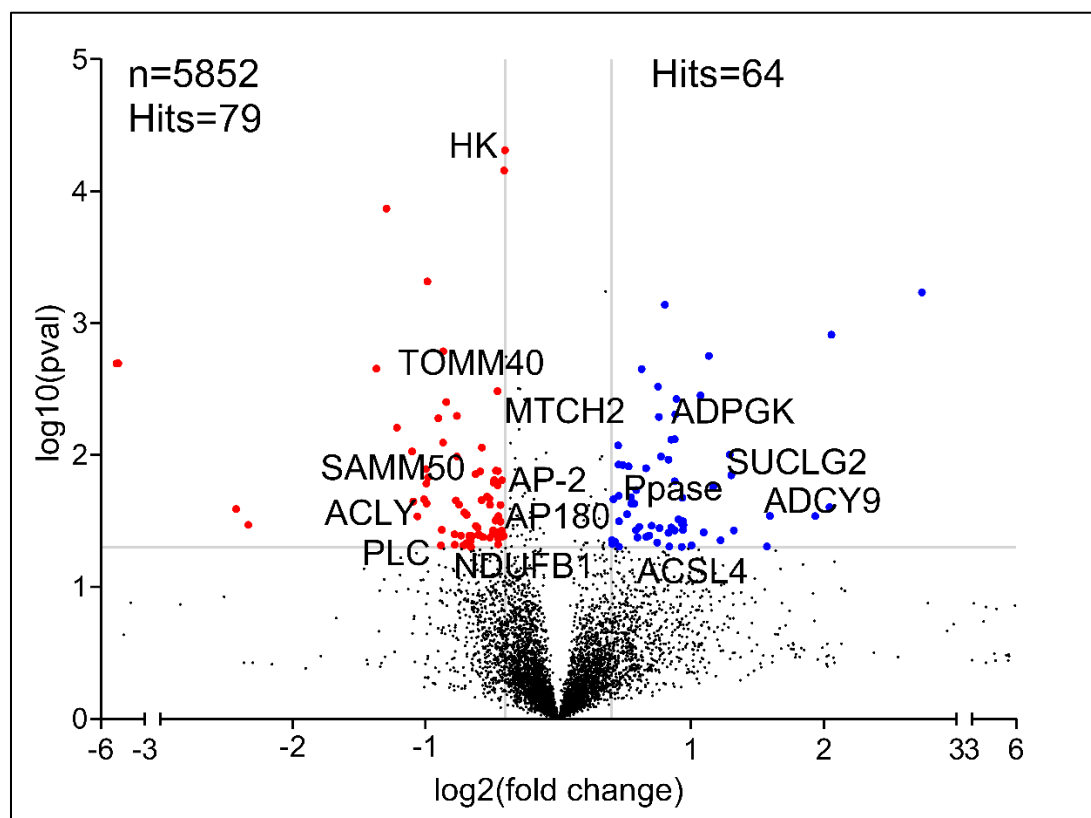


Figure 24: Volcano plot of the quantitative proteomics analysis of brain L2AC31-KO vs WT RTs. Top left: number of identified proteins (n) and significantly down-regulated hits. Top right: number of significantly up-regulated hits. Blue and red dots indicate significantly down- and up-regulated proteins, respectively ($p < 0.05$ and fold change > 1.3).

General discussion

The main objectives of this PhD were to characterize CMA in the RT, uncover its various roles and evaluate its potential as an indicator of cellular stress. The data we gathered suggest that these mechanisms likely appeared sequentially in the course of evolution, with eMI probably being very ancient and CMA appearing much later during the vertebrate radiation. This analysis also indicates that, although CMA certainly exists in the majority of vertebrates, including fish, its physiological role may have evolved.

Anticipating the presence of CMA genetic material in RT, it became necessary to investigate the mRNA expression of the CMA-related genes. These genes were examined throughout developmental stages and in adult tissues to gain insights into potential physiological pathways where CMA might be implicated. The results demonstrated that genes related to CMA machinery were expressed throughout embryogenesis and potentially needed at specific stages (e.g., onset of liver development). Additionally, both *lamp2a* copies displayed a high expression in tissues with metabolic implications. After the first characterization of CMA in RT, a demonstration of its activity was needed. Consequently, we opted to use the established gold standard for quantifying *in vivo* CMA activity. This involves assessing the binding and uptake of a CMA substrate (GAPDH) in isolated CMA-competent (CMA⁺) lysosomes. This method is extensively described in mice and we successfully adapted it to RT. Having confidently isolated CMA⁺ lysosomes, we were then able to quantify the binding and uptake of GAPDH. The findings revealed that the lysosomes in RT exhibited CMA activity, which was reliant on the presence of HSC70 and ATP. Furthermore, we observed that starvation, a well-known inducer of CMA in mammals, also triggered CMA activity in RT.

Being confident that RT exhibited CMA activity, we proceeded to delve deeper into our research to unravel its various roles. To this end, we generated a stable RT KO line lacking *lamp2a* from chromosome 31 (L2AC31-KO), as our latest gene knock-down experiments performed in an RT cell line (RTH-149) demonstrated that the other copy (on chromosome 14) shows little if any involvement in CMA activity²⁵³. As CMA is known to target many metabolic pathways in mammals, we investigated the physiological consequences of *lamp2a* C31 deletion. Our observations revealed that L2AC31-KO RTs displayed significantly higher body weight and length compared to their WT counterparts, indicating that the absence of Lamp2A C31 leads to metabolic changes in this species. As RT is recognized as glucose-intolerant species²⁵⁶, we subjected both WT and L2AC31-KO RTs to a high

carbohydrate diet, mimicking a strong physiological stress. L2AC31-KO fish exhibited significantly higher levels of hepatosomatic (HSI) and gastrosomatic (GSI) indexes as well as clear metabolic defects. Finally, we conducted a proteomics analysis to analyze the disruptions in the proteome experienced by the L2AC31-KO RTs. We observed differentially-regulated proteins involved in both metabolism and the response to oxidative stress, which highlighted CMA's critical role as a gatekeeper of hepatic proteostasis in RT.

Given the role of CMA in maintaining cellular homeostasis upon environmental stress, we decided to use the CMA score as a stress gauge in RT. We used RT cells subjected to different known CMA triggers, as CMA activity can be quantified using a KFERQ-PA-mCherry1 CMA reporter. This study revealed that in the RT analyzed cell line CMA was activated by starvation or oxidative stress. In addition, this allowed us to adjust the CMA score calculation for later utilization.

We exposed RTs to moderate hypoxia, as a way to mimic a current environmental stressor for fish. The RT displayed an overall increased CMA score upon exposure. As the exposure was only moderate, it underscores the sensitivity of the CMA score as a marker for cellular homeostasis.

Certain aspects of the study hinted at possible deviations from the established understanding of CMA, thus introducing novel insights into the exploration of CMA in fish. This discussion will now delve into these emerging perspectives.

PART 1: L2AC31 inactivation and compensation of other proteolytic pathways

As we saw previously, the inactivation of L2AC31 resulted in significant proteome remodeling in the liver, particularly affecting proteins involved in metabolic pathways. However, a large number of proteins associated with other proteolytic pathways were also upregulated (Fig 24), possibly indicating a compensatory response.

Several proteins associated with the proteasome system exhibited upregulation. Notable examples include ubiquitin-26S protease regulatory subunit 4 (Psmc1), which is part of the 19S proteasome complex (Fig 25). Additionally, E3 ubiquitin-protein ligase (Nedd4), UV excision repair protein (Rad23), and probable ubiquitin carboxyl-terminal hydrolase (Faf-x) showed increased expression (Fig 25). These proteins play crucial roles in processing ubiquitin precursors and facilitating the targeting and delivery of polyubiquitinated proteins to the proteasome³⁰³⁻³⁰⁵. Furthermore, the upregulated proteins encompassed enzymes involved in ubiquitination and the subsequent proteasomal degradation of target proteins. This group includes protein ligase (Ubr5), ubiquitin-conjugating enzyme E2 K (Ube2k), and suppressor of the G2 allele of *skp1* (Sgt1)³⁰⁶⁻³⁰⁸ (Fig 25). Overall, the upregulation of many proteasome system components following L2AC31 inactivation suggests a potential compensatory mechanism. Previous studies have also suggested a potential link between

these two mechanisms¹⁹⁰, particularly indicating a proteasome compensation response to CMA inactivation¹⁷².

Interestingly, vacuolar protein sorting-associated protein 4B (Vps4b) was also upregulated in L2AC31-KO RTs (Fig 25). Vps4b is an essential component of the ESCRT machinery, contributing to the formation of multivesicular bodies (MVBs) and playing a critical role in endosomal microautophagy (eMI)³⁰⁹. This upregulation suggests an increase in eMI activity following L2AC31 inactivation, providing further hints that there is a close relationship between CMA and eMI mechanisms.

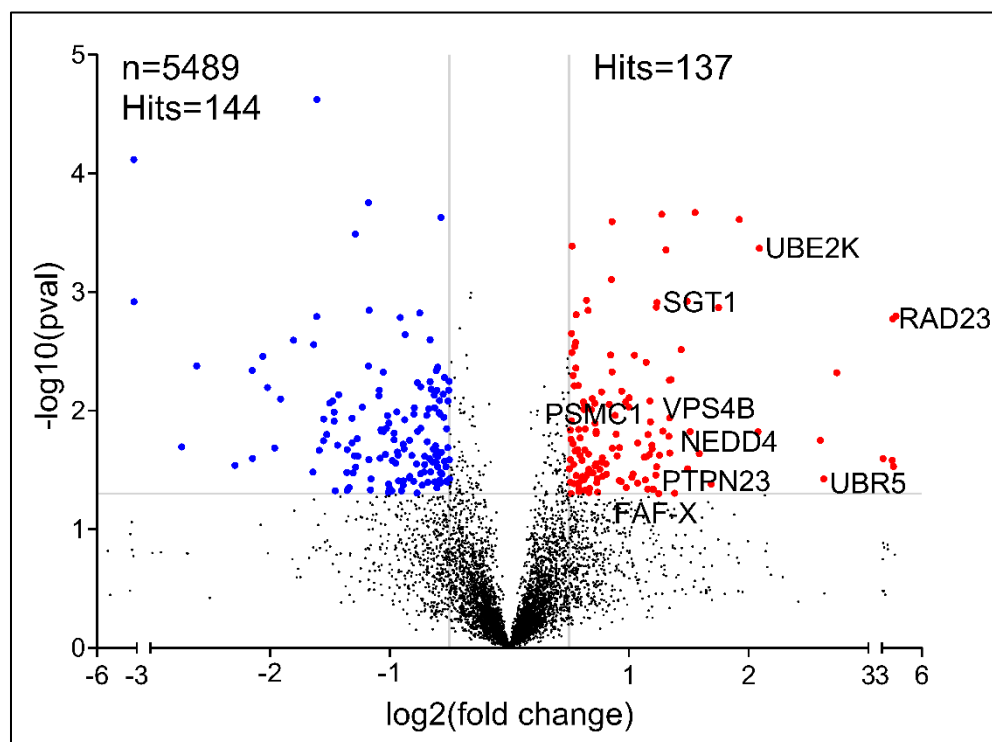


Figure 25: Volcano plot of the quantitative proteomic analysis of liver L2AC31-KO vs WT RTs. Top left: number of identified proteins (n) and significantly down-regulated hits. Top right: number of significantly up-regulated hits. Blue and red dots indicate significantly down- and up-regulated proteins, respectively ($p < 0.05$ and fold change > 1.41).

Vélez et al. 2023 conducted an experiment on a RT hepatocyte cell line and transfected the cells with small interfering RNAs (siRNA) designed to specifically target and knockdown *lamp2a* C31 (si31)²⁵³. 64 proteins were differentially expressed in the knockdown cells (Fig 26). Among the upregulated proteins, Tsg101 was appealing. In mammals, Sahu et al. discovered that this protein is a core component of the ESCRT-1 machinery and plays a vital role in eMI¹⁵⁰. As a result, the increased Tsg101 levels observed in CMA-deficient conditions suggest a potential eMI compensation. In this proposed

scenario, it becomes plausible that CMA activity directly shapes eMI by regulating Tsg101 levels, a hypothesis that undoubtedly warrants in-depth exploration in future research.

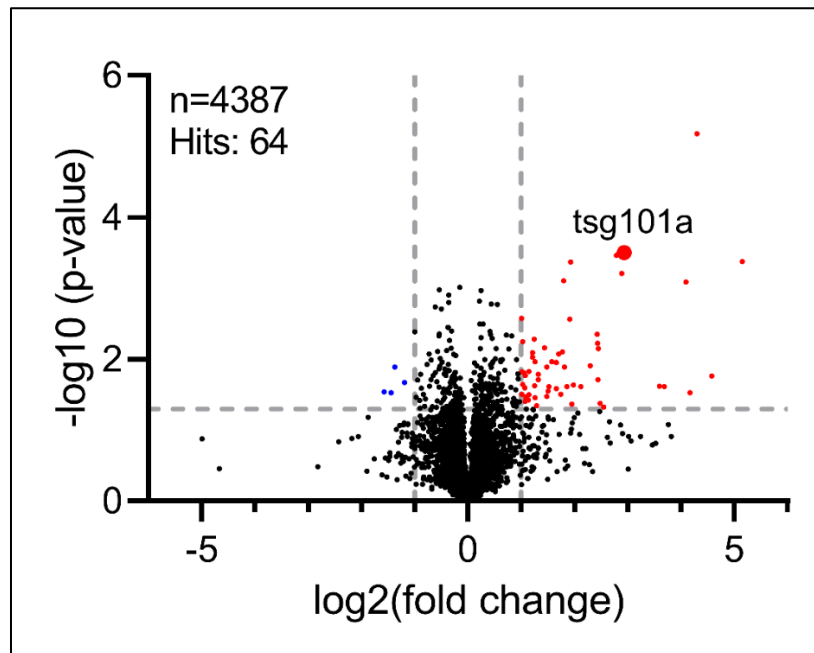


Figure 26: Volcano plot of the quantitative proteomic analysis of RTH-149 cells transfected with si31 and compared to control. Adapted from Vélez et al. 2023.¹¹³ Top left: number of identified proteins (n) and significantly differentially regulated hits. Blue dots indicate differentially downregulated proteins, and red dots correspond to upregulated proteins ($p < 0.05$ with ≥ 2 fold change).

PART 2: The interplay between CMA and eMI

The preceding discussion sheds light on a perspective that, as of now, remains obscure. The interplay between CMA and eMI revolves around the pathway taken by the KFERQ/Hsc70 complex, either toward Lamp2A at the lysosomal membrane (CMA) or transported to the LE/MVB to bind phosphatidylserine residues on the LE/MVB membrane (eMI)^{153,262}. One can then wonder how the complex is directed toward one or the other pathway and what cellular mechanisms lie behind this machinery.

The suggested eMI compensation observed in the proteomic analysis of L2AKO-C31 RTs and si31 cells strongly suggests a mechanistic regulation in the interplay between these two routes. Various hypotheses have emerged as to why certain substrates undergo degradation through either eMI or CMA. It was recently confirmed that if the substrate proteins are in a semi-aggregated state, organized into higher molecular weight complexes, or incapable of unfolding, they cannot be degraded by CMA but remain amenable for eMI degradation¹⁸¹. For instance, an important discovery by Caballero et al.

is that endogenous proteins like TAU, a cytoskeletal protein linked to neurodegeneration, undergo simultaneous degradation through both eMI and CMA¹⁷⁷. They discovered that pathogenic mutations in Tau changed the amount of protein degraded by these two pathways, which implies that inherent characteristics of the protein itself (mutations, post-translational modifications, oligomeric state...) may account for the autophagic shift of the substrate¹⁷⁷. It is also conceivable that under conditions characterized by high CMA activity and low eMI activity, such as during specific stages of starvation, molecular components of eMI may become susceptible to targeting by CMA³¹⁰. In 2022, Krause et al. mention that BAG6, a protein involved in the invagination of the LE/MVB limiting membrane, might be implicated in the crosstalk between endosomal microautophagy and chaperone-mediated autophagy^{150,151}. In our case, Tsg101 bears one phosphorylation-dependent KFERQ-like motif, supporting the idea that it could be a CMA target thus participate in the autophagic switch between both routes.

More hypotheses rise regarding the switch between eMI and CMA, but further research is needed to elucidate the exact molecular mechanisms behind it.

PART 3: Mysteries of *lamp2a* in RT

The presence of CMA in RT initially sparked interest due to the fact that this species carries two copies of the *lamp2* gene. The first genetic investigation of both *lamp2as* shows that both are expressed, albeit not at the same level. Notably, *lamp2a* C14 exhibited lower expression than its counterpart from C31 in nearly all investigated tissues. The visualization of RNA signal using BaseScope in-situ hybridization analysis enabled us to discriminate between both copies. It showed that *lamp2a* C14 has almost no signal in liver and intestine compared to *lamp2a* C31. Simultaneous *in vitro* investigations conducted in the laboratory to assess the contribution of each paralog to CMA activity revealed that Lamp2A from C14 played a minimal role in CMA activity²⁵³. Specifically, this study demonstrated that silencing *lamp2a* C14 had minimal impact on the KFERQ-PA-mCherry puncta formation induced by high glucose conditions, while CMA activity was clearly hampered after silencing *lamp2a* C31.

While this PhD project centered on L2AC31-KO RTs, forthcoming research should delve into the *lamp2a* C14 KO RT line to unveil the physiological role of this paralog. Given that duplicated genes can undergo diverse mutation patterns³¹¹ and the low mRNA expression of *lamp2a* C14, it is possible to imagine that it underwent a pseudogenization event²⁴⁷. This event is defined as “an evolutionary phenomenon whereby a gene loses its function, accumulates mutations and becomes a pseudogene”³¹². Following this hypothesis, it would indicate that *lamp2a* C14 may have undergone mutations, leading to its non-involvement in CMA and loss of contribution to this mechanism. A neofunctionalization event could also have happened, suggesting *lamp2a* C14 might have evolved into an entirely distinct

function³¹¹. Despite the low *lamp2a* C14 expression found in RT tissues, mRNA signal could be detected and perhaps Lamp2A from C14 serves another role.

We observed a higher *lamp2a* C14 mRNA expression in the L2AC31-KO RTs than in WT RTs across all the tissues examined. This suggests a potential compensatory response to the gene deletion. Therefore, it is crucial to investigate the intricate interplay between both paralogs, as they may share regulatory pathways.

Conducting experiments on L2AC14-KO, L2AC31-KO RT, or double L2A-KO RT lines to measure CMA activity could provide valuable insights into the precise contribution of each paralog to CMA activity and their potential paralog-specific roles. These experiments could also shed light on any paralog compensation for Lamp2A loss. Exploring the role of this 'rescued' CMA function is particularly intriguing, considering the structural disparities between both paralogs, as discussed in the first chapter of our study. An additional noteworthy observation pertains to the induction of expression for both *lamp2a* paralogs during fasting. In mammals, CMA activation in response to nutrient deprivation primarily involves diminishing Lamp2A degradation and its relocation to the lysosomal membrane¹⁸⁶, rather than regulating *LAMP2A* transcription. Taken together, these findings emphasize the general preservation of the CMA machinery in RT. Nevertheless, they also indicate variations from mammalian processes in the mechanisms that oversee its regulation, thereby warranting deeper investigation.

PART 4: First *in vivo* CMA activity assay in a fish species

To demonstrate the presence of CMA activity in RT, we proceeded to isolate CMA-active lysosomes from liver samples and confirm their capacity to bind and transport a CMA substrate. To our knowledge, this represents the first evidence of CMA activity (or CMA-like activity) through lysosomal isolation in a non-mammalian organism. This finding confirms previous *in vitro* observations regarding CMA activity in RT cell lines²⁵³, in medaka fish²⁴⁵ and zebrafish (unpublished data). CMA existence is therefore not restricted to only one species of fish but probably others, which opens up new perspectives in the study of this function. For example, it is feasible to imagine that CMA could be present in other vertebrates, as they all display the *lamp2* gene.

In addition to demonstrating the functional capability of RT lysosomes to perform CMA, the lysosome isolation assay also revealed their capacity to recognize the KFERQ-like motif. This discovery raises questions about potential evolutionary changes in the motif within fish species. Notably, the structural differences in RT Lamp2A with human LAMP2A (Fig 27) suggest the possibility that CMA in RTs may target species-specific substrates. Furthermore, it raises the intriguing possibility of 'new KFERQ-like motifs' in species that are capable of CMA but have undergone evolutionary divergence.

neurons but not in other tissues. These findings indicate that CMA's influence on RT metabolic pathways should be further investigated through organ-specific knockout experiments.

In our model species, I believe special attention should be given to the intestine, as it exhibited high *lamp2a* expression and plays key roles in nutrient absorption, metabolism, osmoregulation and the immune response^{313,314}. While most focus was brought on liver in this study, the extensive mRNA signal observed in intestine through BaseScope analysis (Fig 29) strongly suggests CMA activity and a CMA's physiological role in this tissue, potentially unknown. Despite numerous studies on autophagy in intestine³¹⁵⁻³¹⁷, CMA's part in this organ remains completely unexplored.

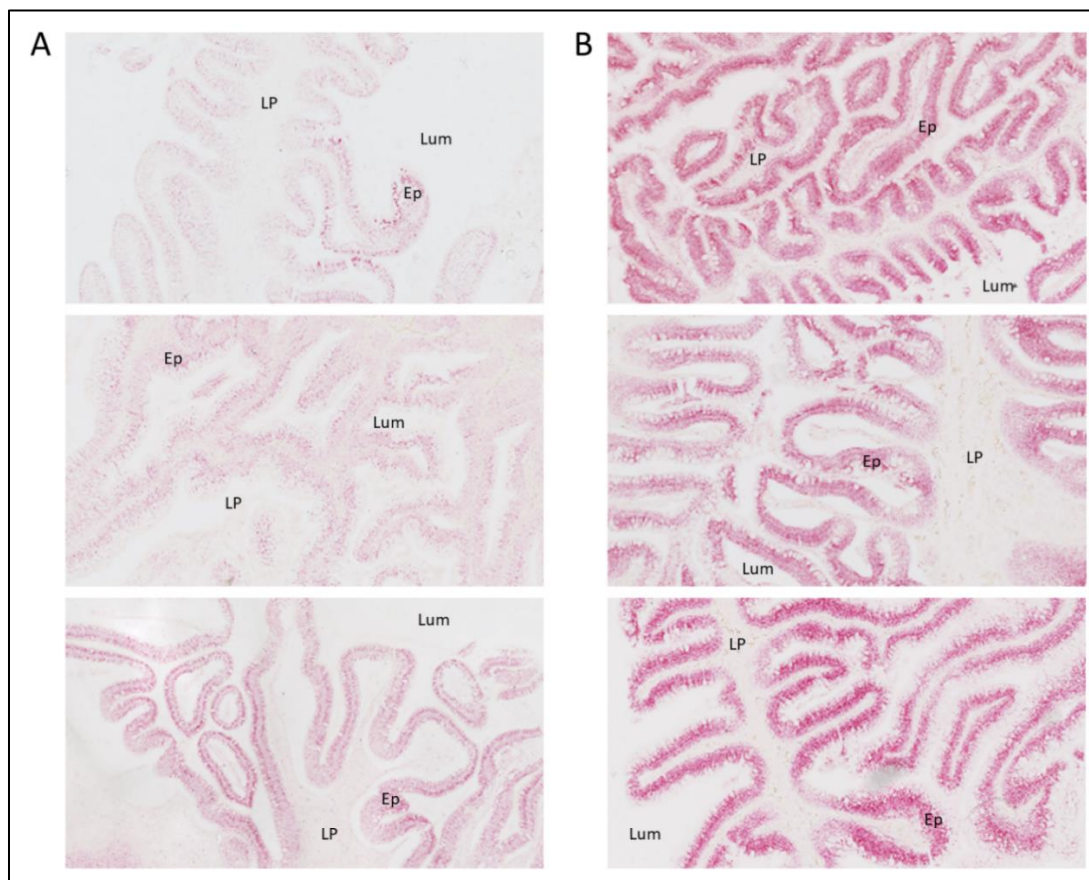


Figure 29: Signal of *lamp2a* C31 probes in distal intestine sections from three different (A) control and (B) starved RTs. mRNA signal is displayed in red dots. Ep: epithelium; Lum: lumen; LP: lamina propria.

PART 5: A previously uncovered role for CMA?

In the additional results, we discovered that L2AC31-KO RTs exhibited different feeding behaviors and significant changes in mRNA levels of targets of appetite regulation, which suggested an involvement of CMA in the control of food intake in RT. Previous studies have focused on the role of macroautophagy and food intake. Kaushik et al. described in 2011 that starvation-induced hypothalamic

macroautophagy mobilizes neuron-intrinsic lipids to generate endogenous free fatty acids, which in turn regulate AgRP levels and food intake³¹⁸. Recently, Bravo-San Pedro et al. discovered that acyl-CoA-binding protein (ACBP), also known as diazepam-binding inhibitor (DBI), functions as an effective promoter of lipogenesis and appetite stimulation in mice³¹⁹. Their research revealed that its plasma concentration is dependent on macroautophagy activity and is activated by starvation³¹⁹. These discoveries clearly open up new perspectives regarding the potential involvement of other autophagy pathways in the regulation of food intake.

Our results suggested that L2AKOC31-RTs displayed a higher food intake, hinting at a potential CMA regulation of appetite. In Kaushik's study, they generated mice that lacked the autophagy gene *ATG7* in AgRP neurons³¹⁹. Interestingly, inhibiting autophagy in AgRP neurons resulted in reduced body weight and decreased food intake compared to controls following a 6 h fast and subsequent refeeding³¹⁹. If CMA indeed plays a role in appetite regulation, it could potentially have contrasting effects on hypothalamic AgRP neurons compared to macroautophagy. It is even possible to imagine that they have contrasting effects to finely calibrate appetite regulation.

To deepen our understanding, future studies should prioritize the quantification of food intake in L2AKO-C31 RTs. While our analysis of mRNA expression and quantitative proteomics in L2AKO-C31 RTs encompassed the whole brain, it is essential to conduct extensive molecular studies, targeting precise genes and proteins, specifically in the hypothalamus. This region plays a central role in regulating energy balance. Moreover, it is interesting to note that the regulators of food intake investigated in the mRNA expression study, namely AgRP/NPY and POMC/CART neurons, might have exhibited differential regulation in the hypothalamus. However, the proteomics analysis, being whole-brain-focused, could have masked these effects. Given the major role of leptin and ghrelin³²⁰ in food intake, measuring levels of these hormones could also provide us with significant information on the effect of CMA on this pathway.

PART 6: Compromised homeostasis and new perspectives for CMA in fish

We discovered that absence of *lamp2a* C31 in RT during a stressful event compromised cellular homeostasis. This revelation highlighted the role of CMA in defending against oxidative stress and regulating metabolic processes under stress conditions. Therefore, we decided to adapt the CMA score originally designed in Bourdenx et al. as a proxy for cellular homeostasis²⁵⁴. While new experimental methods to measure stress physiology in captive or wild fish have emerged, challenges remain to develop more specific and sensitive tools⁹⁸. Subsequently, we subjected RTs to moderate hypoxic conditions and assessed the CMA score in multiple tissues. We found an overall increase in the tissues due to the hypoxic treatment after a four-week exposure. Those results strongly suggested that an

activation of the CMA machinery could indicate a cellular stress. Notably, the activation of the CMA score was achieved solely with moderate hypoxia, underscoring the precision of this method for assessing stress at the tissue level. While we have thoroughly addressed the CMA score approach, there remain many unexplored aspects of this method.

Considering its potential as a cellular homeostasis indicator in fish during environmental challenges, it could become a fast and reliable method. By narrowing down the CMA score network to include only genes directly related to CMA and designing common primers targeting multiple paralogs of the same gene, we can potentially enhance its speed while maintaining its effectiveness. In addition, other proteolytic pathways involved in stress response could be included in the calculation. While examining cellular responses to stress, it is crucial to consider the main actors of macroautophagy and the proteasome system, as highlighted in previous studies^{321,322}. For instance, when it comes to hypoxic stress, the hypoxia-inducible factors HIF-1 α and HIF-2 α play pivotal roles as mediators. Research conducted by Bellot et al. demonstrated that hypoxia triggers autophagy through the activation of these HIFs. Specifically, they found that HIFs activate autophagy via BNIP3 (Bcl-2/E1B 19 kDa-interacting protein 3), a mechanism aimed at protecting cells from damage³²³. Other proteolytic systems should then be explored in fish species to strengthen and refine the CMA score calculation and applications.

Besides its analytical efficiency, we can explore the broader applications of the CMA score method. For instance, CMA has been implicated in the immune response, as observed in T cells²⁰¹. Additionally, as we discovered in the second chapter, red blood cells (which are nucleated in fish) express *lamp2a*, suggesting that the CMA score could be measured in blood samples. This approach could offer a non-lethal method to assess cellular homeostasis in fish.

The types of stress detectable through the CMA score are of particular interest. Major CMA activators include starvation, hypoxia, and oxidative stress²⁶². These stressors can be indirectly linked to environmental factors like temperature and pollutants. A comprehensive study could expose fish to multiple stressors, measuring the CMA score in various tissues. The results could then reveal how the CMA score's sensitivity varies with different stress types and intensities across tissues.

C onclusion

As CMA continues to gain prominence in human therapeutics, there remains a notable gap in our understanding of this pathway in other vertebrate species. Previous research in medaka laid the foundation for the existence of CMA in fish. This thesis has shed light on the presence of CMA activity in the RT, underlining the importance of investigating CMA in fish.

Our research not only confirms the presence of this process but also unravels its critical role in regulating metabolic pathways and maintaining cellular homeostasis, mirroring its significance in mammals. However, the ever-evolving path of evolution for fish species unveils distinct CMA actors, exemplified by structural disparities in LAMP2A, the rate-limiting factor in CMA. This discovery raises intriguing questions about the potential evolution of the KFERQ-like motif and suggests alternative physiological roles for CMA in previously uncharted species.

While our primary focus has centered on the RT, our work opens the door to innovative methods for evaluating cellular stress in a multitude of fish species and, potentially, other aquatic vertebrates. These findings carry the promise of uncovering varied roles of CMA in species dwelling in vastly different and rapidly changing environments.

In conclusion, harnessing the power of CMA as a tool for assessing cellular homeostasis extends the range of potential instruments for evaluating fish welfare, especially for species that have garnered public attention. These findings set the stage for an exciting journey into the uncharted waters of autophagy research, with vast possibilities for applications in aquaculture, conservation, and the broader understanding of the natural world.

References

1. Richmond, R. & Buesseler, K. The future of ocean health. *Science* **381**, 927–927 (2023).
2. Jin, X., Wang, X., Tse, W. K. F. & Shi, Y. Editorial: Homeostasis and physiological regulation in the aquatic animal during osmotic stress. *Front. Physiol.* **13**, 977185 (2022).
3. *Climate Change 2013 – The Physical Science Basis: Working Group I Contribution to the Fifth Assessment Report of the Intergovernmental Panel on Climate Change*. (Cambridge University Press, 2014). doi:10.1017/CB09781107415324.
4. Francis, R. C., Hare, S. R., Hollwed, A. B. & Wooster, W. S. Effects of interdecadal climate variability on the oceanic ecosystems of the NE Pacific: Interdecadal climate variability in the NE Pacific. *Fisheries Oceanography* **7**, 1–21 (1998).
5. Sydeman, W. J., Poloczanska, E., Reed, T. E. & Thompson, S. A. Climate change and marine vertebrates. *Science* **350**, 772–777 (2015).
6. Alfonso, S., Gesto, M. & Sadoul, B. Temperature increase and its effects on fish stress physiology in the context of global warming. *Journal of Fish Biology* **98**, 1496–1508 (2021).
7. Fabbri, E. & Moon, T. W. Adrenergic signaling in teleost fish liver, a challenging path. *Comparative Biochemistry and Physiology Part B: Biochemistry and Molecular Biology* **199**, 74–86 (2016).
8. Schreck, C. B., Olla, B. L. & Davis, M. W. Behavioral responses to stress. *Fish stress and health in aquaculture* **62**, 145–170 (1997).
9. Colson, V. *et al.* Maternal temperature exposure impairs emotional and cognitive responses and triggers dysregulation of neurodevelopment genes in fish. *PeerJ* **7**, e6338 (2019).
10. Pörtner, H. O. & Knust, R. Climate Change Affects Marine Fishes Through the Oxygen Limitation of Thermal Tolerance. *Science* **315**, 95–97 (2007).
11. Mateus, A. P. *et al.* Thermal imprinting modifies adult stress and innate immune responsiveness in the teleost sea bream. *Journal of Endocrinology* **233**, 381–394 (2017).
12. O'Reilly, C. M. *et al.* Rapid and highly variable warming of lake surface waters around the globe. *Geophysical Research Letters* **42**, (2015).
13. Howarth, R. W., Sharpley, A. & Walker, D. Sources of nutrient pollution to coastal waters in the United States: Implications for achieving coastal water quality goals. *Estuaries* **25**, 656–676 (2002).
14. Steckbauer, A., Duarte, C. M., Carstensen, J., Vaquer-Sunyer, R. & Conley, D. J. Ecosystem impacts of hypoxia: thresholds of hypoxia and pathways to recovery. *Environ. Res. Lett.* **6**, 025003 (2011).
15. Diaz, R. J. & Rosenberg, R. Spreading Dead Zones and Consequences for Marine Ecosystems. *Science* **321**, 926–929 (2008).

16. Daskalov, G. Overfishing drives a trophic cascade in the Black Sea. *Mar. Ecol. Prog. Ser.* **225**, 53–63 (2002).
17. Mee, L. D., Friedrich, J. & Gomoiu, M. T. Restoring the Black Sea in times of uncertainty. *Oceanography, Vol.18, No.2* 32–43 (2005).
18. Kideys, A. E. Fall and Rise of the Black Sea Ecosystem. *Science* **297**, 1482–1484 (2002).
19. Breitburg, D. *et al.* Declining oxygen in the global ocean and coastal waters. *Science* **359**, eaam7240 (2018).
20. Vaquer-Sunyer, R. & Duarte, C. M. Thresholds of hypoxia for marine biodiversity. *Proc. Natl. Acad. Sci. U.S.A.* **105**, 15452–15457 (2008).
21. Schmidtko, S., Stramma, L. & Visbeck, M. Decline in global oceanic oxygen content during the past five decades. *Nature* **542**, 335–339 (2017).
22. Stierhoff, K. L., Targett, T. E. & Power, J. H. Hypoxia-induced growth limitation of juvenile fishes in an estuarine nursery: assessment of small-scale temporal dynamics using RNA:DNA. *Can. J. Fish. Aquat. Sci.* **66**, 1033–1047 (2009).
23. Wang, S. Y. *et al.* Hypoxia causes transgenerational impairments in reproduction of fish. *Nat Commun* **7**, 12114 (2016).
24. Busecke, J. J. M., Resplandy, L., Ditkovsky, S. J. & John, J. G. Diverging Fates of the Pacific Ocean Oxygen Minimum Zone and Its Core in a Warming World. *AGU Advances* **3**, e2021AV000470 (2022).
25. Gattuso, J.-P. & Buddemeier, R. W. Calcification and CO₂. *Nature* **407**, 311–313 (2000).
26. Caldeira, K. & Wickett, M. E. Anthropogenic carbon and ocean pH. *Nature* **425**, 365–365 (2003).
27. Kroeker, K. J., Kordas, R. L., Crim, R. N. & Singh, G. G. Meta-analysis reveals negative yet variable effects of ocean acidification on marine organisms: Biological responses to ocean acidification. *Ecology Letters* **13**, 1419–1434 (2010).
28. Munday, P., Crawley, N. & Nilsson, G. Interacting effects of elevated temperature and ocean acidification on the aerobic performance of coral reef fishes. *Mar. Ecol. Prog. Ser.* **388**, 235–242 (2009).
29. Munday, P. L. *et al.* Ocean acidification impairs olfactory discrimination and homing ability of a marine fish. *Proc. Natl. Acad. Sci. U.S.A.* **106**, 1848–1852 (2009).
30. Munday, P. L. *et al.* Replenishment of fish populations is threatened by ocean acidification. *Proc. Natl. Acad. Sci. U.S.A.* **107**, 12930–12934 (2010).
31. Dong, S., Lei, Y., Li, T., Cao, Y. & Xu, K. Biocalcification crisis in the continental shelf under ocean acidification. *Geoscience Frontiers* **14**, 101622 (2023).
32. DeCarlo, T. M. *et al.* Investigating marine bio-calcification mechanisms in a changing ocean with in vivo and high-resolution ex vivo Raman spectroscopy. *Global Change Biology* **25**, 1877–1888 (2019).
33. Beaugrand, G., Brander, K. M., Alistair Lindley, J., Souissi, S. & Reid, P. C. Plankton effect on cod recruitment in the North Sea. *Nature* **426**, 661–664 (2003).

34. Cushing, D. H. Plankton Production and Year-class Strength in Fish Populations: an Update of the Match/Mismatch Hypothesis. in *Advances in Marine Biology* vol. 26 249–293 (Elsevier, 1990).
35. Moullec, F., Benedetti, F., Saraux, C., VAN BEVEREN, E. & Shin, Y.-J. Climate change induces bottom-up changes in the food webs of the Mediterranean Sea. *The Mediterranean region under climate change* 219 (2016).
36. Hedström, P., Bystedt, D., Karlsson, J., Bokma, F. & Byström, P. Brownification increases winter mortality in fish. *Oecologia* **183**, 587–595 (2017).
37. Kokfelt, U. *et al.* Ecosystem responses to increased precipitation and permafrost decay in subarctic Sweden inferred from peat and lake sediments. *Global Change Biology* **15**, 1652–1663 (2009).
38. Larsen, S., Andersen, T. & Hessen, D. O. Climate change predicted to cause severe increase of organic carbon in lakes: CLIMATE CHANGE CAUSE ELEVATED TOC IN LAKES. *Global Change Biology* **17**, 1186–1192 (2011).
39. Kime, D. E. The effects of pollution on reproduction in fish. *Rev Fish Biol Fisheries* **5**, 52–95 (1995).
40. Borrelle, S. B. *et al.* Predicted growth in plastic waste exceeds efforts to mitigate plastic pollution. *Science* **369**, 1515–1518 (2020).
41. Wendelaar Bonga, S. E. The stress response in fish. *Physiological Reviews* **77**, 591–625 (1997).
42. Incardona, J. P. & Scholz, N. L. Environmental Pollution and the Fish Heart. in *Fish Physiology* vol. 36 373–433 (Elsevier, 2017).
43. Evans, D. H. The fish gill: site of action and model for toxic effects of environmental pollutants. *Environ Health Perspect* **71**, 47–58 (1987).
44. Ullrich, S. M., Tanton, T. W. & Abdrashitova, S. A. Mercury in the Aquatic Environment: A Review of Factors Affecting Methylation. *Critical Reviews in Environmental Science and Technology* **31**, 241–293 (2001).
45. Scheuhammer, A. *et al.* Recent progress on our understanding of the biological effects of mercury in fish and wildlife in the Canadian Arctic. *Science of The Total Environment* **509–510**, 91–103 (2015).
46. Cole, M., Lindeque, P., Halsband, C. & Galloway, T. S. Microplastics as contaminants in the marine environment: A review. *Marine Pollution Bulletin* **62**, 2588–2597 (2011).
47. Lusher, A., Hollman, P. & Mendoza-Hill, J. *Microplastics in fisheries and aquaculture: status of knowledge on their occurrence and implications for aquatic organisms and food safety.* (FAO, 2017).
48. Jovanović, B. Ingestion of microplastics by fish and its potential consequences from a physical perspective: Potential Consequences of Fish Ingestion of Microplastic. *Integr Environ Assess Manag* **13**, 510–515 (2017).
49. Deng, J., Liu, C., Yu, L. & Zhou, B. Chronic exposure to environmental levels of tribromophenol impairs zebrafish reproduction. *Toxicology and Applied Pharmacology* **243**, 87–95 (2010).

50. Ferreira, P., Fonte, E., Soares, M. E., Carvalho, F. & Guilhermino, L. Effects of multi-stressors on juveniles of the marine fish *Pomatoschistus microps*: Gold nanoparticles, microplastics and temperature. *Aquatic Toxicology* **170**, 89–103 (2016).
51. Pandey, S. *et al.* Effects of exposure to multiple trace metals on biochemical, histological and ultrastructural features of gills of a freshwater fish, *Channa punctata* Bloch. *Chemico-Biological Interactions* **174**, 183–192 (2008).
52. *The State of World Fisheries and Aquaculture 2022*. (FAO, 2022). doi:10.4060/cc0461en.
53. France - National Aquaculture Sector Overview. https://www.fao.org/fishery/en/countrysector/naso_france.
54. Jansen, M. D. *et al.* The epidemiology of pancreas disease in salmonid aquaculture: a summary of the current state of knowledge. *Journal of Fish Diseases* **40**, 141–155 (2017).
55. Johnson-Mackinnon, J., Oldham, T. & Nowak, B. Amoebic gill disease: a growing threat. *Microbiol. Aust.* **37**, 140 (2016).
56. Aaen, S. M., Helgesen, K. O., Bakke, M. J., Kaur, K. & Horsberg, T. E. Drug resistance in sea lice: a threat to salmonid aquaculture. *Trends in Parasitology* **31**, 72–81 (2015).
57. Pajdak-Czaus, J., Platt-Samoraj, A., Szweda, W., Siwicki, A. K. & Terech-Majewska, E. *Yersinia ruckeri* — A threat not only to rainbow trout. *Aquac Res* **50**, 3083–3096 (2019).
58. Ahmed, N., Thompson, S. & Glaser, M. Global Aquaculture Productivity, Environmental Sustainability, and Climate Change Adaptability. *Environmental Management* **63**, 159–172 (2019).
59. Kent, M., Sawyer, T. & Hedrick, R. *Paramoeba pemaquidensis* (Sarcostigophora: Paramoebidae) infestation of the gills of coho salmon *Oncorhynchus kisutch* reared in sea water. *Dis. Aquat. Org.* **5**, 163–169 (1988).
60. Steinum, T. *et al.* First cases of amoebic gill disease (AGD) in Norwegian seawater farmed Atlantic salmon, *Salmo salar* L., and phylogeny of the causative amoeba using 18S cDNA sequences. *J Fish Diseases* **31**, 205–214 (2008).
61. Oldham, T., Rodger, H. & Nowak, B. F. Incidence and distribution of amoebic gill disease (AGD) — An epidemiological review. *Aquaculture* **457**, 35–42 (2016).
62. Lulijwa, R., Alfaro, A. C. & Young, T. Metabolomics in salmonid aquaculture research: Applications and future perspectives. *Reviews in Aquaculture* **14**, 547–577 (2022).
63. World Population Prospects 2019 Highlights.
64. *The State of World Fisheries and Aquaculture 2022*. (FAO, 2022). doi:10.4060/cc0461en.
65. Aragão, C. *et al.* Alternative Proteins for Fish Diets: Implications beyond Growth. *Animals* **12**, 1211 (2022).
66. Commission, E. *Strategic Guidelines for a More Sustainable and Competitive EU Aquaculture for the Period 2021 to 2030*. (European Commission Brussels, Belgium, 2021).
67. OECD. *Green Growth in Fisheries and Aquaculture*. (OECD, 2015). doi:10.1787/9789264232143-en.

68. Cf, O. Transforming our world: the 2030 Agenda for Sustainable Development. *United Nations: New York, NY, USA* (2015).
69. Freire, R. & Nicol, C. A bibliometric analysis of past and emergent trends in animal welfare science. *Anim. welf.* **28**, 465–485 (2019).
70. Franks, B., Ewell, C. & Jacquet, J. Animal welfare risks of global aquaculture. *Sci. Adv.* **7**, eabg0677 (2021).
71. Gorissen, M. & Flik, G. The Endocrinology of the Stress Response in Fish. in *Fish Physiology* vol. 35 75–111 (Elsevier, 2016).
72. Vallejos-Vidal, E. *et al.* The Direct Exposure of Cortisol Does Not Modulate the Expression of Immune-Related Genes on Tissue Explants of Mucosal Surfaces in Rainbow Trout (*Oncorhynchus mykiss*) Nor in Gilthead Sea Bream (*Sparus aurata*). *Front. Mar. Sci.* **9**, 828050 (2022).
73. Gamperl, A. K., Vijayan, M. M. & Boutilier, R. G. Experimental control of stress hormone levels in fishes: techniques and applications. *Rev Fish Biol Fisheries* **4**, 215–255 (1994).
74. Balasch, J. C. & Tort, L. Netting the Stress Responses in Fish. *Front. Endocrinol.* **10**, 62 (2019).
75. Cruz, S. A., Lin, C.-H., Chao, P.-L. & Hwang, P.-P. Glucocorticoid Receptor, but Not Mineralocorticoid Receptor, Mediates Cortisol Regulation of Epidermal Ionocyte Development and Ion Transport in Zebrafish (*Danio Rerio*). *PLoS ONE* **8**, e77997 (2013).
76. Ellis, T. *et al.* Cortisol and finfish welfare. *Fish Physiol Biochem* **38**, 163–188 (2012).
77. Pottinger, T. G., Pickering, A. D. & Hurley, M. A. Consistency in the stress response of individuals of two strains of rainbow trout, *Oncorhynchus mykiss*. *Aquaculture* **103**, 275–289 (1992).
78. Grutter, A. S. & Pankhurst, N. W. The effects of capture, handling, confinement and ectoparasite load on plasma levels of cortisol, glucose and lactate in the coral reef fish *Hemigymnus melapterus*. *Journal of Fish Biology* **57**, 391–401 (2000).
79. Iwama, G. K., Morgan, J. D. & Barton, B. A. Simple field methods for monitoring stress and general condition of fish. *Aquaculture Res* **26**, 273–282 (1995).
80. Wedemeyer, G. A., Barton, B. A., McLeavy, D. J., Schreck, C. B. & Moyle, P. B. Methods for fish biology. *Stress and Acclimation* 451–489 (1990).
81. Raposo De Magalhães, C. S. F. *et al.* A Proteomics and other Omics approach in the context of farmed fish welfare and biomarker discovery. *Reviews in Aquaculture* **12**, 122–144 (2020).
82. Harman, D. Aging: A Theory Based on Free Radical and Radiation Chemistry. *Journal of Gerontology* **11**, 298–300 (1956).
83. Birnie-Gauvin, K., Costantini, D., Cooke, S. J. & Willmore, W. G. A comparative and evolutionary approach to oxidative stress in fish: A review. *Fish and Fisheries* **18**, 928–942 (2017).
84. Halliwell, B. & Gutteridge, J. M. C. *Free Radicals in Biology and Medicine*. (Oxford University Press, 2015). doi:10.1093/acprof:oso/9780198717478.001.0001.
85. Brookes, P. S. Mitochondrial H⁺ leak and ROS generation: An odd couple. *Free Radical Biology and Medicine* **38**, 12–23 (2005).

86. Jamieson, D., Chance, B., Cadenas, E. & Boveris, A. The Relation of Free Radical Production to Hyperoxia. *Annu. Rev. Physiol.* **48**, 703–719 (1986).
87. Cadenas, E. Basic mechanisms of antioxidant activity. *BioFactors* **6**, 391–397 (1997).
88. Valko, M. *et al.* Free radicals and antioxidants in normal physiological functions and human disease. *The International Journal of Biochemistry & Cell Biology* **39**, 44–84 (2007).
89. Carney Almroth, B. *et al.* Warmer water temperature results in oxidative damage in an Antarctic fish, the bald notothen. *Journal of Experimental Marine Biology and Ecology* **468**, 130–137 (2015).
90. Bagnyukova, T. V., Lushchak, O. V., Storey, K. B. & Lushchak, V. I. Oxidative stress and antioxidant defense responses by goldfish tissues to acute change of temperature from 3 to 23 °C. *Journal of Thermal Biology* **32**, 227–234 (2007).
91. Heise, K., Puntarulo, S., Nikinmaa, M., Abele, D. & Pörtner, H.-O. Oxidative stress during stressful heat exposure and recovery in the North Sea eelpout *Zoarces viviparus* L. *Journal of Experimental Biology* **209**, 353–363 (2006).
92. Nikinmaa, M. *et al.* Transcription and redox enzyme activities: comparison of equilibrium and disequilibrium levels in the three-spined stickleback. *Proc. R. Soc. B.* **280**, 20122974 (2013).
93. Lushchak, V. I., Lushchak, L. P., Mota, A. A. & Hermes-Lima, M. Oxidative stress and antioxidant defenses in goldfish *Carassius auratus* during anoxia and reoxygenation. *American Journal of Physiology-Regulatory, Integrative and Comparative Physiology* **280**, R100–R107 (2001).
94. Lushchak, V. I. *et al.* Hyperoxia results in transient oxidative stress and an adaptive response by antioxidant enzymes in goldfish tissues. *The International Journal of Biochemistry & Cell Biology* **37**, 1670–1680 (2005).
95. Martínez-Álvarez, R. M. *et al.* Physiological changes of sturgeon *Acipenser naccarii* caused by increasing environmental salinity. *Journal of Experimental Biology* **205**, 3699–3706 (2002).
96. Pottinger, T. G. The Stress Response in Fish-Mechanisms, Effects and Measurement. in *Fish Welfare* (ed. Branson, E. J.) 32–48 (Wiley, 2008). doi:10.1002/9780470697610.ch3.
97. Brambell, F. W. Report of the technical committee to enquire into the welfare of animals kept under intensive livestock husbandry systems. (*No Title*) (1965).
98. Sadoul, B. & Geffroy, B. Measuring cortisol, the major stress hormone in fishes. *Journal of Fish Biology* **94**, 540–555 (2019).
99. Auperin, B. & Geslin, M. Plasma cortisol response to stress in juvenile rainbow trout is influenced by their life history during early development and by egg cortisol content. *General and Comparative Endocrinology* **158**, 234–239 (2008).
100. Varsamos, S., Flik, G., Pepin, J. F., Bonga, S. E. W. & Breuil, G. Husbandry stress during early life stages affects the stress response and health status of juvenile sea bass, *Dicentrarchus labrax*. *Fish & Shellfish Immunology* **20**, 83–96 (2006).
101. Sandblom, E. *et al.* Physiological constraints to climate warming in fish follow principles of plastic floors and concrete ceilings. *Nat Commun* **7**, 11447 (2016).

102. Moore, M. N., Allen, J. I. & Somerfield, P. J. Autophagy: Role in surviving environmental stress. *Marine Environmental Research* **62**, S420–S425 (2006).
103. Moore, M. N., Viarengo, A., Donkin, P. & Hawkins, A. J. S. Autophagic and lysosomal reactions to stress in the hepatopancreas of blue mussels. *Aquatic Toxicology* **84**, 80–91 (2007).
104. Sforzini, S. *et al.* Effects of fullerene C60 in blue mussels: Role of mTOR in autophagy related cellular/tissue alterations. *Chemosphere* **246**, 125707 (2020).
105. Shaw, J. P. *et al.* Oxidative stress, lysosomal damage and dysfunctional autophagy in molluscan hepatopancreas (digestive gland) induced by chemical contaminants. *Marine Environmental Research* **152**, 104825 (2019).
106. Hartl, F. U., Bracher, A. & Hayer-Hartl, M. Molecular chaperones in protein folding and proteostasis. *Nature* **475**, 324–332 (2011).
107. de Duve, C., Pressman, B. C., Gianetto, R., Wattiaux, R. & Appelmans, F. Tissue fractionation studies. 6. Intracellular distribution patterns of enzymes in rat-liver tissue. *Biochem J* **60**, 604–617 (1955).
108. Straus, W. ISOLATION AND BIOCHEMICAL PROPERTIES OF DROPLETS FROM THE CELLS OF RAT KIDNEY. *Journal of Biological Chemistry* **207**, 745–755 (1954).
109. Cohn, Z. A. THE FATE OF BACTERIA WITHIN PHAGOCYTTIC CELLS. *The Journal of Experimental Medicine* **117**, 27–42 (1963).
110. Fengsrud, M., Erichsen, E. S., Berg, T. O., Raiborg, C. & Seglen, P. O. Ultrastructural characterization of the delimiting membranes of isolated autophagosomes and amphisomes by freeze-fracture electron microscopy. *European Journal of Cell Biology* **79**, 871–882 (2000).
111. de Duve, C. & Wattiaux, R. Functions of Lysosomes. *Annual Review of Physiology* **28**, 435–492 (1966).
112. Klionsky, D. J. Autophagy: from phenomenology to molecular understanding in less than a decade. *Nat Rev Mol Cell Biol* **8**, 931–937 (2007).
113. Seglen, P. O. Regulation of autophagic degradation in isolated liver cells. *Lysosomes: their role in protein breakdown* 369–414 (1987).
114. Gordon, P. B. & Seglen, P. O. Prelysosomal convergence of autophagic and endocytic pathways. *Biochemical and Biophysical Research Communications* **151**, 40–47 (1988).
115. Takeshige, K., Baba, M., Tsuboi, S., Noda, T. & Ohsumi, Y. Autophagy in yeast demonstrated with proteinase-deficient mutants and conditions for its induction. *The Journal of cell biology* **119**, 301–311 (1992).
116. Liang, X. H. *et al.* Induction of autophagy and inhibition of tumorigenesis by beclin 1. *Nature* **402**, 672–676 (1999).
117. Mathew, R. *et al.* Autophagy suppresses tumor progression by limiting chromosomal instability. *Genes Dev.* **21**, 1367–1381 (2007).
118. Cuervo, A. M. Chaperone-mediated autophagy: Dice’s ‘wild’ idea about lysosomal selectivity. *Nat Rev Mol Cell Biol* **12**, 535–541 (2011).

119. Klionsky, D. J. *et al.* A comprehensive glossary of autophagy-related molecules and processes (2nd edition). *Autophagy* **7**, 1273–1294 (2011).
120. Deffieu, M. *et al.* Glutathione Participates in the Regulation of Mitophagy in Yeast. *Journal of Biological Chemistry* **284**, 14828–14837 (2009).
121. Dunn, Jr., W. A. *et al.* Pexophagy: The Selective Autophagy of Peroxisomes. *Autophagy* **1**, 75–83 (2005).
122. Feng, Y., He, D., Yao, Z. & Klionsky, D. J. The machinery of macroautophagy. *Cell Research* **24**, 24–41 (2014).
123. Klionsky, D. J. The molecular machinery of autophagy: unanswered questions. *Journal of Cell Science* **118**, 7–18 (2005).
124. Yorimitsu, T. & Klionsky, D. J. Autophagy: molecular machinery for self-eating. *Cell Death Differ* **12**, 1542–1552 (2005).
125. Zheng, Q. *et al.* Calcium transients on the ER surface trigger liquid-liquid phase separation of FIP200 to specify autophagosome initiation sites. *Cell* **185**, 4082–4098.e22 (2022).
126. Heras-Sandoval, D., Pérez-Rojas, J. M., Hernández-Damián, J. & Pedraza-Chaverri, J. The role of PI3K/AKT/mTOR pathway in the modulation of autophagy and the clearance of protein aggregates in neurodegeneration. *Cellular Signalling* **26**, 2694–2701 (2014).
127. Munson, M. J. & Ganley, I. G. mTOR, PIK3C3, and autophagy: Signaling the beginning from the end. *Autophagy* **11**, 2375–2376 (2015).
128. Shi, B., Ma, M., Zheng, Y., Pan, Y. & Lin, X. mTOR and Beclin1: Two key autophagy-related molecules and their roles in myocardial ischemia/reperfusion injury. *Journal Cellular Physiology* **234**, 12562–12568 (2019).
129. Noda, T. Regulation of Autophagy through TORC1 and mTORC1. *Biomolecules* **7**, 52 (2017).
130. Kim, J., Kundu, M., Viollet, B. & Guan, K.-L. AMPK and mTOR regulate autophagy through direct phosphorylation of Ulk1. *Nat Cell Biol* **13**, 132–141 (2011).
131. Laplante, M. & Sabatini, D. M. mTOR Signaling in Growth Control and Disease. *Cell* **149**, 274–293 (2012).
132. Jia, J. *et al.* Galectins control mTOR and AMPK in response to lysosomal damage to induce autophagy. *Autophagy* **15**, 169–171 (2019).
133. Russell, R. C., Yuan, H.-X. & Guan, K.-L. Autophagy regulation by nutrient signaling. *Cell Res* **24**, 42–57 (2014).
134. Levine, B. & Kroemer, G. Biological Functions of Autophagy Genes: A Disease Perspective. *Cell* **176**, 11–42 (2019).
135. Menon, M. B. & Dhamija, S. Beclin 1 Phosphorylation – at the Center of Autophagy Regulation. *Front. Cell Dev. Biol.* **6**, 137 (2018).
136. Ghanbarpour, A., Valverde, D. P., Melia, T. J. & Reinisch, K. M. A model for a partnership of lipid transfer proteins and scramblases in membrane expansion and organelle biogenesis. *Proc. Natl. Acad. Sci. U.S.A.* **118**, e2101562118 (2021).

137. Mailler, E. *et al.* The autophagy protein ATG9A enables lipid mobilization from lipid droplets. *Nat Commun* **12**, 6750 (2021).
138. Huang, D. *et al.* TMEM41B acts as an ER scramblase required for lipoprotein biogenesis and lipid homeostasis. *Cell Metabolism* **33**, 1655-1670.e8 (2021).
139. Yamamoto, H. & Matsui, T. Molecular mechanisms of macroautophagy, microautophagy, and chaperone-mediated autophagy. *J Nippon Med Sch JNMS.2024_91-102* (2023)
doi:10.1272/jnms.JNMS.2024_91-102.
140. Nakatogawa, H. Two ubiquitin-like conjugation systems that mediate membrane formation during autophagy. *Essays in Biochemistry* **55**, 39–50 (2013).
141. Takahashi, Y. *et al.* An autophagy assay reveals the ESCRT-III component CHMP2A as a regulator of phagophore closure. *Nat Commun* **9**, 2855 (2018).
142. Reggiori, F. & Ungermann, C. Autophagosome Maturation and Fusion. *Journal of Molecular Biology* **429**, 486–496 (2017).
143. Zhu, L., Jorgensen, J. R., Li, M., Chuang, Y.-S. & Emr, S. D. ESCRTs function directly on the lysosome membrane to downregulate ubiquitinated lysosomal membrane proteins. *eLife* **6**, e26403 (2017).
144. Mehrpour, M., Esclatine, A., Beau, I. & Codogno, P. Overview of macroautophagy regulation in mammalian cells. *Cell Res* **20**, 748–762 (2010).
145. Orsini, M., Morceau, F., Dicato, M. & Diederich, M. Autophagy as a pharmacological target in hematopoiesis and hematological disorders. *Biochemical Pharmacology* **152**, 347–361 (2018).
146. Mijaljica, D., Prescott, M. & Devenish, R. J. Microautophagy in mammalian cells: Revisiting a 40-year-old conundrum. *Autophagy* **7**, 673–682 (2011).
147. Wang, L., Klionsky, D. J. & Shen, H.-M. The emerging mechanisms and functions of microautophagy. *Nat Rev Mol Cell Biol* **24**, 186–203 (2023).
148. Oku, M. & Sakai, Y. Three Distinct Types of Microautophagy Based on Membrane Dynamics and Molecular Machineries. *BioEssays* **40**, 1800008 (2018).
149. Anding, A. L. & Baehrecke, E. H. Cleaning House: Selective Autophagy of Organelles. *Developmental Cell* **41**, 10–22 (2017).
150. Sahu, R. *et al.* Microautophagy of Cytosolic Proteins by Late Endosomes. *Developmental Cell* **20**, 131–139 (2011).
151. Krause, G. J. *et al.* Reduced endosomal microautophagy activity in aging associates with enhanced exocyst-mediated protein secretion. *Aging Cell* **21**, e13713 (2022).
152. Schniewind, I. *et al.* Cellular plasticity upon proton irradiation determines tumor cell radiosensitivity. *Cell Reports* **38**, 110422 (2022).
153. Morozova, K. *et al.* Structural and Biological Interaction of hsc-70 Protein with Phosphatidylserine in Endosomal Microautophagy. *Journal of Biological Chemistry* **291**, 18096–18106 (2016).
154. Hurley, J. H. ESCRT s are everywhere. *The EMBO Journal* **34**, 2398–2407 (2015).

155. Shields, S. B. & Piper, R. C. How Ubiquitin Functions with ESCRTs. *Traffic* **12**, 1306–1317 (2011).
156. Chauhan, A. S. *et al.* Trafficking of a multifunctional protein by endosomal microautophagy: linking two independent unconventional secretory pathways. *FASEB j.* **33**, 5626–5640 (2019).
157. Mesquita, A., Glenn, J. & Jenny, A. Differential activation of eMI by distinct forms of cellular stress. *Autophagy* **17**, 1828–1840 (2021).
158. Caballero, B. *et al.* Acetylated tau inhibits chaperone-mediated autophagy and promotes tau pathology propagation in mice. *Nat Commun* **12**, 2238 (2021).
159. Mukherjee, A., Patel, B., Koga, H., Cuervo, A. M. & Jenny, A. Selective endosomal microautophagy is starvation-inducible in *Drosophila*. *Autophagy* **12**, 1984–1999 (2016).
160. Liu, X.-M. *et al.* ESCRTs Cooperate with a Selective Autophagy Receptor to Mediate Vacuolar Targeting of Soluble Cargos. *Molecular Cell* **59**, 1035–1042 (2015).
161. Backer, J. M., Bourret, L. & Dice, J. F. Regulation of catabolism of microinjected ribonuclease A requires the amino-terminal 20 amino acids. *Proc. Natl. Acad. Sci. U.S.A.* **80**, 2166–2170 (1983).
162. Dice, J. F., Chiang, H. L., Spencer, E. P. & Backer, J. M. Regulation of catabolism of microinjected ribonuclease A. Identification of residues 7-11 as the essential pentapeptide. *Journal of Biological Chemistry* **261**, 6853–6859 (1986).
163. Chiang, H. L., Terlecky, Plant, C. P. & Dice, J. F. A role for a 70-kilodalton heat shock protein in lysosomal degradation of intracellular proteins. *Science* **246**, 382–385 (1989).
164. Cuervo, A. M. & Dice, J. F. A Receptor for the Selective Uptake and Degradation of Proteins by Lysosomes. *Science* **273**, 501–503 (1996).
165. Bandyopadhyay, U., Kaushik, S., Varticovski, L. & Cuervo, A. M. The Chaperone-Mediated Autophagy Receptor Organizes in Dynamic Protein Complexes at the Lysosomal Membrane. *Molecular and Cellular Biology* **28**, 5747–5763 (2008).
166. Bandyopadhyay, U., Sridhar, S., Kaushik, S., Kiffin, R. & Cuervo, A. M. Identification of Regulators of Chaperone-Mediated Autophagy. *Molecular Cell* **39**, 535–547 (2010).
167. Gong, Z. *et al.* Humanin is an endogenous activator of chaperone-mediated autophagy. *Journal of Cell Biology* **217**, 635–647 (2018).
168. Terlecky, S. R., Chiang, H. L., Olson, T. S. & Dice, J. F. Protein and peptide binding and stimulation of in vitro lysosomal proteolysis by the 73-kDa heat shock cognate protein. *Journal of Biological Chemistry* **267**, 9202–9209 (1992).
169. Fred Dice, J. Peptide sequences that target cytosolic proteins for lysosomal proteolysis. *Trends in Biochemical Sciences* **15**, 305–309 (1990).
170. Cuervo, A. M. & Dice, J. F. Age-related Decline in Chaperone-mediated Autophagy*. *Journal of Biological Chemistry* **275**, 31505–31513 (2000).
171. Kirchner, P. *et al.* Proteome-wide analysis of chaperone-mediated autophagy targeting motifs. *PLoS Biol* **17**, e3000301 (2019).

172. Koga, H., Martinez-Vicente, M., Macian, F., Verkhusha, V. V. & Cuervo, A. M. A photoconvertible fluorescent reporter to track chaperone-mediated autophagy. *Nat Commun* **2**, 386 (2011).
173. Kaushik, S. & Cuervo, A. M. **AMPK-dependent phosphorylation of lipid droplet protein PLIN2 triggers its degradation by CMA.** *Autophagy* **12**, 432–438 (2016).
174. Park, C., Suh, Y. & Cuervo, A. M. Regulated degradation of Chk1 by chaperone-mediated autophagy in response to DNA damage. *Nat Commun* **6**, 6823 (2015).
175. Quintavalle, C. *et al.* Phosphorylation-Regulated Degradation of the Tumor-Suppressor Form of PED by Chaperone-Mediated Autophagy in Lung Cancer Cells. *Journal Cellular Physiology* **229**, 1359–1368 (2014).
176. Kaushik, S. & Cuervo, A. M. The coming of age of chaperone-mediated autophagy. *Nature Reviews Molecular Cell Biology* **19**, 365–381 (2018).
177. Caballero, B. *et al.* Interplay of pathogenic forms of human tau with different autophagic pathways. *Aging Cell* **17**, e12692 (2018).
178. Kiffin, R., Christian, C., Knecht, E. & Cuervo, A. M. Activation of Chaperone-mediated Autophagy during Oxidative Stress. *MBoC* **15**, 4829–4840 (2004).
179. Ferreira, J. V. *et al.* STUB1/CHIP is required for HIF1A degradation by chaperone-mediated autophagy. *Autophagy* **9**, 1349–1366 (2013).
180. Agarraberes, F. A. & Dice, J. F. A molecular chaperone complex at the lysosomal membrane is required for protein translocation. *Journal of Cell Science* **114**, 2491–2499 (2001).
181. Tekirdag, K. & Cuervo, A. M. Chaperone-mediated autophagy and endosomal microautophagy: Jointed by a chaperone. *J Biol Chem* **293**, 5414–5424 (2018).
182. Agarraberes, F. A., Terlecky, S. R. & Dice, J. F. An Intralysosomal hsp70 Is Required for a Selective Pathway of Lysosomal Protein Degradation. *Journal of Cell Biology* **137**, 825–834 (1997).
183. Cuervo, A. M., Knecht, E., Terlecky, S. R. & Dice, J. F. Activation of a selective pathway of lysosomal proteolysis in rat liver by prolonged starvation. *American Journal of Physiology-Cell Physiology* **269**, C1200–C1208 (1995).
184. Eskelinen, E. *et al.* Unifying Nomenclature for the Isoforms of the Lysosomal Membrane Protein LAMP-2. *Traffic* **6**, 1058–1061 (2005).
185. Cuervo, A. M. & Dice, J. F. Unique properties of lamp2a compared to other lamp2 isoforms. *Journal of Cell Science* **113**, 4441–4450 (2000).
186. Cuervo, A. M. & Dice, J. F. Regulation of lamp2a levels in the lysosomal membrane. *Traffic* **1**, 570–583 (2000).
187. Rout, A. K., Strub, M.-P., Piszczek, G. & Tjandra, N. Structure of Transmembrane Domain of Lysosome-associated Membrane Protein Type 2a (LAMP-2A) Reveals Key Features for Substrate Specificity in Chaperone-mediated Autophagy. *Journal of Biological Chemistry* **289**, 35111–35123 (2014).
188. Bandyopadhyay, U., Kaushik, S., Varticovski, L. & Cuervo, A. M. The Chaperone-Mediated Autophagy Receptor Organizes in Dynamic Protein Complexes at the Lysosomal Membrane. *Molecular and Cellular Biology* **28**, 5747–5763 (2008).

189. Massey, A. C., Kaushik, S., Sovak, G., Kiffin, R. & Cuervo, A. M. Consequences of the selective blockage of chaperone-mediated autophagy. *Proceedings of the National Academy of Sciences* **103**, 5805–5810 (2006).
190. Schneider, J. L. *et al.* Loss of hepatic chaperone-mediated autophagy accelerates proteostasis failure in aging. *Aging Cell* **14**, 249–264 (2015).
191. Backer, J. M. & Dice, J. F. Covalent linkage of ribonuclease S-peptide to microinjected proteins causes their intracellular degradation to be enhanced during serum withdrawal. *Proceedings of the National Academy of Sciences* **83**, 5830–5834 (1986).
192. Schneider, J. L., Suh, Y. & Cuervo, A. M. Deficient Chaperone-Mediated Autophagy in Liver Leads to Metabolic Dysregulation. *Cell Metabolism* **20**, 417–432 (2014).
193. Cuervo, A. M., Hildebrand, H., Bomhard, E. M. & Dice, J. F. Direct lysosomal uptake of α 2-microglobulin contributes to chemically induced nephropathy. *Kidney International* **55**, 529–545 (1999).
194. Hubbi, M. E. *et al.* Cyclin-dependent kinases regulate lysosomal degradation of hypoxia-inducible factor 1 α to promote cell-cycle progression. *Proceedings of the National Academy of Sciences* **111**, E3325–E3334 (2014).
195. Vasco Ferreira, J., Rosa Soares, A., Silva Ramalho, J., Pereira, P. & Girao, H. K63 linked ubiquitin chain formation is a signal for HIF1A degradation by Chaperone-Mediated Autophagy. *Sci Rep* **5**, 10210 (2015).
196. Bonhoure, A. *et al.* Acetylation of translationally controlled tumor protein promotes its degradation through chaperone-mediated autophagy. *European Journal of Cell Biology* **96**, 83–98 (2017).
197. Cuervo, A. M., Dice, J. F. & Knecht, E. A Population of Rat Liver Lysosomes Responsible for the Selective Uptake and Degradation of Cytosolic Proteins. *Journal of Biological Chemistry* **272**, 5606–5615 (1997).
198. Boya, P. Lysosomal Function and Dysfunction: Mechanism and Disease. *Antioxidants & Redox Signaling* **17**, 766–774 (2012).
199. Mindell, J. A. Lysosomal Acidification Mechanisms. *Annual Review of Physiology* **74**, 69–86 (2012).
200. Pajares, M. *et al.* Transcription factor NFE2L2/NRF2 modulates chaperone-mediated autophagy through the regulation of LAMP2A. *Autophagy* **14**, 1310–1322 (2018).
201. Valdor, R. *et al.* Chaperone-mediated autophagy regulates T cell responses through targeted degradation of negative regulators of T cell activation. *Nat Immunol* **15**, 1046–1054 (2014).
202. Anguiano, J. *et al.* Chemical modulation of chaperone-mediated autophagy by retinoic acid derivatives. *Nature Chemical Biology* **9**, 374–382 (2013).
203. Yang, Q., Wang, R. & Zhu, L. Chaperone-Mediated Autophagy. in *Autophagy: Biology and Diseases: Basic Science* (ed. Qin, Z.-H.) 435–452 (Springer, 2019). doi:10.1007/978-981-15-0602-4_20.

204. Staudt, C., Puissant, E. & Boonen, M. Subcellular Trafficking of Mammalian Lysosomal Proteins: An Extended View. *International Journal of Molecular Sciences* **18**, 47 (2017).
205. Gough, N. R. *et al.* Utilization of the indirect lysosome targeting pathway by lysosome-associated membrane proteins (LAMPs) is influenced largely by the C-terminal residue of their GYXXΦ targeting signals. *Journal of Cell Science* **112**, 4257–4269 (1999).
206. Kaushik, S., Massey, A. C. & Cuervo, A. M. Lysosome membrane lipid microdomains: novel regulators of chaperone-mediated autophagy. *The EMBO Journal* **25**, 3921–3933 (2006).
207. Arias, E. *et al.* Lysosomal mTORC2/PHLPP1/Akt Regulate Chaperone-Mediated Autophagy. *Molecular Cell* **59**, 270–284 (2015).
208. Cuervo, A. M. Cathepsin A regulates chaperone-mediated autophagy through cleavage of the lysosomal receptor. *The EMBO Journal* **22**, 47–59 (2003).
209. Endicott, S. J., Ziemba, Z. J., Beckmann, L. J., Boynton, D. N., Jr. & Miller, R. A. Inhibition of class I PI3K enhances chaperone-mediated autophagy. *Journal of Cell Biology* **219**, (2020).
210. Dohi, E. *et al.* Hypoxic stress activates chaperone-mediated autophagy and modulates neuronal cell survival. *Neurochemistry International* **60**, 431–442 (2012).
211. Cuervo, A. M., Stefanis, L., Fredenburg, R., Lansbury, P. T. & Sulzer, D. Impaired Degradation of Mutant α -Synuclein by Chaperone-Mediated Autophagy. *Science* **305**, 1292–1295 (2004).
212. Martinez-Vicente, M. *et al.* Dopamine-modified α -synuclein blocks chaperone-mediated autophagy. *J. Clin. Invest.* JCI32806 (2008) doi:10.1172/JCI32806.
213. Mizushima, N., Yamamoto, A., Matsui, M., Yoshimori, T. & Ohsumi, Y. In Vivo Analysis of Autophagy in Response to Nutrient Starvation Using Transgenic Mice Expressing a Fluorescent Autophagosome Marker. *MBoC* **15**, 1101–1111 (2004).
214. Zhang, C. & Cuervo, A. M. Restoration of chaperone-mediated autophagy in aging liver improves cellular maintenance and hepatic function. *Nature Medicine* **14**, 959–965 (2008).
215. Kaushik, S. & Cuervo, A. M. Degradation of lipid droplet-associated proteins by chaperone-mediated autophagy facilitates lipolysis. *Nat Cell Biol* **17**, 759–770 (2015).
216. Cuervo, A. M., Hu, W., Lim, B. & Dice, J. F. I κ B Is a Substrate for a Selective Pathway of Lysosomal Proteolysis. *MBoC* **9**, 1995–2010 (1998).
217. Jacobs, M. D. & Harrison, S. C. Structure of an I κ B α /NF- κ B Complex. *Cell* **95**, 749–758 (1998).
218. Franch, H. A., Sooparb, S., Du, J. & Brown, N. S. A Mechanism Regulating Proteolysis of Specific Proteins during Renal Tubular Cell Growth. *Journal of Biological Chemistry* **276**, 19126–19131 (2001).
219. Yang, Q. *et al.* Regulation of Neuronal Survival Factor MEF2D by Chaperone-Mediated Autophagy. *Science* **323**, 124–127 (2009).
220. Zhang, L. *et al.* Disruption of chaperone-mediated autophagy-dependent degradation of MEF2A by oxidative stress-induced lysosome destabilization. *Autophagy* **10**, 1015–1035 (2014).
221. Hu, M.-M. *et al.* Sumoylation Promotes the Stability of the DNA Sensor cGAS and the Adaptor STING to Regulate the Kinetics of Response to DNA Virus. *Immunity* **45**, 555–569 (2016).

222. Juste, Y. R. *et al.* Reciprocal regulation of chaperone-mediated autophagy and the circadian clock. *Nat Cell Biol* **23**, 1255–1270 (2021).
223. Bourdenx, M., Gavathiotis, E. & Cuervo, A. M. Chaperone-mediated autophagy: a gatekeeper of neuronal proteostasis. *Autophagy* **17**, 2040–2042 (2021).
224. Bourdenx, M. Chaperone-mediated autophagy prevents collapse of the neuronal metastable proteome.
225. Patel, B. & Cuervo, A. M. Methods to study chaperone-mediated autophagy. *Methods* **75**, 133–140 (2015).
226. Juste, Y. R. & Cuervo, A. M. Analysis of Chaperone-Mediated Autophagy. in *Autophagy* (eds. Ktistakis, N. & Florey, O.) vol. 1880 703–727 (Springer New York, 2019).
227. Wattiaux, R., Wattiaux-De Coninck, S., Ronveaux-Dupal, M.-F. & Dubois, F. Isolation of rat liver lysosomes by isopycnic centrifugation in a metrizamide gradient. *The Journal of cell biology* **78**, 349–368 (1978).
228. Koga, H., Martinez-Vicente, M., Macian, F., Verkhusha, V. V. & Cuervo, A. M. A photoconvertible fluorescent reporter to track chaperone-mediated autophagy. *Nat Commun* **2**, 386 (2011).
229. Dong, S. *et al.* Monitoring spatiotemporal changes in chaperone-mediated autophagy in vivo. *Nat Commun* **11**, 645 (2020).
230. Kaushik, S. *et al.* Chaperone-mediated autophagy regulates adipocyte differentiation. *Sci. Adv.* **8**, eabq2733 (2022).
231. Dong, S. *et al.* Chaperone-mediated autophagy sustains haematopoietic stem-cell function. *Nature* **591**, 117–123 (2021).
232. Orenstein, S. J. *et al.* Interplay of LRRK2 with chaperone-mediated autophagy. *Nat Neurosci* **16**, 394–406 (2013).
233. Storrie, B. & Amadden, E. [16] Isolation of subcellular organelles. in *Methods in Enzymology* vol. 182 203–225 (Elsevier, 1990).
234. Gomez-Sintes, R. *et al.* Targeting retinoic acid receptor alpha-corepressor interaction activates chaperone-mediated autophagy and protects against retinal degeneration. *Nat Commun* **13**, 4220 (2022).
235. Madrigal-Matute, J. *et al.* Protective role of chaperone-mediated autophagy against atherosclerosis. *Proc. Natl. Acad. Sci. U.S.A.* **119**, e2121133119 (2022).
236. Kuo, S.-H. *et al.* Mutant glucocerebrosidase impairs α -synuclein degradation by blockade of chaperone-mediated autophagy. *Sci. Adv.* **8**, eabm6393 (2022).
237. Levine, B. & Klionsky, D. J. Development by Self-Digestion. *Developmental Cell* **6**, 463–477 (2004).
238. Rusten, T. E. *et al.* Programmed Autophagy in the Drosophila Fat Body Is Induced by Ecdysone through Regulation of the PI3K Pathway. *Developmental Cell* **7**, 179–192 (2004).
239. Scott, R. C., Schuldiner, O. & Neufeld, T. P. Role and Regulation of Starvation-Induced Autophagy in the Drosophila Fat Body. *Developmental Cell* **7**, 167–178 (2004).

240. Tesseraud, S. *et al.* Autophagy in farm animals: current knowledge and future challenges. *Autophagy* **17**, 1809–1827 (2021).
241. Gough, N. R. & Fambrough, D. M. Different Steady State Subcellular Distributions of the Three Splice Variants of Lysosome-associated Membrane Protein LAMP-2 Are Determined Largely by the COOH-terminal Amino Acid Residue. *The Journal of Cell Biology* **137**, 1161–1169 (1997).
242. Lescat, L. *et al.* CMA restricted to mammals and birds: myth or reality? *Autophagy* **14**, 1267–1270 (2018).
243. Williams, M. A. & Fukuda, M. Accumulation of membrane glycoproteins in lysosomes requires a tyrosine residue at a particular position in the cytoplasmic tail. *The Journal of cell biology* **111**, 955–966 (1990).
244. Guarnieri, F. G., Arterburn, L. M., Penno, M. B., Cha, Y. & August, J. T. The motif Tyr-X-X-hydrophobic residue mediates lysosomal membrane targeting of lysosome-associated membrane protein 1. *Journal of Biological Chemistry* **268**, 1941–1946 (1993).
245. Lescat, L. *et al.* Chaperone-Mediated Autophagy in the Light of Evolution: Insight from Fish. *Molecular Biology and Evolution* **37**, 2887–2899 (2020).
246. Inoue, J., Sato, Y., Sinclair, R., Tsukamoto, K. & Nishida, M. Rapid genome reshaping by multiple-gene loss after whole-genome duplication in teleost fish suggested by mathematical modeling. *Proc. Natl. Acad. Sci. U.S.A.* **112**, 14918–14923 (2015).
247. Lescat, L. Caractérisation et étude du rôle de lamp2a chez les poissons. (Pau, 2019).
248. Berthelot, C. *et al.* The rainbow trout genome provides novel insights into evolution after whole-genome duplication in vertebrates. *Nature communications* **5**, 3657 (2014).
249. Vernier, J. M. Table chronologique du développement embryonnaire de la truite arc-en-ciel, *Salmo gairdneri* Rich. *Ann. Embryol. Morphogenet.* **2**, 495–520 (1969).
250. Cuervo, A. M., Terlecky, S. R., Dice, J. F. & Knecht, E. Selective binding and uptake of ribonuclease A and glyceraldehyde-3-phosphate dehydrogenase by isolated rat liver lysosomes. *Journal of Biological Chemistry* **269**, 26374–26380 (1994).
251. Juste, Y. R. & Cuervo, A. M. Analysis of chaperone-mediated autophagy. *Autophagy: Methods and Protocols* 703–727 (2019).
252. Donzeau, M. *et al.* Tim23 Links the Inner and Outer Mitochondrial Membranes. *Cell* **101**, 401–412 (2000).
253. Vélez, E. J. *et al.* Chaperone-mediated autophagy protects against hyperglycemic stress. *Autophagy* 15548627.2023.2267415 (2023) doi:10.1080/15548627.2023.2267415.
254. Bourdenx, M. *et al.* Chaperone-mediated autophagy prevents collapse of the neuronal metastable proteome. *Cell* **184**, 2696–2714.e25 (2021).
255. Klionsky, D. J. *et al.* Guidelines for the use and interpretation of assays for monitoring autophagy. *autophagy* **17**, 1–382 (2021).
256. Krishnan, J. & Rohner, N. Sweet fish: Fish models for the study of hyperglycemia and diabetes. *Journal of Diabetes* **11**, 193–203 (2019).

257. Puri, P. *et al.* A lipidomic analysis of nonalcoholic fatty liver disease. *Hepatology* **46**, 1081–1090 (2007).
258. Tasset, I. & Cuervo, A. M. Role of chaperone-mediated autophagy in metabolism. *The FEBS journal* **283**, 2403–2413 (2016).
259. Schlegel, A. *Zebrafish models for dyslipidemia and atherosclerosis research. Front Endocrinol* **7**: 159. (2016).
260. Wood, C. M. & Eom, J. The osmorepiratory compromise in the fish gill. *Comparative Biochemistry and Physiology Part A: Molecular & Integrative Physiology* **254**, 110895 (2021).
261. Abdel-Tawwab, M., Monier, M. N., Hoseinifar, S. H. & Faggio, C. Fish response to hypoxia stress: growth, physiological, and immunological biomarkers. *Fish Physiol Biochem* **45**, 997–1013 (2019).
262. Kaushik, S. & Cuervo, A. M. The coming of age of chaperone-mediated autophagy. *Nat Rev Mol Cell Biol* **19**, 365–381 (2018).
263. Pérez, L. *et al.* LAMP-2C Inhibits MHC Class II Presentation of Cytoplasmic Antigens by Disrupting Chaperone-Mediated Autophagy. *The Journal of Immunology* **196**, 2457–2465 (2016).
264. Kiffin, R. *et al.* Altered dynamics of the lysosomal receptor for chaperone-mediated autophagy with age. *Journal of Cell Science* **120**, 782–791 (2007).
265. Murphy, K. E. *et al.* Lysosomal-associated membrane protein 2 isoforms are differentially affected in early Parkinson's disease: Early loss of LAMP2A protein in PD. *Mov Disord.* **30**, 1639–1647 (2015).
266. Cleveland, B. M., Yamaguchi, G., Radler, L. M. & Shimizu, M. Editing the duplicated insulin-like growth factor binding protein-2b gene in rainbow trout (*Oncorhynchus mykiss*). *Sci Rep* **8**, 16054 (2018).
267. Wargelius, A. *et al.* Dnd knockout ablates germ cells and demonstrates germ cell independent sex differentiation in Atlantic salmon. *Sci Rep* **6**, 21284 (2016).
268. Marandel, L., Véron, V., Surget, A., Plagnes-Juan, É. & Panserat, S. Glucose metabolism ontogenesis in rainbow trout (*Oncorhynchus mykiss*) in the light of the recently sequenced genome: new tools for intermediary metabolism programming. *Journal of Experimental Biology* jeb.134304 (2016) doi:10.1242/jeb.134304.
269. Cardona, E. *et al.* Tissue origin of circulating microRNAs and their response to nutritional and environmental stress in rainbow trout (*Oncorhynchus mykiss*). *Science of The Total Environment* **853**, 158584 (2022).
270. Kawano, A. *et al.* Development of a rainbow trout intestinal epithelial cell line and its response to lipopolysaccharide. *Aquaculture Nutrition* **17**, e241–e252 (2011).
271. Plagnes-Juan, E. *et al.* Insulin regulates the expression of several metabolism-related genes in the liver and primary hepatocytes of rainbow trout (*Oncorhynchus mykiss*). *Journal of Experimental Biology* **211**, 2510–2518 (2008).
272. Gudrun, T. The E-Method: a highly accurate technique for gene-expression analysis. *Nat. Methods* **3**, i–ii (2006).

273. Pfaffl, M. W. A new mathematical model for relative quantification in real-time RT-PCR. *Nucleic Acids Res* **29**: e45. *Find this article online* (2001).
274. Schindelin, J. *et al.* Fiji: an open-source platform for biological-image analysis. *Nat Methods* **9**, 676–682 (2012).
275. Folch, J., Lees, M. & Sloane Stanley, G. H. A simple method for the isolation and purification of total lipids from animal tissues. *J Biol Chem* **226**, 497–509 (1957).
276. Alannan, M. *et al.* Targeting PCSK9 in Liver Cancer Cells Triggers Metabolic Exhaustion and Cell Death by Ferroptosis. *Cells* **12**, 62 (2022).
277. Kuleshov, M. V. *et al.* Enrichr: a comprehensive gene set enrichment analysis web server 2016 update. *Nucleic Acids Res* **44**, W90–W97 (2016).
278. Cardoso, O. *et al.* Oxidative stress profiles in brain point out a higher susceptibility of fish to waterborne divalent mercury compared to dietary organic mercury. *Marine Pollution Bulletin* **122**, 110–121 (2017).
279. Zulkipli, S. Z. *et al.* A review of mercury pathological effects on organs specific of fishes. *Environmental Pollutants and Bioavailability* **33**, 76–87 (2021).
280. Näslund, E. & Hellström, P. M. Appetite signaling: From gut peptides and enteric nerves to brain. *Physiology & Behavior* **92**, 256–262 (2007).
281. Morton, G. J., Meek, T. H. & Schwartz, M. W. Neurobiology of food intake in health and disease. *Nat Rev Neurosci* **15**, 367–378 (2014).
282. Nuzzaci, D. *et al.* Plasticity of the Melanocortin System: Determinants and Possible Consequences on Food Intake. *Front. Endocrinol.* **6**, (2015).
283. Cerdá-Reverter, J. M., Ringholm, A., Schiöth, H. B. & Peter, R. E. Molecular Cloning, Pharmacological Characterization, and Brain Mapping of the Melanocortin 4 Receptor in the Goldfish: Involvement in the Control of Food Intake. *Endocrinology* **144**, 2336–2349 (2003).
284. Kalanathan, T. *et al.* The Melanocortin System in Atlantic Salmon (*Salmo salar* L.) and Its Role in Appetite Control. *Front. Neuroanat.* **14**, 48 (2020).
285. Soengas, J. L., Cerdá-Reverter, J. M. & Delgado, M. J. Central regulation of food intake in fish: an evolutionary perspective. *Journal of Molecular Endocrinology* **60**, R171–R199 (2018).
286. Delgado, M. J., Cerdá-Reverter, J. M. & Soengas, J. L. Hypothalamic Integration of Metabolic, Endocrine, and Circadian Signals in Fish: Involvement in the Control of Food Intake. *Front. Neurosci.* **11**, 354 (2017).
287. Polakof, S., Rodríguez-Alonso, M. & Soengas, J. L. Immunohistochemical localization of glucokinase in rainbow trout brain. *Comparative Biochemistry and Physiology Part A: Molecular & Integrative Physiology* **153**, 352–358 (2009).
288. Yan, P. *et al.* Duplication of neuropeptide Y and peptide YY in Nile tilapia *Oreochromis niloticus* and their roles in food intake regulation. *Peptides* **88**, 97–105 (2017).
289. Tolås, I. *et al.* Regional Expression of npy mRNA Paralogs in the Brain of Atlantic Salmon (*Salmo salar*, L.) and Response to Fasting. *Front. Physiol.* **12**, 720639 (2021).

290. Lu, W. *et al.* Dual Proteolytic Pathways Govern Glycolysis and Immune Competence. *Cell* **159**, 1578–1590 (2014).
291. Beutler, E. Disorders Due to Enzyme Defects in the Red Blood Cell. in *Advances in Metabolic Disorders* vol. 6 131–160 (Elsevier, 1972).
292. Endicott, S. J. & Miller, R. A. PTEN activates chaperone-mediated autophagy to regulate metabolism. *Autophagy* 1–2 (2023) doi:10.1080/15548627.2023.2255966.
293. Zaltsman, Y. *et al.* MTCH2/MIMP is a major facilitator of tBID recruitment to mitochondria. *Nat Cell Biol* **12**, 553–562 (2010).
294. Utsumi, T. *et al.* Identification and characterization of protein N-myristoylation occurring on four human mitochondrial proteins, SAMM50, TOMM40, MIC19, and MIC25. *PLoS ONE* **13**, e0206355 (2018).
295. Fuhrmann, D. C. & Brüne, B. Mitochondrial composition and function under the control of hypoxia. *Redox Biology* **12**, 208–215 (2017).
296. Kaufman, D. M. *et al.* Ageing and hypoxia cause protein aggregation in mitochondria. *Cell Death Differ* **24**, 1730–1738 (2017).
297. Sivanesan, S., Chang, E., Howell, M. D. & Rajadas, J. Amyloid protein aggregates: new clients for mitochondrial energy production in the brain? *The FEBS Journal* **287**, 3386–3395 (2020).
298. Zhang, L. *et al.* Differential effect of amyloid beta peptides on mitochondrial axonal trafficking depends on their state of aggregation and binding to the plasma membrane. *Neurobiology of Disease* **114**, 1–16 (2018).
299. Rebecchi, M. J. & Pentylala, S. N. Structure, Function, and Control of Phosphoinositide-Specific Phospholipase C. *Physiological Reviews* **80**, 1291–1335 (2000).
300. Verschueren, K. H. G. *et al.* Structure of ATP citrate lyase and the origin of citrate synthase in the Krebs cycle. *Nature* **568**, 571–575 (2019).
301. Kelly, D. J. & Hughes, N. J. The Citric Acid Cycle and Fatty Acid Biosynthesis. in *Helicobacter pylori* (eds. Mobley, H. L. T., Mendz, G. L. & Hazell, S. L.) 135–146 (ASM Press, 2014). doi:10.1128/9781555818005.ch12.
302. Xue, B. & Kahn, B. B. AMPK integrates nutrient and hormonal signals to regulate food intake and energy balance through effects in the hypothalamus and peripheral tissues. *The Journal of Physiology* **574**, 73–83 (2006).
303. Yang, B. & Kumar, S. Nedd4 and Nedd4-2: closely related ubiquitin-protein ligases with distinct physiological functions. *Cell Death Differ* **17**, 68–77 (2010).
304. Schaubert, C. *et al.* Rad23 links DNA repair to the ubiquitin/proteasome pathway. *Nature* **391**, 715–718 (1998).
305. Pickart, C. M. & Rose, I. A. Ubiquitin carboxyl-terminal hydrolase acts on ubiquitin carboxyl-terminal amides. *Journal of Biological Chemistry* **260**, 7903–7910 (1985).
306. Hughes, D. C. *et al.* Knockdown of the E3 ubiquitin ligase UBR5 and its role in skeletal muscle anabolism. *American Journal of Physiology-Cell Physiology* **320**, C45–C56 (2021).

307. Fatima, A. *et al.* The ubiquitin-conjugating enzyme UBE2K determines neurogenic potential through histone H3 in human embryonic stem cells. *Commun Biol* **3**, 262 (2020).
308. Kitagawa, K., Skowyra, D., Elledge, S. J., Harper, J. W. & Hieter, P. SGT1 Encodes an Essential Component of the Yeast Kinetochore Assembly Pathway and a Novel Subunit of the SCF Ubiquitin Ligase Complex. *Molecular Cell* **4**, 21–33 (1999).
309. Yuliandari, P. *et al.* Hepatitis C virus NS5A protein promotes the lysosomal degradation of diacylglycerol O-acyltransferase 1 (DGAT1) via endosomal microautophagy. *Autophagy Reports* **1**, 264–285 (2022).
310. Mejlvang, J. *et al.* Starvation induces rapid degradation of selective autophagy receptors by endosomal microautophagy. *Journal of Cell Biology* **217**, 3640–3655 (2018).
311. Ohno, S. *Evolution by gene duplication*. (Springer Science & Business Media, 2013).
312. Albalat, R. & Cañestro, C. Evolution by gene loss. *Nat Rev Genet* **17**, 379–391 (2016).
313. Bieczynski, F., Paineofilú, J. C., Venturino, A. & Luquet, C. M. Expression and Function of ABC Proteins in Fish Intestine. *Front. Physiol.* **12**, 791834 (2021).
314. Salinas, I. & Parra, D. Fish mucosal immunity: intestine. in *Mucosal Health in Aquaculture* 135–170 (Elsevier, 2015). doi:10.1016/B978-0-12-417186-2.00006-6.
315. Wu, Y. *et al.* The role of autophagy in maintaining intestinal mucosal barrier. *Journal Cellular Physiology* **234**, 19406–19419 (2019).
316. Hansen, M., Rubinsztein, D. C. & Walker, D. W. Autophagy as a promoter of longevity: insights from model organisms. *Nat Rev Mol Cell Biol* **19**, 579–593 (2018).
317. Li, H.-Y. *et al.* Autophagy in intestinal injury caused by severe acute pancreatitis. *Chinese Medical Journal* **134**, 2547–2549 (2021).
318. Kaushik, S. *et al.* Autophagy in Hypothalamic AgRP Neurons Regulates Food Intake and Energy Balance. *Cell Metabolism* **14**, 173–183 (2011).
319. Bravo-San Pedro, J. M., Sica, V., Madeo, F. & Kroemer, G. Acyl-CoA-binding protein (ACBP): the elusive ‘hunger factor’ linking autophagy to food intake. *CST* **3**, 312–318 (2019).
320. Unniappan, S. & Peter, R. E. Structure, distribution and physiological functions of ghrelin in fish. *Comparative Biochemistry and Physiology Part A: Molecular & Integrative Physiology* **140**, 396–408 (2005).
321. Kroemer, G., Mariño, G. & Levine, B. Autophagy and the Integrated Stress Response. *Molecular Cell* **40**, 280–293 (2010).
322. Shang, F. & Taylor, A. Ubiquitin–proteasome pathway and cellular responses to oxidative stress. *Free Radical Biology and Medicine* **51**, 5–16 (2011).
323. Bellot, G. *et al.* Hypoxia-Induced Autophagy Is Mediated through Hypoxia-Inducible Factor Induction of BNIP3 and BNIP3L via Their BH3 Domains. *Molecular and Cellular Biology* **29**, 2570–2581 (2009).

ECOLE DOCTORALE : UPPA

LABORATOIRE : NUMEA/INRAE

CONTACT

simon.schnebert@inrae.fr

simonschnbebert@gmail.com